ABSTRACTS

Mikołaj Busłowicz
Robust stability of convex combination of two fractional degree characteristic polynomials

The paper considers the problem of robust stability of convex combination of two fractional degree characteristic polynomials. This problem is equivalent to the problem of robust stability of linear continuous-time fractional systems with characteristic polynomial linearly dependent on one uncertain parameter. Frequency domain methods for robust stability analysis of such a combination are given. The methods proposed are based on the Zero Exclusion Condition known from the theory of robust stability of families of natural degree polynomials. The considerations are illustrated by numerical example.

Giancarlo Genta , Andrea Festini, Xavier Delepine
From oil to magnetic fields: active and passive vibration control

When a reduction of vibration amplitude usually designers resort to dampers based either on dry friction, internal material damping or fluid viscosity, each one of these mechanisms having its peculiar field of application. To improve performance while at the same time reducing costs and environmental load, electromagnetic damping devices are finding new applications, beyond the fields where they have a long history. Moreover, electromagnetic dampers can be easily controlled, obtain active or even 'intelligent' vibration control. Three examples from the internal combustion engines, automotive and gas turbine fields are discussed in some detail to show the potential advantages of this technology.
Keywords: Vibration control, eddy current dampers, active damping.

Zdzisław Gosiewski
Control-oriented modeling and control of rotor vibration

Deep analysis of the control plant brings many useful information for the designer of the control system. The analysis is also important part in the design of active vibration control system. The coupling of different dynamical phenomena in rotating machinery leads to unstable vibrations. Usually, the coupling effects are caused by changing parameters. Angular speed or rotor unbalance in some applications are such parameters which change in the wide range. The problem is to find for which angular speeds we have unstable torsional/lateral vibrations. Usually, the unstable regions are in the vicinity of angular speeds where maps of natural frequencies for both dynamical systems cross each other. In the paper there was explained which intersection of torsional and lateral natural frequencies are unstable and why. The root locus method was used to explain the phenomenon. It indicated such control procedures which amplify the positive (stabilizing) mechanisms in the rotor dynamics. Such procedures can also lead to the energy saving control laws. In the case of lateral vibrations there were considered four control strategies. And these strategies were compared to indicate optimal one.

Zdzisław Gosiewski, Grzegorz Michałowski
H∞ control of robot arm with hydraulic drive

In the paper an H_∞ velocity control of the robot arm in combination with the hydraulic drive is presented. The open-loop system consists of a manipulator with one rotary degree of freedom, a hydraulic servomotor, and an electrohydraulic amplifier. The mathematical model of the system is derived. Due to the nonlinearity in the model, which is caused by varying operating point parameters and the direction of the servomotor motion, the model of multiplicative uncertainty was defined. The plant model transfer function parameters were assumed to be variable. To limit error signal, control signal, and output signal three weighting functions were designed. The simulation results of the designed $H\infty$ optimal closed-loop system were compared to the standard PID closed-loop system. The solution ensuring robust performance was achieved and proved.

Tadeusz Kaczorek
Realization problem for singular positive single-input single-output continuous-time systems with delays in state and in inputs

The positive realization problem for singular continuous-time linear single-input single-output systems with delays in state and in inputs is addressed. The notion of canonical forms of matrices are extended for singular linear systems with delays. Necessary and sufficient conditions for positivity of the singular continuous-time systems with delays and sufficient conditions for the existence of a positive singular realization are established. A procedure for computation of a positive singular realization of a given transfer function is proposed and illustrated by a numerical example.

Tadeusz Kaczorek
Positive different orders fractional 2D linear systems

A new class of positive different orders fractional 2D linear systems is introduced. A notion of (α, β) orders difference of 2D function is proposed. Fractional 2D state equations of linear systems are given and their solutions are derived using 2D Z-transform. The classical Cayley-Hamilton theorem is extended to the 2D fractional linear systems. Neccesary and sufficient conditions for the positivity, reachability and controllability to zero of the fractional 2D linear systems are established.

Tadeusz Kaczorek, Vladimir Marchenko, Łukasz Sajewski
Solvability of 2D hybrid linear systems – comparison of three different methods

A class of positive hybrid linear systems is introduced. Three different methods for computation of solutions of the hybrid system are proposed. The considerations are illustrated by numerical example. Simulations of solution have been shown for the methods.

Jerzy T. Sawicki

Rationale for mu-synthesis control of flexible rotor-magnetic bearing systems

The emergence of sophisticated formal control synthesis tools provokes important questions for any prospective user: why learn to use these new tools, what will they offer me? In synthesis of magnetic bearing controllers, it turns out that the range of stabilizing controllers is often quite narrow so that the difference between a poor controller and an "optimal" one may be small. Hence, the product of formal control synthesis tools often looks and performs much like what a reasonably clever control engineer would produce by hand. This paper demonstrates that the real value of these tools lies in a) generation of a performance benchmark which can be used to firmly establish the best performance relative to a specification and b) change of design parameter space to one which is relatively easy to maintain and represents a durable investment from an engineering process view.

Krzysztof Sibilski

Microelectromechanical flying robots - state of the art

Micro Air Vehicles (MAVs) are miniature airplanes constructed from state-of-the-art materials, designed to be small, light, and highly resilient. Current applications include surveillance, reconnaissance, and munitions. Many of the planes, because of their size, have unconventional designs with respect to the wings and control surfaces. Instability introduced by the small non-traditional aircraft designs must be addressed, to eliminate the need for an expert pilot for aircraft control and navigation. In this paper we present a state-of-the-art technology development focused on the technologies and components required to enable flight at small scales, including flight control, power and propulsion, navigation, multi-purpose structures, advanced communications and information systems, Micro-electro-mechanical Systems (MEMS), advanced sensors, and lightweight, efficient high-density power sources.

ROBUST STABILITY OF CONVEX COMBINATION OF TWO FRACTIONAL DEGREE CHARACTERISTIC POLYNOMIALS

Mikołaj BUSŁOWICZ[*]

[*]Chair of Automatics and Electronics, Faculty of Electrical Engineering
ul. Wiejska 45D, Białystok Technical University, 15-351 Białystok

Abstract: The paper considers the problem of robust stability of convex combination of two fractional degree characteristic polynomials. This problem is equivalent to the problem of robust stability of linear continuous-time fractional systems with characteristic polynomial linearly dependent on one uncertain parameter. Frequency domain methods for robust stability analysis of such a combination are given. The methods proposed are based on the Zero Exclusion Condition known from the theory of robust stability of families of natural degree polynomials. The considerations are illustrated by numerical example.

1. INTRODUCTION

In the last decades, the problem of analysis and synthesis of dynamical systems described by fractional order differential (or difference) equations was considered in many papers. For review of the previous results see (Ortigueira, 2000a; Ortigueira, 2000b; Sierociuk, 2007; Ma, 2004; Valerio, 2005; Vinagre et al., 2002), for example.

The problems of stability and robust stability of linear fractional continuous-time systems were studied among others in (Matignon, 1996; Matignon, 1998; Vinagre et al., 2002) and (Ahn et al., 2006; Busłowicz and Kalinowski, 2008; Chen et al., 2006; Petras et al., 2002), respectively.

The new class of the linear discrete-time fractional order systems, namely the positive systems of fractional order
is considered by Kaczorek (2007).

Recently, the new frequency domain methods for stability analysis of linear continuous-time fractional systems of non-commensurate and commensurate orders was proposed by Busłowicz (2008a, 2008b).

The aim of the paper is to give the frequency domain methods for robust stability analysis of convex combination of two fractional non-commensurate degree characteristic polynomials. This problem is equivalent to the problem of robust stability of linear continuous-time fractional non-commensurate order systems with characteristic polynomial linearly dependent on one uncertain parameter. This problem in the case of commensurate order systems was considered by Busłowicz and Kalinowski (2008).

The problem of robust stability analysis of linear systems was considered in the monographs (Ackermann et al., 1994; Barmish, 1995; Bhattacharyya et al., 1995; Białas, 2002; Busłowicz, 1997). To the best knowledge of the Author, the robust stability problem of convex combination of two fractional non-commensurate degree polynomials has not been considered yet.

2. PROBLEM FORMULATION

Let us consider the fractional degree polynomial

$$w(s,p)=w_1(s)+pw_2(s),\quad p\in P, \tag{1}$$

linearly dependent on one uncertain parameter p where $P=[p^-,\ p^+]$ with $p^- < p^+$ is the value set of uncertain parameter and

$$w_1(s)=a_{1,n}s^{\alpha_n}+a_{1,n-1}s^{\alpha_{n-1}}+...+a_{1,1}s^{\alpha_1}+a_{1,0}, \tag{2a}$$

$$w_2(s)=a_{2,m}s^{\beta_m}+a_{2,m-1}s^{\beta_{m-1}}+...+a_{2,1}s^{\beta_1}+a_{2,0}, \tag{2b}$$

are given polynomials of fractional degrees where $\alpha_n>\alpha_{n-1}>\ldots>\alpha_1>0$ and $\beta_m>\beta_{m-1}>\ldots>\beta_1>0$are arbitrary real numbers, $\alpha_{1,i}$ (i=0, 1, …, n) and $\alpha_{2,k}$ (k=0, 1, …, m) are real coefficients.

The polynomial (1) with uncertain parameter can be written in the form of convex combination of two fractional degrees polynomials

$$W(s,Q)=\{w(s,q):q\in Q=[0,1]\}, \tag{3}$$

where

$$w(s,q)=(1-q)w_a(s)+qw_b(s), \tag{4}$$

with $q=(p-p^-)/(p^+-p^-)$ and

$$\begin{aligned}w_a(s)&=w(s,p^-)=w_1(s)+p^-w_2(s)\\&=a_ns^{\gamma_n}+a_{n-1}s^{\gamma_{n-1}}+\ldots+a_1s^{\gamma_1}+a_0\end{aligned} \tag{5a}$$

$$w_b(s) = w(s, p^+) = w_1(s) + p^+ w_2(s) \\ = b_n s^{\gamma_n} + b_{n-1} s^{\gamma_{n-1}} + \ldots + b_1 s^{\gamma_1} + b_0 \tag{5b}$$

with $\gamma_n = \alpha_n$ and $\gamma_n > \gamma_{n-1} > \cdots > \gamma_1 > 0$.

The family (3) of fractional polynomials is of the non-commensurate degree, in general.

This family is of the commensurate degree, if polynomials (5) have commensurate degrees, i.e. if $\gamma_i = i\gamma$ for i=0, 1, …, n and $0<\gamma<1$. In such a case polynomials (5) can be written in the forms of natural degree polynomials

$$w_a(\lambda) = a_n \lambda^n + a_{n-1}\lambda^{n-1} + \ldots + a_1\lambda + a_0 \tag{6a}$$

$$w_b(\lambda) = b_n \lambda^n + b_{n-1}\lambda^{n-1} + \ldots + b_1\lambda + b_0 \tag{6b}$$

where $\lambda = s^{\gamma}$.

In the paper we will assume that the leading coefficient of the polynomial (4) is non-zero for all $q \in Q$ i. e.

$$(1-q)a_n + qb_n \neq 0, \quad \forall q \in Q.$$

If the above condition holds then the family (3) of fractional polynomials is degree invariant.

From the theory of stability of fractional order systems given by Matignon (1996, 1998) and Vinagre et al. (2002), for example, we have the following theorem.

Let $w(s)$ be any fixed fractional degree polynomial.

Theorem 1.

The fractional order system with characteristic polynomial $w(s)$ is bounded-input bounded-output (BIBO) stable (shortly stable) if and only if the fractional degree characteristic polynomial $w(s)$ is stable, i.e. $w(s)$ has no zeros in the closed right-half of the Riemann complex surface, i.e.

$$w(s) \neq 0 \ \text{ for } \ \mathrm{Re}\, s \geq 0. \tag{7}$$

The fractional order polynomial $w(s)$ is a multivalued function whose domain is a Riemann surface. In general, this surface has an infinite number of sheets and the fractional polynomial $w(s)$ has an infinite number of zeros. Only a finite number of which will be in the main sheet of the Riemann surface. For stability reasons only the main sheet defined by $-\pi < \arg s < \pi$ can be considered (Vinagre et al., 2002).

Definition 1.

The family (3) of fractional degree polynomials is called robustly stable, if polynomial $w(s,q)$ is stable for all $q \in Q$

By generalization of Theorem 1 to the robust stability case we obtain the following theorem.

Theorem 2.

An uncertain system of fractional order with characteristic polynomial (3) is robustly bounded-input bounded-output (BIBO) stable (shortly robustly stable) if and only if the family (3) of fractional degree characteristic polynomials is robustly stable, i.e. $w(s,p)$ has no zeros in the closed right-half of the Riemann complex surface for all $q \in Q$, that is

$$w(s,q) \neq 0 \ \text{ for } \ \mathrm{Re}\, s \geq 0 \ \text{ and for all } \ q \in Q. \tag{8}$$

The problem of robust stability analysis of family (3) of fractional polynomials was considered by Busłowicz and Kalinowski (2008) in the case of commensurate degrees of polynomials (5), i.e. with $\gamma_i = i\gamma$, i=0, 1, …, n, $0<\gamma<1$. In such a case family (3) is robustly stable if and only if all zeros of the polynomial $w(\lambda, q) = (1-q)w_a(\lambda) + qw_b(\lambda)$ with $w_a(\lambda)$ and $w_b(\lambda)$ of the forms (6) satisfy the condition $|\arg \lambda| > 0.5\gamma\pi$ for all $q \in Q=[0,1]$.

The aim of this paper is to give the frequency domain methods for robust stability analysis of family (3) of fractional polynomials of non-commensurate degrees. The methods proposed are based on the Argument Principle and they are a generalization to the fractional polynomials case of the methods given by Busłowicz (1997) in the case of natural degree polynomials.

3. SOLUTION OF THE PROBLEM

First we consider the problem of stability analysis of fixed fractional polynomial of non-commensurate degree, in general, of the form

$$w(s) = a_n s^{\alpha_n} + a_{n-1} s^{\alpha_{n-1}} + \ldots + a_1 s^{\alpha_1} + a_0, \tag{9}$$

where $\alpha_n > \alpha_{n-1} > \cdots > \alpha_1 > 0$ are real numbers.

From (Busłowicz, 2008a) we have the following frequency domain method for stability analysis of the fractional polynomial (9).

Theorem 3.

The fractional degree polynomial (9) is stable if and only if

$$\underset{\omega \in (-\infty, \infty)}{\Delta \arg} \ \psi(j\omega) = 0, \tag{10}$$

with $\psi(j\omega) = \psi(s)$ for $s = j\omega$ and

$$\psi(s) = \frac{w(s)}{w_r(s)}, \tag{11}$$

Where $w_r(s)$ is the reference fractional polynomial of the same order α_n as (9) and it is stable, i.e.

$$w_r(s) \neq 0 \ \text{ for } \ \mathrm{Re}\, s \geq 0. \tag{12}$$

Proof.

From (11) for $s = j\omega$ it follows that

$$\Delta \arg \psi(j\omega) = \Delta \arg w(j\omega) - \Delta \arg w_r(j\omega).$$

The reference polynomial $w_r(s)$ of the same fractional degree as polynomial (9) is stable by the assumption.

Therefore, the fractional polynomial (9) is stable if and only if

$$\underset{\omega\in(-\infty,\infty)}{\Delta\arg}\ w(j\omega)=\underset{\omega\in(-\infty,\infty)}{\Delta\arg}\ w_r(j\omega),$$

which holds if and only if (10) is satisfied.

The reference fractional polynomial $w_r(s)$ can be chosen in the form

$$w_r(s)=a_n(s+c)^{\alpha_n},\ \ c>0. \tag{13}$$

Note that for $c>0$ the reference polynomial (13) is stable.

Condition (10) of Theorem 3 holds if and only if the plot of $\psi(j\omega)$ does not encircle the origin of the complex plane as ω runs from $-\infty$ to $+\infty$.

From (11), (9) and (13) we have

$$\lim_{\omega\to\pm\infty}\psi(j\omega)=\lim_{\omega\to\pm\infty}\frac{w(j\omega)}{w_r(j\omega)}=1, \tag{14}$$

and

$$\psi(j0)=\frac{w(j0)}{w_r(j0)}=\frac{a_0}{a_n c^{\alpha_n}}. \tag{15}$$

From the above and Theorem 3 it follows that the fractional degree characteristic polynomial (9) is not stable if $\alpha_0/\alpha_n\leq 0$.

Now we consider the robust stability problem of the family (3) of fractional polynomials.

Without loss of generality we will assume that $w_a(s)$ is the nominal polynomial of this family and that $w_a(s)$ is stable, i.e. $w_a(s)\neq 0$ for $\mathrm{Re}s\geq 0$. Theorem 3 can by used for stability analysis of this polynomial.

Let ω be any fixed real number. Substituting $s=j\omega$ in (5) one obtain complex numbers $w_\alpha(j\omega)$ and $w_b(j\omega)$ - values of polynomials $w_a(s)$ and $w_b(s)$ for $s=j\omega$.

Definition 2.

For any fixed complex number $s=j\omega$ the set defined by

$$w(j\omega,Q)=\{w(j\omega,q):q\in Q=[0,1]\}, \tag{16}$$

where $w(j\omega,q)$ has the form (4) for $s=j\omega$ is called the value set of the family (3) of fractional polynomials.

The value set (16) is the straight line segment joining the points $w_\alpha(j\omega)$ and $w_b(j\omega)$ in the complex plane.

Theorem 4.

Let the polynomial $w_a(s)$ be stable. Family (3) of fractional polynomials is robustly stable if and only if the following condition (called as the Zero Exclusion Condition)

$$0\notin w(j\omega,Q),\ \ \forall\omega\in\Omega=[0,\infty), \tag{17}$$

holds, where $w(j\omega,Q)$ is defined by (16).

Proof.

If the condition (17) does not hold, then there exist $\omega=\overline{\omega}\in\Omega$ and $q=\overline{q}\in Q$ such that $w(j\overline{\omega},\overline{q})=0$. This means that polynomial $w(s,\overline{q})\in W(s,Q)$ has zero $s=j\overline{\omega}$ on the imaginary axis and the family (3) is not robustly stable.

Now we assume that the family (3) of fractional polynomials is not robustly stable. Then in this family exists at least one unstable polynomial $w(s,\tilde{q})$ with $\tilde{q}>0$. This follows from the fact that the nominal polynomial $w_a(s)=w(s,0)$ is stable by the assumption.

From the above and continuous dependence of coefficients of the polynomial $w(s,q)$ on uncertain parameter q it follows that there exists $\overline{q}\in(0,\tilde{q})$ such that polynomial $w(s,\overline{q})$ has at least one zero on the imaginary axis, i.e. $w(j\omega,\overline{q})=0$ for a some fixed $\omega\in\Omega$ and the condition (17) is not satisfied.

If the condition (17) holds then the origin of the complex plane is excluded from the value set (16) for all $\omega\in\Omega=[0,\infty)$. Therefore, the condition (17) is called as the Zero Exclusion Condition, see (Barmish, 1995), for example.

It is easy to see that $w_\alpha(j\omega)$ and $w_b(j\omega)$ (endpoints of the value set (16) for fixed ω) quickly tend to infinity as $\omega\to\infty$. Therefore, application of Theorem 4 a difficult problem in general.

To remove this difficulty, similarly as in (Busłowicz, 1997) in the case of natural degree polynomials, we will consider the normalized value set instead of the value set (16).

Definition 3.

Let the polynomial $w_a(s)$ be stable. For the fixed complex number $s=j\omega$ the value set defined by

$$w_{nor}(j\omega,Q)=\{w_{nor}(j\omega,q):q\in Q=[0,1]\}, \tag{18}$$

with

$$w_{nor}(j\omega,q)=w(j\omega,q)/w_a(j\omega),\ \ w_a(j\omega)\neq 0, \tag{18a}$$

where $w(j\omega,q)$ has the form (4) for $s=j\omega$ is called the normalized value set of the family (3) of fractional polynomials.

For any fixed complex number $s=j\omega$ the normalized value set (18) is the straight line segment with endpoints $w_{nor}(j\omega,0)=1+j0$ and $w_{nor}(j\omega,1)=w_b(j\omega)/w_a(j\omega)$. Because $w_{nor}(j\omega,0)=1+j0$ for all $\omega\in\Omega$ the normalized value set (18) always lies near of the origin of the complex plane.

From the above and Theorem 4 it follows that the Zero Exclusion Condition for the normalized value set (18) can be formulated as follows.

Theorem 5.

Let the nominal polynomial $w_a(s)$ be stable. Family of polynomials (3) is robustly stable if and only if the following condition holds

$$0\notin w_{nor}(j\omega,Q),\ \ \forall\omega\in\Omega=[0,\infty). \tag{19}$$

The parametric description of the boundary of stability region, i.e. of the imaginary axis of the complex plane, has the form $s=j\omega$, $\omega\in(-\infty,\ \infty)$. Zeroes of fractional polynomials with real coefficients are complex conjugate. Therefore,
in the Zero Exclusion Conditions (17) and (19) we can consider only the interval $\Omega=[0,\infty)$ of the parameter ω.

Satisfaction of the condition (19) can be checked directly by plotting the normalized value set (18) (straight line segment) for all fixed $\omega=i\Delta\omega$, $i=0,1,\ldots$, where $\Delta\omega$ is the sufficiently small step.

Now we consider the methods for checking of the Zero Exclusion Condition (19) without plotting the normalized value set (18).

It is easy to see that if for fixed $\omega=\overline{\omega}\in\Omega$ the straight line segment (18) crosses the origin of the complex plane then

$$w_{nor}(j\overline{\omega},1)=w_b(j\overline{\omega})/w_a(j\overline{\omega})<0,$$

because $w_{nor}(j\overline{\omega},0)=1+j0.$ In such a case the following condition holds

$$|\arg(w_a(j\overline{\omega}))-\arg(w_b(j\overline{\omega}))|=\pi, \tag{20}$$

where $\arg(\cdot)\in[-\pi,\pi)$.

From the above it follows that the condition (19) of Theorem 5 holds if and only if

$$\varphi(\omega)\neq 0,\ \forall\omega\in\Omega, \tag{21}$$

where

$$\varphi(\omega)=\pi-|\arg(w_a(j\omega))-\arg(w_b(j\omega))| \tag{22}$$

is the testing function.

Hence, we have the following lemma.

Lemma 2.

Let the nominal polynomial $w_a(s)$ be stable. Family of polynomials (3) is robustly stable if and only if the condition (21) holds. Now we prove the following theorem.

Theorem 6.

Let the nominal polynomial $w_a(s)$ be stable. Family of polynomials (3) is robustly stable if and only if plot of the function

$$\vartheta(j\omega)=\frac{w_b(j\omega)}{w_a(j\omega)},\ \ \omega\in\Omega, \tag{23}$$

does not cross the non-positive part $(-\infty,0]$ of the real axis in the complex plane.

Proof.

From the above considerations it follows that for any fixed $\omega\in\Omega$ the straight line segment $w_{nor}(j\omega,Q)$ with one endpoint $w_{nor}(j\omega,0)=1+j0$ does not cross the origin of the complex plane for all $\omega\in\Omega$ if and only if plot of the function $w_b(j\omega)/w_a(j\omega)$, $\omega\in\Omega$ does not cross the non-positive part of the real axis.

From (23) and (5) it follows that

$$\vartheta(j0)=\frac{b_0}{a_0},\qquad \lim_{\omega\to\pm\infty}\vartheta(j\omega)=\frac{b_n}{a_n}. \tag{24}$$

Lemma 3.

Let the nominal polynomial $w_a(s)$ be stable. Family (3) of fractional polynomials is not robustly stable if $b_0/a_0\leq 0$ or $b_n/a_n\leq 0$

Proof.

If $b_0/a_0\leq 0$ or $b_n/a_n\leq 0$ then plot of the function (23) crosses the non-positive part of the real axis and the family (3) of fractional polynomials is not stable, according to Theorem 6.

4. ILLUSTRATIVE EXAMPLE

Consider the control system shown in Figure 1 with the fractional order plant described by the nominal transfer function

$$G_0(s)=\frac{1}{0.8s^{2.2}+0.5s^{0.9}+1}=\frac{1}{D_0(s)} \tag{25}$$

and fractional order PID controller

$$C(s)=k_p+\frac{k_i}{s^{\lambda}}+k_d s^{\mu}. \tag{26}$$

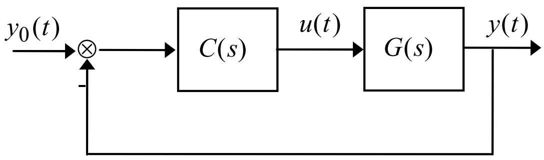

Fig. 1. The feedback control system

In (Zhao et al. 2005) it was shown that closed loop system with the plant (25) is stable and it has the gain margin A_m=1.3 and phase margin $\phi_m=60^{\circ}$ for the controller (26) with λ=0.1, μ=1.15, k_p=233.4234, k_i=22.3972 and k_d=18.5274 i.e. for the controller PID with the transfer function

$$C(s)=\frac{18.5274s^{1.25}+233.4234s^{0.1}+22.3972}{s^{0.1}}=\frac{N_c(s)}{D_c(s)}. \tag{27}$$

Characteristic polynomial of the closed loop system with the plant (25) and controller (27) has the form

$$\begin{aligned} w_{c0}(s)&=D_0(s)D_c(s)+N_c(s)\\ &=0.8s^{2.3}+18.5274s^{1.25}+0.5s+234.4234s^{0.1}+22.3971. \end{aligned} \tag{28}$$

Let us assume that the model of the plant is not precisely known and it is described by the family of transfer functions

$$G(s,p)=\frac{1}{D_0(s)+p\Delta(s)}=\frac{1}{D(s,p)},\quad p\in P=[-1,1],\tag{29}$$

where $D_0(s)$ has the form shown in (25) and

$$\Delta(s)=0.4s^{2.2}+0.2s^{0.9}+0.5\tag{30}$$

is the perturbation polynomial.

Characteristic polynomial of the closed loop system with the plant (29) and controller (27) has the form

$$\begin{aligned}w_c(s,p)&=D(s,p)D_c(s)+N_c(s)\\&=[D_0(s)D_c(s)+N_c(s)]+p\Delta(s)D_c(s)\\&=w_{c0}(s)+p\Delta(s)D_c(s)=w_{c0}(s)+pd(s),\end{aligned}\tag{31}$$

where $p\in P=[-1,1]$, $w_{c0}(s)$ has the form (28) and

$$d(s)=0.4s^{2.3}+0.2s+0.5s^{0.1}.\tag{32}$$

The polynomial (31) with uncertain parameter $p\in P=[-1,1]$ can be written in the form

$$w(s,q)=(1-q)w_a(s)+qw_b(s),\quad q\in Q=[0,1],\tag{33}$$

where

$$w_a(s)=w_c(s,p^-)=w_{c0}(s)-d(s),\tag{34a}$$

$$w_b(s)=w_c(s,p^+)=w_{c0}(s)+d(s).\tag{34b}$$

For the given polynomials $w_{c0}(s)$ and $d(s)$ from (34) we have

$$\begin{aligned}w_a(s)&=0.4s^{2.3}+18.5274s^{1.25}+0.3s\\&\quad+233.9234s^{0.1}+22.3971\end{aligned}\tag{35}$$

$$\begin{aligned}w_b(s)&=1.2s^{2.3}+18.5274s^{1.25}+0.7s\\&\quad+234.9234s^{0.1}+22.3971\end{aligned}\tag{36}$$

First, we check stability of the polynomial (35).

Plot of the function

$$\psi(j\omega)=\frac{w_a(j\omega)}{w_r(j\omega)},\tag{37}$$

where $w_a(s)$ has the form (35) and $w_r(s)$=0.4(s+10)$^{2.3}$ is the reference fractional polynomial, is shown in Figure 2. From (14), (15) we have

$$\psi(0)=\frac{22.3971}{0.4\cdot 10^{2.3}}=0.2806,\quad \lim_{\omega\to\pm\infty}\psi(j\omega)=1.$$

From Figure 2 it follows that the plot of $\psi(j\omega)$ does not encircle the origin of the complex plane. This means, according to Theorem 3, that the nominal polynomial (35) is stable.

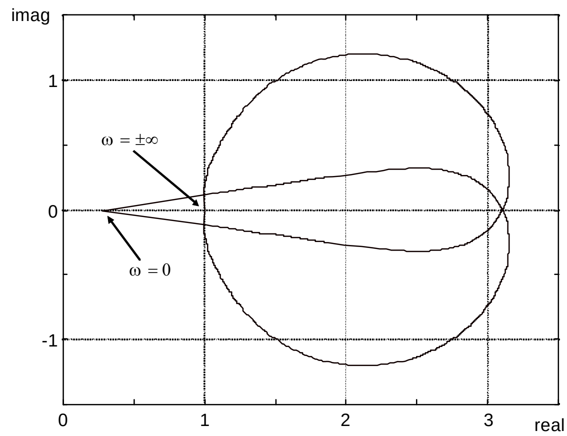

Fig. 2. Plot of the function (37)

Plot of the function (23) with $w_a(s)$ and $w_b(s)$ of the forms (35) and (36), respectively, is shown in Figure 3. From (24) and (35), (36) we have

$$\vartheta(j0)=\frac{w_b(j0)}{w_a(j0)}=1,\quad \lim_{\omega\to\pm\infty}\vartheta(j\omega)=\frac{1.2}{0.4}=3.\tag{38}$$

The plot of $\vartheta(j\omega)$ does not cross of the non-positive part of the real axis and the system is robustly stable, according to Theorem 6. This means that the control system with the controller (27) and uncertain plant (29) is stable for all $p\in P=[-1,1]$.

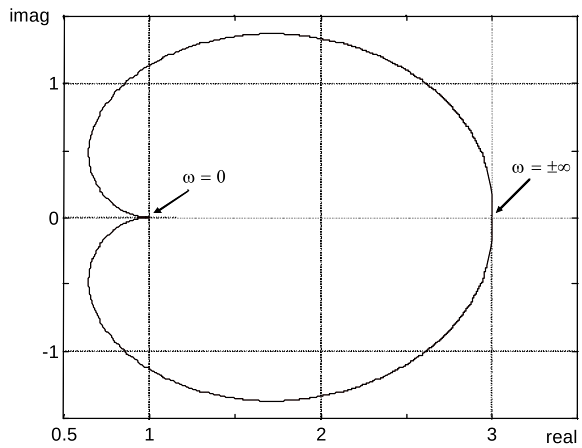

Fig. 3. Plot of the function $\vartheta(j\omega)$ defined by (23)

5. CONCLUDING REMARKS

New frequency domain methods for robust stability analysis of convex combination of two fractional degree characteristic polynomials have been given. These methods can be used for robust stability analysis of linear continuous-time fractional systems with characteristic polynomial linearly dependent on one uncertain parameter.

The methods proposed are based on the Zero Exclusion Condition given in Theorem 4 (for the value set of the family (3) of fractional polynomials) and in Theorem 5 (for the normalized value set of this family).

The main result has been established in Theorem 6. The effectiveness of the method has been illustrated by a numerical example.

REFERENCES

1. **Ackermann J., Bartlett A., Kaesbauer D., Sienel W., Steinhauser R.** (1994), *Robust Control: Systems with Uncertain Physical Parameters,* Springer-Verlag, London.
2. **Ahn H-S., Chen Y-Q., Podlubny I.** (2006), Robust stability checking of a class interval fractional order linear systems using Lyapunov inequality, *2nd IFAC Workshop on Fractional Differentiation and its Applications*, Porto, Portugal.
3. **Barmish B. R.** (1995), *New Tools for Robustness of Linear Systems*, Macmillan Publishing Company, New York.
4. **Bhattacharyya S. P., Chapellat H., Keel L. H.** (1995), *Robust Control: The Parametric Approach*, Prentice Hall PTR, New York.
5. **Białas S.** (2002), *Robust stability of polynomials and matrices*, Publishing Department of University of Mining and Metallurgy, Kraków (in Polish).
6. **Busłowicz M.** (1997), *Stability of linear time-invariant systems with uncertain parameters*, Publishing Department of Technical University of Białystok, Białystok (in Polish).
7. **Busłowicz M.** (2008a), Frequency domain method for stability analysis of linear continuous-time fractional systems, In: K. Malinowski and L. Rutkowski (Eds.): *Recent Advances in Control and Automation*, Academic Publishing House EXIT, Warsaw, 83-92.
8. **Busłowicz M.** (2008b), Stability of linear continuous-time fractional systems of commensurate order, *Proc. XII National Conference Automation'2008,* Pomiary Automatyka Robotyka, No. 2, 475-484 (on CD-ROM) (in Polish).
9. **Busłowicz M., Kalinowski T.** (2008), Robust stability of linear continuous-time fractional system with characteristic function linearly dependent on one uncertain parameter, *Proc. XII National Conference Automation'2008,* Pomiary Automatyka Robotyka, No. 2, 465-474 (on CD-ROM) (in Polish).
10. **Chen Y.-Q., Ahn H.-S., Podlubny I.** (2006), Robust stability check of fractional order linear time invariant systems with interval uncertainties, *Signal Processing*, Vol. 86, 2611-2618.
11. **Matignon D.** (1996), Stability results on fractional differential equation with applications to control processing, *Proc. of IMACS*, Lille, France.
12. **Matignon D.** (1998), Stability properties for generalized fractional differential systems, *Proc. of ESAIM*, 145-158.
13. **Ortigueira M. D.** (2000a), Introduction to fractional linear systems. Part 1: Continuous-time case, *IEE Proc - Vis. Image Signal Process*, Vol. 147, No.1, 62-70.
14. **Ortigueira M. D.** (2000b), Introduction to fractional linear systems. Part 2: Discrete-time systems, *IEE Proc - Vis. Image Signal Process*, Vol. 147, No.1, 71-78.
15. **Petras I., Chen Y.-Q., Vinagre B. M.** (2002), A robust stability test procedure for a class of uncertain LTI fractional order systems, *Proc. Int. Carpatian Control Conf. ICCC'2002,* Malenovice, Czech Republic, 247-252.
16. **Sierociuk D.** (2007), *Estimation and control of discrete dynamical systems of fractional order in state space,* PhD Dissertation, Faculty of Electrical Engineering, Warsaw University of Technology (in Polish).
17. **Kaczorek T.** (2007), Reachability and controllability to zero of positive fractional discrete-time systems, *Machine Intelligence and Robotics Control,* 6(4).
18. **Ma C.** (2004), *Fractional order control and its applications in motion control,* PhD Dissertation, Department of Electrical Engineering, University of Tokyo.
19. **Valerio D.** (2005), *Fractional Robust Systems Control*, PhD Dissertation, Techn. Univ. of Lisbona.
20. **Vinagre B. M., Monje C. A., Calderon A. J.** (2002), Fractional order systems and fractional order control actions, Lecture 3, *IEEE Proc. CDC'02 TW#2: Fractional Calculus Applications in Automatic Control and Robotics*, Las Vegas.
21. **Zhao Ch., Xue D., Chen Y.-Q.** (2005), A fractional order PID tuning algorithm for a class of fractional order plants, *Proc. IEEE Intern. Conf. on Mechatronics & Automation*, 216-221, Niagara Falls, Canada.

The work was supported by the Ministry of Science and High Education of Poland under grant No. N N514 1939 33.

CONTENTS

FROM OIL TO MAGNETIC FIELDS: ACTIVE AND PASSIVE VIBRATION CONTROL

Giancarlo Genta [*], Andrea Festini[*], Xavier Delepine[*]

[*] Department of Mechanics, Politecnico di Torino, Corso Duca degli Abruzzi 24, 10129 Torino, Italy

giancarlo.genta@polito.it, andrea.festini@polito.it, xavier.delepine@polito.it

Abstract: When a reduction of vibration amplitude usually designers resort to dampers based either on dry friction, internal material damping or fluid viscosity, each one of these mechanisms having its peculiar field of application. To improve performance while at the same time reducing costs and environmental load, electromagnetic damping devices are finding new applications, beyond the fields where they have a long history. Moreover, electromagnetic dampers can be easily controlled, obtain active or even 'intelligent' vibration control. Three examples from the internal combustion engines, automotive and gas turbine fields are discussed in some detail to show the potential advantages of this technology.
Keywords: Vibration control, eddy current dampers, active damping.

1. INTRODUCTION

Mechanical systems (actually not only mechanical) are prone to vibrate if they can store energy in two different forms, usually potential and kinetic, in a way that energy can flow from one form to the other. Vibration is the process in which this energy exchange takes place.

Since every time energy is transformed from one form to another some of it is dissipated (usually converted into low temperature thermal energy, from which it cannot be transformed back), any vibrating system is bound to come to rest eventually, unless it is connected to some energy source, providing to refurbish its energy level. This process of energy dissipation is usually referred to as damping.

The designer of any machine has usually to deal with vibration. Although there are cases where vibration is a desired effect (vibrating sieves, vibration welding machines, etc.), usually the task of the designer is to minimize, or at least to control, it.

When it is not possible to act on what excites vibration or to insulate the relevant element from it, the traditional approach to keep vibration under control is to act on the elastic and inertial characteristics of the system to modify the frequencies at which free vibration takes place (these modifications may include the addition of a further mechanical system operating as a vibration absorber) or to increase the damping properties of the system. Often both actions are required, like when using damped vibration absorbers.

Several mechanisms can be used to dissipate energy during vibration. Those traditionally employed are:

– Dry friction between two surfaces moving in contact with each other;
– Internal damping of some materials;
– Viscous forces in a fluid.

Dry friction is today relied upon only for small quantities of energy, and in very simple machines. Its major disadvantage, introducing nonlinearities into the system, is considered a serious drawback, both for its performance and owing to difficulties in modeling its behavior.

Internal damping of most engineering materials is too low to be used to dissipate large quantities of energy, so that dampers of this kind have some restricted fields of application. Elastomeric materials may be tailored to have the required damping characteristics, but their low thermal conductivity and poor high temperature characteristics limit their applications. Nevertheless many small automotive diesel engines use torsional vibration dampers based on elastomeric elements.

Viscous dampers are widely used in many applications, from torsional vibration dampers in reciprocating engines to squeeze film dampers in turbines, from automotive shock absorbers to large dampers used in large buildings, just to name a few examples. In their basic form they are linear devises, since the force they supply is proportional to the velocity

$$F = c\dot{x}, \tag{1}$$

to the point that viscous damper has become a synonymous of linear damper. It is however possible to obtain different law $F(\dot{x})$ by adequately designing the system.

Another way for dissipating energy in a vibrating system is transforming the (mechanical) vibration energy into electric energy and then dissipating it through Joule effect. This can be done both in a solid conductor, by generating eddy currents, or through purposely built electric circuits in which a current can flow. All these electromagnetic devices need a magnetic field to operate: if this is produced by permanent magnets no external power is required, and a passive system is obtained. If, on the contrary, an electromagnet is used, some external power is required and then the system must be considered as active (Some confusion about this terminology is sometimes found. Here a passive system is intended as a system requiring no external energy to work, while an active system is a system that needs to receive power. This has nothing to do with whether the system is controlled or not: an eddy current damper in which the magnetic field is produced by an electromagnet fed by a constant current is active but not controlled. The term semiactive is also used, often with the meaning of a controlled system needing a limited amount of energy. What limited means is clearly arbitrary). In principle, the vibration energy extracted from the system may be converted into some useful form of energy to be used somewhere else: this require a transducer working on four quadrants instead of a simple energy dissipator (usually a resistor).

Electric and magnetic circuits may be coupled to the mechanical system through transducers of various kind, so that to modify the dynamics of the system. Electromagnetic damped vibration absorbers may use electric damped oscillators instead of springs, masses and dampers.

Active devices, based on actuators exerting forces on the system with the aim of reducing vibration, can nowadays be added to these more or less classical ways of controlling vibration. Since they supply energy to the system, the actuators must be carefully controlled to avoid instabilities. While passive systems based on energy dissipators are intrinsically stable, the stability of active systems must be checked carefully in each case.

2. OIL AND RUBBER VS. MAGNETIC FIELDS

The trend towards electromagnetic dampers, be they active or passive, controlled or not, is clear. It is due to both new needs and new opportunities.

Viscous and elastomeric dampers have basically 3 problems.

The first is thermal stability. The viscosity or oil and the internal damping of rubber are strongly dependent of temperature. Specific problems are then cavitation in oleodynamic dampers (cavitation is an important problem in automotive shock absorbers) and overeating with subsequent failure in elastomeric dampers. Elastomeric materials show also a large dependence of their damping characteristics on frequency.

The second problem is linked with manufacturing and disposal. Environmental laws cause the cost of dealing with oils and above all to dispose of used oil to increase steadily. Strict rules are also imposed on the manufacture and disposal of rubber machine components. These rules are bound to become more strict in the future with further increasing costs.

A third point, linked with viscous damping devices, is the difficulty of controlling the characteristics of the fluid. Electrorheological and magnetorheological fluids have been investigated showing attractive potentialities for tuning damping forces according to the operating conditions. However they too have problems related to the ageing of the fluid and to the tuning required for the compensation of the temperature and frequency effects.

Electromagnetic dampers improve much this situation. Although the resistivity of conductors (a property that determines the characteristics of electromagnetic dampers) is a function of the temperature, this dependence is much weaker that that of the viscosity of oils or the internal damping of rubbers. Their manufacture and disposal is much less subject to restrictions and they are easily controlled by electronic, possibly digital, microprocessor-based, devices.

Electromagnetic dampers were often discarded in the past for many applications because they were considered too heavy, bulky and costly. Recently the situation has much improved.

New opportunities have opened with the introduction of high-performance rare-earths permanent magnets. They allow generating magnetic fields much more intense than those due to traditional magnets for a given quantity of magnetic material. The mass and bulk of electromagnetic dampers is thus reduced a great deal. After the expiry of the original patents, their cost started decreasing and today it is possible to build electromagnetic passive dampers that are competitive with traditional dampers.

Even if slower, there has been also a progress in the field of soft magnetic materials, which helps in containing the size and weight of electromagnetic dampers.

To describe the potentialities of electromagnetic dampers, three applications will be described in detail. They deal with vibration in widely different frequency range, and are based on different layouts.

Electromagnetic dampers can be built following two different schemes: vibrational motion can cause electric currents to be generated, which flowing either n a solid conductor or a resistor of various type produces the required energy dissipation. Alternatively, electromagnetic forces can be produced by controlled actuators, either of the Lorentz or the Maxwell type. While in the first case damping is automatically produced, in the second case the controller must ensure that the forces oppose vibrational motion, so that energy is dissipated and vibration is quenched.

3. MOTIONAL EDDY CURRENT DAMPERS FOR TORSIONAL VIBRATION CONTROL

The electromechanical dynamics of a torsional eddy current damper of motional type can be studied using the model shown in Fig. 1. Such a configuration is characterized by a single magnetic pole pair (Tonoli, 2007; Graves et al., 2000). The rotor is made by two windings 1, 1’ and 2, 2’ installed on orthogonal planes. It is crossed by the constant magnetic field (flux density Bs) generated by the stator. The analysis is performed under the following assumptions:

– The two rotor coils have the same electric parameters and are shunted,
– The reluctance of the magnetic circuit is constant. The analysis is therefore only applicable to motional eddy current devices and not to transformer ones (Graves et al., 2000; Kamerbeek, 1973),

- The magnetic flux generated by the stator is constant as if it were produced by permanent magnets or by current driven electromagnets,
- All quantities are assumed to be independent from the axial coordinate,
- Every electric parameter is assumed to be lumped.

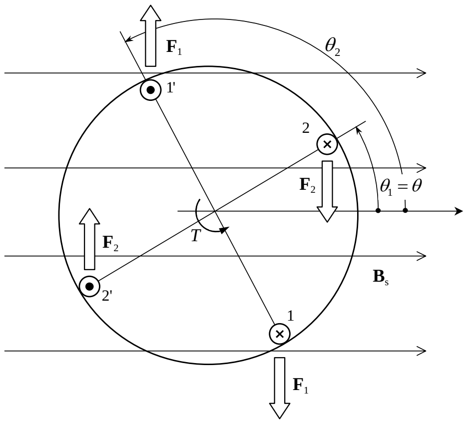

Fig. 1. Sketch of the eddy current damper

Angle $\theta(t)$ between the plane of winding 2 and the direction of the magnetic field indicates the angular position of the rotor relative to the stator. When currents $i_{\gamma 1}$ and $i_{\gamma 2}$ flow in the windings, they interact with the magnetic field of the stator and generate a pair of Lorentz forces $F_{1,2}$ in Fig. 1. Each force is perpendicular to both the magnetic field and the axis of the conductors. Their magnitudes are:

$$F_1 = N l_r i_{r1} B_s,\ F_2 = N l_r i_{r2} B_s, \tag{2}$$

where N and l_γ indicate the number of winding in each coil and their axial length, respectively.

The total torque T acting on the rotor is:

$$T = \phi_{rs0}\left[\sin(\theta) i_{r1} + \cos(\theta) i_{r2}\right]. \tag{3}$$

For constant rotation speeds ω, the torque to speed characteristics is found:

$$T = \frac{c_0}{1+(p\omega)^2/\omega_p^2},\ \text{with}\ c_0 = \frac{\phi_{rs0}^2}{R_r},\ \omega_p = \frac{R_r}{L_r}, \tag{4}$$

where, c_0, p and ω_p are respectively the damping at low frequencies, the number of magnet poles and the frequency of the electric pole of the system, and $\phi_{\gamma s0}$ is the equivalent crank radius. R_γ and L_γ are the resistance and inductance of the rotating coils. The mechanical impedance can also be obtained using the Laplace transform as:

$$Z_m(s) = \frac{T(s)}{\dot{\theta}(s)} = \frac{c_{em}}{1+s/\omega_p} = \frac{c_{em}}{1+s(k_{em}/c_{em})}. \tag{5}$$

This impedance corresponds to a viscous torsional damper and a torsional spring connected in series, whose parameters are:

$$c_{em} = \frac{p\phi_{rs0}^2}{R_r}\ \text{and}\ k_{em} = \frac{p\phi_{rs0}^2}{L_r}. \tag{6}$$

The model has been validated experimentally (Tonoli and Amati, 2008) using a test rig based on a four pole pairs axial flux induction machine (Fig. 2, steady state tests).

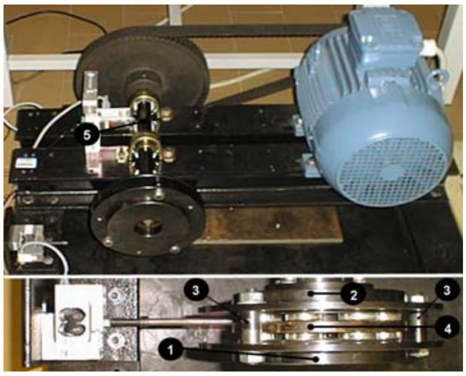

Fig. 2. Test used for the identification of the induction machine at steady state

In Fig. 2, the magnetic flux is generated by permanent magnets while energy is dissipated in a solid conductive disk. The first array of 8 circular permanent magnets is bond on the iron disk (1) with alternate axial magnetization. The second array is bond on the disk (2) with the same criterion. Three calibrated pins (3) are used to face the two iron disk - permanent magnet assemblies ensuring a 1 mm airgap between the conductor and the magnet arrays. The latter are circumferentially oriented so that the magnets with opposite magnetization are faced to each other. In the following such an assembly is named "stator". The conductor disk (4) is placed in between the two arrays of magnets and is fixed to the shaft (5). It can rotate relative to the stator by means of two ball bearings installed in the hub. The magnetic circuit has been designed using a simplified one-dimensional analysis with the aim of avoiding saturation in the iron parts. The main features of the induction machine are summarized in Tab. 1.

Tab. 1. Main features of the induction machine used for the tests

Number of pole pairs	-	4
Diameter of the magnets	mm	30
Thickness of the magnets	mm	6
Magnets' geometry	-	Circular
Magnets' material	-	Nd-Fe-B(N45)
Residual magnetization of the magnets	T	1.22
Thickness of conductor disk	mm	7
Resistivity of conductor (Cu)	Ohm m	$57\ 10^{-6}$
Airgap	mm	1

Experimental tests at constant speed have been carried out to identify the slope c_0 of the torque to speed characteristic at zero or low speed and the pole frequency ω_p. While the former has been identified in quasi-static tests, the latter has been identified as best fit of the experimental points reported in Fig. 3 (Tonoli and Amati, 2008). The identified parameters are c_0 = 1.24 Nms/rad and ω_p = 51.1 Hz, from which the induction machine characteristics can be obtained.

An interesting field of application of this technology is the vibration damping of the crankshafts in internal combustion engines. In fact, technological issues make active solutions difficult to be implemented, which naturally lead to passive solutions. Nowadays, the common solutions involve either elastomers or viscous fluids. However, they undergo a large number of stress-strain cycles, and consequently their working life is reduced to approximately half the working life of a motor. Instead, eddy current damping does not imply the deformation of the material of the actuator, Therefore, the working life is increased, and the efficiency of the apparatus is improved (Fig. 4).

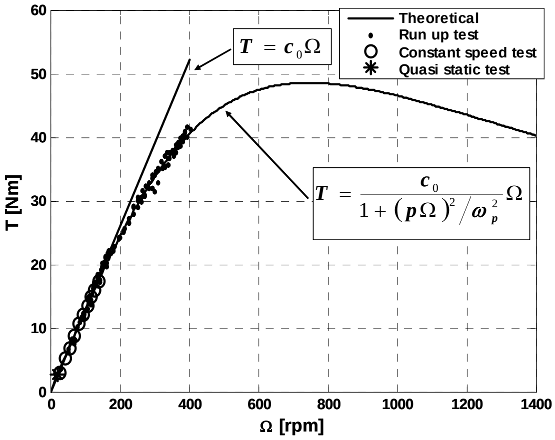

Fig. 3. Experimental results of the induction machine characterization at steady state

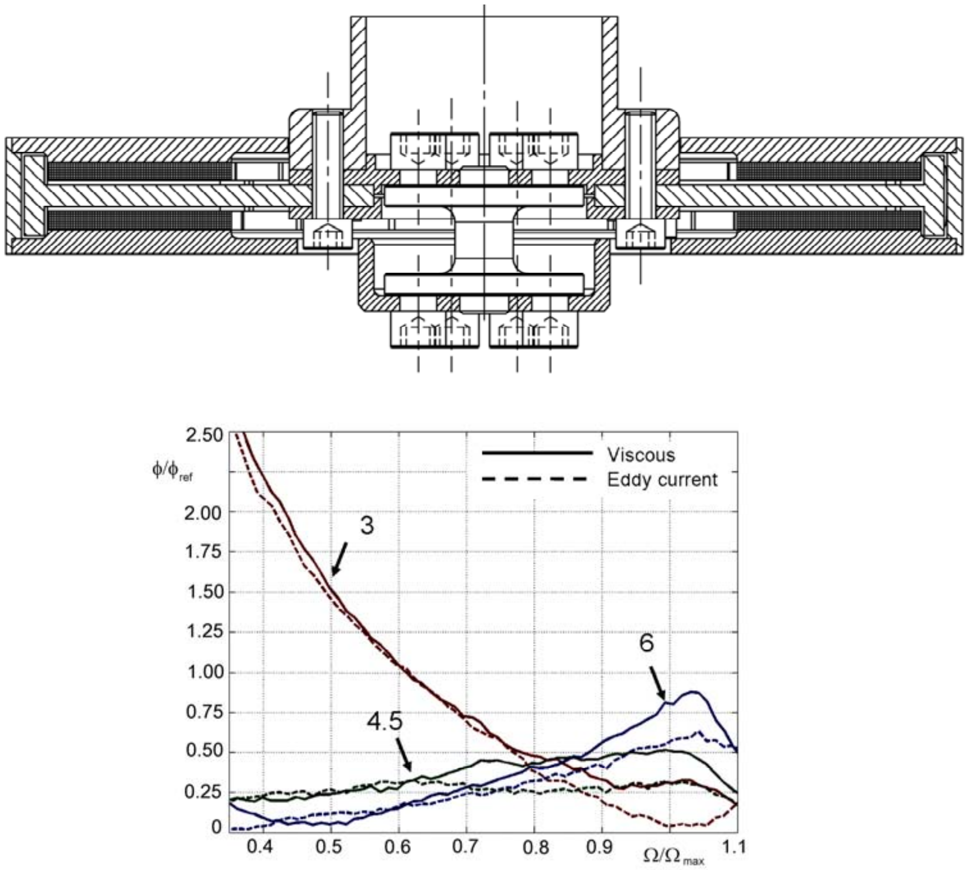

Fig. 4. Torsional damper: schematic cross section and comparison of the amplitude of three harmonics in the nondimensional torsional response of the engine using a viscous and an eddy current damper

4. ELECTROMAGNETIC AUTOMOTIVE SHOCK ABSORBERS

Working principle. Main tasks of automotive shock absorbers are the capability of reducing transmission of vibration and controlling the applied load. Active solution can be used to achieve these goals, but very good results may be obtained also from semi-active configurations, allowing to change the value of damping, depending on the driving conditions. Conventional solutions are nowadays based on hydraulic dampers, whose characteristics may be variable as a result of modifications in the hydraulic circuit or in the oil physical properties (magnetorheologic fluids). Solution based on linear electric motors were proposed to solve the typical problems related to the use of fluids, but they lead to an increase of size and mass (Karnopp, 1989). This is due to the fact that, while in rotary electric motors all the magnetic and conductor material is always active, in linear motors only a relatively small part of it is working at each time. Moreover, rotating electric motors are based on a more consolidated design practice and on a higher technology background.

The electromagnetic technology based on brushless motors allows obtaining a tunable suspension damper with many advantages and limited disadvantages. The capability of being tunable, and regenerating energy (four-quadrant operation) with limited increase of mass and size using an actuator that can become fully active are considered important features.

The tunable electromechanical damper described in the following section is based on a DC electric motor whose electric terminals are shunted on a resistive load instead of being connected to a converter: the torque needed to rotate the shunted motor can be computed from the characteristic equations of the electric machine. They link the back electromotive force V_{emf} and the electromechanical torque T_{em} to the rotating speed ω and the electric current i

$$V_{emf} = K_e \cdot \omega \ ; \ T_{em} = K_t \cdot i . \tag{7}$$

K_e and K_t indicate the back electromotive force constant and the torque constant, respectively. If the electric terminals of the motor are shunted by a resistance R, the current i (eddy current) is induced by the back electromotive force V_{emf}, so that (in case of a constant speed ω)

$$V_{emf} = R \cdot i . \tag{8}$$

Substituting the Ohm equation (8), into the motor characteristic equations (7) allows to get rid of the back electromotive force and of the eddy current. The back electromotive force and the torque constants are the same, both are indicated as K_m. The electromechanical torque T_{em} is then related to the angular speed ω as shown in Fig. 3a:

$$T_{em} = c_\omega \cdot \omega \text{, where } c_\omega = \frac{K_m{}^2}{R} . \tag{9}$$

From the mechanical point of view the resistively shunted electric motor behaves as a torsional viscous damper (Graves et al., 2000; Karnoppm 1987, Amati et al., 2006). The torsional damping coefficient c_ω can be tuned by acting on the shunt resistance. The lower is the resistance, the higher is the damping. The solution in

Fig. 5 shows a linear electromechanical damper including a rotary motor and a ball screw transmission.

From the electrical point of view, the motor of

Fig. 5 is represented as a universal motor with two electric terminals (such as a brush motor). R includes the resistance of the motor windings (R_m) and the external one (R_{ext}) that allows to tune the damping coefficient ($R = R_m + R_{ext}$). As the effect of the inductance of the motor coil L is unwanted, no external contribution is usually added to it. From the mechanical point of view, the contribution of the masses and inertias on the dynamic performances of the damper cannot be neglected.

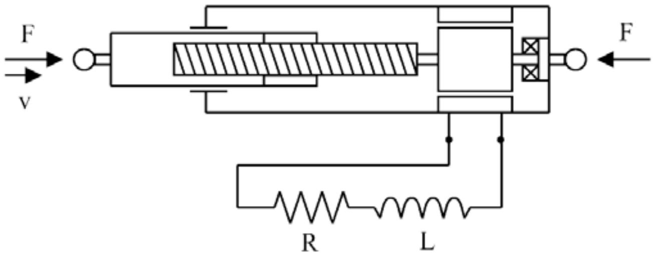

Fig. 5. Sketch of the electromechanical shock absorber

The equivalent mechanical model of the device shown in

Fig. **5** is reported in Fig. 6. It takes into account the contribution of the electric and mechanical part of the motor written at the level of the damper. A detailed description of the model, that allows to take into account its frequency dependency, is reported in Amati et al (2006). To this end, the effect of the rotor inertia J, the motor inductance (L) and resistance (R) can be written as:

$$m_{eq} = \tau^2 \cdot J \ , \ c_{eq} = c_s + \tau^2 \cdot c_\omega \ , \ k_{em} = \tau^2 \cdot k_\omega \ , \tag{10}$$

where $c_\omega = K_m{}^2/R$ and $k_\omega = K_m{}^2/L$, are the torsional damping and stiffness produced by the shunted motor.

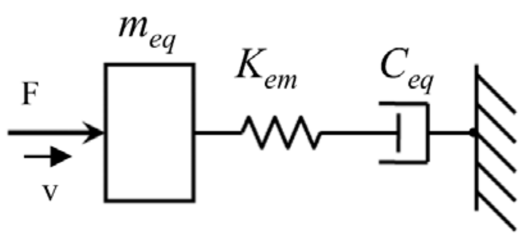

Fig. 6. Mechanical analogue of the electric motor

The dynamic behavior of the damper can therefore be characterized by the mechanical impedance given by the following equation:

$$\frac{F}{v} = m_{eq} \frac{s^2 + 2\zeta_0 \omega_0 s + \omega_0{}^2}{s + \omega_p} , \tag{11}$$

where s is the Laplace variable. The pole frequency ω_p, the zero frequency ω_0, and damping factor ζ_0 are

$$\omega_p = \frac{k_{em}}{c_{eq}} \ , \ \ \omega_0^{\,2} = \frac{k_{em}}{m_{eq}} \ , \ \ \zeta_0 = \frac{\sqrt{m_{eq} k_{em}}}{2c_{eq}} \tag{12}$$

Fig. 7 holds in the case where ω_p is lower than ω_0 (0 ζ_0 1 2). Between the pole and the zeros the system behaves as a spring of stiffness k_{em} as shown by the -20 dB/dec slope of the mechanical impedance. A detailed study of the frequency behavior is reported in Amati et al (2006).

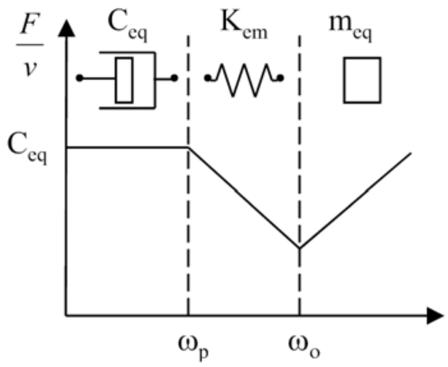

Fig. 7. Mechanical impedance of the damper

4.1. Electromechanical design

The rather typical design situation is strive to obtain the specified damping coefficient while keeping the equivalent mass (Equation 10) as small as possible. Since the equivalent mass is related to the moment of inertia of the rotor, the aim of this section is to find a relationship between the electromechanical damping coefficient c_ω in equation 9 and the moment of inertia J of the rotor. The analysis is performed assuming a conventional brushless motor with permanent magnets on the rotor surface running in a the toothed and slotted stator.

The analysis performed in Amati et al (2006) leads to the following expression of the damping coefficient

$$c_\omega = \Gamma_c r^4 l \ , \tag{13}$$

where parameter Γ_c is a function of the motor shape and technology.

From the mechanical point of view it is worth to notice that the torsional damping coefficient is proportional to the moment of inertia of the rotor J_{em}. Under the assumption that the rotor is an homogeneous cylinder made of an material with density ρ this is

$$J_{em} = \frac{\pi}{2} \rho \cdot r^4 \cdot l \ . \tag{14}$$

By introducing Eq. (13) into Eq. (14), it follows that

$$J_{em} = \frac{\pi}{2} \rho \cdot \frac{c_\omega}{\Gamma_c} \ . \tag{15}$$

Coming back to the layout of

Fig. 5, the equivalent mechanical parameters of equation (10) are linked together similarly to torsional damping and rotor inertia. The ratio between the equivalent mass and damping due to the electromechanical effects is constant, its value being a function of the motor shape and technology

$$\frac{m_{eq}}{c_{eq} - c_s} = \frac{J_{em}}{c_\omega} = \frac{\pi}{2} \frac{\rho}{\Gamma_c} \ . \tag{16}$$

This is a very important result from the design point of view. Once the equivalent damping is specified, the equivalent mass to be minimized is just a function of the motor shape and technology (ρ Γ_c), and not of the transmission ratio τ. The only way to reduce it is to improve constant Γ_c.

In addition to the rotor inertia, the overall mass of the electric motor m_{em} is the other important mechanical feature of the damper.

For what is concerned to the total mass, in Amati et al (2006) with reference to the shock absorber of

Fig. 5, the mass of the electrical motor is expressed as function of the equivalent damping of Eq. (10) as

$$m_{em} = \frac{\Gamma_m}{\Gamma_c} \frac{(c_{eq} - c_s)}{(\tau r)^2} r^4 l \ . \tag{17}$$

Equation (17) shows it is related to technology and $(\tau\ r)^2$ once the desired damping coefficient is chosen. For a given equivalent damping (c_{eq}), motor shape and technology (this gives Γ_m and Γ_c) the larger the rotor radius r and the transmission ratio τ, the smaller the mass of the electric motor. The apparently unreasonable lower mass corresponding to a larger radius is due to the smaller amount of conductor necessary to obtain the desired damping c_{eq}.

To conclude the present section, equations (10), (13), (16), and (17) outline a design procedure of the electromechanical damper.

4.2. Application example

To analyze the potentialities of electromechanical dampers in automotive applications, the previously outlined procedure has been applied to design the damper of a C-segment vehicle front suspension. The application example was done on a Mc Pherson suspension using the same mechanical interfaces as the original system, and using the inner space of the coil spring with an appropriate allowance (device data are reported in Tab. 2). With reference to the layout of Fig. 8 the electromagnetic damper is represented in shade.

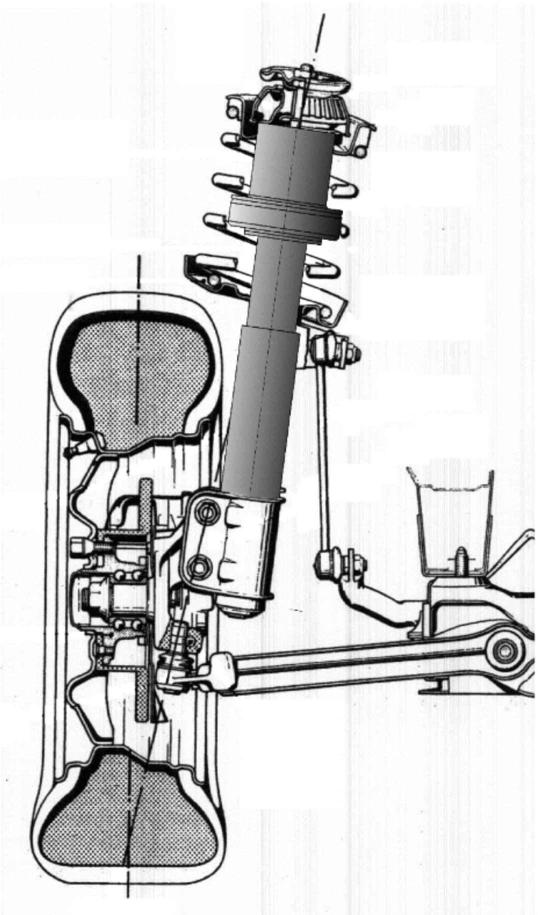

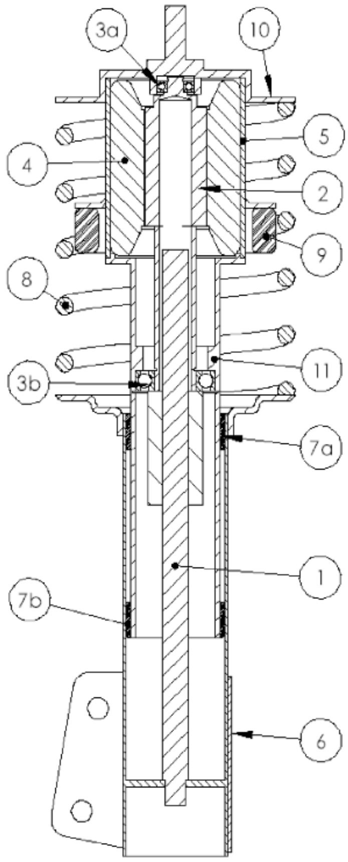

Fig. 8. Electromechanical damper integrated in a Mc Pherson suspension and cross section of the damper

The electric motor (2) (4) (5) is housed in upper part of the cylinder close to the upper strut mount (10). This choice allows to exploit the relatively large diameter inside the spring (8) while keeping a small diameter close to the wheel. The screw (1) is rigidly connected to the moving piston (6), bolted to the hub. The motor, the nut of the ball screw, and the guiding tubes (11) are connected to the sprung mass. The rotor of the electric motor and the nut of the ball screw are rotating on ball bearings (3a) (3b) and connected together, this reduces considerably the axial length of the device as it exploits the room inside the rotor of the motor.

The total mass of the electric damper is shown in Fig. 8 is 5 kg. This mass has to be compared to the 4.1 kg of a hydraulic solution with continuously variable damping. The proposed damper is still heavier than the hydraulic one but is much lighter than the configurations found in the literature with comparable performances. A passive electromechanical damper based on a linear electric motor was designed using the same specifications (Karnopp, 1989) and lead to a device of more than 15 kg of mass.

The effects of the damper in the car suspension have been investigated by integrating the model in a simple quarter car model. Fig. 9 shows the transfer function between the displacement of the contact point of the tire to the ground and the acceleration of the sprung mass.

Tab. 2. Damper specifications and parameters of the single corner suspension

Max damp. Coeff. (rebound)		>10	kNs/m
Max speed		1	m/s
Max stroke (peak to peak)		150	Mm
Spring stiffness	K_s	18	kN/m
Tire radial stiffness	K_p	150	kN/m
Tire radial damping	C_p	50	Ns/m
Sprung mass	M_s	450	kg
Unsprung mass	M_n	30	kg
Axial length at midstroke		450	Mm
Max force		1.8	kN

The undamped response curves is that of the open circuit damper ($R_{ext} = \infty$: no electro-mechanical damping); the other ones to some values the external resistance R_{ext} . The equivalent mass (m_{eq} q. 10) due to the rotor inertia introduces a sort of inertial coupling between the sprung and unsprung masses. The effect is, at any rate, not large as demonstrated by the fact that the two undamped natural frequencies of the suspension go from 0.95 Hz and 11.91 Hz (no electromechanical damper installed) to 0.94 Hz and 11.12 Hz (open circuited electromechanical damper).

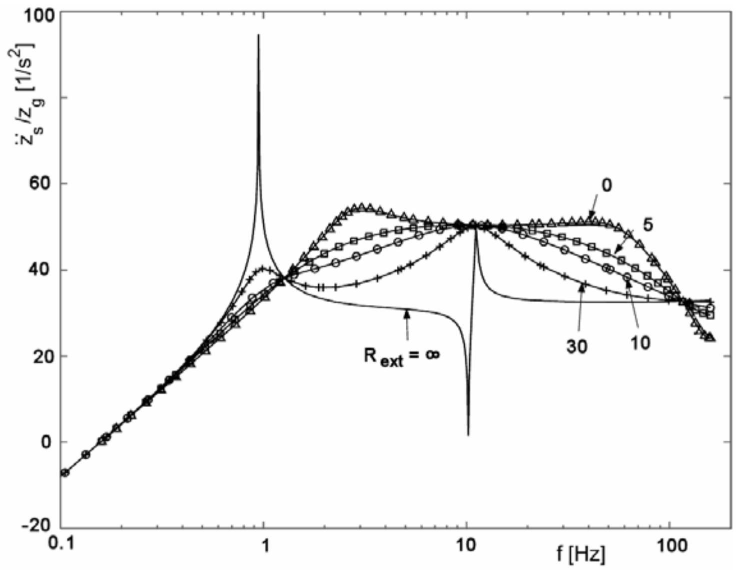

Fig. 9. Transfer function between displacement of the ground (input) and acceleration of the sprung mass (output)

5. ACTIVE AND PASSIVE DAMPERS FOR ROTATING MACHINES

5.1. Active magnetic damper (AMD)

In the present section the use of active magnetic bearings (AMB, Fig. 10a) for vibration damping (active magnetic damper referred to as AMD, Fig. 10b) (Amati et al., 2006) is introduced. Those two configurations differ only by the function of the force generated by the actuator. While for the AMB, the actuator is used for both suspension and damping, the AMD is used only to introduce damping into the system and the of the suspension must be insured by mechanical means. The static stability of the suspension is thus guaranteed if the mechanical stiffness is greater than the open-loop negative stiffness of the AMD.

The AMD technology is particularly well suited in the field of rotating machines, where they can replace with advantages squeeze film dampers.

A model of the actuator is needed for the design of the control law of the AMD. To this aim, the usual expression of the force generated by one electromagnet is used:

$$F = \frac{\mu_0 N^2 A}{4}\left(\frac{i(t)}{q_0 + q(t)}\right)^2, \tag{18}$$

where N is the number of turns of each winding, A is the area of the magnetic circuit at the air gap, μ_0 is the magnetic permeability of vacuum, i is the current, q_0 is the nominal air gap and q is the displacement.

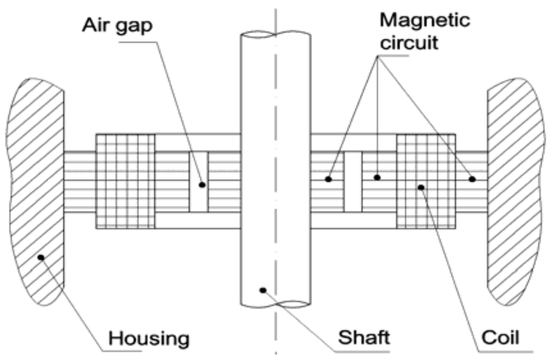

a)

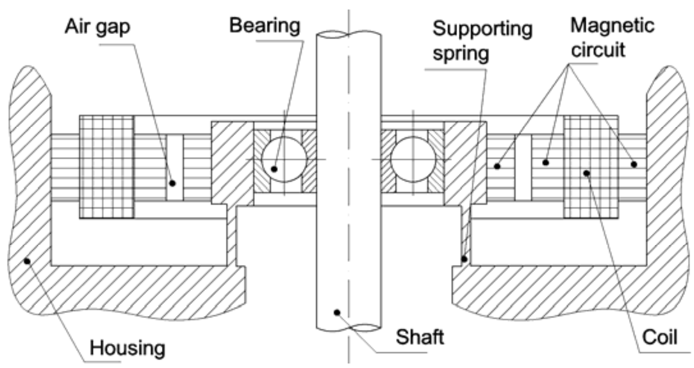

b)

Fig. 10. Sketch of an active magnetic bearing (a) and of an active magnetic damper (b) operating also as an elastic support

5.2. Transformer eddy current dampers

A "transformer" eddy current damper may use the same configuration as an AMD, although in this case the coils are supplied with constant voltage through which the magnetic field is generated. Damping is thus provided by eddy currents instead by control forces as in AMDs. Both AMD and transformer operation is possible in the case shown in Fig. 10b. However, in the latter case, the absence of a control law can make the implementation easier.

The basic principle of transformer eddy current dampers is the following: the displacement with speed $\dot{q}$ of the anchor changes the reluctance of the magnetic circuit causing the flux linkage to change in time, which generates a back electromotive force in the coils, and consequently eddy currents in the coils. The current in the coils has thus two contributions: a fixed one due to the voltage applied, and a variable one induced by the back electromotive force. The first contribution generates a force that increases when the air-gap decreases, which produces a negative stiffness. The damping force is generated by the contribution due to the anchor speed $\dot{q}$, that acts against the motion of the moving element. In these terms, this configuration can be called semi-active, as power is initially required to produce the initial magnetic field, but damping is introduced without a traditional feedback law (i.e. using sensors).

The transfer function between the speed $\dot{q}$ and the electromagnetic force F shows a first order dynamics with pole frequency ω_{RL} due to the R-L nature of each circuit

$$\frac{F}{\dot{q}} = \frac{1}{s}\frac{K_{em}}{\left(1+s/\omega_{RL}\right)}, \tag{19}$$

where $K_{em} = -\dfrac{2V^2/R}{q_0^2\omega_{RL}}$, $\omega_{RL} = \dfrac{R}{L_0}$, $L_0 = \dfrac{\mu_0 N^2 A}{2q_0}$.

The mechanical impedance has the form of a band limited negative stiffness. The value of the negative stiffness is proportional to the electrical power (V^2/R) dissipated at steady state by the electromagnet. For given values of the number of turns (N), of the air gap area (A), and nominal air-gap (q_0), the mechanical impedance and the pole frequency are functions of the voltage applied V and the resistance R.

As mentioned earlier, a mechanical spring must be located in parallel to the electromagnets to compensate their negative stiffness. For static stability, the additional stiffness K_m must be larger than the negative stiffness of the electromagnets ($K_m \geq |K_{em}|$). For the analysis, the mechanical spring in parallel to the transformer damper can be considered as a part of the damper, and from now on the whole "electromagnet + mechanical spring" will be referred to as "transformer electromechanical damper" (TEMD). The mechanical impedance of the damper in parallel with the mechanical spring, i.e. of the TEMD, is studied:

$$\frac{F}{\dot{q}} = \frac{1}{s}\left(\frac{K_{em}}{\left(1+s/\omega_{RL}\right)} + K_m\right) = \frac{K_{eq}}{s}\frac{1+s/\omega_z}{1+s/\omega_{RL}}, \tag{20}$$

where $K_{eq} = K_m + K_{em}$; $\omega_z = \omega_{RL}\dfrac{K_{eq}}{K_m}$.

Apart from the pole at null frequency, the impedance shows a zero-pole behavior. To ensure stability, the frequency of the zero must to be smaller than the frequency ($0 < \omega_z < \omega_{RL}$) of the pole. As shown in Fig. 11a, it is possible to identify three different frequency ranges.

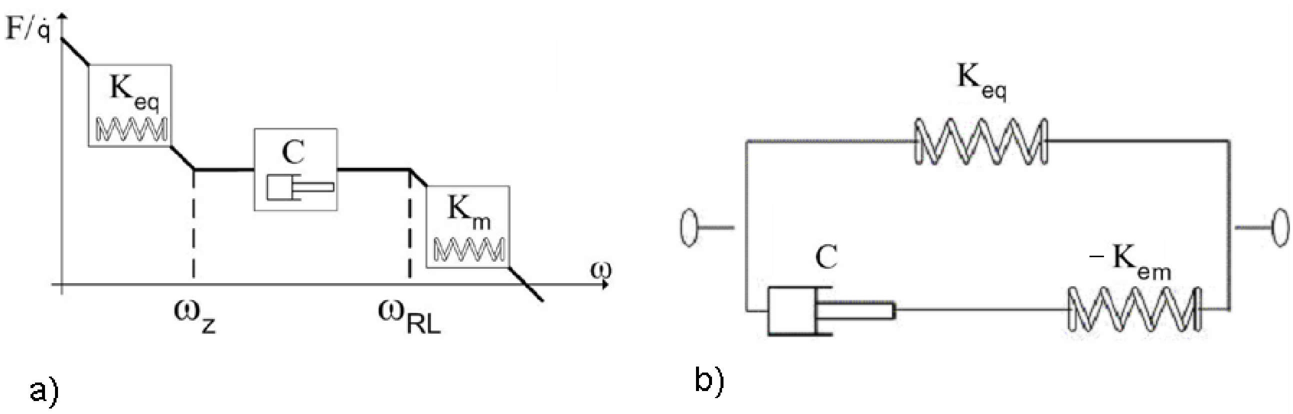

Fig. 11. "Transformer" eddy current damper. A) Mechanical impedance of a transformer damper in parallel to a spring of stiffness K_{eq} and b) mechanical equivalent

– Equivalent stiffness range $\omega << \omega_z < \omega_{RL}$: the system behaves as a spring of stiffness $K_{eq} > 0$.
– Damping range $\omega_z < \omega < \omega_{RL}$: the system behaves as a viscous damper with coefficient C defined as:

– $$C = \frac{K_m}{\omega_{RL}} . \quad (21)$$

– Mechanical stiffness range $\omega_z < \omega_{RL} << \omega$: the transformer damper contribution vanishes and the remaining stiffness contribution is provided by the mechanical spring (K_m).

It can be concluded that the association of electromagnets with a mechanical suspension opens interesting perspectives for the vibration control of rotating machines. As the AMD and TEMD configurations are identical, it is possible to switch from one strategy to the other while the machine is running.

5. CONCLUSIONS

'More electric' or even 'All electric' are more than fashionable catch phrases. They synthesize a tendency gaining momentum in many fields of technology towards a larger use of electric machines to control motion and to distribute power, while trying to do without lubricating or damping fluids. Even in cases where it is impossible to avoid hydraulic transmission, the electrohydraulic approach allows to mate the great compactness of hydraulic machinery and transmission lines with the ease of control of electric machines.

While the road to build an 'all electric' turbojet or power turbine (to quote two examples) is still long and full of obstacles, the use of electromagnetic devices to control vibration and to manage power is in many cases mature for applications. Passive, semiactive and fully active dampers find increasing applications not only in those high technology fields in which they were first used, but also in low cost consumer markets.

The automotive shock absorber and the internal combustion engine torsional dampers here shown are two examples of this trend. In eddy current dampers, usually passive or semiactive, the substitution of magnetic fields instead of oil or elastomers is straightforward and the only difficulties are costs and sometimes still mass and bulk.

Fully active devices on the contrary, apart from being more complex and usually costly, require accurate studies since their behavior is not intrinsically stable. As usual with active systems, their control laws must be designed with both cost and performance and stability in mind.

Although being still far in the future, the vision of machines with no part in contact and hence requiring no lubricant and displaying no wear, and with vibration control that does not involve energy dissipation, is a clear goal that can guide designers and scientists.

REFERENCES

1. **Tonoli, A.** (2007), "Dynamic characteristics of eddy current dampers and couplers," *Elsevier J. Sound Vib.*, 301, pp. 576-591.
2. **Graves, K. E., Toncich, D., and Iovenitti, P. G.** (2000), "Theoretical comparison of motional and transformer emf device damping efficiency", *Journal of Sound and Vibration*, vol. 233, no. 3, pp. 441–453.
3. **Kamerbeek, E. M. H.** (1973), "Electric motors", *Philips tech. Rev.*, vol. 33, pp. 215–234.
4. **Tonoli, A., and Amati, N.** (2008), "Dynamic modeling and experimental validation of eddy current dampers and couplers", *Journal of Vibration and Acoustics*, vol. 130.
5. **Macchi, P., Silvagni, M., Amati, N., Carabelli, S. and Tonoli, A.** (2006), "Transformer eddy current dampers for the vibration control of rotating machines", Proceedings of the 8th Biennial ASME Conference on Engineering System Design and Analysis, Torino, Italy, pp. 1–10.
6. **Karnopp, D.** (1989), "Permanent magnets linear motors used as variable mechanical dampers for vehicle suspensions". *Vehicle System Dynamics*, 18, pp. 187–200.
7. **Karnopp, D.** (1987). "Force generation in semi-active suspensions using modulated dissipative elements". *Vehicle System Dynamics*, 16, pp. 333–343.
8. **Amati, N., Canova, A., Cavalli, F., Caviasso, G., Carabelli, S., Festini, A., and Tonoli, A.** (2006), "Electromagnetic shock absorbers for automotive suspensions: electromechanical design". ESDA-ASME 95339.
9. **Amati, N., Carabelli, S., Genta G., Macchi P., Nicolotti F., Silvagni M., Tonoli, A., Vinsconti, M.** (2006), Vibration control of rotors: trade off between active, semi-active and passive solutions. The IX Finnish Mechanics Day. Lapperanta, Finland. June 13-14. (pp. 1-15). ISBN/ISSN: 952-214- 227-1/1459-2924.

CONTROL-ORIENTED MODELLING AND CONTROL OF ROTOR VIBRATION

Zdzisław GOSIEWSKI*

* Faculty of Mechanical Engineering, Białystok Technical University, ul. Wiejska 45 C, 15-351 Białystok

gosiewski@pb.edu.pl

Abstract: Deep analysis of the control plant brings many useful information for the designer of the control system. The analysis is also important part in the design of active vibration control system. The coupling of different dynamical phenomena in rotating machinery leads to unstable vibrations. Usually, the coupling effects are caused by changing parameters. Angular speed or rotor unbalance in some applications are such parameters which change in the wide range. The problem is to find for which angular speeds we have unstable torsional/lateral vibrations. Usually, the unstable regions are in the vicinity of angular speeds where maps of natural frequencies for both dynamical systems cross each other. In the paper there was explained which intersection of torsional and lateral natural frequencies are unstable and why. The root locus method was used to explain the phenomenon. It indicated such control procedures which amplify the positive (stabilizing) mechanisms in the rotor dynamics. Such procedures can also lead to the energy saving control laws. In the case of lateral vibrations there were considered four control strategies. And these strategies were compared to indicate optimal one.

1. INTRODUCTION

The modal control of flexible structures is usually applied in analytical papers [Preumont, 2002, Ulbrich and Gunther, 2005). The modal control is a global one, while the sensors and actuators are located pointy. In control-oriented modeling it is important to find input-output relations among these points. So more, the simpler model of plant the simpler is the control design. The following disadvantages of the modal control can be noticed:

- Global approach leads to a plant model which has non-physical parameters.
- The reduction of the modal model leads to “the spillover” of the measurement and control effects.
- The control system is usually far from the optimal one from the energy point of view.
- During the control design we omit the knowledge about the plant.

The disadvantages of modal approach are particular well seen in the case of the rotor vibration control. The coupled vibrations are often met in the rotordynamics and small changes of the value of the coupling parameters can lead to the unstable behavior of the rotating machinery. So it is important to divide dynamical system into smaller subsystems and to find which parameter is responsible for the coupling of the subsystems. Such vibration analysis can indicate what one should do to design the energy saving control system.

The design procedure of the vibration control system is realized in four stages (Fig. 1a). They are: modeling of the plant and control system elements, analysis of the plant vibrations (in our case of the rotor), the design of the control law and after the implementation of the control system the experimental validation of the design procedure and dynamical behavior of the closed-loop system.

When the identification procedures were discovered (Ejkchoff, 1980; Juang, 1994) the design procedure of vibration control system can be realized in the closed loop (Fig. 1b). The experimental results can be used to identify the real rotor model. So, the improved rotor model can be again used in the next steps of the design procedure. So more, the identified model is an input-output model, so it perfectly suits the design of the control system. In the fast prototyping of the mechatronic systems we intensively apply the computer aid design methods. So, all design steps can be in practice realized parallel (Fig.1c). So more, as it was mentioned, the synthesis methods can be used to the rotor vibration analysis.

In the paper the coupling effects will be analyzed in the case of the a few-mode rotor model (similar to the Jeffcott’s model (Gosiewski and Muszynska, 1992)). In the considered case we have coupled torsional/lateral vibrations which are described by three nonlinear equations. To obtain rotor motion equations one can apply the Lagrange’s equations. After linearization in the inertial co-ordinate system the equations of rotor vibrations will be transformed to the system of co-ordinates which rotates together with rotor.

First, the coupling effect and its influence on the stability will be considered in the classical way (Muszynska et al., 1992). Next, we define the feedback in the coupled system and carry out investigation of the system stability with help of Evans method (root locus) known from the control theory (Kaczorek, 1993). Such approach leads to simple explanation whether given intersection on the map of natural frequencies is stable or not.

In the second part of the paper different control schemes will be used to stabilize the rotor vibrations in the wide range of the rotor angular speed. The energy effective control law will be applied to stabilize the laterarl vibrations of the rotor. We will check whether the controller also correctly stabilize the closed-loop system in the case of the torsional/lateral vibrations.

All considerations will be illustrated by the results of the computer simulations.

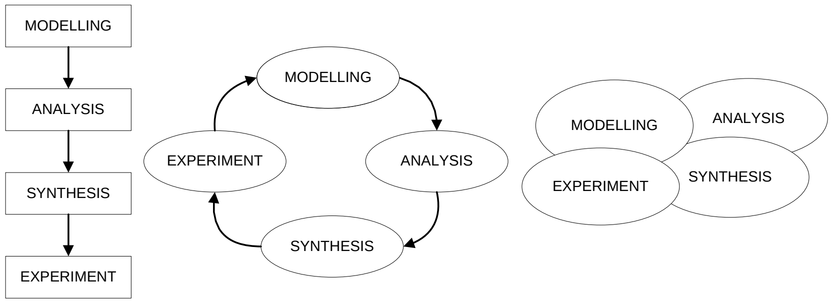

Fig. 1. Design procedure steps of the vibration control system

2. MATHEMATICAL MODEL

We consider the physical model of flexible rotor shown in Fig. 2. The model consists of a rigid disc and a massless flexible shaft. The static unbalanced disc is located in the center of the shaft. The shaft is drived by a high power motor which rotates with constant angular speed Ω. The disc has mass m and inertia momentum I_0 We assume that flexibilities of the shaft in both directions: ξ, η are: k_1, k_2, respectively. The torsional flexibility coefficient is k_t.

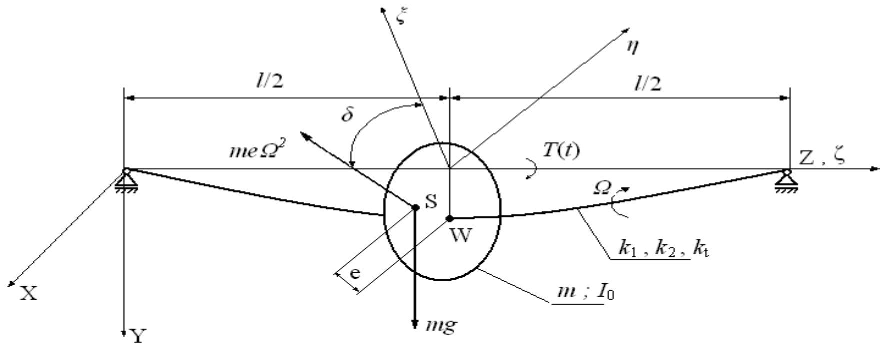

Fig. 2. Physical model of the anisotropic rotor

Kinetic energy E_k i potential energy E_p of such dynamical system are as follows:

$$E_k = \frac{m}{2}\left(\dot{x}_S^2 + \dot{y}_S^2\right) + \frac{I_O}{2}\dot{\gamma}^2,$$

$$E_p = \frac{k}{2}\xi^2 + \frac{k}{2}\eta^2 + \frac{k_t}{2}\left(\gamma - \Omega t\right)^2 - mgy,$$

where: $x_s = x - e\cos(\gamma + \delta)$, $y_s = y + e\sin(\gamma + \delta)$ are coordinates of the disc mass centre S in inertial coordinate system XYZ, while: $\xi = x\cos\gamma + y\sin\gamma$, $\eta = -x\sin\gamma + y\cos\gamma$ are co-ordinates of the disc geometrical centre W in rotating co-ordinate system $\xi\eta\zeta$, which rotates with rotor angular velocity Ω. Furthermore: γ – is the angle of the shaft twist, e - is the eccentricity (distance) of rotor mass centre S from its geometrical centre W, while δ – is the angle between unbalance vector and axis ξ.

Rayleigh's function of energy dissipation in the lateral vibrations consists of two components. One component describes the dissipation caused by external vibration damping and second one describes the dissipation caused by internal damping. We assume that external damping is proportional to the rotor velocity in inertial coordinate system while internal damping is proportional to the rotor velocity in rotating coordinate system. Therefore, the Rayleigh's function is as follows:

$$E_r = \frac{1}{2}b_z\left(\dot{x}^2 + \dot{y}^2\right) + \frac{1}{2}b_w\left(\dot{\xi}^2 + \dot{\eta}^2\right) + b_t(\dot{\gamma} - \Omega)^2 =$$

$$= \frac{1}{2}b_z\left(\dot{x}^2 + \dot{y}^2\right) + \frac{1}{2}b_w\left[\left(\dot{x} + \Omega y\right)^2 + \left(\dot{y} - \Omega x\right)^2\right] + b_t(\dot{\gamma} - \Omega)^2$$

where: b_z – coefficient of external damping, b_w - coefficient of internal damping b_t - coefficient of torsional damping.

Lagrange's equations were used to obtain the motion equations of the rotor. The set of three nonlinear motion equations with periodic time-varying coefficients was obtained. So the system describes the parametric vibrations, where coefficients are a function of the rotor angular speed. To obtain the system with linear time invariant equations the non-linear equations were linearized and transformed to the rotating coordinate system (Fig.3).

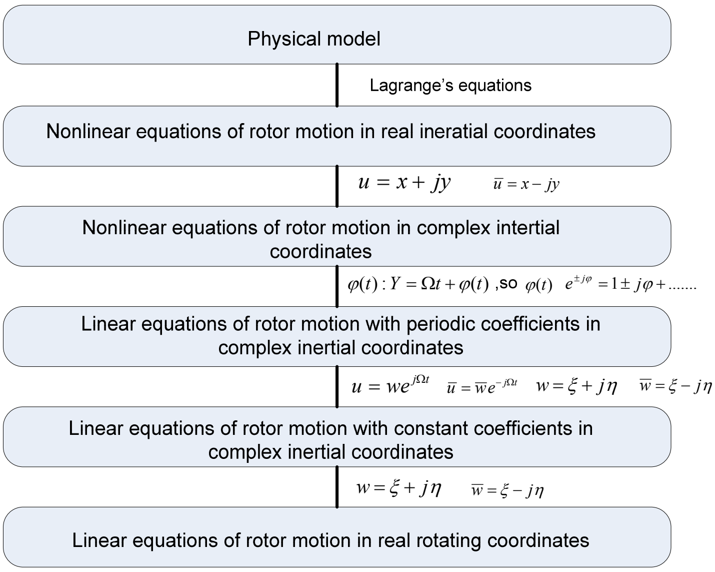

Fig. 3. Linearization and transformation of the equations describing the torsional/lateral vibrations of the rotor

The final version of the rotor model is as follows:

$$\begin{aligned}
&\ddot{\xi} - 2\Omega\dot{\eta} - \Omega^2\xi + 2h_z\left(\dot{\xi} - \Omega\eta\right) + 2h_w\dot{\xi} + \omega_1^2\xi + \\
&e\Omega^2\sin\delta\phi - 2e\Omega\cos\delta\dot{\phi} - e\sin\delta\ddot{\phi} = e\Omega^2\cos\delta + g\sin\Omega t, \\
&\ddot{\eta} + 2\Omega\dot{\xi} - \Omega^2\eta + 2h_z\left(\dot{\eta} + \Omega\xi\right) + 2h_w\dot{\eta} + \\
&\omega_2^2\eta + e\Omega^2\cos\delta\phi - 2e\Omega\sin\delta\dot{\phi} + e\cos\delta\ddot{\phi} = \\
&e\Omega^2\sin\delta + g\cos\Omega t, \\
&\ddot{\phi} + 2h_t\dot{\phi} + Rh\Omega^2\phi + \mu^2\phi + R\omega_1^2\sin\delta\xi - R\omega_2^2\cos\delta\eta = \\
&-Rg\cos\left(\Omega t + \delta\right).
\end{aligned} \tag{1}$$

where:

$$\omega_1^2 = \frac{k_1}{m}, \quad \omega_2^2 = \frac{k_2}{m}, \quad \mu^2 = \frac{k_t}{I_0}, \quad R = \frac{me}{I_0}, \quad h_t = \frac{b_t}{2I_o},$$

$$h_z = \frac{b_z}{2m}, \quad h_w = \frac{b_w}{2m}.$$

It is seen that equations are coupled by rotor unbalance ($e \neq 0$).

The linearized equations in inertial coordinates have time dependent coefficients. It means that the rotor vibrations can by considered as a parametric vibrations. From vibration theory we know that such vibrations for some range of parameters are unstable. The angular speed Ω is one of the main rotor parameters. Equations in rotating coordinates (1) have constant coefficients. Therefore, the calculations of unstable ranges of angular speed will be much simple, by the analysis of the equations in rotating coordinates.

3. FREE TORSIONAL/LATERAL ROTOR VIBRATIONS

We omit external excitations. In this case the motion equations (1) describe free rotor vibrations:

$$\begin{aligned}
&\ddot{\xi} - 2\Omega\dot{\eta} - \Omega^2\xi + 2h_z\left(\dot{\xi} - \Omega\eta\right) + 2h_w\dot{\xi} + \omega_1^2\xi + \\
&e\Omega^2\phi\sin\delta - 2e\Omega\dot{\phi}\cos\delta - e\ddot{\phi}\sin\delta = 0, \\
&\ddot{\eta} + 2\Omega\dot{\xi} - \Omega^2\eta + 2h_z\left(\dot{\eta} + \Omega\xi\right) + 2h_w\dot{\eta} + \omega_2^2\eta + \\
&e\Omega^2\cos\delta\phi - 2e\Omega\sin\delta\dot{\phi} + e\cos\delta\ddot{\phi} = 0, \\
&\ddot{\phi} + h_t\dot{\phi} + Rh\Omega^2\phi + \mu^2\phi + R\omega_1^2\sin\delta\xi - \\
&R\omega_2^2\cos\delta\eta = 0.
\end{aligned} \tag{2}$$

When we use Laplace transform the differential equations (2) will be changed to the algebraic form:

$$\begin{bmatrix} A_{1d}(s) & -B_d(s) & -D(s) \\ B_d(s) & A_{2d}(s) & -F(s) \\ -H(s) & -K(s) & C(s) \end{bmatrix} \begin{bmatrix} \xi \\ \eta \\ \phi \end{bmatrix} = \begin{bmatrix} 0 \\ 0 \\ 0 \end{bmatrix}, \tag{3}$$

where:

$$\begin{aligned}
&A_{1d}(s) = s^2 + 2(h_z + h_w)s + \omega_1^2 - \Omega^2; \\
&A_{2d}(s) = s^2 + 2(h_z + h_w)s + \omega_2^2 - \Omega^2, \\
&B_d(s) = 2\Omega(s + h_z); \\
&C(s) = s^2 + 2h_t s + eR\Omega^2 + \mu^2 \\
&D(s) = -e(\Omega^2\sin\delta - 2\Omega s\cos\delta - s^2\sin\delta); \\
&F(s) = e(\Omega^2\cos\delta + 2\Omega s\sin\delta - s^2\cos\delta); \\
&H(s) = -R\omega_2^2\sin\delta; \quad K(s) = R\omega_1^2\cos\delta.
\end{aligned} \tag{4}$$

The determinant of the main matrix in equation (3) is a characteristic polynomial. When characteristic polynomial equals zero we have characteristic equation:

$$A_{1d}(s)A_{2d}(s)C(s) - B_d(s)F(s)H(s) + D(s)B_d(s)K(s) + \\ -A_{2d}(s)D(s)H(s) - A_{1d}(s)F(s)K(s) + C(s)B_d^2(s) = 0 \tag{5}$$

When system is stable the roots (all poles) of the characteristic equation have negative real parts.

The roots have been calculated in function of rotor speed Ω for the following parameters: ω_1= 90 [rad/s], ω_2= 100 [rad/s], μ=150 [rad/s], R_h=0.01, h_z=h_w=0.04ω_1, h_t=0.02μ, ρ=30°. The results are presented in Fig. 4.

a)

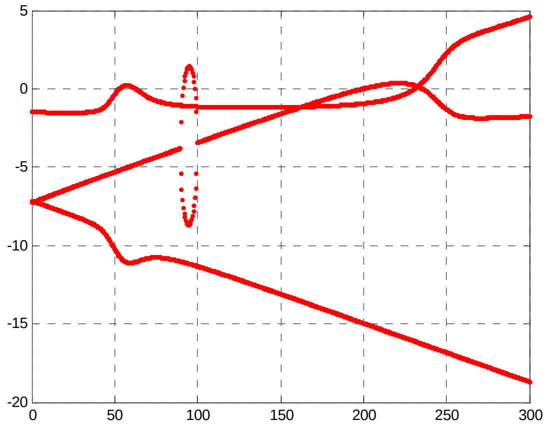

b)

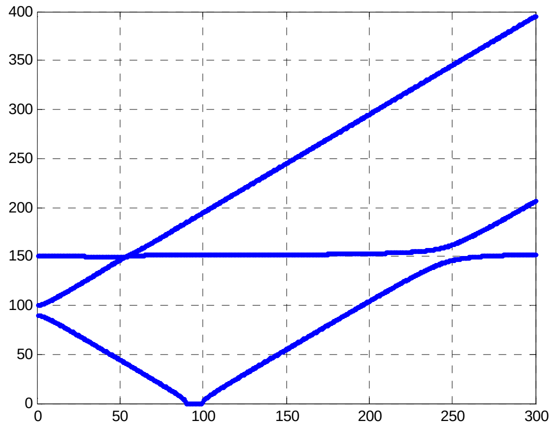

Fig. 4. Map of real part (a) and imaginary part (b) of characteristic equation roots (poles) for the torsional/lateral vibrations of the rotor with anisotropic flexibility

In the upper right quarter of the natural frequency map (Fig. 4b) we can notice three crossings of the natural frequency lines. Two crossings are in spots where torsional map meets lateral map: $\Omega \cong \mu_z-(\omega_1+\omega_2)/2$, $\Omega \cong \mu_z+(\omega_1+\omega_2)/2$. The third crossing is in the vicinity of the frequency $\Omega \cong (\omega_1+\omega_2)/2$ where the natural frequencies of lateral vibrations in two perpendicular directions ζ, η approach each other. In the vicinity of two crossings there are unstable ranges of the rotor speeds Ω.

We will show that the particular subsystems are coupled by two particular parameters: rotor unbalance R_h and rotor angular speed Ω as it is shown in Fig 5.

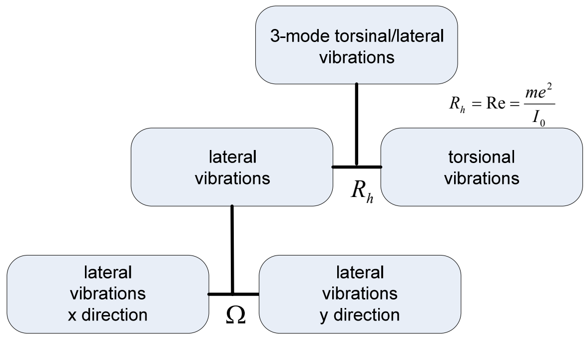

Fig. 5. Coupling parameters in considered rotor model

3.1 Undamped free vibrations of isotropic rotor

Now, we neglect the damping and assume a rotor with isotropic flexibility ω=ω_1=ω_2=100[rad/s]. In this case some of the polynomials (4) reduce to the form:

$$\begin{aligned} &A = A_{1d}(s) = A_{2d}(s) = s^2 + \omega^2 - \Omega^2, \\ &B = B_d(s) = 2\Omega s, \\ &C(s) = s^2 + eR\Omega^2 + \mu^2 \end{aligned} \tag{6}$$

and characteristic equation can be expressed as the algebraic equation:

$$s^6 + a_1 s^4 + a_2 s^2 + a_3 = 0, \tag{7}$$

where:

$$\begin{aligned} &a_1 = 2\omega^2 + 2\Omega^2 + \mu_z^2 + pR_h, \\ &a_2 = \left(\omega^2 - \Omega^2\right)^2 + 2\left(\omega^2 + \Omega^2\right)\mu_z^2 + \omega^4 R_h + 2\Omega^2 pR_h, \\ &a_3 = \mu_z^2\left(\omega^2 - \Omega^2\right)^2 - \omega^4 R_h + \Omega^4 pR_h, \\ &p = \omega^2 \sin^2\delta + \omega^2\cos^2\delta = \omega^2, \\ &R_h = Re = \frac{me^2}{I_o}, \quad \mu_z^2 = \mu^2 + R_h\Omega^2. \end{aligned}$$

From above coefficients of the characteristic equation it results that δ (angle between unbalance vector and axis ξ) does not influence the roots in the case of the isotropic rotor. So, we can orient the rotating coordinate system in any way against the rotor.

The stability condition is that all roots of characteristic equations have negative real parts. So using Cardan solution of the bi-3-order equation (7) we have obtained the stability conditions:

$$a_3 > 0, a_1 > 0,$$

and: (8)

$$a_1^2 < 3a_2 \quad \text{or} \quad 2(a_1^2 - 3a_2)^3 > [a_1(9a_2 - 2a_1^2) - 27a_3]^2,$$

when: $a_1^2 > 3a_2$.

From the first inequality (8) we can calculate one of the unstable ranges of the rotor speed:

$$\omega\sqrt{\frac{\mu_z^2}{R_h\omega^2+\mu_z^2}} \langle\ \Omega\ \langle\ \omega\ .$$

It is seen that unstable range always exists when the rotor is unbalanced ($e \neq 0$). Second inequality (8) is always fulfilled. From the third inequality (8) we have one more range of the unstable rotor speeds. Second range of the unstable rotor speeds is in the vicinity of the value: $\Omega=\omega+\mu$.

Typical maps of real and imaginary (natural frequencies) parts of the roots of characteristic equation in function of the rotor angular speed are shown in Fig. 6. The analytical considerations are confirmed by the computer simulation results. The both mentioned ranges of unstable rotor speeds are well seen in Fig.6.

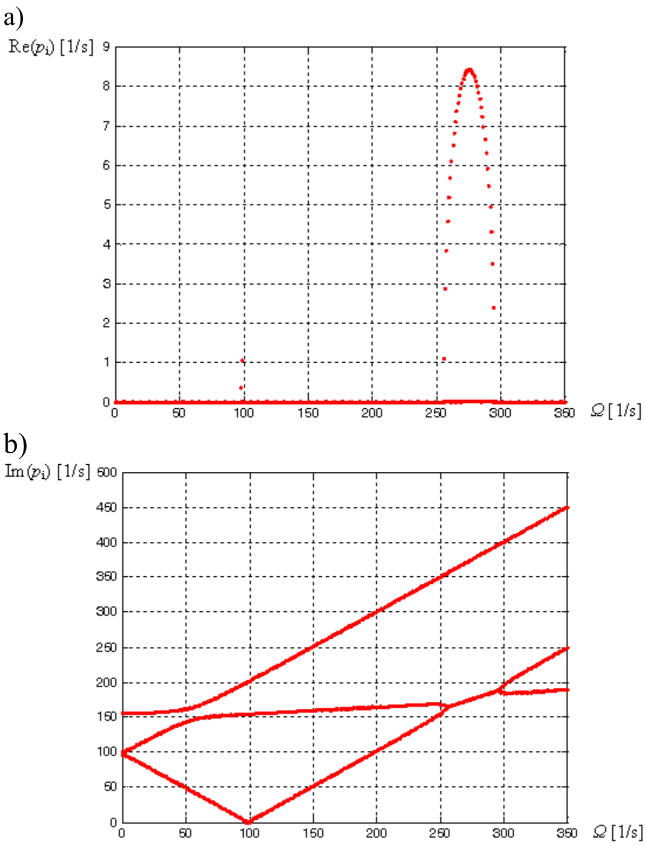

Fig. 6. Real part(a) and imaginary part (b) of characteristic polynomial roots versus rotor speed Ω for data: ω= 100 [rad/s], μ=150 [rad/s], R_h=0.1. Two ranges of unstable rotor speeds: 97 [rad/s] <Ω< 100 [rad/s], 256 [rad/s]<Ω<292 [rad/s].

The unstable speeds are in the vicinity of some natural frequency intersections (Fig. 6b). For these frequencies real part of roots have positive values (see Fig. 4a). We denote: p_i – i-th pole of transfer function (root of characteristic polynomial), z_i – i-th zero of transfer function. This time however, in comparison to Fig.4, the intersection $\Omega\cong\mu_z-(\omega_1+\omega_2)/2$ is stable while the crossing $\Omega\cong\mu_z+(\omega_1+\omega_2)/2$ is unstable. So, the problem is how to recognize which crossing indicate the unstable ranges. To answer question we will reach for a synthesis method known from the control theory.

We consider separately lateral and torsional vibrations. The coupling forces from (3) will be taken as external excitations:

$$\begin{aligned}&A(s)\xi(s)-B(s)\eta(s)=D(s)\varphi(s),\\&B(s)\xi(s)+A(s)\eta(s)=F(s)\varphi(s),\\&C(s)\varphi(s)=H(s)\xi(s)+K(s)\eta(s).\end{aligned} \tag{9}$$

Two first equations describe lateral vibrations and third one describes torsional vibrations. The mathematical model can be presented in the form of block scheme, given in Fig.7.

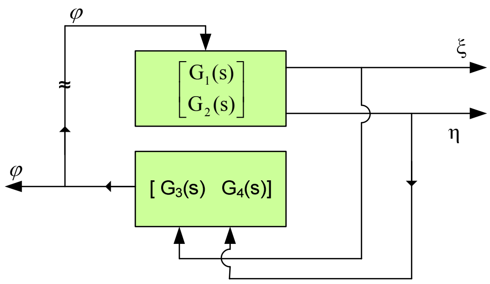

Fig. 7. Block scheme of the torsional/lateral vibrations of the flexible rotor

It is a dynamical system with feedback loop very well known from control theory, where particular transfer functions have the form:

$$\begin{aligned}G_1(s)&=\frac{\xi(s)}{\varphi(s)}=\frac{B(s)F(s)+A(s)D(s)}{A^2(s)+B^2(s)};\\G_2(s)&=\frac{\eta(s)}{\varphi(s)}=\frac{A(s)F(s)-B(s)D(s)}{A^2(s)+B^2(s)};\\G_3(s)&=\frac{\varphi(s)}{\xi(s)}=\frac{H(s)}{C(s)};\\G_4(s)&=\frac{\varphi(s)}{\eta(s)}=\frac{K(s)}{C(s)}.\end{aligned} \tag{10}$$

We break the feedback loop in the place indicated by tildes to obtain open-loop system. The open-loop transfer function is obtained by the multiplication of matrices:

$$G_o(s)=\begin{bmatrix}G_3(s) & G_4(s)\end{bmatrix}\begin{bmatrix}G_1(s)\\G_2(s)\end{bmatrix}=G_3(s)G_1(s)+G_4(s)G_2(s).$$

Taking into account transfer functions (10) we have:

$$G_o(s)=\frac{H(s)B(s)F(s)+H(s)A(s)D(s)+K(s)A(s)F(s)-K(s)B(s)D(s)}{[A^2(s)+B^2(s)]C(s)}. \tag{11}$$

When we introduce the rotor parameters (4), (6) the open-loop transfer function has the form:

$$G_o(s) = \frac{-R_h\omega^2\{s^4 + s^2(3\Omega^2+\omega^2) - (\omega^2-\Omega^2)\Omega^2\}}{\{s^4 + 2s^2(\omega^2-\Omega^2) + (\omega^2-\Omega^2)^2\}(s^2+\mu_z^2)} = R_h G_r(s) \qquad (12)$$

In the Evans method we will consider rotor unbalance parameter R_h as a gain which changes from zero to the infinity.

Now, we analyze the influence of the unbalance on the system dynamics. Closed-loop system from Fig.7 have the following characteristic equation:

$1 + R_h G_r(s) = 0$ or:

$$G_r(s) = -\frac{1}{R_h}, \quad \text{for } R_h \geq 0, \qquad (13)$$

In our case characteristic equation of the closed-loop system has the form:

$$1 + \frac{-R_h\omega^2\{s^4 + s^2(3\Omega^2+\omega^2) - (\omega^2-\Omega^2)\Omega^2\}}{\{s^4 + 2s^2(\omega^2-\Omega^2) + (\omega^2-\Omega^2)^2\}(s^2+\mu_z^2)} = 0$$

or (14)

$$\frac{\{s^4 + 2s^2(\omega^2-\Omega^2) + (\omega^2-\Omega^2)^2\}(s^2+\mu_z^2) - R_h\omega^2\{s^4 + s^2(3\Omega^2+\omega^2) - (\omega^2-\Omega^2)\Omega^2\}}{\{s^4 + 2s^2(\omega^2-\Omega^2) + (\omega^2-\Omega^2)^2\}(s^2+\mu_z^2)} = 0.$$

The numerator of the transfer function (14) is a characteristic polynomial of the closed-loop system (13) and denominator is a characteristic polynomial of the open-loop system.

$G_r(s)$ is a complex number and can be presented as a vector in the complex (Gauss) plane. According to the equation (13) the transfer function $G_r(s)$ should fulfill two conditions put on the angular location of the vector: arg $G_r(s)$=-180°±360°N, N – integer number and on its absolute value: $|G_r(s)| = 1/R_h$.

From above conditions it results that for R_h increasing from zero to the infinity the open-loop poles (roots of denominator polynomial in the transfer function $G_r(s)$) move towards zeros of the same open-loop transfer function $G_r(s)$ (roots of numerator in equation (11)). If the number of poles is bigger then the number of zeros the other poles escape to the infinity along asymptotes which start from the central point in the complex plane.

It means that zeros of the open-loop transfer function should play important role in the analysis of the unbalance influence on the dynamic behavior of the coupled torsional/lateral vibrations of the flexible rotor. The real and imaginary part of transfer function zeros for rotor parameter: ω=100 [rad/s], μ=150 [rad/s], R_h=0.1 are presented in Fig 8. It is a rotor which poles (natural frequencies) are shown in Fig. 5.

As we can see in Fig. 8 the positive real parts of the zeros exist only for the rotor speed Ω range from 0 to 100 [rad/s]. Imaginary parts (frequencies) of zeros changestogether with rotor angular speed Ω and increase parallel to real parts of poles (natural frequencies) of the lateral vibrations.

For small angular speed of rotor the system can be unstable for very big values of R_h because two of zeros in transfer function $G_r(s)$ are real and positive. But value of unbalance for which it happens is unrealistic. When all zeros and poles of transfer function are purely imaginary the root locus plot moves along imaginary axis. In this case each pole has its associated zero which is a target for locus line. Two biggest poles moves to infinity along imaginary axis. Such rotor is completely stable for all values of unbalance R_h.

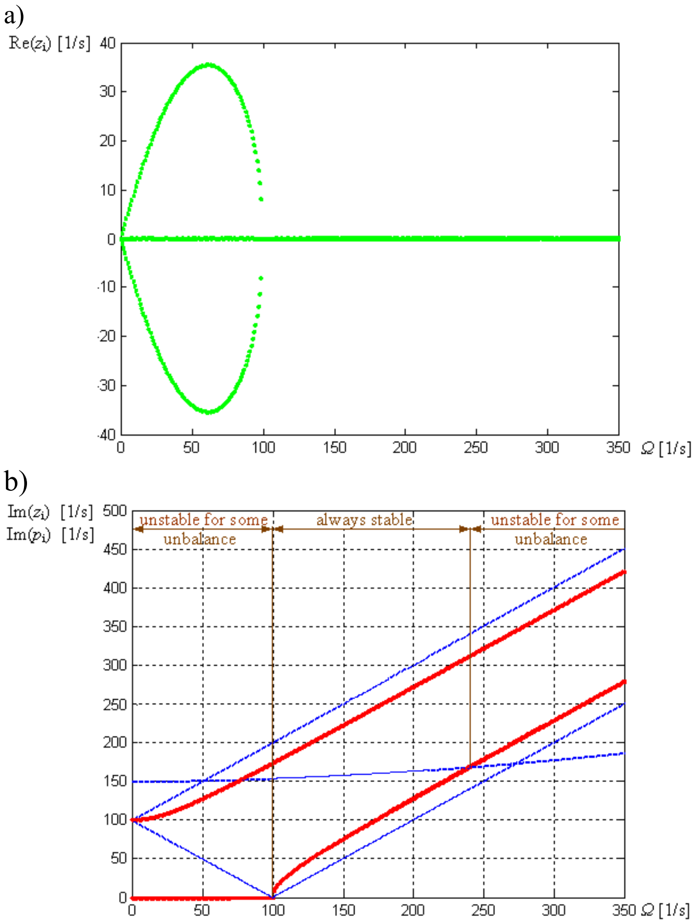

Fig. 8. The ranges of rotor speed where we can find such unbalance, which destabilize rotor vibrations Real parts (a) and imaginary parts (b) of zeros in the transfer function $G_r(S)$ versus rotor angular speed Ω drown as a bold lines. Slim lines in Fig.(b) show the natural frequencies of uncoupled torsional/lateral vibrations (poles of the transfer function $G_r(S)$).

Such harmony is destroyed when rotor angular speed cross value 245 [rad/s] (see Fig. 8). For angular speeds Ω>245[rad/s] the alteration of poles and zeros is replaced by close neighborhood of two poles. To reach open-loop zeros the locus lines are forced to make a circles. The circle enter the positive side of the complex plane. It means the motion becomes unstable for some values of unbalance.

We conclude that by analysis of the pole and zero values we are able to show the ranges of unstable vibrations (Fig.8). In first range (to 100 [rad/s]) the instability is connected with the real part positive value of two zeros of the open-loop transfer function. In second range of the unstable rotor angular speeds the alternating pole-zero pattern [Preumont, 2002] was destroyed. The neighborhood of two zeros and two poles is a simple way to detect the unstable behavior of the system. The closer to the crossing point on natural frequency map the smaller value of unbalance is needed to trigger the instability in both ranges.

3.2 Damped lateral vibrations of anisotropic rotor

Now, we will consider free damped lateral vibrations of an anisotropic rotor. To do this we reduce (3) to the following algebraic equations:

$$\begin{bmatrix} A_{1d} & -B_d \\ B_d & A_{2d} \end{bmatrix}\begin{bmatrix} \xi \\ \eta \end{bmatrix} = \begin{bmatrix} 0 \\ 0 \end{bmatrix}. \tag{15}$$

The determinant of the left matrix compared to zero is a characteristic equation:

$$\begin{aligned}&[s^2+2(h_z+h_w)s+\omega_1^2-\Omega^2]\\&[s^2+2(h_z+h_w)s+\omega_2^2-\Omega^2]+4\Omega^2\left(s+h_z\right)^2=0.\end{aligned} \tag{16}$$

The roots of the characteristic equation in the function of rotor angular speed Ω are presented in Fig.9.

After some manipulations of characteristic equation (16) we can find the ranges of the unstable rotor speeds. For ω_1<ω_2 the first range is: $\sqrt{\omega_1^2-h_z^2}<\Omega<\sqrt{\omega_2^2-h_z^2}$.

The second range is when angular speed crosses the value: $\Omega>\left\{\dfrac{h_z+h_w}{h_w}\right\}\omega_1$. The first range of unstable rotor speeds vanishes when external damping crosses the value: $h_z^2\rangle\dfrac{(\omega_1-\omega_2)^2}{8\left(\omega_1^2+\omega_2^2\right)}$.

As it is seen in Fig.9a for both unstable ranges the real parts of some roots become positive.

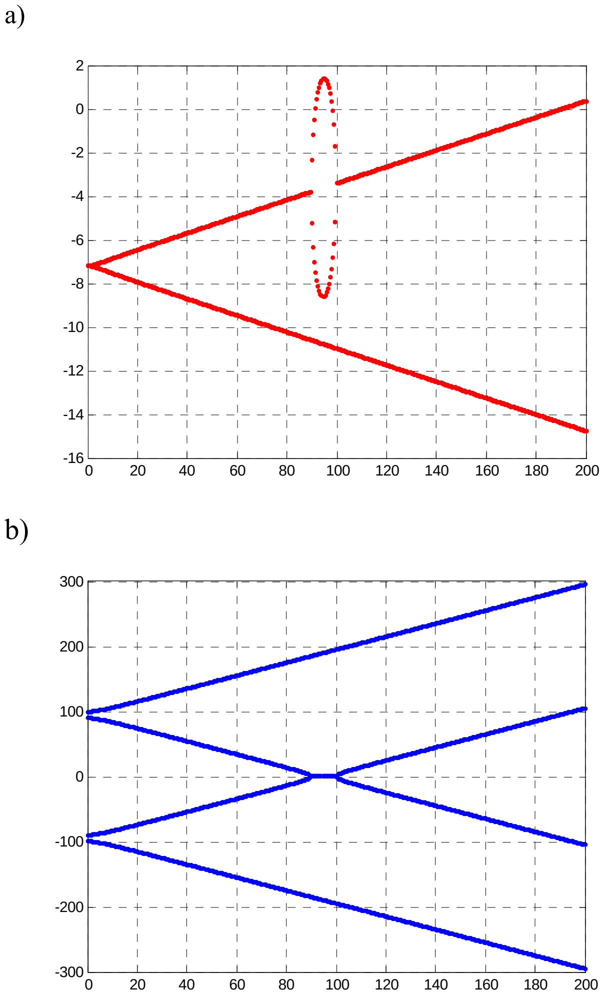

Fig. 9. Real (a) and imaginary (b) parts of the characteristic polynomial roots versus rotor angular speed Ω for lateral vibrations.

Once again we use feedback loop to decompose the system into smaller parts. We separate two perpendicular directions of the rotor lateral vibrations. The block scheme of the system is shown in Fig. 10.

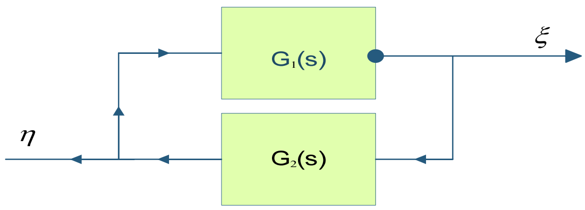

Fig. 10. The block scheme of rotor lateral vibrations

The open-loop transfer function is as follows:

$$G_{od}(s)=G_{1d}(s)G_{2d}(s), \tag{17}$$

where:

$$G_{1d}(s)=\frac{B(s)}{A_{1d}(s)};\quad G_{2d}(s)=\frac{-B(s)}{A_{2d}(s)};$$

Finally, we have:

$$G_{od}(s) = \frac{4\Omega^2 (s+h_z)^2}{[s^2 + 2(h_z + h_w)s + \omega_1^2 - \Omega^2][s^2 + 2(h_z + h_w)s + \omega_2^2 - \Omega^2]} = R_d G_{rd}(s) \tag{18}$$

The poles of the open-loop system for different rotor speeds are presented in Fig.11. The transfer function of the open-loop system has one doubled zero and it is negative since: $z_1 = z_2 = -h_z$. It is evident (see Fig.11)) that open-loop system is unstable for: $\Omega > \omega_1$ while closed-loop system (Fig. 9) is stable also in the range $\omega_2 < \Omega < \omega_1 (h_w + h_z)/h_w$. To find mechanism which extends the range of stable rotor speeds we will again use the Evans method. According to the method some system poles will approach negative open-loop zeros while the remain ones escape along the vertical asymptotes. We assume that rotor rotation is a cause of this mechanism so we introduce an artificial Evans' gain in the form:

$$R_D = \rho 4 \Omega^2 \tag{19}$$

For $\rho=1$ we have nominal state of the open-loop system (18). It is interesting to find for what values of the gain ρ the root locus cross the stability border on the Gauss plane.

a)

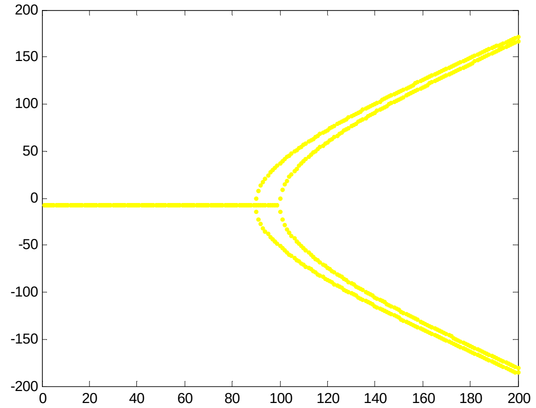

b)

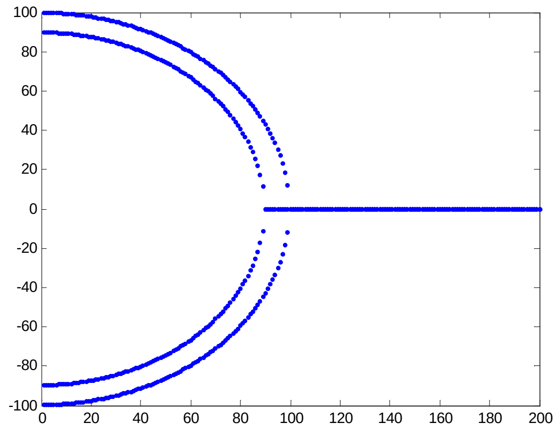

Fig. 11. Real (a) and imaginary (b) parts of the open-loop system poles versus rotor angular speed

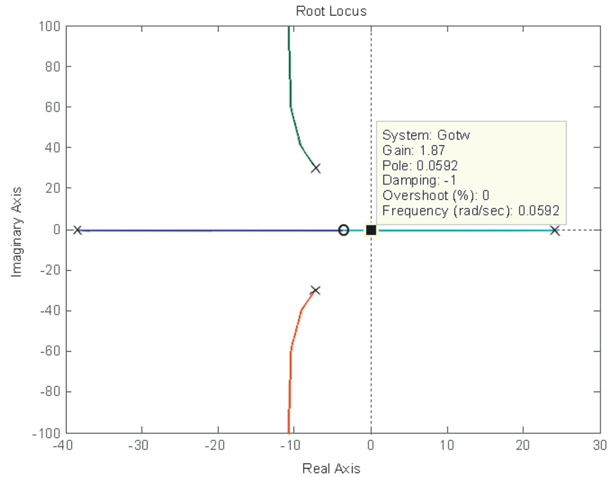

Fig. 12. Root locus of the rotor lateral vibrations in function of the gain ρ for angular speed Ω=95[rad/s]

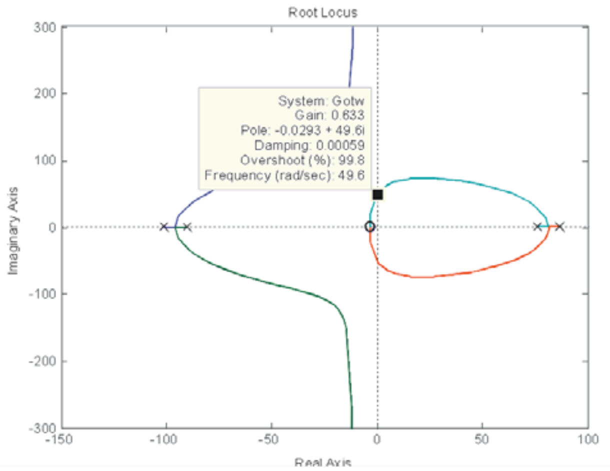

Fig. 13. Root locus of the rotor lateral vibrations in function of the gain ρ for angular speed Ω=130 [rad/s].

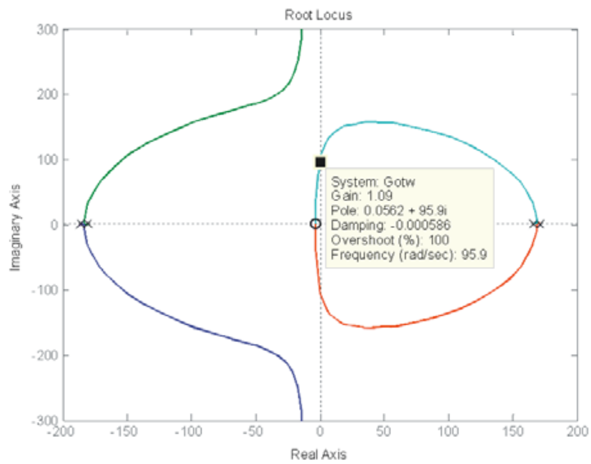

Fig. 14. Root locus of the rotor lateral vibrations in function of the gain ρ for angular speed Ω=200 [rad/s]

The root locus for unstable rotor speeds 95 [rad/s] and 200[rad/s] are presented in Fig. 12 and 14, respectively. The root locus for stable rotor speed 130[rad/s] is shown in Fig.13. The black square in Figures indicate the point on one of the root locus lines which is connected with the pole on the stability threshold. The parameters of the point are described in the Figure. For example, the overshoot on the stability border should be 100% for complex poles. The gain is the Evans gain (value of considered coupling parameter).

The imaginary axis divides the poles into stable and unstable ones. In the case of unstable rotor speeds the gain ρ crosses value 1 (ρ>1) when root locus cross the imaginary axes. It means that actual rotor speed Ω^2 is insufficient to stabilize the rotor for given speed.

3.3. Full model

Now, we return to the full model (8) whose poles are presented in Fig.2. Since now we know that zeros of open-loop system play important role in the stability analysis we have calculated them and they are presented in Fig. 15.

a)

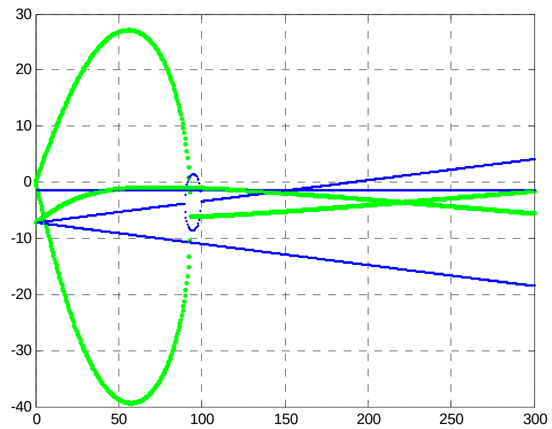

b)

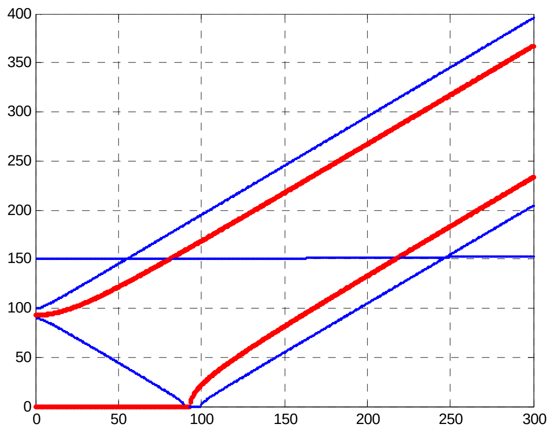

Fig. 15. Real (a) and imaginary (b) parts of zeros (bold lines) and poles (slim lines) of the open-loop transfer function designed for damped anisotropic rotor

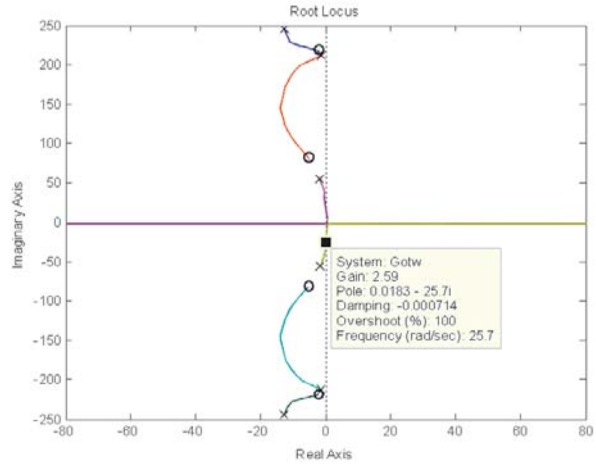

Fig. 16. Root locus for rotor angular speed Ω=150[rad/s]

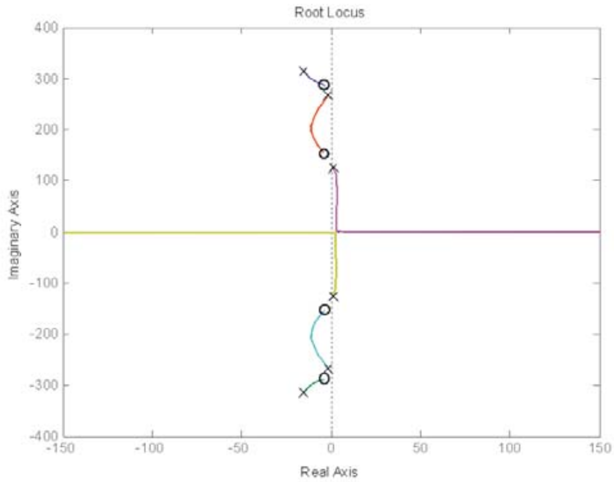

Fig. 17. Root locus for rotor angular speed Ω=220[rad/s]

We have shown in Figs 16, 17 the root locus for the two rotor speeds: 150, 220 [rad/s], respectively. In the case of Ω=150[rad/s] the rotor motion is practically stable for any unbalance. When rotor rotates with angular speed Ω=220[rad/s] the system is unstable and the unbalance practically has no influence of the dynamical state. The instability of the system is connected with internal damping.

The decomposition of coupled vibrations gives many advantages in the analysis of the system stability. The deviation of the system into smaller ones allows to reduce the calculations. It gives deeper insight into connections of the vibrations with changes of chosen parameters. Many vibration phenomena can be simply explain.

In the case of the considered torsional/lateral rotor vibrations we have carried out decoupling of the vibrations on two levels. First, we separated the torsional and lateral vibrations to analyze influence of the rotor unbalance on the rotor dynamics. Next we decoupled lateral vibrations into vibrations of the perpendicular directions. Such decomposition allowed us to show the stabilizing mechanism generated by rotor rotation.

Such approach give deeper insight into dynamical system as a control plant. Analysis of the plant dynamics allows to find the best strategy of the design procedure of the active vibration control system. We hope that the decomposition will also be useful in the diagnostic systems.

4. CONTROL OF THE DAMPED LATERAL VIBRATIONS OF THE ANISOTROPIC ROTOR

After reanalysis of the results from section 3.2 we can improve dynamic performance of the closed-loop system (stabilization of the rotor displacement and improvement of the transient parameters) by:
- additional external damping,
- additional gyroscopic effect,
- change of system stiffness,
- active rotor balancing.

Let us consider the equations of lateral vibrations of the anisotropic rotor in form convenient to design the control law. First, the control forces are introduced to rotor movement equation (15):

$$\begin{bmatrix} A_{1d} & -B_d \\ B_d & A_{2d} \end{bmatrix} \begin{bmatrix} \xi \\ \eta \end{bmatrix} = \begin{bmatrix} f_\xi \\ f_\eta \end{bmatrix}, \tag{20}$$

where:

$$A_{1d}(s) = s^2 + 2(h_z + h_w)s + \omega_1^2 - \Omega^2\,;$$
$$A_{2d}(s) = s^2 + 2(h_z + h_w)s + \omega_2^2 - \Omega^2\,;$$
$$B_d(s) = 2\Omega(s + h_z)\,.$$

After some calculations the relationships between control forces and rotor displacements have the form:

$$\begin{bmatrix} \xi(s) \\ \eta(s) \end{bmatrix} = \frac{1}{D_{op}} \begin{bmatrix} A_{2d}(s) & B_d(s) \\ -B_d(s) & A_{1d}(s) \end{bmatrix} \begin{bmatrix} f_\xi(s) \\ f_\eta(s) \end{bmatrix} \tag{21}$$

where:

$$D_{op} = A_{1d}(s)A_{2d}(s) + B_d^2(s) \tag{22}$$

is a characteristic polynomial of the plant.

This is the control model which has two inputs (control forces) and two outputs (measurement signals) connecting with two directions of analysed rotor vibrations: ξ, η. This relationship can be presented in matrix form as follows:

$$\mathbf{Y}_r(s) = \mathbf{G}_r(s)\mathbf{F}_r(s)\,, \tag{23}$$

where:

$$\mathbf{Y}_r(s) = \begin{bmatrix} \xi(s) \\ \eta(s) \end{bmatrix},$$
$$\mathbf{G}_r(s) = \frac{1}{D_{op}} \begin{bmatrix} A_{2d}(s) & B_d(s) \\ -B_d(s) & A_{1d}(s) \end{bmatrix}, \tag{24}$$
$$\mathbf{F}_r(s) = \begin{bmatrix} f_\xi(s) \\ f_\eta(s) \end{bmatrix}.$$

The denominator of transfer function $\mathbf{G}(s)$ is a characteristic equation of the control plant given as follows:

$$D_{op} = (A_{1d}A_{2d} + B_d^2) = s^4 + b_3 s^3 + b_2 s^2 + b_1 s + b_0 = 0. \tag{25}$$

Where:

$$\begin{aligned} b_3 &= 4(h_z + h_w), \\ b_2 &= 4(h_z + h_w)^2 + (\omega_1^2 + \omega_2^2 + 2\Omega^2), \\ b_1 &= 2(h_z + h_w)(\omega_1^2 + \omega_2^2) + 4\Omega^2(h_z - h_w), \\ b_0 &= (\omega_1^2 - \Omega^2)(\omega_2^2 - \Omega^2) + 4\Omega^2 h_z^2 = \\ &= (\omega_2^2 - \Omega^2)^2 + 4\Omega^2 h_z^2 + (\omega_1^2 - \omega_2^2)(\omega_2^2 - \Omega^2). \end{aligned} \tag{26}$$

According to Hurwitz criterion, the open-loop system is stable if all coefficients (26) of the polynomial have the same sign (positive) and minor determinants of Hurwitz matrix are positive. As it results from equations (26) coefficients b_3, b_2 are always positive. The coefficient b_1 is positive for rotational speeds described by condition:

$$\Omega^2 < \frac{(h_z + h_w)(\omega_1^2 + \omega_2^2)}{2(h_w - h_z)}. \tag{27}$$

The condition above confirms the known phenomena - external damping increases and internal damping decreases the range of stable rotor speeds. The coefficient b_0 has two parts. The second part $4\Omega^2 h_z^2$ is always positive and the first one $(\omega_1^2-\Omega^2)(\omega_2^2-\Omega^2)$ is positive for all rotor speeds except the range:

$$\omega_1 < \Omega < \omega_2. \tag{28}$$

This unstable range of rotational speeds was earlier considered and it is a result of anisotropic rotor stiffness.

According to Hurwitz criterion in case of considered rotor system the additional two minor determinants should be positive:

$$\begin{aligned} \Delta_2 &= b_3 b_2 - b_1 > 0, \\ \Delta_3 &= b_3 b_2 b_1 - b_3^2 b_0 - b_1^2 > 0. \end{aligned} \tag{29}$$

After calculations the first minor determinant is given by:

$$\begin{aligned} \Delta_2 &= 16(h_z + h_w)^3 + 2(h_z + h_w)(\omega_1^2 + \omega_2^2) + \\ &4\Omega^2(3h_z + h_w). \end{aligned} \tag{30}$$

Thus, the minor determinant Δ_2 is positive for any rotational speed of the rotor. The stable range of rotational speeds can be calculated from condition: $\Delta_3 = b_3 b_2 b_1 - b_3^2 b_0 - b_0^2 > 0$.

It is quite difficult to calculate the condition analytically. If we assume zero damping, the condition above can be written in simpler form: $\Delta_3 = -b_0^2 > 0$. For this condition the stable range of rotational speeds is given by inequality (28).

The control forces can be written as functions of measurement signals. These relationships are called control law. Let us consider four control laws. To compare the control laws in all control directions let introduce similary gain coefficients k. In general case, the control law can be presented as follows:

$$\mathbf{F}_r(s) = -\mathbf{K}_r(s)\mathbf{Y}_r(s)\,. \qquad (31)$$

After introducing of the control law to the equation of control plant (23) the closed-loop system is as follows:

$$[\mathbf{I} + \mathbf{G}_r(s)\mathbf{K}_r(s)]\mathbf{Y}_r(s) = \mathbf{0}\,, \qquad (32)$$

where, the characteristic equation of the closed-loop system is given by:

$$\det[\mathbf{I} + \mathbf{G}_r(s)\mathbf{K}_r(s)] = 0. \qquad (33)$$

In order to estimate the stability range of closed-loop system and to obtain the proper parameters of the controller (in our case the gain parameter k), the roots of the closed-loop characteristic equation should be analyzed.

The equation (31) describes the control law in rotational coordinate system. In practice, the rotor vibrations are controlled in non-rotating inertial coordinate system. Thus, we introduce the transformation matrix between coordinates of rotating and non-rotating coordinate systems:

$$\begin{bmatrix} \xi(t) \\ \eta(t) \end{bmatrix} = \begin{bmatrix} \sin\Omega t & \cos\Omega t \\ -\cos\Omega t & \sin\Omega t \end{bmatrix} \begin{bmatrix} x(t) \\ y(t) \end{bmatrix}, \qquad (34a)$$

that is:

$$\mathbf{Y}_r(t) = \mathbf{T}\mathbf{Y}(t)\,. \qquad (34b)$$

The transformation matrix $\mathbf{T}$ is orthonormal. Thus, the inverse matrix is obtained as: $\mathbf{T}^{-1}=\mathbf{T}^{T}$.

The control forces (31) should also be calculated in inertial coordinate system. Thus, we also introduce the transformation matrix $\mathbf{T}$ to obtain the control forces:

$$\begin{bmatrix} f_\xi(t) \\ f_\eta(t) \end{bmatrix} = \begin{bmatrix} \sin\Omega t & \cos\Omega t \\ -\cos\Omega t & \sin\Omega t \end{bmatrix} \begin{bmatrix} f_x(t) \\ f_x(t) \end{bmatrix}, \qquad (35a)$$

that is:

$$\mathbf{F}_r(t) = \mathbf{T}\mathbf{F}(t)\,. \qquad (35b)$$

After putting the formulas (34b) and (35b) into the control law (31) we obtain:

$$\mathbf{T}\mathbf{F}(t) = -\mathbf{K}_r(t)\mathbf{T}\mathbf{Y}(t) \qquad (36)$$

After some calculations the control law in non-rotating coordinate system is as follows:

$$\mathbf{F}(s) = -\mathbf{K}(s)\mathbf{Y}(s)\,, \qquad (37)$$

where, the gain parameter of controller can be obtained from relation:

$$\mathbf{K}(s) = \mathbf{T}^T\mathbf{K}_r(s)\mathbf{T}\,. \qquad (38)$$

So the control law can be calculated in rotating coordinate system (which is advantageous in case of parametric vibrations) and the last equation can be used to transform it to the inertial coordinate system.

4.1 Active damping of rotor vibrations

The damping forces are proportional to the velocity of vibrations. Let us introduce the control law where the control forces are proportional to the vibration velocity and there are no crossing couplings (see Fig. 18). Without cross couplings there are only two paths in the controller between particular control forces and rotor velocity in each of the control directions. Thus, the control law is given by formula:

$$\mathbf{F}_r(s) = \begin{bmatrix} f_\xi(s) \\ f_\eta(s) \end{bmatrix} = -k_1 s \begin{bmatrix} 1 & 0 \\ 0 & 1 \end{bmatrix} \begin{bmatrix} \xi(s) \\ \eta(s) \end{bmatrix}. \qquad (39)$$

that is:

$$\mathbf{K}_{r1}(s) = \begin{bmatrix} k_1 s & 0 \\ 0 & k_1 s \end{bmatrix}. \qquad (40)$$

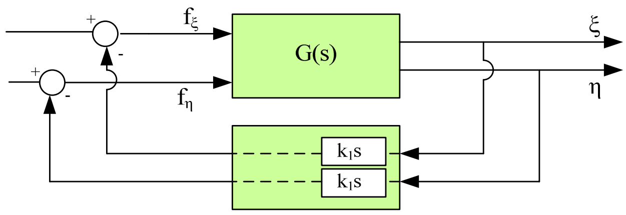

Fig. 18. The closed-loop system with the active damping f rotor vibrations

The characteristic equation of closed-loop system with control gain $\mathbf{K}_{r1}$ is given by:

$$\det[\mathbf{I} + \mathbf{G}_r(s)\mathbf{K}_{r1}(s)] = D_{op} + k_1^2 s^2 + k_1(A_{1d} + A_{2d})s = 0. \qquad (41)$$

The first part of equation (41) is the characteristic equation of control plant (23). The another two parts are an appendix to the rotor dynamics introduced by the control law and the appendix has the form of the polynomial:

$$k_1^2 s^2 + k_1(A_{1d} + A_{2d})s = b_{13}s^3 + b_{12}s^2 + b_{11}s, \qquad (42)$$

where:

$$\begin{aligned} b_{13} &= 2k_1, \\ b_{12} &= 4k_1(h_z + h_w) + k_1^2, \\ b_{11} &= k_1[(\omega_1^2 - \Omega^2) + (\omega_2^2 - \Omega^2)]. \end{aligned} \qquad (43)$$

From above results the control law influences three middle coefficients of the characteristic equation of the plant.

For the control plant with parameters: ω_1= 90 [rad/s], ω_2= 100 [rad/s], R_h=0.01, h_z=h_w=0.04ω_1, we have calculated such gain coefficient k_1 of controller which brings the closed-loop system at the stability limit. These values of coefficient k_1 for different rotor angular speed Ω are called the critical coefficients. We are looking for such control systems which stabilize rotor dynamics in given range of the rotor speeds.

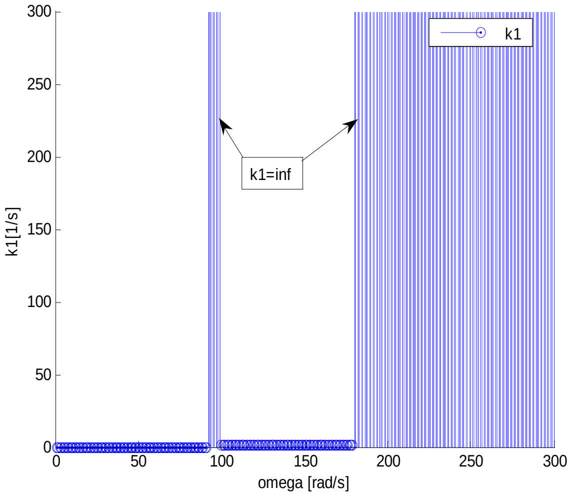

Fig. 19. Critical gain coefficients k_1 in the $\mathbf{K}_{r1}$ controller for rotor angular speed Ω from 0 to 300 [rad/s]

Unfortunately, the active control of rotor vibration damping does not ensure the stability for all rotor angular speeds (see Fig. 19). That is because the controller with gain coefficient k_1 do not influences the coefficient b_0 in the characteristic equation. Therefore, we have two unstable ranges of rotor vibrations: 92 [rad/s]<Ω<98 [rad/s] and Ω>179 [rad/s], which do not depend on controller coefficient k_1.

According to equation (38) we can control law in rotating coordinate system transform to the non-rotating coordinate system. The matrix $\mathbf{K}_{r1}$ is an identity matrix multiplied by scalar $k_1 s$. Therefore, the control law in the non-rotating coordinate system according to the equation (38) have the form:

$$\mathbf{K}_1(s) = \mathbf{T}^T \mathbf{K}_{r1}(s)\mathbf{T} = \mathbf{K}_{r1}(s). \tag{44}$$

In this case the control laws in both coordinate systems - rotating and non-rotating - are identical.

4.2. Active gyroscopic damping

The gyroscopic forces are proportional to values of rotor rotational speed. However, their direction is perpendicular to considered rotor movement. Let us introduce the control law where the control forces are perpendicular proportional to vibrations speed. There are only two feedback loops between particular control forces and rotor speeds which directions are perpendicular to directions of control forces. Thus, the control law is given by:

$$\mathbf{K}_{r2}(s) = \begin{bmatrix} 0 & -k_2 s \\ k_2 s & 0 \end{bmatrix}. \tag{45}$$

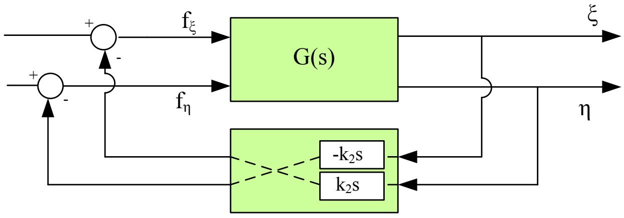

Fig. 20. The closed-loop system with the active gyroscopic damping of rotor vibrations

The characteristic equation of closed-loop system with $\mathbf{K}_{r2}$ control law is given by:

$$\det[\mathbf{I} + \mathbf{G}_r(s)\mathbf{K}_{r2}(s)] = D_{op} + k_2{}^2 s^2 + 2k_2 B_d s = 0. \tag{46}$$

The first part of equation (46) is the characteristic equation of control plant (21). The another two parts are introduced by
the control law of rotor dynamic and are given by:

$$k_2{}^2 s^2 + 2k_2 B_d s = b_{22} s^2 + b_{21} s, \tag{47}$$

where:

$$\begin{aligned} b_{22} &= 4k_2\Omega + k_2{}^2, \\ b_{21} &= 4k_2\Omega h_z. \end{aligned} \tag{48}$$

The control law (described above) have positive influence on the two coefficients but does not change the rest coefficients of the characteristic equation..

Unfortunately, the active gyroscopic damping of rotor vibrations does not ensure the stability for all rotational speeds (see Fig. 21). That is because the controller with gain coefficient k_2 does not influence the coefficient b_0 in the characteristic equation. Therefore, we have one unstable range of rotor vibrations: 92 [rad/s]<Ω<98 [rad/s], which does not depend of the controller coefficient k_2. For rotational speed higher than 98 [rad/s] the small value of gain coefficient k_2 is necessary to stabilize the closed-loop system. The critical value of gain coefficient k_2 increases with rotational speed Ω.

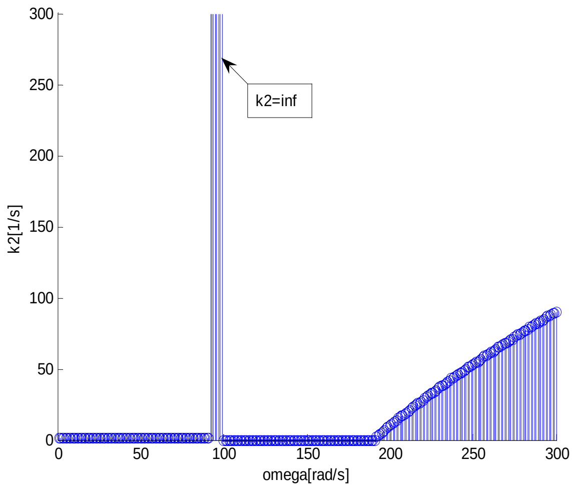

Fig. 21. Critical value of gain coefficient k_2 in the $\mathbf{K}_{r1}$ controller stabilizing the rotor vibrations for angular speeds Ω from 0 to 300 [rad/s]

Now, let us to investigate the dynamic of the closed-loop system for rotor speed Ω=300 [rad/s]. For this rotational speed the critical gain k_2 of the controller equals 91 [1/s]. The impulse response of the closed-loop rotor system in two directions of the vibrations: ξ, η for gain k_2=100 [1/s] (about 10% over critical one) is shown in Fig. 22.

The small damping of rotor vibrations in both control directions can be observed. The impulse response of the closed-loop system for gain k_2=200 [1/s] is shown in Fig. 23. The higher gain only slight improves the intensity of vibration damping.

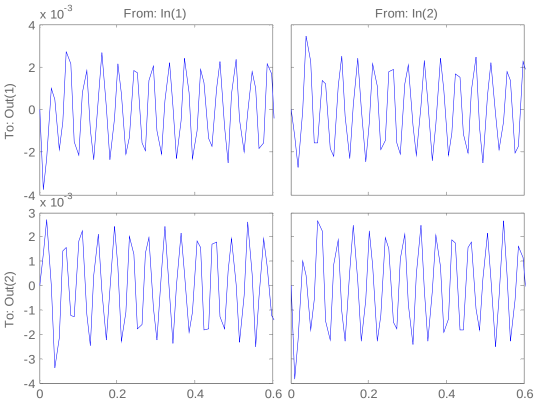

Fig. 22. The impulse response of the closed-loop system for the controller gain k_2=100 [1/s]

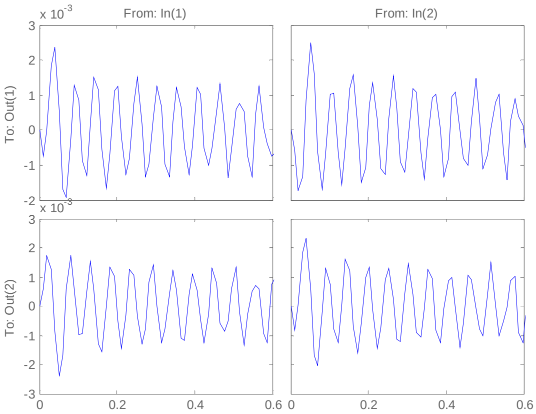

Fig. 23. The impulse response of the closed-loop for the controller gain k_2=200 [1/s]

Basing on the equation (38) we can control law transfer to the non-rotating coordinate system. The matrix $\mathbf{K}_{r2}$ is an identity matrix multiplied by scalar $k_2 s$. Therefore, in non-rotating coordinate system we have:

$$\mathbf{K}_2(s) = \mathbf{T}^T \mathbf{K}_{r2}(s)\mathbf{T} = \mathbf{K}_{r2}(s). \tag{49}$$

In this case the control laws in both coordinate systems - rotating and no rotating - are also identical.

4.3. Active change of rotor direct stiffness

According to Hurwitz criterion, all coefficients of characteristic equation of the closed-loop system should be positive. If the external damping is not big enough the last one of coefficients: $b_0=(\omega_1^2-\Omega^2)(\omega_2^2-\Omega^2)+4\Omega^2 h_z^2$ in the characteristic equation of control plant (25) is negative for the rotational speeds Ω between frequency ω_1 and ω_2. What more, any of above control laws do not change the value of coefficient b_0. Therefore, the another control law which can change the value of coefficient b_0 is necessary to be considered. The most advantageous is a control law which leads to the isotropy of the rotor system. In this case the unstable region of rotor vibrations is reduced to zero.

The stiffness forces are proportional to the displacement of rotor vibrations. Let us introduce the control law in which the control forces are proportional to the rotor displacements and there are no cross coupling. Thus, we obtain two independent feedback loops between particular control forces and rotor displacements in each of control directions (Fig.24).

The control law is given by formula:

$$\mathbf{F}_r(s) = \begin{bmatrix} f_\xi(s) \\ f_\eta(s) \end{bmatrix} = -\begin{bmatrix} k_{31} & 0 \\ 0 & k_{32} \end{bmatrix} \begin{bmatrix} \xi(s) \\ \eta(s) \end{bmatrix}. \tag{50}$$

It means:

$$\mathbf{K}_{r3}(s) = \begin{bmatrix} k_{31} & 0 \\ 0 & k_{32} \end{bmatrix}. \tag{51}$$

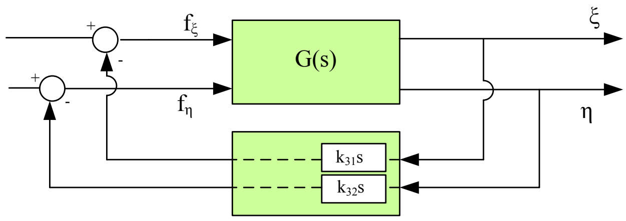

Fig. 24. The closed-loop system with controller which change the lateral system stiffness

The characteristic equation of the closed-loop system with control law $\mathbf{K}_3$ is given by:

$$\det[\mathbf{I} + \mathbf{G}_r(s)\mathbf{K}_{r3}(s)] = D_{op} + k_{31}k_{32} + k_{32}A_{1d} + k_{31}A_{2d} = 0. \tag{52}$$

The first part of equation (52) is the characteristic equation of the control plant (23). The another two parts present the influence of the controller on the closed-loop dynamics. The difference between the characteristic equation of closed-loop system and the characteristic equation of the plant is a polynomial:

$$k_{31}k_{32} + k_{32}A_{1d} + k_{31}A_{2d} = b_{32}s^2 + b_{31}s + b_{30}, \tag{53}$$

where:

$$\begin{aligned} b_{32} &= k_{31} + k_{32}, \\ b_{31} &= 2(k_{31} + k_{32})(h_z + h_w), \\ b_{30} &= k_{32}(\omega_1^2 - \Omega^2) + k_{31}(\omega_2^2 - \Omega^2) + k_{31}k_{32}. \end{aligned} \tag{54}$$

We assume first that the values of gain coefficients are the same: k_3=k_{31}=k_{32}. Thus, for the same values of the gain coefficients the closed-loop system is stable in full range of considered rotor angular speeds Ω (see Fig. 25).

However, the value of the critical coefficient strongly increases with the increase of the rotational speed.

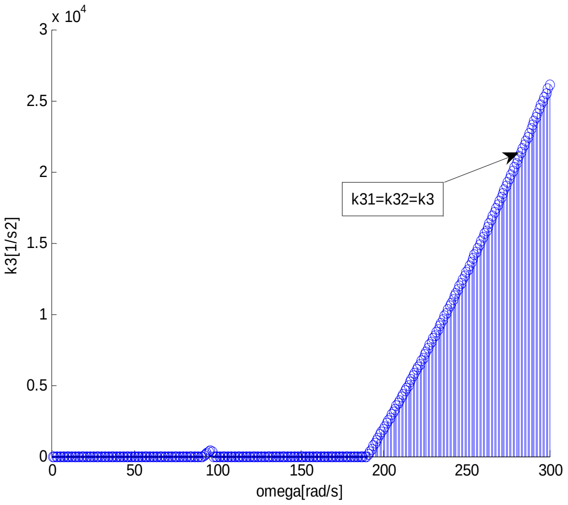

Fig. 25. The critical coefficient k_3 of $\mathbf{K}_{r3}$ controller with the same values of all gain parameters

The controller gain k_3 influences three coefficients of characteristic equation of the control plant including b_0.

Thus, the last coefficient of the characteristic equation (52) of closed-loop system is given by:

$$\begin{aligned} b_0 + b_{30} &= (\omega_1^2 - \Omega^2)(\omega_2^2 - \Omega^2) + 4\Omega^2 h_z^2 + \\ &+ k_{32}(\omega_1^2 - \Omega^2) + k_{31}(\omega_2^2 - \Omega^2) + k_{31}k_{32} = \\ &= (\omega_1^2 + k_{31} - \Omega^2)(\omega_2^2 - \Omega^2) + \\ &4\Omega^2 h_z^2 + k_{32}(\omega_1^2 - \Omega^2) + k_{31}k_{32}. \end{aligned} \tag{55}$$

If we assume:

$$\begin{aligned} k_{32} &= 0, \\ \omega_1^2 + k_{31} &= \omega_2^2, \end{aligned} \tag{56}$$

the closed-loop system with rotating rotor is stable and isotropic.

In this case the gain matrix of the controller (51) in rotating coordinate system has different elements. Thus, the gain matrix of controller in non-rotating coordinate system basing on the transformation (38) has the form:

$$\mathbf{K}_3(s) = \mathbf{T}^T \mathbf{K}_{r3}(s)\mathbf{T} = \begin{bmatrix} k_{31}\sin^2\Omega t + k_{32}\cos^2\Omega t & k_{31}\sin\Omega t\cos\Omega t - k_{32}\sin\Omega t\cos\Omega t \\ k_{31}\sin\Omega t\cos\Omega t - k_{32}\sin\Omega t\cos\Omega t & k_{32}\sin^2\Omega t + k_{31}\cos^2\Omega t \end{bmatrix}. \tag{57}$$

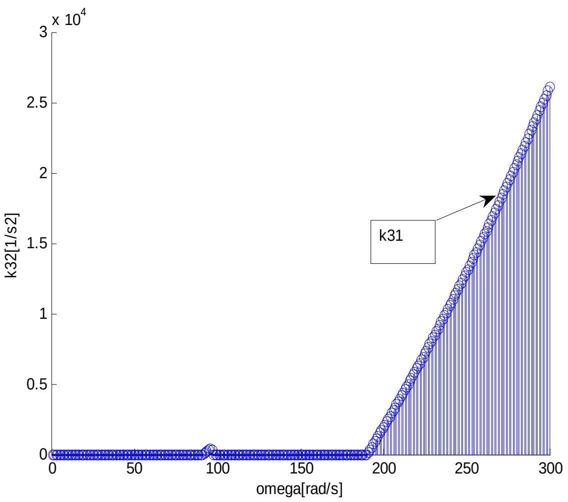

Fig. 26. The critical gain coefficient k_{31} of $\mathbf{K}_{r3}$ controller when gain parameter k_{32}=0

When we assume in (57) that k_{32}=0, we obtain the control law in inertial coordinate system given by:

$$\mathbf{K}_3(s) = \begin{bmatrix} k_{31}\sin^2\Omega t & k_{31}\sin\Omega t\cos\Omega t \\ k_{31}\sin\Omega t\cos\Omega t & k_{31}\cos^2\Omega t \end{bmatrix}. \tag{58}$$

The control law (58) means that two control inputs and two measurement output must be used to ensure the rotor isotropic stiffness.

Let us check the case when gain coefficient k_{32}=0. Now, we try to find a value of the gain k_{31} for which the SISO closed-loop system is stable. This situation is presented in Fig. 26. It is the same as is Fig. 25. where both gain coefficients had the same value. That means, we can apply the SISO control system and obtain the same results as in two input-two output control. However, the SISO control in rotating coordinate system must be transformed to two input-two output control system in non-rotoating coordinate system (see equation 58). Therefore, it is more convenient to apply two input-two output control with the same gains in order to avoid time-variant gain parameters in the $\mathbf{K}_3$ controller.

4.4 Active change of cross symmetry stiffness

Now, we consider the control law where the control forces are proportional to rotor displacements in the cross configuration. Thus, we obtain two feedback loops between particular control forces and rotor displacements which directions are perpendicular to directions of control forces (see Fig. 27). The control law is given by:

$$\mathbf{K}_{r4}(s) = \begin{bmatrix} 0 & -k_4 \\ k_4 & 0 \end{bmatrix}. \tag{59}$$

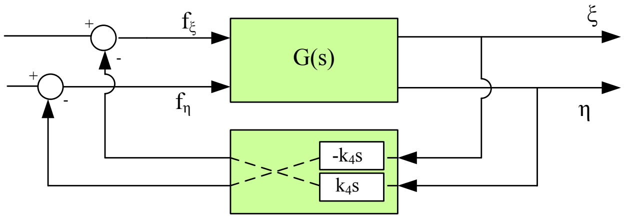

Fig. 27. The closed-loop system with controller which change the lateral stiffness in cross configuration of the rotor system

The characteristic equation of the closed-loop system with control gain $\mathbf{K}_4$ is given as follows:

$$\det[\mathbf{I} + \mathbf{G}_r(s)\mathbf{K}_{r4}(s)] = D_{op} + 2B_d k_4 + k_4^2 = 0. \tag{60}$$

The two last parts of equation (60) present influence of the control law onto rotor dynamics:

$$2B_d k_4 + k_4 = b_{41}s + b_{40}, \tag{61}$$

where:

$$b_{41} = 4\Omega k_4, \qquad b_{40} = 4\Omega k_4 h_z + k_4^2. \tag{62}$$

This control law (described above) has positive influence on the dynamics of the closed-loop. For any values of angular speed this control law increases the value of coefficients b_1 and b_0 which represent the negative effects of the internal damping and of the rotor anisotropic stiffness.

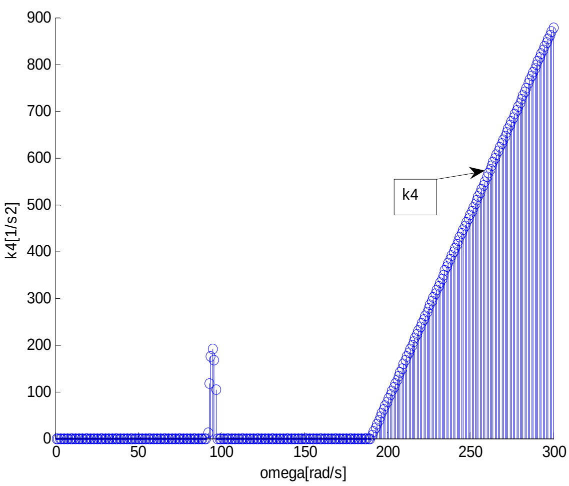

Fig. 28. The critical gain parameter k_4 in $\mathbf{K}_{r4}$ controller versus the angular speed Ω

The critical value of gain k_4 was presented in the Fig. 28. The cross change of system stiffness by $\mathbf{K}_{r4}$ controller require significantly reduces the critical gains in the comparison with the $\mathbf{K}_{r3}$ controller.

Therefore, we check dynamical behaviour of closed-loop system for rotational speed Ω=300[rad/s]. For this rotational speed the critical gain parameter is k_4=900 [1/s]. First, we apply the gain parameter k_4=1000[1/s^2] (about 10% over the critical one). The impulse responses of the closed-loop system in two vibration directions: ξ, η for critical gain parameter k_4=1000 [1/s] are shown in Fig. 29.

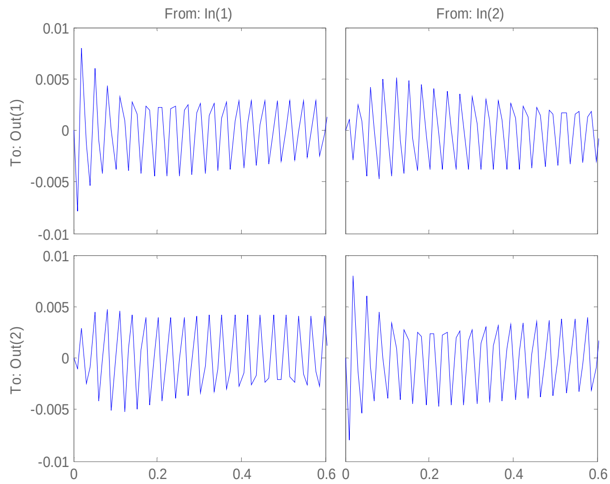

Fig. 29. The impulse response of closed-loop system for cross symmetric $\mathbf{K}_{r4}$ controller with gain k_4=1000 [1/s]

In above case we can observe small damping of rotor vibrations in both control directions. In the next step we increase the gain of the controller. The impulse responses of closed-loop system for gain controller k_4=1500 [1/s] atr shown in Fig. 30. It is evident the bigger gain parameter k_4 improves intensity of vibrations damping.

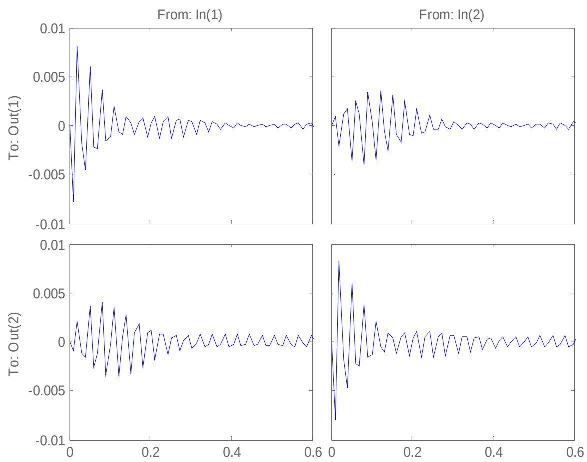

Fig. 30. The impulse response of closed-loop system for cross symmetric $\mathbf{K}_{r4}$ controller with gain k_4=1500 [1/s]

Now, we will check the stability of the system in full range of the considered angular speeds (from 0 to 300 [rad/s]). The real and imaginary parts of the roots of characteristic equation for closed-loop system with controller gain k_4=1500 [1/s] are shown in Fig. 31.

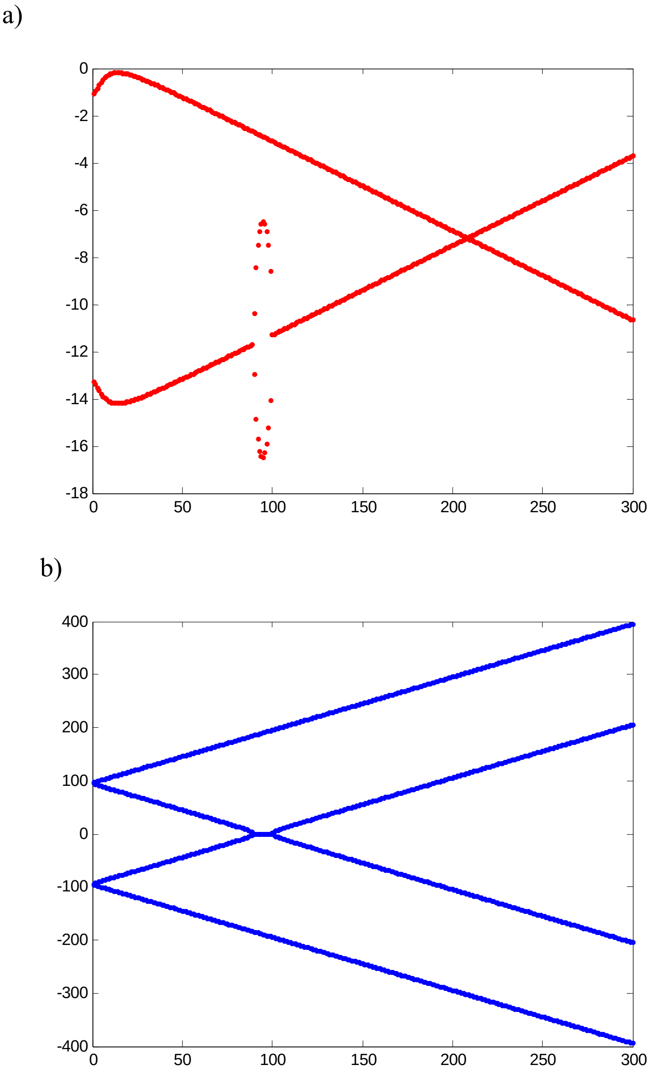

Fig. 31. Real (a) and imaginary (b) parts of the characteristic equation for gain k_4=1500 [1/s]

The closed-loop system is on the border of the stability for low rotor angular speeds (in the vicinity of 20 [rad/s]). It is appeared that there is upper limit on the value of the controller gain to stabilize the system in considered range of the rotor speeds. The upper limit is just k_4=1500 [1/s]. The lower limit of the controller gain was shown in Fig.28.

The gain matrix of controller (59) in the rotating coordinate system has the same two elements with opposite signs. The gain matrix of controller in non-rotating coordinate system has the form:

$$\mathbf{K}_4(s) = \mathbf{T}^T \mathbf{K}_{r4}(s)\mathbf{T} = \mathbf{K}_{r4}(s). \tag{63}$$

The control laws in both coordinate systems - rotating and no rotating - are identical.

4.5. Comparison of control systems

To compare the different control systems we have taken into account the power consumption of power amplifiers which is the multiplication of control force and the velocity of the rotor vibrations. The most interesting are closed-loop systems with controllers $\mathbf{K}_{r2}$ i $\mathbf{K}_{r4}$. Thus, let us compare the power consumption by these control systems. In the case of $\mathbf{K}_{r2}$ controller the control force is proportional to rotational speed and in the second case of $\mathbf{K}_{r4}$ controller the control force is proportional to rotor displacement. The main rotor vibration movement is connected with angular speed Ω. Therefore, we assume that speeds v_x or v_y in motion directions are proportional to displacements in directions x or y and to angular speed Ω. Fig. 32 shows comparison of critical gain parameters for the $\mathbf{K}_{r2}$ i $\mathbf{K}_{r4}$ controllers. The $\mathbf{K}_{r4}$ closed-loop system is definitely the best one.

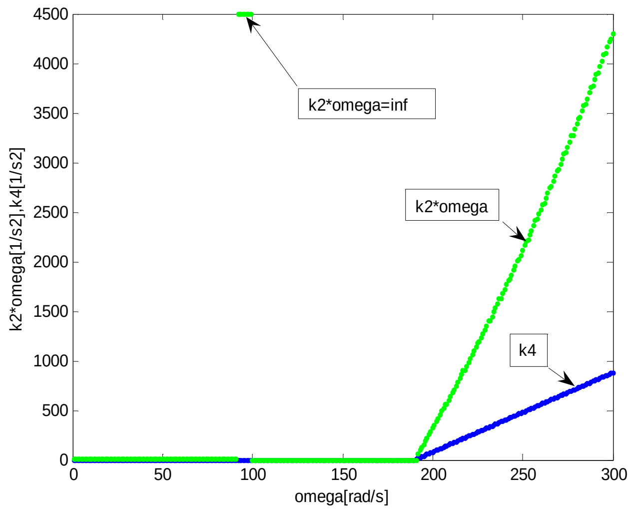

Fig. 32. The comparison of two critical gain parameters of control system

The closed-loop system with $\mathbf{K}_{r4}$ controller ensure the stability in full range of considered angular speeds. What more, for high rotational speeds the $\mathbf{K}_{r4}$ controller consume less power than others controllers. The $\mathbf{K}_{r4}$ controller has also good transient response (compare Figs 23 and 31).

5. CONTROL OF TORSIONAL/LATERAL ROTOR VIBRATIONS

Presently, the controller $\mathbf{K}_4$ will be joined to the full model of the rotor torsional/lateral vibrations. Its influence on the dynamic behaviour of the closed-loop system will be checked. The full rotor model with control of the lateral vibrations is presented in Fig.33.

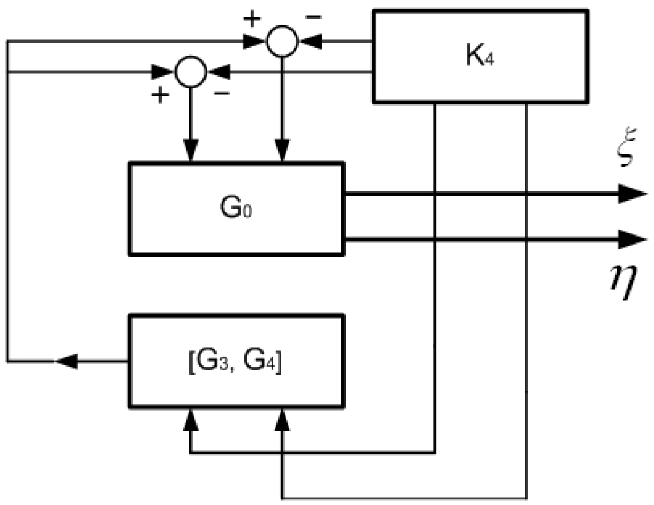

Fig. 33. Block scheme of the considered model for the rotor with active control of the lateral vibrations

To analyze the closed loop system the control forces defined as:

$$\mathbf{F}_r(s)=\begin{bmatrix} f_\xi(s) \\ f_\eta(s) \end{bmatrix} = -\begin{bmatrix} 0 & -k_4 \\ k_4 & 0 \end{bmatrix}\begin{bmatrix} \xi(s) \\ \eta(s) \end{bmatrix} + \begin{bmatrix} D(s) \\ F(s) \end{bmatrix}\phi(s).$$

The above input forces are introduced to the lateral vibrations model (21) to obtain the relations between the torsional and lateral vibrations in the closed loop system:

$$\frac{1}{D_{op}}\begin{bmatrix} D_{op}+Bk_4 & -A_2k_4 \\ A_1k_4 & D_{op}+Bk_4 \end{bmatrix}\begin{bmatrix} \xi \\ \eta \end{bmatrix} = \frac{1}{D_{op}}\begin{bmatrix} A_{2d} & B_d \\ -B_d & A_{1d} \end{bmatrix}\begin{bmatrix} D \\ F \end{bmatrix}\phi$$

Using above relation we can find the transfer functions between the lateral vibrations and torsional vibrations in the following form:

$$\begin{bmatrix} \xi \\ \eta \end{bmatrix} = \frac{1}{D_{op}D_{cl}}\begin{bmatrix} \left(D_{op}+Bk_4\right)\left(A_2D+BF\right)-A_1k_4\left(A_1F-BD\right) \\ A_2k_4\left(A_2D+BF\right)+\left(D_{op}+Bk_4\right)\left(A_1F-BD\right) \end{bmatrix}\phi$$

where D_{cl} is the characteristic polynomial of the closed-loop system (60) designed to control lateral vibrations:

$$D_{cl}=D_{op}+2B_dk_4+k_4^2.$$

In case of the minimal realization of the transfer functions the polynomial D_{op} from the denominator should be compensated by the same polynomial in the numerator. The above considerations lead to the reduced scheme (Fig. 34) were we have the following transfer functions:

$$G_{1c}=\frac{\left(D_{op}+Bk_4\right)\left(A_2D+BF\right)-A_1k_4\left(A_1F-BD\right)}{D_{op}D_{cl}},$$

$$G_{2c}=\frac{A_2k_4\left(A_2D+BF\right)+\left(D_{op}+Bk_4\right)\left(A_1F-BD\right)}{D_{op}D_{cl}}.$$

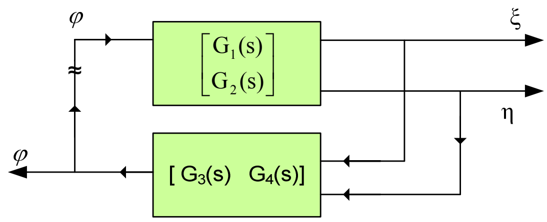

Fig. 34. Reduced block scheme of the closed-loop system with separated transfer functions of lateral and torsional vibrations.

The scheme from the Fig. 34 is very similar to the scheme from Fig. 7. Only the transfer functions $G_1(s)$, $G_2(s)$ was replaced by transfer functions $G_{1c}(s)$, $G_{2c}(s)$.
It means that full analysis of the system dynamics can be carried out according to procedure shown in Chapter 3.

6. SUMMARY

The full analysis of the rotor torsional/lateral vibrations is much simpler when we can divide the system into smaller subsystems. In this case the calculations are simplified
and we have deep insight into mechanisms leading to good or bed behaviour of the rotor motion. It is particularly important in the case of the rotor working in the wide range of the angular speeds. Turbo jet engines and flywheels are such rotors. For the vibration analysis the methods known from control theory was applied. In the paper it is Evans method. As well some other control methods can also be used to the vibration analysis.

The proposed approach was testified in the paper on the simple 3-mode rotor model (Jeffcott model). The torsional vibrations were separated from lateral vibrations and a feedback among subsystem was established. The subsystems are coupled by rotor unbalance and Evans method allows us show the critical values of the unbalance which destabilize rotor motion for different angular speeds. The lateral vibrations are stabilized by angular speed (rather gyroscopic effects proportional to the angular speed) and using again Evans method it is possible to find how big value of the rotor speed is sufficient to stabilize rotor motion.

Such analysis of the rotor vibrations appeared very useful for the choice of the control strategy. It indicated such control procedures which amplify the positive (stabilizing) mechanisms in the rotor dynamics. Such procedures can also lead to the energy saving control laws. In the case of lateral vibrations there were considered four control strategies. And these strategies were compared to indicate optimal one.

REFERENCES

1. **Ejkchoff P.** (1980), *Identyfikacja w układach dynamicznych*, PWN, Warszawa.
2. **Gosiewski Z.** (2008), Analysis of coupling mechanism in lateral/torsional rotor vibrations, *Journal of Theoretical and Applied Mechanics*, No. 4, Warsaw.
3. **Gosiewski Z., Muszyńska A.** (1992), *Dynamika maszyn wirnikowych* (*Dynamics of rotating machinery*), Publishing Office of WSInż. Koszalin.
4. **Juang J.-N**. (1994), *Applied System Identification*. Prentice-Hall Inc., (UK).
5. **Kaczorek T. (**1993), *Teoria sterowania i systemów* (*Theory of control and systems*), Wydawnictwo Naukowe PWN.
6. **Muszynska A., Goldman P., Bently D.E.** (1992), Torsional/lateral vibration cross-coupled responses due to shaft anisotropy: a new tool in shaft crack detection, *Conference of Institution of Mechanical Engineers*, Bath, Great Britain.
7. **Preumont A.** (2002), *Vibration Control of Active Structures: An Introduction*, Kluwer Academic Publishers, Dordrecht.
8. **Ulbrich H., Gunthner W.** (Editors) (2005), *Proc. IUTAM Symposium on Vibration Control of Nonlinear Mechanisms and Structures*. Munich, Germany. Springer, Dordrecht, the Netherlands.

The work is a part of project number PBZ-KBN-109/T-10/2004 supported by State Committee for Scientific Research.

H_∞ CONTROL OF ROBOT ARM WITH HYDRAULIC DRIVE

Zdzisław GOSIEWSKI*, Grzegorz MICHAŁOWSKI*

* Faculty of Mechanical Engineering, Białystok Technical University, ul. Wiejska 45 C, 15-351 Białystok

gosiewski@pb.edu.pl, g.m@onet.eu

Abstract: In the paper an H_∞ velocity control of the robot arm in combination with the hydraulic drive is presented. The open-loop system consists of a manipulator with one rotary degree of freedom, a hydraulic servomotor, and an electrohydraulic amplifier. The mathematical model of the system is derived. Due to the nonlinearity in the model, which is caused by varying operating point parameters and the direction of the servomotor motion, the model of multiplicative uncertainty was defined. The plant model transfer function parameters were assumed to be variable. To limit error signal, control signal, and output signal three weighting functions were designed. The simulation results of the designed H_∞ optimal closed-loop system were compared to the standard PID closed-loop system. The solution ensuring robust performance was achieved and proved.

1. INTRODUCTION

Nowadays, industrial robots (manipulators) are widely used in manufacturing tasks. The manipulators are driven by hydraulic servomotors, and there is an obvious need to achieve robust performance in case of, for example, varying parameters that describe such systems. These factors influence on time and frequency quality of the system, and the standard control methods may not be sufficient in such cases. Thus, in this paper the H_∞ robust control is analyzed. The considered system consists of three main elements: the manipulator, which angular velocity is to be controlled, the hydraulic servomotor, and the electrohydraulic amplifier as an actuator. Models of these elements are combined to form the plant model with uncertain values of the transfer function parameters. The servomotor with the manipulator is a simplified, plane mechanism with one rotary degree of freedom. To obtain a simple model of the plant some simplifications were necessary. Moment of inertia of the servomotor, clearance between joints, and friction forces were omitted. Additionally, the stiffness of the structure was assumed to be infinite. Design procedure of the H_∞ robust controller requires the model of uncertainty and the weighting functions to be included, thus, they are to be designed. Every transfer function presented in the article is taken to be a function of s, therefore the (s) notation will be dropped henceforth.

2. CONTROL PLANT

All the considered elements of the open-loop system have been identified in (Henzel, 2004) and (Cedro, 2007). The first element of the plant is the electrohydraulic amplifier with the following 2nd-order transfer function:

$$G_1 = \frac{4800}{s^2 + 400\,s + 48000} \text{ (Henzel, 2004).} \tag{1}$$

The model of the servomotor with the manipulator, shown in Fig. 1, has been experimentally derived and has the general 2nd-order form with three varying parameters:

$$G_2 = \frac{b_0}{s^2 + a_1\,s + a_0} \text{ (Cedro, 2007).} \tag{2}$$

The possible values of parameters: b_0, a_1 and a_0, depending on the operating point parameters, have been determined as well (Fig. 2). Due to the structural constraints, the rotational angle of the robot arm can vary from 0.4 to 1.5 rad.

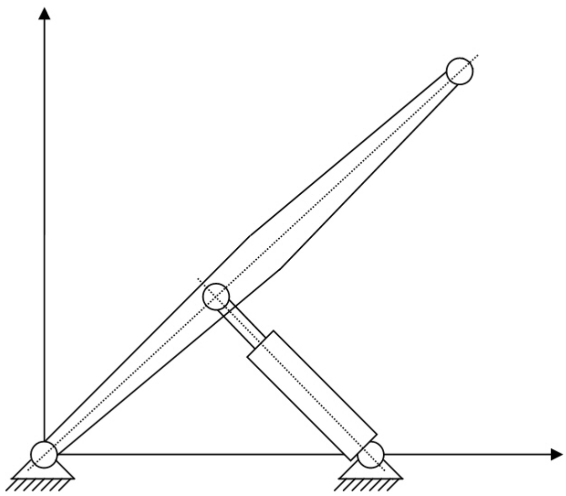

Fig. 1. Sample configuration of servomotor and manipulator with one rotary degree of freedom

Introduced elements are combined to form the open-loop system model, which is assumed to be the product of transfer function of the actuator (1) and transfer function of the servomotor/arm (2) with three varying parameters, and it has the following 4th-order form:

$$G = \frac{4800}{s^2 + 400s + 48000} \cdot \frac{b_0}{s^2 + a_1 s + a_0}. \tag{3}$$

The voltage is the input signal to the plant, and the angular velocity of the robot arm, φ_0, is the output signal. The displacement of the hydraulic piston, x_0 is the transitional signal between amplifier and servomotor.

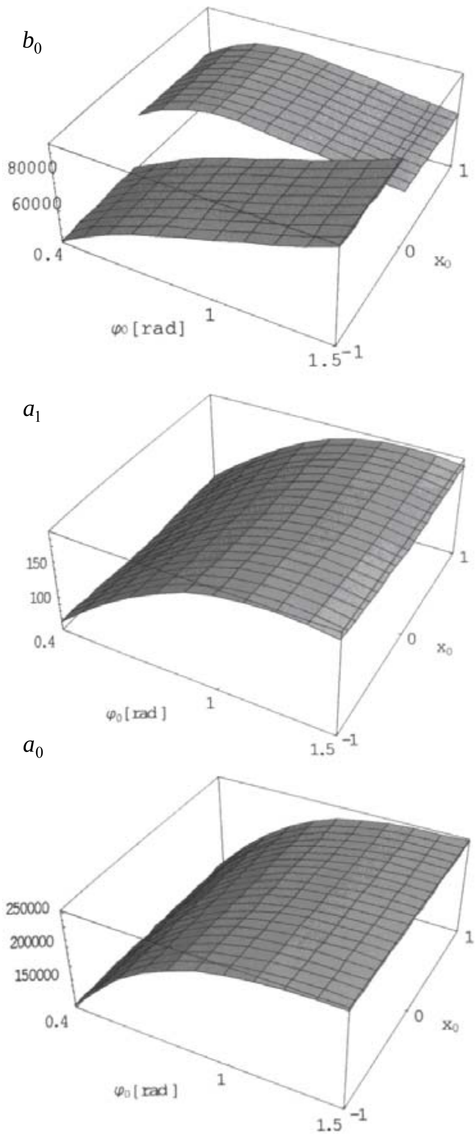

Fig. 2. Relationship between plant model parameters and operating point parameters, φ_0 – rotational angle of the robot arm, x_0 – displacement of the hydraulic piston (Henzel, 2004)

To reduce the number of considered variants resulting from (3) and Fig. 2, the nominal (4), the minimal (5), and the maximal (6) transfer functions were defined as follows:

$$G_0 = \frac{4800}{s^2 + 400s + 48000} \cdot \frac{65000}{s^2 + 125s + 175000}, \tag{4}$$

$$G_{\min} = \frac{4800}{s^2 + 400s + 48000} \cdot \frac{40000}{s^2 + 50s + 100000}, \tag{5}$$

$$G_{\max} = \frac{4800}{s^2 + 400s + 48000} \cdot \frac{90000}{s^2 + 200s + 250000}. \tag{6}$$

The nominal plant model was assumed to be the transfer function with parameters: b_0, a_1, and a_0, calculated as the arithmetic mean of their extreme values. The minimal and the maximal plant models were taken to have respectively minimal and maximal values of the transfer function parameters: b_0, a_1, and a_0. Notice that the maximal model has the least gain (Figs. 3, 4).

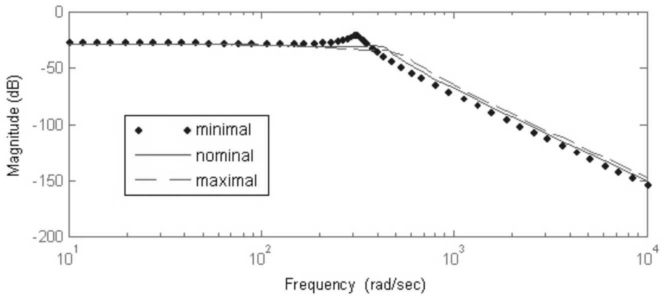

Fig. 3. Magnitude-frequency plots of the nominal, the minimal, and the maximal plant model

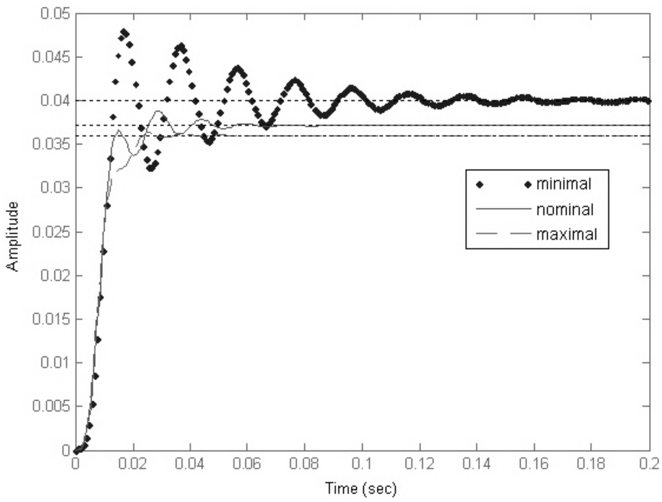

Fig. 4. Step responses of the nominal, the minimal, and the maximal plant model

3. DESIGN PROCESS OF H_∞ ROBUST CONTROL SYSTEM

The H_∞ robust control problem is to achieve such K controller that provides minimization of the H_∞ norm of the considered closed-loop system described by the transfer function $F(G, K)$, where G is the plant model:

$$\|H\|_\infty = \sup_{\omega \in R} \left(F(G,K)(j\omega) \right). \tag{7}$$

H_∞ norm is the supremum (upper bound) of the maximum singular value of the closed-loop system represented in the frequency domain.

3.1. Design process of PID controller

The design of the PID controller is based on the nominal plant model G_0 and is required to obtain the sensitivity function, the control function, and the complementary sensitivity function, which are essential to the further weighting functions design. The ideal PID controller parameters were selected to achieve zero overshoot and sufficiently short settling time of the closed-loop system:

$$K_{\mathrm{PID}} = K_{\mathrm{p}}\left(1+\frac{1}{T_{\mathrm{i}}s}+T_{\mathrm{d}}s\right)=10\left(1+\frac{1}{0.01s}+0.001s\right), \qquad (8)$$

where: K_p – proportional gain, T_i – integral time, T_d – derivative time.

The transfer function (8) was then approximated by the proper transfer function of the physically realizable PID controller that is described as follows:

$$K_{\mathrm{PID}} = 10\left(1+\frac{1}{0.01s}+\frac{0.001s}{0.001s+1}\right). \qquad (9)$$

3.2. Weighting functions

The first requirement of the H_∞ robust controller design procedure is the proper choice of the weighting functions that limit the error signal, the control signal, and the output signal. For the purpose of the robust design three weighting functions W_e, W_u, and W_y were designed. They are based on the sensitivity function, the control function, and the complementary sensitivity function, respectively:

$$S=\left(I+K\,G_0\right)^{-1}, \qquad (10)$$

$$R=K\left(I+K\,G_0\right)^{-1}, \qquad (11)$$

$$T=K\,G_0\,S, \qquad (12)$$

where K was taken to be K_{PID} (9). The designed weighting functions have the forms:

$$W_\mathrm{e}=\frac{8.5s+100}{30s+0.1}, \qquad (13)$$

$$W_\mathrm{u}=\frac{s+22}{22s+720}, \qquad (14)$$

$$W_\mathrm{y}=\frac{s+1500}{0.1s+1500}. \qquad (15)$$

Magnitude-frequency plots of the weighting functions (13)–(15) with corresponding system functions for standard PID closed-loop system are presented in Fig. 5.

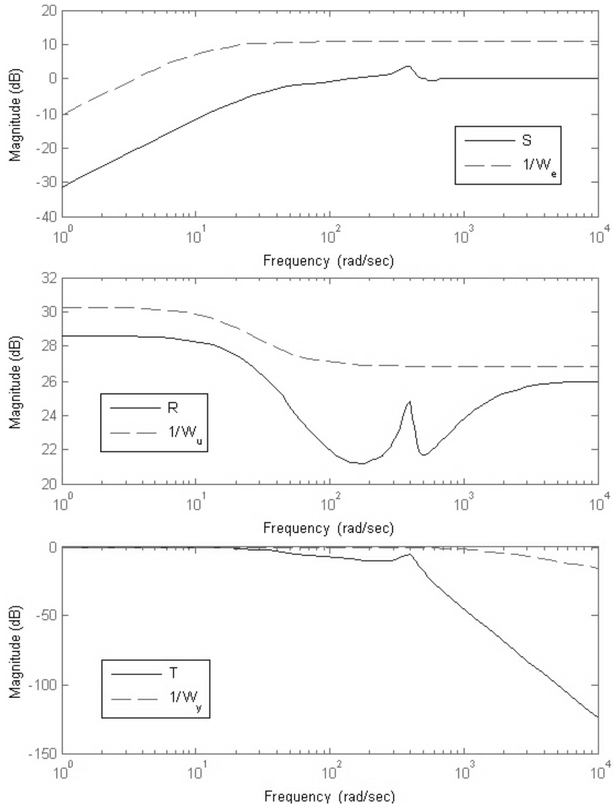

Fig. 5. Magnitude-frequency plots of the weighting functions W_e, W_u, W_y and corresponding standard PID system functions

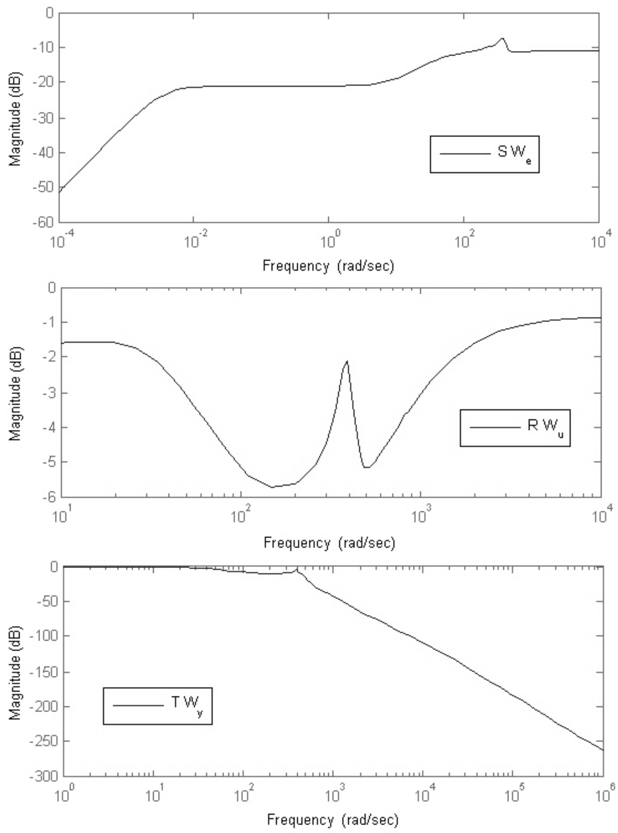

Fig. 6. Graphic interpretation of the conditions (16)–(18)

Weighting functions are properly designed since they satisfy conditions:

$$\left|W_e(j\omega)S(j\omega)\right| \le 1, \quad \forall \omega \,, \tag{16}$$

$$\left|W_u(j\omega)R(j\omega)\right| \le 1, \quad \forall \omega \,, \tag{17}$$

$$\left|W_y(j\omega)T(j\omega)\right| \le 1, \quad \forall \omega \,. \tag{18}$$

The maximal gain of the considered products does not exceed the magnitude of 1, which in the logarithmic scale equals 0 dB, for every case (Fig. 6).

3.3. Model of uncertainty

The second requirement of the H_∞ controller design procedure is connected with the definition of uncertainty. The robust controller should ensure sufficient time and frequency quality of the closed-loop system even in case of the difference between the real plant and its assumed nominal model. In general, there are two kinds of uncertainty models: additive and multiplicative, which we define as follows:

$$\Delta_A = G_{max} - G_0 \,, \tag{19}$$

$$\Delta_M = \frac{G_{max} - G_0}{G_0} \,. \tag{20}$$

Thus, the nominal model of the plant with each uncertainty will have the general form, respectively:

$$G_A = G_0 + \Delta_A \,, \tag{21}$$

$$G_M = G_0 \cdot (1 + \Delta_M) \,. \tag{22}$$

In both cases, the 8th-order uncertainty model is produced. To check the differences between each interconnection to the nominal plant model, consider Fig. 7.

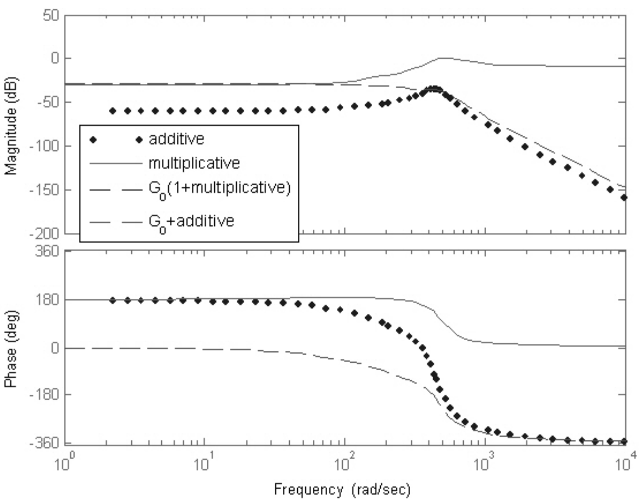

Fig. 7. Bode plots of additive and multiplicative uncertainty models, and their interconnection to the nominal plant model

It is shown that there is no difference between each interconnection (two dashed lines agree with each other), thus, to include varying model parameters the multiplicative uncertainty was chosen (22, Fig. 8b).

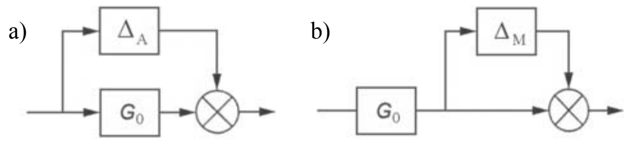

Fig. 8. Representation of additive (a) and multiplicative (b) uncertainty

3.4. Design process of H_∞ controller

To obtain the H_∞ robust controller a plant augmentation is required. The expanded model includes 4th-order nominal plant model G_0, 8th-order multiplicative uncertainty Δ_M, and three of 1st-order weighting functions W_e, W_u, W_y what produces 15th-order augmented plant model. Due to the above, the designed controller is described by 15th-order transfer function as well. Therefore, to reduce system complexity, the controller reduction should be applied. To do it, the *Hankel Singular Values* method was used. This technique estimates the "energy" of each controller state, keeping major states and discarding the minor ones. Keeping larger "energy" states of the controller preserves most of its characteristics in terms of stability, frequency, and time responses (Balas et al., 2007). Due to the only one dominant state in this case, the 14 states were safely rejected (Fig. 9).

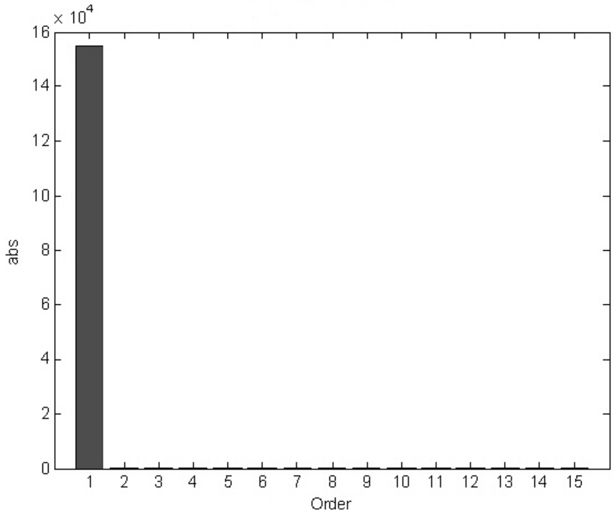

Fig. 9. Hankel singular value plot of the 15th-order controller

Thus, the H_∞ robust controller can be simplified to the 1st-order transfer function:

$$K = \frac{1033}{s + 0.003334} \,. \tag{23}$$

The time-domain comparison between 15th-order robust controller, reduced 1st-order robust controller, and standard PID controller (9) is shown in Fig. 10.

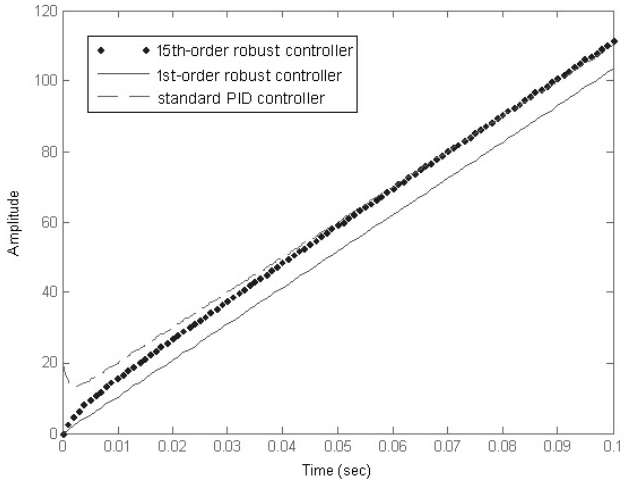

Fig. 10. Step responses: 15th-order robust controller, reduced 1st-order robust controller, and standard PID controller

It is shown that in the transient state of the closed-loop system the reduced robust controller acts as an integrator, and due to its very high gain the steady-state error is almost equal to zero. This can be proved using the *Final Value Theorem* (Franklin et al., 2002).

To determine the H_∞ system functions *S*, *R*, *T* the designed robust controller (23) can be substituted for *K* in equations (10)–(12). Magnitude-frequency plots of the weighting functions (13)–(15) with corresponding H_∞ system functions are presented in Fig. 11.

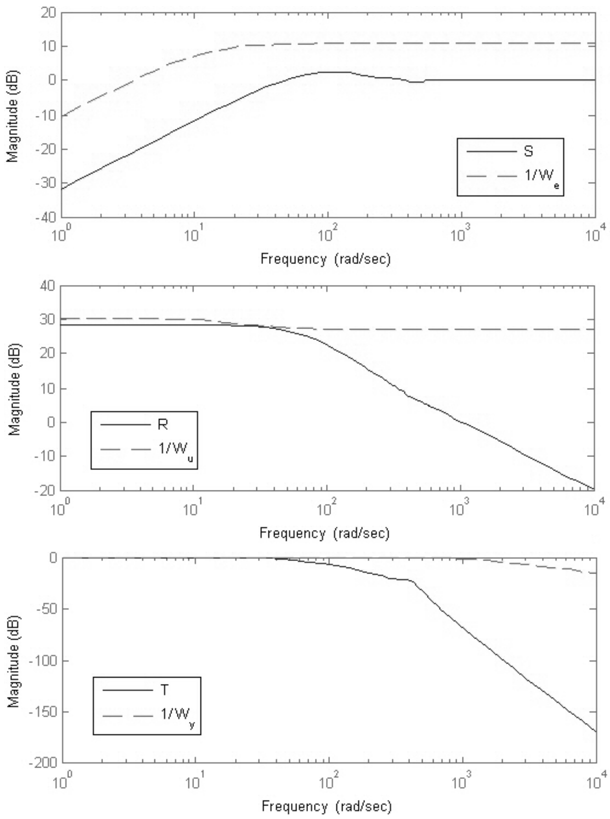

Fig. 11. Magnitude-frequency plots of the weighting functions W_e, W_u, W_y and corresponding H_∞ system functions

The comparison between Figs. 5 and 11 shows that the H_∞ system functions do not contain as high resonant peaks for some frequency as the standard PID system functions, what is the result of the H_∞ norm minimization.

The comparison between step responses of the designed H_∞ closed-loop system and the PID closed-loop system for the uncertainty model is shown in Fig. 12.

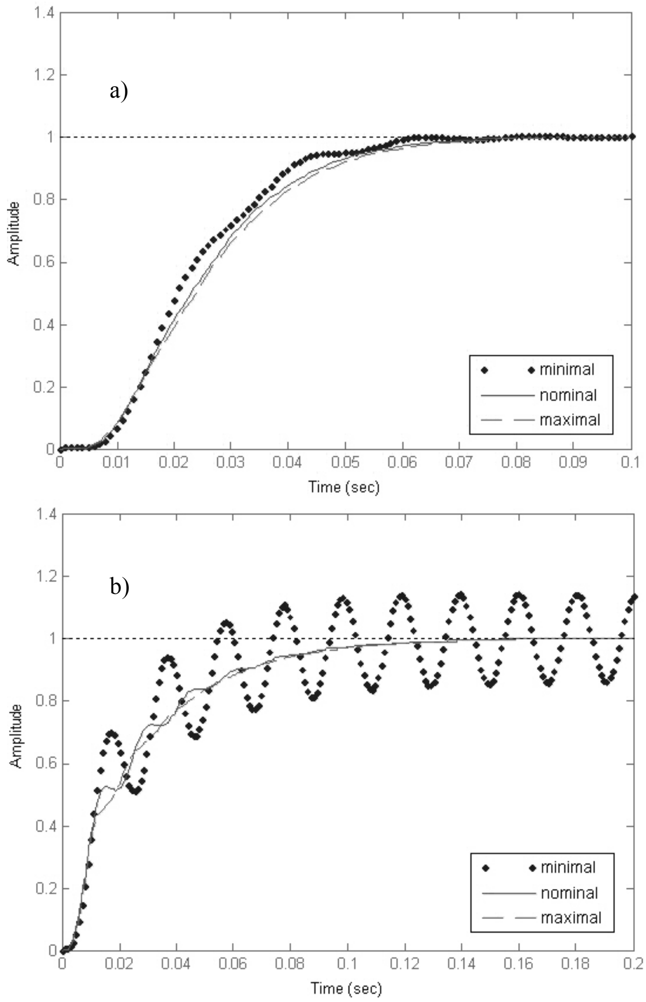

Fig. 12. Step responses: H_∞ closed-loop system (a), PID closed-loop system (b)

The investigated dynamic responses show that the H_∞ closed-loop system achieves better time-domain quality than the PID closed-loop system, since there is no overshoot and settling time is sufficiently short for each plant model with extreme values of varying parameters. Using standard PID control in this case can lead to oscillations of the output signal. Thus, PID controller might not provide stability of the system with, for example, higher ranges of varying parameters.

The comparison between frequency responses of the H_∞ closed-loop system and the PID closed-loop system for the uncertainty model is shown in Fig. 13.

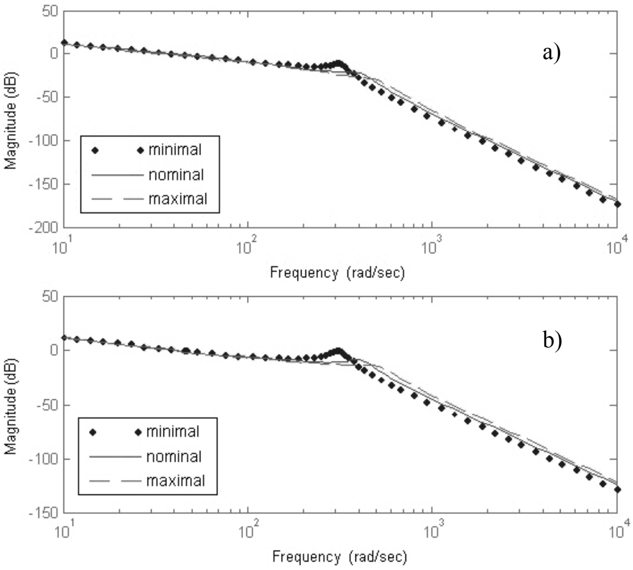

Fig. 13. Magnitude-frequency plots: H_∞ closed-loop system (a), PID closed-loop system (b)

The investigated responses show that the H_∞ closed-loop system achieves better frequency-domain quality than PID closed-loop system, since there is higher high-frequency decrease than in the standard PID closed-loop system. Therefore, the robust control system can more effectively attenuate sensor noises and other high-frequency disturbances, which could otherwise shift themselves to lower frequencies.

4. CONCLUSION

In the paper the H_∞ robust control method was applied to control the robot arm angular velocity. Due to time-varying plant model parameters, the multiplicative uncertainty model was defined. To satisfy the H_∞ robust controller design procedure requirements, three weighting functions were taken into account as well. The time and frequency responses of the robust control system and the standard PID closed-loop system were investigated. The H_∞ robust system showed better quality and manifested robust performance in spite of uncertainties in the plant model.

REFERENCES

1. **Balas G.**, **Chiang R., Packard A., Safonov M.** (2007), *Robust Control Toolbox*. *User's Guide*, The MathWorks Inc.
2. **Cedro L.** (2007), *Identification of the systems with hydraulic drives by using of differential filters* (in Polish), Ph.D. Thesis, Kielce University of Technology.
3. **Dorf R.C., Bishop R.H.** (2005), *Modern Control Systems*, 10th Edition, Prentice Hall.
4. **Franklin G.F., Powell J.D., Emami-Naeini A.** (2002), *Feedback Control of Dynamic Systems*, 4th Edition, Prentice Hall.
5. **Gosiewski Z., Mystkowski A.** (2006), One-DoF robust control of shaft supported magnetically, *Archives of Control Sciences*, Vol. 16, No. 3, 327–339.
6. **Henzel M.** (2004), *New control methods of aircraft's electrohydraulic servodrive* (in Polish), Ph.D. Thesis, Military University of Technology, Warsaw.
7. **Zhou K., Doyle J.C.** (1998), *Essentials of Robust Control*, Prentice Hall.

REALIZATION PROBLEM FOR SINGULAR POSITIVE SINGLE-INPUT SINGLE-OUTPUT CONTINUOUS-TIME SYSTEMS WITH DELAYS IN STATE AND IN INPUTS

Tadeusz Kaczorek*

* Faculty of Electrical Engineering, Bialystok Technical University, ul. Wiejska 45D, 15-351 Bialystok

kaczorek@isep.pw.edu.pl

Abstract: The positive realization problem for singular continuous-time linear single-input single-output systems with delays in state and in inputs is addressed. The notion of canonical forms of matrices are extended for singular linear systems with delays. Necessary and sufficient conditions for positivity of the singular continuous-time systems with delays and sufficient conditions for the existence of a positive singular realization are established. A procedure for computation of a positive singular realization of a given transfer function is proposed and illustrated by a numerical example.

1. INTRODUCTION

In positive systems inputs, state variables and outputs take only non-negative values. Examples of positive systems are industrial processes involving chemical reactors, heat exchangers and distillation columns, storage systems, compartmental systems, water and atmospheric pollution models. A variety of models having positive linear systems behaviour can be found in engineering, management science, economics, social sciences, biology and medicine, etc.

Positive linear systems are defined on cones and not on linear spaces. Therefore, the theory of positive systems is more complicated and less advanced. An overview of state of the art in standard delay systems is given in Górecki et all (1989) and in positive systems theory is given in the monographs Farina and Rinaldi (2000), Kaczorek (2002). Recent developments in positive systems theory and some new results are given in Kaczorek (2003). Realizations problem of positive linear systems without time-delays has been considered in many papers and books (Benvenuti and Farina, 2004; Farina and Rinaldi 2000; Kaczorek, 2002) .

Recently, the reachability, controllability and minimum energy control of positive linear discrete-time systems with time-delays have been considered in Busłowicz and Kaczorek (2004), Kaczorek (2005), Klamka (1997).

The realization problem for positive multivariable discrete-time systems with one time-delay was formulated and solved in Kaczorek (2004), Kaczorek (2005) and the realization problem for positive continuous-time systems with delays was investigated in Kaczorek (2005).

The main purpose of this paper is to present a method for computation of positive singular realization of a transfer function for singular continuous-time linear systems with delays in state and in input. Sufficient conditions for the existence of a positive singular realization will be established and a procedure for computation of a positive singular realization of a given transfer function will be proposed.

To the best knowledge of the author the realization problem for singular continuous-time linear systems with delays in state vector and in inputs has not been considered yet.

2. POSITIVE SINGULAR SYSTEMS WITH DELAYS

Consider the singular single-input single-output continuous-time linear systems with h delays in state and q delays in inputs

$$E\dot{x}(t) = \sum_{i=0}^{h} A_i x(t-id) + \sum_{j=0}^{q} B_j u(t-jd) \tag{1a}$$

$$y(t) = Cx(t) \tag{1b}$$

where $x(t)\in R^n$, $u(t)$, $y(t)\in R$ are the state vector and scalar input and output, respectively and E, $A_i\in R^{n\times n}$, $i = 0,1,...,h$, $B_j\in R^n$, $j = 0,1,...,q$, $C\in R^{1\times n}$, $d > 0$ is delay.
It is assumed that det E=0 and the characteristic polynomial is nonzero, i.e.

$$d(s,w) = \det[Es - A_0 - A_1 w - \dots - A_h w^h] \neq 0, \quad w = e^{-sd} \tag{2}$$

It is also assumed that the initial conditions for (1a)

$$x_0(t),\ t\in[-hd,\ 0),\ u_0(t),\ t\in[-qd,\ 0) \tag{3}$$

belong to the set of admissible initial conditions.

The transfer function of the system (1) is given by

$$T(s,w) = C[Es - A_0 - A_1 w - \ldots - A_h w^h]^{-1}(B_0 + B_1 w + \ldots + B_q w^q) \tag{4}$$

Let us assume that the matrices of the system (1) have the following canonical forms

$$E = \left[\begin{array}{c|c} I_{n-1} & 0 \\ \hline 0 & 0 \end{array}\right] \in R^{n\times n},\ A_0 = \begin{bmatrix} 0 & 0 & \cdots & 0 & 0 & 0 & \cdots & 0 & a_{01} \\ 1 & 0 & \cdots & 0 & 0 & 0 & \cdots & 0 & a_{02} \\ \cdots & \cdots & \cdots & \cdots & \cdots & \cdots & \cdots & \cdots & \cdots \\ 0 & 0 & \cdots & 1 & 0 & 0 & \cdots & 0 & a_{0r} \\ 0 & 0 & \cdots & 0 & -1 & 0 & \cdots & 0 & 1 \\ 0 & 0 & \cdots & 0 & 0 & 1 & \cdots & 0 & 0 \\ \cdots & \cdots & \cdots & \cdots & \cdots & \cdots & \cdots & \cdots & \cdots \\ 0 & 0 & \cdots & 0 & 0 & 0 & \cdots & 1 & 0 \end{bmatrix} \in R^{n\times n}$$

$$A_i = [0 \mid a_i] \in R^{n\times n},\ i = 1,\ldots,h,\ a_i = [a_{i1}\ \ a_{i2}\ \ \ldots\ \ a_{ir}\ \ 0\ \ \ldots\ \ 0]^T \tag{5}$$

$$B_j = [b_{j1}\ \ b_{j2}\ \ \ldots\ \ b_{jr}\ \ -b_{jr+1}\ \ \ldots\ \ -b_{jn}]^T,\ j = 0,1,\ldots,q,\ C = [0\ \ \ldots\ \ 0\ \ 1] \in R^{1\times n}$$

where the superscript T denotes the transpose.

Definition 1.

The system (1) is called (internally) positive if for any admissible conditions $x_0(t)\in R^n_+$, $t \in [-hd, 0)$, $u_0(t) \in R_+$, $u^{(p)}(t)=d^p u(t)/dt^p \in R_+$ for $t\in [-pd, 0)$ and all inputs $u(t)\in R_+$, $u^{(p)}(t) \in R_+$, $(0 \le p < n)$, $t \ge 0$, $x(t)\in R_+$, for $t \ge 0$. Let M_n be the set of Metzler matrices, i.e. the set of real matrices with nonnegative off-diagonal entries.

Theorem 1.

The system (1) with matrices in the canonical forms (5) is positive if and only if

– the entries of A_i, i=0,1,…,h are nonnegative except α_{0r} which can be arbitrary
– the entries b_{ji}, j=0,1,…,q; i=1,…,n of B_j, j=0,1,…q of the form (5) are nonnegative

Proof.

Let $x(t)=[x_1(t)\ \ x_2(t)\ \ \ldots\ \ x_n(t)]^T$. Then from (1a) and (5) we obtain

$$\begin{cases} \dot{x}_1(t) = a_{01}x_n(t) + \sum_{i=1}^{h} a_{i1}x_n(t-id) + \sum_{j=0}^{q} b_{j1}u(t-jd) \\ \dot{x}_2(t) = x_1(t) + \sum_{i=0}^{h} a_{i2}x_n(t-id) + \sum_{j=0}^{q} b_{j2}u(t-jd) \\ \cdots\cdots\cdots\cdots\cdots\cdots\cdots\cdots\cdots \\ \dot{x}_r(t) = x_{r-1}(t) + \sum_{i=0}^{h} a_{ir}x_n(t-id) + \sum_{j=0}^{q} b_{jr}u(t-jd) \end{cases} \tag{6}$$

$$\begin{cases} \dot{x}_{r+1}(t) = -x_r(t) + x_n(t) - \sum_{j=0}^{q} b_{jr+1}u(t-jd) \\ \dot{x}_{r+2}(t) = x_{r+1}(t) - \sum_{j=0}^{q} b_{jr+2}u(t-jd) \\ \cdots\cdots\cdots\cdots\cdots\cdots\cdots\cdots\cdots \\ \dot{x}_{n-1}(t) = x_{n-2}(t) - \sum_{j=0}^{q} b_{jn-1}u(t-jd) \end{cases} \tag{7}$$

$$0 = x_{n-1}(t) - \sum_{j=0}^{q} b_{jn}u(t-jd) \tag{8}$$

From (8) and (7) we have

$$\begin{cases} x_{n-1}(t) = \sum_{j=0}^{q} b_{jn}u(t-jd) \\ x_{n-2}(t) = \sum_{j=0}^{q}\left(b_{jn}\dot{u}(t-jd) + b_{jn-1}u(t-jd)\right) \\ \cdots\cdots\cdots\cdots\cdots\cdots\cdots\cdots\cdots \\ x_{r+1}(t) = \sum_{j=0}^{q}\left(b_{jn}u^{(p-1)}(t-jd) + b_{jn-1}u^{(p-2)}(t-jd) + \ldots + b_{jr+2}u(t-jd)\right) \\ x_n(t) = x_r(t) + \sum_{j=0}^{q}\left(b_{jn}u^{(p)}(t-jd) + b_{jn+1}u^{(p-1)}(t-jd) + \ldots + b_{jr+1}u(t-jd)\right), \\ p = n-r-1 \end{cases} \tag{9}$$

Substitution of the last equation of (9) into (6) yields a system of r differential equations with delays and constant coefficients.

The system is a positive one if and only if the conditions i) and ii) are satisfied.

3. FORMULATION OF THE REALIZATION PROBLEM

Definition 2.

Matrices $A_0 \in M_n$, E, $A_i \in R_+^{n\times n}$, i=1,…,h the entries b_{ji} of B_j, i=1,…,n; j=0,1,…,q of the form (5) are nonnegative,

$$C \in R_+^{1\times n} \tag{10}$$

are called a positive singular realization of a given transfer function $T(s,w)$ if they satisfy the equality (4). A realization is called minimal if the dimension $n\times n$ of E and A_i i=0,1,…,h is minimal among all realizations of $T(s,w)$.

The positive singular realization problem can be stated as follows. Given an improper transfer function of the form

$$T(s,w) = \frac{b_m(w)s^m + \ldots + b_{r+1}(w)s^{r+1} + b_r(w)s^r + \ldots + b_1(w)s + b_0(w)}{s^n - a_{n-1}(w)s^{n-1} - \ldots - a_1(w)s - a_0(w)} \quad (r = m - n \geq 0) \tag{11a}$$

where

$$\begin{aligned} a_i(w) &= a_{iq}w^q + \ldots + a_{i1}w + a_{i0}, \quad i = 0,1,...,n-1 \\ b_j(w) &= b_{q,j+1}w^q + \ldots + b_{1,j+1}w + b_{0,j+1}, \quad j = 0,1,...,m \end{aligned} \tag{11b}$$

Find a positive singular realization (10) of $T(s,w)$.

In this paper sufficient conditions for the existence of the positive singular realization (10) of $T(s,w)$ will be established and a procedure for computation of a positive singular realization will be proposed.

4. SOLUTION OF THE PROBLEM

Solution of the problem is based on the following two lemmas.

Lemma 1.

If

$$E = \left[\begin{array}{c|c} I_m & 0 \\ \hline \multicolumn{2}{c}{0} \end{array}\right] \in R^{(m+1)\times(m+1)},$$

$$A_0 = \begin{bmatrix} 0 & 0 & \cdots & 0 & 0 & 0 & \cdots & 0 & a_{00} \\ 1 & 0 & \cdots & 0 & 0 & 0 & \cdots & 0 & a_{10} \\ \cdots & \cdots & \cdots & \cdots & \cdots & \cdots & \cdots & \cdots & \cdots \\ 0 & 0 & \cdots & 1 & 0 & 0 & \cdots & 0 & a_{n-1,0} \\ 0 & 0 & \cdots & 0 & -1 & 0 & \cdots & 0 & 1 \\ 0 & 0 & \cdots & 0 & 0 & 1 & \cdots & 0 & 0 \\ \cdots & \cdots & \cdots & \cdots & \cdots & \cdots & \cdots & \cdots & \cdots \\ 0 & 0 & \cdots & 0 & 0 & 0 & \cdots & 1 & 0 \end{bmatrix} \in R^{(m+1)\times(m+1)}$$

$$A_i = \begin{bmatrix} 0 & \cdots & 0 & a_{0i} \\ 0 & \cdots & 0 & a_{1i} \\ \cdots & \cdots & \cdots & \cdots \\ 0 & \cdots & 0 & a_{n-1,i} \\ 0 & \cdots & 0 & 0 \\ \cdots & \cdots & \cdots & \cdots \\ 0 & \cdots & 0 & 0 \end{bmatrix} \in R^{(m+1)\times(m+1)}, i = 1,...,h \tag{12}$$

then

$$d(s,w) = \det[Es - A_0 - A_1w - \ldots - A_hw^h] = -s^n + a_{n-1}(w)s^{n-1} + \ldots + a_1(w)s + a_0(w) \tag{13}$$

Proof.

The expansion of the determinant with respect to m+1-th column yields

$$\det[Es - A_0 - A_1w - ... - A_hw^h] = \begin{vmatrix} s & 0 & ... & 0 & 0 & 0 & ... & 0 & -a_0(w) \\ -1 & s & ... & 0 & 0 & 0 & ... & 0 & -a_1(w) \\ ... & ... & ... & ... & ... & ... & ... & ... & ... \\ 0 & 0 & ... & -1 & s & 0 & ... & 0 & -a_{n-1}(w) \\ 0 & 0 & ... & 0 & 1 & s & ... & 0 & -1 \\ 0 & 0 & ... & 0 & 0 & -1 & ... & 0 & 0 \\ ... & ... & ... & ... & ... & ... & ... & ... & ... \\ 0 & 0 & ... & 0 & 0 & 0 & ... & -1 & 0 \end{vmatrix} = -s^n + a_{n-1}(w)s^{n-1} + ... + a_1(w)s + a_0(w)$$

where $\alpha_i(w)$, $i=0,1,\ldots,n$-1 are defined by (11b).

Lemma 2.

If the matrices E and A_i i=0,1,…,h have the forms (12) then the m+1-th row of the adjoint matrix

$$\mathrm{Adj}\ [Es - A_0 - A_1 w - \ldots - A_h w^h] \tag{14}$$

has the form

$$R_{m+1}(s) = [-1 \quad -s \quad \ldots \quad -s^r \quad s^{r+1} \quad \ldots \quad s^m] \tag{15}$$

Proof.

Taking into account that

$$\mathrm{Adj}\ [Es - A_0 - A_1 w - \ldots - A_h w^h][Es - A_0 - A_1 w - \ldots - A_h w^h] = I_{m+1} d(s,w)$$

it is easy to verify that

$$R_{m+1}(s)[Es - A_0 - A_1 w - \ldots - A_h w^h] = [0 \quad \ldots \quad 0\ 1] d(s,w)$$

Taking into account (4), (5) (13) and (15) we may write

$$T(s,w) = C[Es - A_0 - A_1 w - \ldots - A_h w^h]^{-1} (B_0 + B_1 w + \ldots + B_q w^q] =$$

$$\frac{[-1 \quad -s \quad \ldots \quad -s^r \quad s^{r+1} \quad \ldots \quad s^m]}{-s^n + a_{n-1}(w)s^{n-1} + \ldots + a_1(w)s + a_0(w)} \begin{bmatrix} b_{01} + b_{11}w + \ldots + b_{q1}w^q \\ \ldots\ldots\ldots\ldots \\ b_{0r} + b_{1r}w + \ldots + b_{qr}w^q \\ -b_{0r+1} - b_{1r+1}w - \ldots - b_{qr+1}w^q \\ \ldots\ldots\ldots\ldots \\ -b_{0m+1} - b_{1m+1}w - \ldots - b_{qm+1}w^q \end{bmatrix} = \tag{16}$$

$$\frac{b_m(w)s^m + \ldots + b_{r+1}(w)s^{r+1} + b_r(w)s^r + \ldots + b_1(w)s + b_0(w)}{s^n - a_{n-1}(w)s^{n-1} - \ldots - a_1(w)s - a_0(w)}$$

where $\alpha_i(w)$ and $b_j(w)$ are defined by (11b).

Comparison of the coefficients at the same power of s and w of the numerators of the equality (16) yields the desired entries of B_j, j = 0,1,…,q.

Knowing the coefficients $\alpha_{ii,}$ i = 0,1,…,n-1; j = 0,1,…,q of the denominator $d(s,w)$ of the transfer function (11) we may find the matrices A_i, i = 0,1,…,h and knowing the coefficients of its numerator we may find the matrices B_j of the form

$$B_j = \left[b_{j1} \cdots b_{jr} - b_{j,r+1} \cdots - b_{j,m+1}\right]^T, \quad j = 0,1,...,q \tag{17}$$

Theorem 2.

There exist a positive singular realization of the form (5) of the transfer function (11) if

– the coefficients $\alpha_{ii,}$ i = 0,1,…,n-1; j = 0,1,…,q are nonnegative except α_{0r} which can be arbitrary
– the coefficients $b_{ji,}$ j = 0,1,…,m; i = 1,…,q are nonnegative

Proof.

If the condition i) is satisfied then A_0 is a Metzler matrix and $A_i \in R_+^{(m+1)\times(m+1)}$, i = 1,…,h. From (17) it follows that if the condition ii) is met then the matrices B_j, j = 0,1,…,q have nonnegative entries. The matrix C is independent of $T(s,w)$ and has the canonical form (5). Therefore, if both conditions are satisfied then by Theorem 1 the realization is a positive one.

If the conditions of Theorem 2 are satisfied then the positive singular realization (10) of (11) can be found by the use of the following procedure.

Procedure:

Step 1.

For a given transfer function (11) find n, m, r and

$$q = \max_{i,j} \ \deg_w[a_i(w),\ b_j(w)] \quad \text{for} \quad i = 0,1,...,n-1;\ j = 0,1,...,m \tag{18}$$

($\deg_w(\cdot)$ denotes the degree of (·)with respect to w)

Step 2.

Knowing the coefficients $\alpha_{ii,}$ i = 0,1,…,n-1; j = 0,1,…,q of the denominator $d(s,w)$ of (11) find the matrices (12) satisfying (13).

Step 3.

Knowing the coefficients $b_{ji,}$ j = 0,1,…,$m+1$; i = 0,1,…,q and using (17) find the matrices $B_j \in R_+^{m+1}$, j = 0,1,…,q and the matrix C of the form (5).

Example.

Compute a positive singular realization (5) of the transfer function

$$T(s,w)=\frac{w^3s^3+(w^3+1)s^2+(w+2)s+(w^2+2w+1)}{s^2-(2w^2+1)s-(w+1)} \quad (19)$$

It is easy to verify that the transfer function (19) satisfies the conditions of Theorem 2. Using the Procedure we obtain

Step 1.

In this case using (18) for (19) we obtain n = 2, m = 3 and

$$q=\max_{i,j}\ \deg_w[a_i(w),\ b_j(w)]=3 \text{ and } r=1 \quad (20)$$

Step 2.

Taking into account that

$a_0(w)=w+1,\ \ a_1(w)=2w^2+1$

we obtain

$$E=\begin{bmatrix}1&0&0&0\\0&1&0&0\\0&0&1&0\\0&0&0&0\end{bmatrix},\ A_0=\begin{bmatrix}0&0&0&1\\1&0&0&1\\0&-1&0&1\\0&0&1&0\end{bmatrix},$$
$$A_1=\begin{bmatrix}0&0&0&1\\0&0&0&0\\0&0&0&0\\0&0&0&0\end{bmatrix},\ A_2=\begin{bmatrix}0&0&0&0\\0&0&0&2\\0&0&0&0\\0&0&0&0\end{bmatrix} \quad (21)$$

Step 3.

From (19) we have

$$\begin{aligned}
b_0(w)&=w^2+2w+1=b_{01}+b_{11}w+b_{21}w^2+b_{31}w^3,\\
b_1(w)&=w+2=b_{02}+b_{12}w+b_{22}w^2+b_{32}w^3,\\
b_2(w)&=w^3+1=b_{03}+b_{13}w+b_{23}w^2+b_{33}w^3,\\
b_3(w)&=w^3=b_{04}+b_{14}w+b_{24}w^2+b_{34}w^3
\end{aligned} \quad (22)$$

Using (22) and (17) we obtain

$$B_0=\begin{bmatrix}1\\2\\-1\\0\end{bmatrix},\ B_1=\begin{bmatrix}2\\1\\0\\0\end{bmatrix},\ B_2=\begin{bmatrix}1\\0\\0\\0\end{bmatrix},\ B_3=\begin{bmatrix}0\\0\\-1\\-1\end{bmatrix}, \quad (23)$$

and

$$C=\begin{bmatrix}0&0&0&1\end{bmatrix} \quad (24)$$

The desired positive singular realization of (19) is given by (21), (23) and (24).

5. CONCLUDING REMARKS

The positive realization problem for singular continuous-time linear single-input single-output system with delays in state and in inputs has been considered. The notion of canonical forms of matrices has been extended for singular linear continuous-time systems with delays. Conditions for positivity and for the existence of positive singular realizations have been established for singular linear continuous-time single-input single-output system with delays in state and in inputs. A procedure for computation of a positive singular realization of a given transfer function has been proposed and illustrated by a numerical example.

The considerations can be extended for multi-input multi-output singular continuous-time linear systems with delays in state and in inputs. An extension of these considerations for 2D singular linear systems with delays is an open problem.

REFERENCES

1. **Benvenuti L., Farina L.** (2004), A tutorial on the positive realization problem, *IEEE Trans. Autom. Control*, vol. 49, No 5, pp. 651-664.
2. **Busłowicz M., Kaczorek T.** (2004), Reachability and minimum energy control of positive linear discrete-time systems with one delay, *12th Mediterranean Conference on Control and Automation,* June 6-9, Kuasadasi, Izmir, Turkey.
3. **Farina L., Rinaldi S.** (2000), *Positive Linear Systems*; Theory and Applications, J. Wiley, New York.
4. **Górecki H., Fuksa S., Grabowski P., Korytowski A.** (1989), *Analysis and Synthesis of Time delay Systems*, PWN and J. Wiley. Warszawa.
5. **Kaczorek T.** (2004), Realization problem for positive multivariable linear systems with time-delay, *Proc. Int. Workshop Computational Problems of Electrical Engineering*, Zakopane , pp. 186-192.
6. **Kaczorek T.** (2002), *Positive 1D and 2D Systems*, Springer-Verlag, London.
7. **Kaczorek T.** (2003), Some recent developments in positive systems, *Proc. 7th Conference of Dynamical Systems Theory and Applications*, pp. 25-35, Łódź.
8. **Kaczorek T.** (2004), Realization problem for positive discrete-time systems with delay, *System Science*, vol. 30, No. 4, pp. 117-130.

9. **Kaczorek T.** (2005), Positive minimal realizations for singular discrete-time systems with one delay in state and one delay in control. *Bull. Pol. Acad. Sci. Techn*., vol 52, No 3, pp. 293-298.
10. **Kaczorek T.** (2005), Realization problem for a class of positive continuous-time systems with delays, *Int. J. Appl. Math. Comp. Sci.*, vol. 15, No. 4, pp. 101-107.
11. **Kaczorek T.** (2005), Reachability and minimum energy control of positive discrete-time linear systems with multiple delay in state and control, *44th IEEE CDC-ECC'05*.
12. **Klamka J.** (1977), Relative and absolute controllability of discrete systems with delays in control. *Int. Journal of Control*, vol. 26, no. 1, pp. 65-74.
13. **Klamka J.** (1977), Minimum energy control of discrete systems with delays in control. *Int. Journal of Control,* vol. 26, no. 5, pp. 737-744.

The work was supported by the State Committee for Scientific Research of Poland under grant No. 3 T11A 0006 27

POSITIVE DIFFERENT ORDERS FRACTIONAL 2D LINEAR SYSTEMS

Tadeusz KACZOREK*

* Bialystok Technical University, Faculty of Electrical Engineering, Wiejska 45 D, 15-351 Bialystok

kaczorek@isep.pw.edu.pl

Abstract : A new class of positive different orders fractional 2D linear systems is introduced. A notion of (α, β) orders difference of 2D function is proposed. Fractional 2D state equations of linear systems are given and their solutions are derived using 2D $\mathcal{Z}$-transform. The classical Cayley-Hamilton theorem is extended to the 2D fractional linear systems. Neccesary and sufficient conditions for the positivity, reachability and controllability to zero of the fractional 2D linear systems are established.

1. INTRODUCTION

The most popular models of two-dimensional (2D) linear systems are the models introduced by Roesser (1975), Fornasini-Marchesini (1976, 1978) and Kurek (1985).
The models have been extended for positive systems in Kaczorek (1996, 2002, 2005) and Valcher (1987). An overview of 2D linear system theory is given in Bose (1982, 1985), Gałkowski (1977, 2001), Kaczorek (1985) and some recent result in positive systems has been given in the monographs Farina and Marchesini (2000), Kaczorek (2002) and in paper Valcher (1977). Reachability and minimum energy control of positive 2D systems with one delay in states have been considered in Kaczorek (2005). The notion of internally positive 2D system (model) with delay in states and in inputs has been introduced and necessary and sufficient conditions for the internal positivity, reachability, controllability, observability and the minimum energy control problem have been established in Kaczorek (2005). The notions of positive fractional discrete-time and continuous-time linear systems have been introduced in Kaczorek (2003, 2007). The notion for 2D positive fractional hybrid linear systems has been extended in Kaczorek (2008). The realization problem for positive 1D and 2D linear systems has been considered in Kaczorek (2003, 2005), Kaczorek and Busłowicz (2004) and Kaczorek (2007). Recently, a new class of fractional 2D linear systems has been introduced in Kaczorek (2008).

In this paper a new class of positive fractional 2D linear systems will be introduced. A notion of (α, β) orders difference of 2D function will be proposed. Solution to the fractional 2D state equations of the linear systems will be derived using the 2D $\mathcal{Z}$-transform. The classical Cayley-Hamilton theorem will be extended to the 2D fractional linear systems. Necessary and sufficient conditions for the positivity, reachability and controllability of the 2D linear fractional systems are established.

To the best knowledge of the author the positive fractional 2D linear systems have not been considered yet.

2. FRACTIONAL 2D STATE EQUATIONS AND THEIR SOLUTIONS

Let $\Re_+^{n\times m}$ be the set of nonnegative real $n\times m$ matrices and $\Re_+^n = \Re_+^{n\times 1}$. The set of nonnegative integers will be denoted by Z_+ and the $n\times n$ identity matrix will be denoted by I_n.

Definition 1.

The (α, β) orders fractional difference of an 2D function x_{ij} is defined by the formula

$$\Delta^{\alpha,\beta} x_{ij} = \sum_{k=0}^{i}\sum_{l=0}^{j} c_{\alpha\beta}(k,l) x_{i-k,j-l}, \tag{1a}$$

$$n-1 < \alpha < n, \quad n-1 < \beta < n; \quad n \in N = \{1,2,...\}$$

where $\Delta^{\alpha,\beta} x_{ij} = \Delta_i^{\alpha}\Delta_j^{\beta} x_{ij}$ and

$$c_{\alpha,\beta}(k,l) = \begin{cases} 1 & \text{for } k=0 \text{ or/and } l=0 \\ (-1)^{k+l}\dfrac{\alpha(\alpha-1)...(\alpha-k+1)\beta(\beta-1)...(\beta-l+1)}{k!l!} \\ \text{for } k+l>0 \end{cases} \tag{1b}$$

The justification of Definition 1 is given in Appendix A. Consider the (α, β) order fractional 2D linear system, described by the state equations

$$\begin{aligned}\Delta^{\alpha,\beta} x_{i+1,j+1} &= A_0 x_{ij} + A_1 x_{i+1,j} + A_2 x_{i,j+1} \\ &+ B_0 u_{ij} + B_1 u_{i+1,j} + B_2 u_{i,j+1}\end{aligned} \tag{2a}$$

$$y_{ij} = Cx_{ij} + Du_{ij} \tag{2b}$$

where $x_{ij} \in \Re^n, u_{ij} \in \Re^m, y_{ij} \in \Re^p$ are the state, input and output vectors and $A_k \in \Re^{n\times n}$, $B_k \in \Re^{n\times m}$, $k = 0,1,2,$ $C \in \Re^{p\times n}$, $D \in \Re^{p\times m}$.

Using Definition 1 we may write the equation (2a) in the form

$$x_{i+1,j+1} = \bar{A}_0 x_{ij} + \bar{A}_1 x_{i+1,j} + \bar{A}_2 x_{i,j+1} - \sum_{\substack{k=0 \\ k+l>0}}^{i+1} \sum_{l=0}^{j+1} c_{\alpha\beta}(k,l) x_{i-k+1,j-l+1} + B_0 u_{ij} + B_1 u_{i+1,j} + B_2 u_{i,j+1} \tag{3}$$

where $\bar{A}_0 = A_0 - I_n\alpha\beta$, $\bar{A}_1 = A_1 + I_n\beta$, $\bar{A}_2 = A_2 + I_n\alpha$.

From (1b) it follows that the coefficients $c_{\alpha,\beta}(k,l)$ in (1a) strongly decrease when k and l increase. Therefore, in practical problems it is assumed that i and j are bounded by some natural numbers L_1 and L_2. In this case the equation (3) takes the form

$$x_{i+1,j+1} = \bar{A}_0 x_{ij} + \bar{A}_1 x_{i+1,j} + \bar{A}_2 x_{i,j+1} - \sum_{k=0}^{L_1+1} \sum_{l=0}^{L_2+1} c_{\alpha\beta}(k,l) x_{i-k+1,j-l+1} + B_0 u_{ij} + B_1 u_{i+1,j} + B_2 u_{i,j+1} \tag{3a}$$

Note that the fractional systems are 2D linear systems with delays increasing with i and j.

The boundary conditions for the equation (3) (and (3a)) are given in the form

$$x_{i0},\ i \in Z_+ \quad \text{and} \quad x_{0j},\ j \in Z_+ \tag{4}$$

Theorem 1.

The solution of equation (3) with boundary conditions (4) is given by

$$\begin{aligned} x_{ij} &= \sum_{p=1}^{i} T_{i-p,j-1}(\bar{A}_1 x_{p0} + B_1 u_{p0}) + \sum_{q=1}^{j} T_{i-1,j-q}(\bar{A}_2 x_{0q} + B_2 u_{0q}) + \sum_{p=1}^{i-1} T_{i-p-1,j-1}\bar{A}_0 x_{p0} + \\ &\sum_{q=1}^{j-1} T_{i-1,j-q-1}\bar{A}_0 x_{0q} + T_{i-1,j-1}\bar{A}_0 u_{00} + \sum_{p=0}^{i-1}\sum_{q=0}^{j-1} T_{i-p-1,j-q-1} B_0 u_{pq} + \sum_{p=0}^{i}\sum_{q=0}^{j} (T_{i-p-1,j-q-1}B_1 + T_{i-p,j-q-1}B_2) u_{pq} \end{aligned} \tag{5}$$

where the transition matrices T_{pq} are defined by the formula

$$T_{pq} = \begin{cases} I_n \ \text{for}\ p = q = 0 \\ \bar{A}_0 T_{p-1,q-1} + \bar{A}_1 T_{p,q-1} + \bar{A}_2 T_{p-1,q} - \\ -\sum_{\substack{k=0 \\ k+l<p+q-2}}^{p-1} \sum_{l=0}^{q-1} c_{\alpha,\beta}(p-k, q-l) T_{kl} \quad \text{for} \quad p+q>0 \\ 0\ (\text{zero matrix})\ \text{for}\ p<0\ \text{or/and}\ q<0 \end{cases}$$

(6)

Proof.

Let $X(z_1, z_2)$ be the 2D $\mathcal{Z}$-transform of x_{ij} defined by

$$X(z_1,z_2) = \mathcal{Z}[x_{ij}] = \sum_{i=0}^{\infty}\sum_{j=0}^{\infty} x_{ij} z_1^{-i} z_2^{-j} \tag{7}$$

Taking into account that

$$\begin{aligned} &\mathcal{Z}[x_{i+1,j+1}] = z_1 z_2 [X(z_1,z_2) - X(z_1,0) - X(0,z_2) + x_{00}] \\ &\mathcal{Z}[x_{i+1,j}] = z_1[X(z_1,z_2) - X(0,z_2)],\ X(0,z_2) = \sum_{j=0}^{\infty} x_{0j} z_2^{-j} \\ &\mathcal{Z}[x_{i,j+1}] = z_2[X(z_1,z_2) - X(z_1,0)],\ X(z_1,0) = \sum_{i=0}^{\infty} x_{i0} z_1^{-i} \\ &\mathcal{Z}[x_{i-k,j-l}] = z_1^{-k} z_2^{-l} X(z_1,z_2) \end{aligned} \tag{8}$$

then from (3) with (4) we obtain

$$\begin{aligned} X(z_1,z_2) = G^{-1}(z_1,z_2)\Big\{&(B_0 + B_1 z_1 + B_2 z_2)U(z_1,z_2) - \\ &z_1[\bar{A}_1 B_1]\begin{bmatrix} X(0,z_2) \\ U(0,z_2) \end{bmatrix} - z_2[\bar{A}_2 B_2]\begin{bmatrix} X(z_1,0) \\ U(z_1,0) \end{bmatrix} + \\ &z_z z_2[X(z_1,0) + X(0,z_2) - x_{00}]\Big\} \end{aligned} \tag{9}$$

where

$$G(z_1,z_2) = \left[I_n z_1 z_2 + \sum_{\substack{k=0 \\ k+l>1}}^{j+1} \sum_{l=0}^{j+1} I_n c_{\alpha\beta}(k,l) z_1^{-(k-1)} z_2^{-(l-1)} - \bar{A}_0 - \bar{A}_1 z_1 - \bar{A}_2 z_2 \right], \tag{10}$$

and $U(z_1,z_2) = \mathcal{Z}[u_{ij}]$

Let

$$G^{-1}(z_1,z_2) = \sum_{p=0}^{\infty}\sum_{q=0}^{\infty} T_{pq} z_1^{-(p+1)} z_2^{-(q+1)} \tag{11}$$

From the equality

$$G^{-1}(z_1,z_2)G(z_1,z_2) = G(z_1,z_2)G^{-1}(z_1,z_2) = I_n$$

it follows that

$$\left(\sum_{p=0}^{\infty}\sum_{q=0}^{\infty} T_{pq} z_1^{-(p+1)} z_2^{-(q+1)}\right) G(z_1,z_2) = G(z_1,z_2)\left(\sum_{p=0}^{\infty}\sum_{q=0}^{\infty} T_{pq} z_1^{-(p+1)} z_2^{-(q+1)}\right) = I_n \tag{12}$$

Comparison of the coefficients at the same powers of z_1 and z_2 of (12) yields the formula (6).
Substituting (11) into (9) we obtain

$$X(z_1,z_2) = \left(\sum_{p=0}^{\infty}\sum_{q=0}^{\infty} T_{pq} z_1^{-(p+1)} z_2^{-(q+1)}\right)\times \left\{(B_0 + B_1 z_1 + B_2 z_2)U(z_1,z_2) - z_1[\overline{A}_1 B_1]\begin{bmatrix} X(0,z_2) \\ U(0,z_2)\end{bmatrix} - z_2[\overline{A}_2 B_2]\begin{bmatrix} X(z_1,0) \\ U(z_1,0)\end{bmatrix} + z_1 z_2[X(z_1,0) + X(0,z_2) - x_{00}]\right\} \tag{13}$$

Using the 2D inverse Z transform to (13) we obtain the desired formula (5).

3. EXTENSION OF THE CAYLEY-HAMILTON THEOREM

From (10) we have

$$G(z_1,z_2) = z_1 z_2 \overline{G}(z_1,z_2) \tag{14}$$

where

$$\overline{G}(z_1,z_2) = I_n + \sum_{k=0}^{L_1+1}\sum_{l=0}^{L_2+1} I_n c_{\alpha\beta}(k,l) z_1^{-k} z_2^{-l} - \overline{A}_0 z^{-1} z_2^{-1} - \overline{A}_q z_2^{-1} - \overline{A}_2 z_1^{-1} \tag{15}$$

Let

$$\det \overline{G}(z_1,z_2) = \sum_{k=0}^{N_1}\sum_{l=0}^{N_2} a_{N_1-k,N_2-l} z_1^{-k} z_2^{-l} \tag{16}$$

It is assumed that i and j are bounded by some natural numbers L_1, L_2 which determine the degrees N_1, N_2.
From (14) and (11) it follows that

$$G^{-1}(z_1,z_2) = z_1^{-1} z_2^{-1} \overline{G}^{-1}(z_1,z_2) = z_1^{-1} z_2^{-1} \sum_{p=0}^{\infty}\sum_{q=0}^{\infty} T_{pq} z_1^{-p} z_2^{-q} \tag{17}$$

and

$$\overline{G}^{-1}(z_1,z_2) = \sum_{p=0}^{\infty}\sum_{q=0}^{\infty} T_{pq} z_1^{-p} z_2^{-q} \tag{18}$$

where T_{pq} are defined by (6).

Theorem 2.

Let (16) be the characteristic polynomial of the system (2). Then the matrices T_{kl} satisfy the equation

$$\sum_{k=0}^{N_1}\sum_{l=0}^{N_2} a_{kl} T_{kl} = 0 \tag{19}$$

Proof.

From the definition of inverse matrix and (16), (18) we have

$$\text{Adj } \overline{G}(z_1,z_2) = \left(\sum_{k=0}^{N_1}\sum_{l=0}^{N_2} a_{N_1-k,N_2-l} z_1^{-k} z_2^{-l}\right)\left(\sum_{p=0}^{\infty}\sum_{q=0}^{\infty} T_{pq} z_1^{-p} z_2^{-q}\right) \tag{20}$$

where $\text{Adj}\,\overline{G}(z_1,z_2)$ is the adjoint matrix of $\overline{G}(z_1,z_2)$.
Comparison of the coefficients at the same power $z_1^{-N_1} z_2^{-N_2}$ of the equality (20) yields (19) since the degrees of $\text{Adj}\,\overline{G}(z_1,z_2)$ are less than N_1 and N_2.
Theorem 2 is an extension of the well-known classical Cayley-Hamilton theorem for the 2D fractional system (2).

4. POSITIVITY OF THE FRACTIONAL 2D LINEAR SYSTEMS

Lemma 1.

a) If $0 < \alpha < 1$ and $1 < \beta < 2$ then

$$c_{\alpha\beta}(k,l) < 0 \text{ for } k = 1,2,...;\ l = 2,3,... \tag{21a}$$

b) If $1 < \alpha < 2$ and $0 < \beta < 1$ then

$$c_{\alpha\beta}(k,l) < 0 \text{ for } k = 2,3,...;\ l = 1,2,... \tag{21b}$$

Proof.

The proof will be accomplished by induction.
The hypothesis is true for $k = 1$ and $l = 2$ in (21a) since

$$c_{\alpha\beta}(1,2) = (-1)^3 \frac{\alpha\beta(\beta-1)}{2} < 0$$

Assuming that the hypothesis is true for the pair (k,l), $k + l \geq 3$ we shall show that it is also valid for the pairs $(k+1,l)$, $(k,l+1)$ and $(k+1,l+1)$.
From (1b) we have

$$c_{\alpha\beta}(k+1,l) = c_{\alpha\beta}(k,l)\frac{l-\alpha}{k+1} < 0$$

since $c_{\alpha\beta}(k,l) < 0$ for $k = 1,2,...;\ l = 2,3,...$
Similarly

$$c_{\alpha\beta}(k,l+1)=c_{\alpha\beta}(k,l)\frac{k-\alpha}{l+1}<0$$

since $c_{\alpha\beta}(k,l)<0$ for $k=1,2,...;\ l=2,3,...$
and

$$c_{\alpha\beta}(k+1,l+1)=c_{\alpha\beta}(k,l)\frac{(\alpha-\beta)(l-\beta)}{(k+1)(l+1)}<0$$

since $c_{\alpha\beta}(k,l)<0$ for $k=1,2,...;\ l=2,3,...$
The proof of (21b) is similar.

Lemma 2.

If (21) is met and

$$\overline{A}_k\in\Re_+^{n\times n}\ \text{ for } k=0,1,2 \tag{22}$$

then

$$T_{pq}\in\Re_+^{n\times n}\ \text{ for } p,q\in Z_+ \tag{23}$$

Proof.

If the conditions (21) and (22) are satisfied then from (6) we have (23).

Definition 2.

The system (2) is called the (internally) positive fractional 2D system if and only if $x_{ij}\in\Re_+^n$ and $y_{ij}\in\Re_+^p$, $i,j\in Z_+$ for any boundary conditions $x_{i0}\in\Re_+^n$, $i\in Z_+$ $x_{0j}\in\Re_+^n$, $j\in Z_+$ and all input sequences $u_{ij}\in\Re_+^m$, $i,j\in Z_+$.

Theorem 3.

The fractional 2D system (2) for $0<\alpha<1$ and $1<\beta<2$ (or $1<\alpha<2$ and $0<\beta<1$) is positive if and only if

$$\begin{aligned}&\overline{A}_k\in\Re_+^{n\times n},\ B_k\in\Re_+^{n\times m},\ k=0,1,2,\\ &C\in\Re_+^{p\times n},\ D\in\Re_+^{p\times m}\end{aligned} \tag{24}$$

Proof. Necessity.

Let us assume that the system is positive and x_{00}–e_{ni}, i=1,…,n (e_{ni} is the ith column of I_n) x_{01}=x_{10}=0 $u_{ij}=0$, $i,j\in Z_+$. Then from (3) for i=j=0 and $u_{i,j}$=0 $i,j\in Z_+$ we obtain $x_{11}=\overline{A}_0e_{ni}=\overline{A}_{0i}\in\Re_+^n$, where $\overline{A}_{0i}$ is the ith column of the matrix $\overline{A}_0$. This implies $\overline{A}_0\in\Re_+^{n\times n}$ since i=1,…,n. If we assume that x_{10}=e_{ni}, x_{00}=x_{01}=0 and $u_{ij}=0$, $i,j\in Z_+$ then from (3) for i=j=0 we obtain $x_{11}=\overline{A}_1e_{ni}=\overline{A}_{1i}\in\Re_+^n$ and this implies $\overline{A}_1\in\Re_+^{n\times n}$. In a similar way we may prove that $\overline{A}_2\in\Re_+^{n\times n}$. Assuming u_{00}=e_{ni}, $u_{i,j}$=0 $i,j\in Z_+$ $i+j>0$ and x_{00}=x_{10}=x_{01}=0 from (3) for i=j=0 we obtain $x_{11}=B_0e_{mi}=B_{0i}\in\Re_+^m$ for i=1,…,m and this implies $B_0\in\Re_+^{n\times m}$. In a similar way it can be shown that $B_k\in\Re_+^{n\times m}$ for $k=1,2$ and $C\in\Re_+^{p\times n}$, $D\in\Re_+^{p\times m}$.

Sufficiency.

If the conditions (24) are met then by Lemma 2 $T_{pq}\in\Re_+^{n\times n}$ and from (5) we have $x_{ij}\in\Re_+^n$ for $i,j\in Z_+$ since $x_{i0}\in\Re_+^n$, $x_{0j}\in\Re_+^n$ and $u_{ij}\in\Re_+^m$ for $i,j\in Z_+$. From (2b) we have $y_{ij}\in\Re_+^p$ since $C\in\Re_+^{p\times n}$, $D\in\Re_+^{p\times m}$ and $x_{ij}\in\Re_+^n$, $u_{ij}\in\Re_+^m$ for $i,j\in Z_+$.

Remark.

From (1b) and (3) it follows that if $\alpha=\beta$, $0<\alpha<1$ then $c_{\alpha\beta}(k,l)>0$ for $k,l=1,2,...$ and the fractional 2D system (2) is not positive.

5. REACHABILITY AND CONTROLLABILITY TO ZERO

Definition 3.

The positive fractional 2D system (2) is called reachable at the point $(h,k)\in Z_+\times Z_+$ if and only if for zero boundary conditions (4) (x_{i0}=0, $i\in Z_+$, x_{0j}=0, $j\in Z_+$) and every vector $x_f\in\Re_+^n$ there exists a sequence of inputs $u_{ij}\in\Re_+^m$ for

$$\begin{aligned}&(i,j)\in D_{hk}=\\ &\{(i,j)\in Z_+\times Z_+:0\le i\le h,\ 0\le j\le k,\ i+j\ne h+k\}\end{aligned} \tag{25}$$

such that $x_{hk}=x_f$.

A vector is called monomial if and only if its one component is positive and the remaining components are zero.

Theorem 4.

The positive 2D fractional system (2) is reachable at the point (h, k) if and only if the reachability matrix

$$R_{hk}=[M_0,M_1^1,...,M_h^1,M_1^2,...,M_k^2,M_{11},...,M_{1k},M_{21},...,M_{hk-1}] \tag{26}$$

$$M_0 = T_{h-1,k-1}B_0,\ M_i^1 = T_{h-i,k-1}B_1 + T_{h-i-1,k-1}B_0,\ i = 1,...,h$$
$$M_j^2 = T_{h-1,k-1}B_2 + T_{h-1,k-j-1}B_0,\ j = 1,...,k \tag{27}$$
$$M_{ij} = T_{h-i-1,k-j-1}B_0 + T_{h-i,k-j-1}B_1 + T_{h-i-1,k-1}B_2,\ i = 1,...,h,\ j = 1,...,k$$

contains n linearly independent monomial columns.

Proof.

Using the solution (5) for $i = h, j = k$ and zero boundary conditions we obtain

$x_f = R_{hk}u(h,k)$
(28)

where

$$u(h,k) = [u_{00}^T, u_{10}^T, ..., u_{h0}^T, u_{01}^T, ..., u_{0k}^T, u_{11}^T, ..., u_{1k}^T, u_{21}^T, ..., u_{h,k-1}^T]^T \tag{29}$$

and T denotes the transpose.

For the positive fractional 2D system (2) from (27) and (26) we have $M_0 \in \Re_+^{n\times m}$, $M_i^1 \in \Re_+^{n\times m}$, $M_j^2 \in \Re_+^{n\times m}$, $M_{ij} \in \Re_+^{n\times m}, i = 1,...,h, j = 1,...,k$ and $R_{hk} \in \Re_+^{n\times[(h+1)(k+1)-1]m}$.

From (28) it follows that there exists a sequence $u_{ij} \in \Re_+^m$ for $(i,j) \in D_{hk}$ for every $x_f \in \Re_+^n$ if and only if the matrix (26) contains n linearly independent monomial columns.

The following theorem gives sufficient conditions for the reachability of the positive fractional 2D system (2).

Theorem 5.

The positive fractional 2D system (2) is reachable at the point (h,k) if rank $R_{hk}=n$ and the right inverse R^r_{hk} of the matrix (26) has nonnegative entries

$$R_{hk}^r = R_{hk}^T [R_{hk} R_{hk}^T]^{-1} \in \Re_+^{[(h+1)(k+1)-1]m\times n} \tag{30}$$

Proof.

If rank $R_{hk}=n$ then there exists the right inverse R^r_{hk} of the matrix R_{hk}. If the condition (30) is met then from (28) we obtain

$$u(h,k) = R_{hk}^r x_f \in \Re_+^{[(h+1)(k+1)-1]m}$$

for every $x_f \in \Re_+^n$.

Example 1.

Consider the positive fractional 2D system (2) with

$$\overline{A}_0 = \begin{bmatrix} 0 & 1 \\ 1 & 0 \end{bmatrix}, \overline{A}_1 = \begin{bmatrix} 1 & 0 \\ 0 & 1 \end{bmatrix}, \overline{A}_2 = \begin{bmatrix} 1 & 0 \\ 1 & 1 \end{bmatrix},$$
$$B_0 = \begin{bmatrix} 1 \\ 0 \end{bmatrix}, B_1 = \begin{bmatrix} 0 \\ 1 \end{bmatrix}, B_2 = \begin{bmatrix} 1 \\ 1 \end{bmatrix} \tag{31}$$

To check the reachability at the point $(h,k) = (1,1)$ of the system we use Theorem 4. From (27) and (26) we obtain

$$M_0 = B_0 = \begin{bmatrix} 1 \\ 0 \end{bmatrix}, M_1^1 = B_1 = \begin{bmatrix} 0 \\ 1 \end{bmatrix},$$
$$M_1^2 = B_2 = \begin{bmatrix} 1 \\ 1 \end{bmatrix}, M_{ij} = 0$$

for $i \ge 1, j \ge 1$

$$R_{11} = [M_0, M_1^1, M_1^2] = \begin{bmatrix} 1 & 0 & 1 \\ 0 & 1 & 1 \end{bmatrix} \tag{32}$$

The first two columns of (32) are linearly independent monomial columns and by Theorem 4 the positive fractional 2D system (2) with (31) is reachable at the point (1,1). The sequence of inputs steering the state of the system from zero boundary conditions to an arbitrary state $x_f \in \Re_+^2$ at the point (1,1) is given by $\begin{bmatrix} u_{00} \\ u_{10} \end{bmatrix} = x_f$ and $u_{01} = 0$.

Using (30) and (32) we obtain

$$R_{hk}^r = R_{hk}^T [R_{hk} R_{hk}^T]^{-1} =$$
$$= \begin{bmatrix} 1 & 0 \\ 0 & 1 \\ 1 & 1 \end{bmatrix} \begin{bmatrix} 2 & 1 \\ 1 & 2 \end{bmatrix}^{-1} = \frac{1}{3} \begin{bmatrix} 2 & -1 \\ -1 & 2 \\ 1 & 1 \end{bmatrix} \tag{33}$$

From (33) it follows that the condition (30) is not satisfied in spite of the fact that the system is reachable at the point (1,1). Note that the system is reachable at the point (1,1) for any fractional orders (α, β) $0 < \alpha < 1$, $1 < \beta < 2$ (or $1<\alpha<2$, $0 < \beta < 1$) and any matrices $\bar{A}_k$, $k = 0, 1, 2$.

Definition 4.

The positive fractional 2D system (2) is called the system with finite memory if its characteristic polynomial has the form

$$\det G(z_1, z_2) = cz_1^{n_1} z_2^{n_2} \tag{34}$$

where c is a constant coefficient.

Lemma 3.

If the positive fractional 2D system (2) is with finite memory then

$$x_{bc}(i,j) = \sum_{p=1}^{i}(T_{i-p,j-1}\bar{A}_1 + T_{i-p-1,j-1}\bar{A}_0)x_{p0} + \sum_{q=1}^{j}(T_{i-1,j-q}\bar{A}_2 + T_{i-1,j-q-1}\bar{A}_0)x_{0q} + T_{i-1,j-1}\bar{A}_0 x_{00} = 0 \tag{35}$$

for $i \geq n_1, j \geq n_2$ and any nonzero boundary conditions (4).

Proof.

Using the expansion (11) and (34) we obtain $T_{ij} = 0$ for $i \geq n_1, j \geq n_2$ and the equality (35) for any nonzero boundary conditions (4).

Definition 5.

The positive fractional 2D system (2) is called reachable for the nonzero boundary conditions (NBC)

$$x_{i0} \in \Re_+^n, i \in Z_+ \text{ and } x_{0j} \in \Re_+^n, j \in Z_+ \tag{36}$$

at the point $(h,k) \in Z_+ \times Z_+$ if for every vector $x_f \in \Re_+^n$ there exists a sequence of inputs $u_{ij} \in \Re_+^m$ for $(i,j) \in D_{hk}$ such that $x_{hk} = x_f$.

Theorem 6.

The positive fractional 2D system (2) is reachable for NBC at the point (h,k) $(h \geq n_1, k \geq n_2)$ if and only if the system is with finite memory and the reachabilty matrix (26) contains n linearly independent monomial columns.

Proof.

Using the solution (5) for $i = h, j = k$ and taking into account that $x_{hk} = x_f$ we obtain

$$x_f - x_{bc}(h,k) = R_{hk}u(h,k) \tag{37}$$

where R_{hk} and $x_{bc}(h,k)$ are defined by (26) and (35) respectively.

If the positive fractional 2D system (2) is with finite memory then by Lemma 3 there exists a point (h,k) ($h \geq n_1$, $k \geq n_2$) such that (35) holds and $x_f = R_{hk}u(h,k)$. In this case by Theorem 4 there exists a sequence of inputs $u_{ij} \in \Re_+^m$ for $(i,j) \in D_{hk}$ satisfying the equality (28). If it is not the case then $x_f - x_{bc}(h,k) \notin R_{hk}u(h,k)$ since by assumption the NBC (36) are arbitrary and the vector $x_f \in \Re_+^n$ is also arbitrary. In this case there does not exist a sequence of inputs $u_{ij} \in \Re_+^m$ for $(i,j) \in D_{hk}$ satisfying (37).

Definition 6.

The positive fractional 2D system (2) is called controllable to zero at the point (h,k) ($h \geq n_1$, $k \geq n_2$) if and only if for any NBC (36) there exists a sequence of inputs $u_{ij} \in \Re_+^m$ for $(i,j) \in D_{hk}$ such that $x_{hk} = 0$.

Theorem 7.

The positive fractional 2D system (2) is controllable to zero at the point (h,k) ($h \geq n_1$, $k \geq n_2$) if and only if the system is with finite memory.

Proof.

If the system is with finite memory then by Lemma 3 (35) holds for $h \geq n_1$ and $k \geq n_2$. For $x_f = 0$ from (37) we have

$$x_{bc}(h,k) + R_{hk}u(h,k) = 0 \tag{38}$$

The equation (38) is satisfied for $u(h,k) = 0$.
If the condition (35) is not satisfied then does not exist $u(h,k) \in \Re_+^{[(h+1)(k+1)-1]m}$ satisfying (38) since for the positive system $R_{hk} \in \Re_+^{n \times [(h+1)(k+1)-1]m}$ and $x_{bc}(h,k) \in \Re_+^n$.

6. CONCLUDING REMARKS

A new class of 2D fractional linear systems has been introduced. The notion of (α, β) orders $0 < \alpha < 1$, $1 < \beta < 2$ or $1 < \alpha < 2$, $0 < \beta < 1$ fractional 2D difference has been proposed. The fractional 2D state equations of linear systems have been given and their solutions have been derived using the 2D Z transform. The classical Cayley-Hamilton theorem has been extended for the fractional 2D systems. Necessary and sufficient conditions have been established for the positivity, reachability and controllability to zero of the fractional 2D linear systems.
It has been shown that the fractional 2D system (2) is positive if $0 < \alpha < 1$, $1 < \beta < 2$ or $1 < \alpha < 2$, $0 < \beta < 1$. The fractional 2D system is not positive if $\alpha = \beta$
The considerations can be easily extended for fractional 2D linear systems with delays.
An extension of these considerations for fractional 2D continuous-time linear systems is an open problem.

Appendix. Justification of the definition 1.

It is well-known that for a discrete function x_i the n-order difference is given by

$$\Delta_i^n x_i = \Delta^{n-1} x_i - \Delta^{n-1} x_{i-1} = \sum_{k=0}^{i} (-1)^k \binom{n}{k} x_{i-k} \qquad \text{(A.1)}$$

$n \in N = \{1,2,...\}, \quad i = Z_+ \{0,1,...\}$

where

$$\binom{n}{k} = \begin{cases} 1 & \text{for } k = 0 \\ \dfrac{n!}{k!\,(n\text{-}k)!} \end{cases} \qquad \text{(A.2)}$$

Using (A.1) for an 2D discrete function x_{ij} we obtain

$$\Delta_i^{n_1} \Delta_j^{n_2} x_{ij} = \Delta_j^{n_2} \Delta_i^{n_1} x_{ij} = \sum_{k=0}^{i} (-1)^k \binom{n_1}{k} \Delta_j^{n_2} x_{i-k,j} = \sum_{k=0}^{i} (-1)^k \binom{n_1}{k} \sum_{l=0}^{j} (-1)^l \binom{n_2}{l} x_{i-k,j-l} =$$

$$\sum_{l=0}^{j} (-1)^l \binom{n_2}{l} \sum_{k=0}^{i} (-1)^k \binom{n_1}{k} x_{i-k,j-l} = \sum_{k=0}^{i} \sum_{l=0}^{j} (-1)^{k+l} \binom{n_1}{k} \binom{n_2}{l} x_{i-k,j-l} \qquad \text{(A.3)}$$

for $n_1, n_2 \in N$ and $i, j \in Z_+$

Note that

$$\binom{n_1}{k}\binom{n_2}{l} = \begin{cases} 1 \ \text{ for } k = 0 \ \text{ or/and } l = 0 \\ \dfrac{n_1(n_1-1)...(n_1-k+1)n_2(n_2-1)...(n_2-l+1)}{k!\,l!} \\ \text{for } k + l > 0 \end{cases} \qquad \text{(A.4)}$$

is also well defined for $n_1 = \alpha$ and $n_2 = \beta$, where α and β are any real numbers. Thus (A.4) can be used for defining the α, β orders of an 2D function x_{ij}.

REFERENCES

1. **Bose N.K** (1982), *Applied Multidimensional Systems Theory*, Van Nonstrand Reinhold Co, New York.
2. **Bose N.K** (1985) *Multidimensional Systems Theory Progress, Directions and Open Problems*, D. Reidel Publishing Co.
3. **Farina L., Rinaldi S.**, (2000) *Positive Linear Systems; Theory and Applications*, J. Wiley, New York.
4. **Fornasini E., Marchesini G.,** (1976) State-space realization theory of two-dimensional filters, *IEEE Trans. Autom. Contr.,* Vol. AC-21, 484-491.
5. **Fornasini E., Marchesini G**. (1978) Double indexed dynamical systems, *Math. Sys. Theory,* 12, 59-72.
6. **Gałkowski K.** (1977), Elementary operation approach to state space realization of 2D systems, *IEEE Trans. On Circuit and Systems*, Vol. 44, 120-129.
7. **Gałkowski K.** (2001*), State space realizations of linear 2D systems with extensions to the general nD (n>2) case*, Springer Verlag, London.
8. **Kaczorek T.** (1985), *Two-Dimensional Linear Systems*, Springer Verlag, Berlin.
9. **Kaczorek T.** (2002) *Positive 1D and 2D Systems*, Springer Verlang, London.
10. **Kaczorek T.** (1996), Reachability and controllability of non-negative 2D Roesser type models, *Bull. Acad. Pol. Sci. Ser. Sci. Techn.*, Vol. 44, No 4, 405-410
11. **Kaczorek T.** (2008) Realization problem of positive fractional 2D hybrid linear systems, *COMPEL 2008*, vol. 27, No. 3, 613-623.

12. **Kaczorek T.** (2007) Realization problem for positive 2D systems with delays. *Machine Intelligence and Robotic Control*, vol. 6, No. 1 (in Press).
13. **Kaczorek T.** (2005) Reachability and minimum energy control of positive 2D systems with delays, *Control and Cybernetics*, vol. 34, No 2, 411-423.
14. **Kaczorek T.** (2007) Reachabilty and controllability to zero of positive fractional discrete-time systems. *Machine Intelligence and Robotic Control*, vol. 6, no. 2 (in Press).
15. **Kaczorek T.** (2008) Fractional positive continuous-time linear systems and their reachability. *Int. J. Appl. Math. Comp. Sci*., vol. 18, No. 2, 1-6.
16. **Kaczorek T.** (2003) Realization problem for positive discrete-time systems with delays, System Science, vol. 29, No 1,15-29.
17. **Kaczorek T.** (2005) Realization problem for a class of positive continuous-time systems with delays, *Int. J. Appl. Math. Comp. Sci*., vol. 15, No. 4, 101-107.
18. **Kaczorek T.** (2005) Realization problem for a class of positive continuous-time systems with delays, *Int. J. Appl. Math Comput. Sci*, vol. 15, No 4, 101-107.
19. **Kaczorek T.** (2008) Fractional 2D linear systems. *Automation, Mobile Robotics and Intelligent Systems*, vol. 2, no. 2, 1-6.
20. **Kaczorek T.** (2007) Reachability and controllability to zero of cone fractional linear systems. *Archives of Control Scienes*, vol. 17, No. 3, 357-367.
21. **Kaczorek T., Busłowicz M.** (2004) Minimal realization for positive multivariable linear systems with delay, *Int. J. Appl. Math. Comput. Sci*., vol. 14, No 2, 181-187.
22. **Klamka J.** (1991) *Controllability of Dynamical Systems*, Kluwer Academic Publ., Dordrecht, 1991.
23. **Kurek J.** (1985) The general state-space model for a two-dimensional linear digital systems, *IEEE Trans. Autom. Contr*. AC-30, 600-602.
24. **Roesser R. P.** (1975) A discrete state-space model for linear image processing, IEEE Trans. on Automatic Control, AC-20, 1, 1-10.
25. **Valcher M. E.** (1987) On the initial stability and asymptotic behavior of 2D positive systems, *IEEE Trans. On Circuits and Systems – I*, vol. 44, No 7, 602-613.

This work was supported by the Ministry of Science and High Education of Poland under grant NN 514 1939 33.

SOLVABILITY OF 2D HYBRID LINEAR SYSTEMS – COMPARSION OF THREE DIFFERENT METHODS

Tadeusz KACZOREK[*], Vladimir MARCHENKO[**], Łukasz SAJEWSKI[*]

[*]Faculty of Electrical Engineering, Bialystok Technical University, ul. Wiejska 45D, 15-351 Białystok
[**]Faculty of Informatics, Bialystok Technical University, ul. Wiejska 45A, 15-351 Białystok

kaczorek@isep.pw.edu.pl, vmar@bstu.unibel.by, lsajewski@doktoranci.pb.edu.pl

Abstract: A class of positive hybrid linear systems is introduced. Three different methods for computation of solutions of the hybrid system are proposed. The considerations are illustrated by numerical example. Simulations of solution have been shown for the methods.

1. INTRODUCTION

In positive systems, inputs, state variables and outputs take only non-negative values. Examples of positive systems are industrial processes involving chemical reactors, heat exchangers and distillation columns, storage systems, compartmental systems, water and atmospheric pollution models. A variety of models having positive linear systems behavior can be found in engineering, management science, economics, social sciences, biology and medicine, etc.

Positive linear systems are defined on cones, not on linear spaces. Therefore, the theory of positive systems is more complicated and less advanced. An overview of state of the art in positive systems theory is given in the monographs Benvenuti and Farina (2004), Kaczorek (2001). Recent developments in positive systems theory and some new results are given in Kaczorek (2003). The realization problem for positive discrete-time and continuos-time systems without and with delays was considered in Benvenuti and Farina (2004), Farina and Rinaldi (2000), Kaczorek (2001, 2004, 2005, 2006), Kaczorek and Busłowicz (2004).

The main purpose of this paper is presentation and comparison of three methods for computation of solution of positive 2D hybrid systems. Three different solutions of the hybrid linear systems will be derived. The considered methods will be illustrated by numerical example. Using Matlab/Simulink there will be performed comparison simulations of the methods.

2. EQUATIONS OF THE HYBRID SYSTEMS

Let $R^{n\times m}$ be the set of $n\times m$ matrices with entries form the field of real number R and Z_+ be the set of nonnegative integers. The $n\times n$ identity matrix will be denoted by I_n.

Equations of the 2D hybrid linear system have the form

$$\dot{x}_1(t,i) = A_{11}x_1(t,i) + A_{12}x_2(t,i) + B_1u(t,i)\,,\ t \in R_+ \tag{1a}$$

$$x_2(t,i+1) = A_{21}x_1(t,i) + A_{22}x_2(t,i) + B_2u(t,i)\,,\ i \in Z_+ \tag{1b}$$

$$y(t,i) = C_1x_1(t,i) + C_2x_2(t,i) + Du(t,i) \tag{1c}$$

where $\dot{x}_1(t,i) = \frac{\partial x_1(t,i)}{\partial t}$, $x_1(t,i) \in R^{n_1}$, $x_2(t,i) \in R^{n_2}$, $u(t,i)\in R^m$, $y(t,i)\in R^P$ and A_{11}, A_{12}, A_{21}, A_{22}, B_1, B_2, C_1, C_2, D are real matrices with appropriate dimensions.

Boundary conditions for (1a) and (1b) have the form

$$x_1(0,i) = x_1(i)\,,\ i \in Z_+ \ \text{and}\ x_2(t,0) = x_2(t)\,,\ t \in R_+ \tag{2}$$

Note that the hybrid system (1) has a similar structure as the Roesser model (Kaczorek, 2001; Klamka, 1991; Roesser, 1975).

Let $R_+^{n\times m}$ be the set of $n\times m$ real matrices with nonnegative entries and R_+^n, $R_+^{n\times 1}$.

Definition 1.

The hybrid system (1) is called internally positive if $x_1(t,i) \in R_+^{n_1}$, $x_2(t,i) \in R_+^{n_2}$, and $y(t,i) \in R_+^p$, $t \in R_+$, $i \in Z_+$ for arbitrary boundary conditions $x_1(i) \in R_+^{n_1}$, $i \in Z_+$, $x_2(t) \in R_+^{n_2}$, $t \in R_+$ and inputs $u(t,i) \in R_+^m$, $t \in R_+$, $i \in Z_+$.

Let M_n be the set of $n\times m$ Metzler matrices (real matrices with nonnegative off-diagonal entries).

Theorem 1.

(Kaczorek, 2001) The hybrid system (1) is internally positive if and only if

$$A_{11} \in M_{n_1}, A_{12} \in R_+^{n_1\times n_2}, A_{21} \in R_+^{n_2\times n_1}, A_{22} \in R_+^{n_2\times n_2},$$

$$B_1 \in R_+^{n_1\times m}, B_2 \in R_+^{n_2\times m}, C_1 \in R_+^{p\times n_1}, C_2 \in R_+^{p\times n_2}, D \in R_+^{p\times m}$$

3. COMPUTATION OF SOLUTIONS

Method 1.

Along with equations (1a), (1b), consider the following determining equations

$$X^1_{k+1,i} = A_{11}X^1_{k,i} + A_{12}X^2_{k,i} + B_1U_{k,i} \tag{3a}$$

$$X^2_{k,i+1} = A_{21}X^1_{k,i} + A_{22}X^2_{k,i} + B_2U_{k,i} \tag{3b}$$

with initial conditions of the form

$$X^1_{0,i} = 0 \text{ for i} = 0,1,... \tag{4a}$$

$$X^2_{k,0} = 0 \text{ for } k = 0,1,... \tag{4b}$$

$$U_{k,i} = \begin{cases} I_m, & k = i = 0 \\ 0, & k^2 + i^2 \neq 0 \end{cases} \tag{4c}$$

Lemma 1.

The following conditions hold:
for $k = 1,2,...$

$$(A_{11} + A_{12}w(I_{n_2} - A_{22}w)^{-1}A_{21})^{k-1} \times$$

$$(B_1 + A_{12}w(I_{n_2} - A_{22}w)^{-1}B_2) \equiv \sum_{j=0}^{\infty} X^1_{k,j}w^j$$

$$(I_{n_2} - A_{22}w)^{-1}A_{21}w(A_{11} + A_{12}w(I_{n_2} - A_{22}w)^{-1}A_{21})^{k-1} \times$$

$$(B_1 + A_{12}w(I_{n_2} - A_{22}w)^{-1}B_2) \equiv \sum_{j=0}^{\infty} X^2_{k,j}w^j$$

for $j = 1,2,...$

$$(A_{22} + A_{21}w(I_{n_1} - A_{11}w)^{-1}A_{12})^{j-1} \times$$

$$(B_2 + A_{21}w(I_{n_1} - A_{11}w)^{-1}B_1) \equiv \sum_{k=0}^{\infty} X^2_{k,j}w^k$$

$$(I_{n_1} - A_{11}w)^{-1}A_{12}w(A_{22} + A_{21}w(I_{n_1} - A_{11}w)^{-1}A_{12})^{j-1} \times$$

$$(B_2 + A_{21}w(I_{n_1} - A_{11}w)^{-1}B_1) \equiv \sum_{j=0}^{\infty} X^1_{k,j}w^k$$

and

$$(I_{n_2} - A_{22}w)^{-1}B_2w \equiv \sum_{j=0}^{\infty} X^2_{0,j}w^j$$

$$(I_{n_1} - A_{11}w)^{-1}B_1w \equiv \sum_{k=0}^{\infty} X^1_{k,0}w^k$$

Where $|w| < w_1$, $w \in C$ and w_1 is a sufficiently small positive number. Proof by induction is given in (Marchenko and Poddubnaya (2005), Marchenko at al (2005).
Applying the Laplace transformation with respect to t and the Z-transformation with respect to i, we write the equations (1a), (1b) in the form

$$\begin{bmatrix} I_{n_1}s - A_{11} & -A_{12} \\ -A_{21} & I_{n_2}z - A_{22} \end{bmatrix}\begin{bmatrix} X_1(s,z) \\ X_2(s,z) \end{bmatrix} = \begin{bmatrix} B_1 \\ B_2 \end{bmatrix}U(s,z) + \begin{bmatrix} X_1(0,z) \\ zX_2(s,0) \end{bmatrix} \tag{5}$$

where $X_k(s,z) = Z[L(x_k(t,i))]$, $k = 1,2$
$X_1(0,z) = Z[x_1(0,i))]$, $X_2(s,0) = L[x_2(t,0)]$.

The equations (5) can be rewritten as

$$\begin{bmatrix} I_{n_1}s - A_{11} - A_{12}(I_{n_2}z - A_{22})^{-1}A_{21} & 0 \\ -A_{21} & I_{n_2}z - A_{22} \end{bmatrix}\begin{bmatrix} X_1(s,z) \\ X_2(s,z) \end{bmatrix} =$$

$$\begin{bmatrix} B_1 + A_{12}(I_{n_2}z - A_{22})^{-1}B_2 \\ B_2 \end{bmatrix}U(s,z) + \tag{6a}$$

$$\begin{bmatrix} X_1(0,z) + A_{12}(I_{n_2}z - A_{22})^{-1}zX_2(s,0) \\ zX_2(s,0) \end{bmatrix}$$

and

$$\begin{bmatrix} I_{n_1}s - A_{11} & -A_{12} \\ 0 & I_{n_2}z - A_{22} - A_{21}(I_{n_1}s - A_{11})^{-1}A_{12} \end{bmatrix}\begin{bmatrix} X_1(s,z) \\ X_2(s,z) \end{bmatrix} =$$

$$\begin{bmatrix} B_1 \\ B_2 + A_{21}(I_{n_1}s - A_{11})^{-1}B_1 \end{bmatrix}U(s,z) + \tag{6b}$$

$$\begin{bmatrix} X_1(0,z) \\ zX_2(s,0) + A_{21}(I_{n_1}s - A_{11})^{-1}X_1(0,z) \end{bmatrix}$$

It follows from (6) and Lemma 1 given in (Marchenko and Poddubnaya (2005), Marchenko at al (2005), that

$$X_1(s,z) = \sum_{k=0}^{\infty}\frac{1}{s^{k+1}}(A_{11} + A_{12}(I_{n_2}z - A_{22})^{-1}A_{21})^k \times$$

$$\{(B_1 + A_{12}(I_{n_2}z - A_{22})^{-1}B_2)U(s,z) +$$

$$X_1(0,z) + A_{12}(I_{n_2}z - A_{22})^{-1}zX_2(s,0)\} =$$

$$\sum_{k=1}^{\infty}\frac{1}{s^k}(A_{11} + A_{12}z^{-1}(I_{n_2} - A_{22}z^{-1})^{-1}A_{21})^{k-1} \times$$

$$\{(B_1 + A_{12}z^{-1}(I_{n_2} - A_{22}z^{-1})^{-1}B_2)U(s,z) +$$

$$X_1(0,z) + A_{12}(I_{n_2}z - A_{22})^{-1}zX_2(s,0)\} =$$

$$\sum_{k=1}^{\infty}\frac{1}{s^k}\sum_{j=0}^{\infty}X^1_{k,j}\frac{1}{z^j}U(s,z) +$$

$$\sum_{k=1}^{\infty}\frac{1}{s^k}(A_{11} + A_{12}z^{-1}(I_{n_2} - A_{22}z^{-1})^{-1}A_{21})^{k-1}X_1(0,z) +$$

$$\sum_{k=1}^{\infty}\frac{1}{s^k}(A_{11} + A_{12}z^{-1}(I_{n_2} - A_{22}z^{-1})^{-1}A_{21})^{k-1} \times$$

$$A_{12}z^{-1}(I_{n_2} - A_{22}z^{-1})^{-1}zX_2(s,0) \tag{7a}$$

Similarly, we obtain

$$X_2(s,z)=\sum_{j=1}^{\infty}\frac{1}{z^j}(A_{22}+A_{21}s^{-1}(I_{n_1}-A_{11}s^{-1})^{-1}A_{12})^{j-1}\times$$
$$\{(B_2+A_{21}s^{-1}(I_{n_1}-A_{11}s^{-1})^{-1}B_1)U(s,z)+$$
$$zX_2(s,0)+A_{21}s^{-1}(I_{n_1}-A_{11}s^{-1})^{-1}X_1(0,z)\}=$$
$$\sum_{j=1}^{\infty}\frac{1}{z^j}\sum_{k=0}^{\infty}X_{k,j}^2\frac{1}{s^k}U(s,z)+ \tag{7b}$$
$$\sum_{j=1}^{\infty}\frac{1}{z^j}(A_{22}+A_{21}s^{-1}(I_{n_1}-A_{11}s^{-1})^{-1}A_{12})^{j-1}zX_2(s,0)+$$
$$\sum_{j=1}^{\infty}\frac{1}{z^j}(A_{22}+A_{21}s^{-1}(I_{n_1}-A_{11}s^{-1})^{-1}A_{12})^{j-1}\times$$
$$A_{21}s^{-1}(I_{n_1}-A_{11}s^{-1})^{-1}X_1(0,z)$$

Let $X_{k,i}^1=X_{k,i}^{11}$, $X_{k,i}^2=X_{k,i}^{21}$ be the solution of (3a), (3b) with $B_1=I_{n_1}$, $B_2=0$ and $X_{k,i}^1=X_{k,i}^{12}$, $X_{k,i}^2=X_{k,i}^{22}$ with $B_1=0$, $B_2=I_{n_2}$.

Then we have $X_{k,0}^{12}=A_{11}{}^{k-1}B_1=0$, $X_{0,k}^{21}=A_{22}{}^{k-1}B_2=0$, $k=1,2,...$ and

$$X_1(s,z)=\sum_{k=1}^{\infty}\sum_{j=0}^{\infty}\frac{1}{z^j}\frac{1}{s^k}X_{k,j}^1U(s,z)+$$
$$\sum_{k=1}^{\infty}\sum_{j=0}^{\infty}\frac{1}{z^j}\frac{1}{s^k}X_{k,j}^{11}X_1(0,z)+\sum_{k=1}^{\infty}\sum_{j=1}^{\infty}\frac{1}{z^{j-1}}\frac{1}{s^k}X_{k,j}^{12}X_2(s,0) \tag{8a}$$

$$X_2(s,z)=\sum_{k=0}^{\infty}\sum_{j=1}^{\infty}\frac{1}{z^j}\frac{1}{s^k}X_{k,j}^2U(s,z)+$$
$$\sum_{k=0}^{\infty}\sum_{j=1}^{\infty}\frac{1}{z^{j-1}}\frac{1}{s^k}X_{k,j}^{22}X_2(s,0)+\sum_{k=1}^{\infty}\sum_{j=1}^{\infty}\frac{1}{z^j}\frac{1}{s^k}X_{k,j}^{21}X_1(0,z) \tag{8b}$$

Using inverse transforms to (8), we obtain the solution (8b)of hybrid linear system (1) in the form

$$x_1(t,i)=\sum_{k=1}^{\infty}\sum_{j=0}^{i}X_{k,j}^1\int_0^t\frac{(t-\tau)^{k-1}}{(k-1)!}u(\tau,i-j)d\tau\ +$$
$$\sum_{k=1}^{\infty}\sum_{j=0}^{i}X_{k,j}^{11}\frac{t^{k-1}}{(k-1)!}x_1(0,i-j)+ \tag{9a}$$
$$\sum_{k=1}^{\infty}X_{k,i+1}^{12}\int_0^t\frac{(t-\tau)^{k-1}}{(k-1)!}x_2(\tau,0)d\tau$$

$$x_2(t,i)=\sum_{k=1}^{\infty}\sum_{j=1}^{i}X_{k,j}^2\int_0^t\frac{(t-\tau)^{k-1}}{(k-1)!}u(\tau,i-j)d\tau+$$
$$\sum_{k=1}^{\infty}\sum_{j=1}^{i}X_{k,j}^{21}\frac{t^{k-1}}{(k-1)!}x_1(0,i-j)+$$
$$\sum_{j=1}^{i}X_{0,j}^2u(t,i-j)+X_{0,i+1}^{22}x_2(t,0)+ \tag{9b}$$
$$\sum_{k=1}^{\infty}X_{k,i+1}^{22}\int_0^t\frac{(t-\tau)^{k-1}}{(k-1)!}x_2(\tau,0)d\tau$$

Method 2.

Applying the Laplace transformation with respect to t and the Z-transformation with respect to i, we write the equations (1a), (1b) in the form

$$\begin{bmatrix}I_{n_1}-s^{-1}A_{11} & -s^{-1}A_{12}\\ -z^{-1}A_{21} & I_{n_2}-z^{-1}A_{22}\end{bmatrix}\begin{bmatrix}X_1(s,z)\\ X_2(s,z)\end{bmatrix}=$$
$$\begin{bmatrix}s^{-1}B_1\\ z^{-1}B_2\end{bmatrix}U(s,z)+\begin{bmatrix}s^{-1}X_1(0,z)\\ X_2(s,0)\end{bmatrix} \tag{10}$$

and

$$\begin{bmatrix}X_1(s,z)\\ X_2(s,z)\end{bmatrix}=\begin{bmatrix}I_{n_1}-s^{-1}A_{11} & -s^{-1}A_{12}\\ -z^{-1}A_{21} & I_{n_2}-z^{-1}A_{22}\end{bmatrix}^{-1}\times$$
$$\left(\begin{bmatrix}s^{-1}B_1\\ z^{-1}B_2\end{bmatrix}U(s,z)+\begin{bmatrix}s^{-1}X_1(0,z)\\ X_2(s,0)\end{bmatrix}\right) \tag{11}$$

where $X_k(s,z)=Z[L(x_k(t,i))],\ \ k=1,2$
$X_1(0,z)=Z[x_1(0,i))],\ \ X_2(s,0)=L[x_2(t,0)]$.

Let

$$T_{1,0}=\begin{bmatrix}A_{11} & A_{12}\\ 0 & 0\end{bmatrix},\ T_{0,1}=\begin{bmatrix}0 & 0\\ A_{21} & A_{22}\end{bmatrix} \tag{12}$$

and

$$\begin{bmatrix}I_{n_1}-s^{-1}A_{11} & -s^{-1}A_{12}\\ -z^{-1}A_{21} & I_{n_2}-z^{-1}A_{22}\end{bmatrix}^{-1}=$$
$$[I_{n_1+n_2}-T_{1,0}s^{-1}-T_{0,1}z^{-1}]^{-1}=\sum_{i=0}^{\infty}\sum_{j=0}^{\infty}T_{i,j}s^{-i}z^{-j} \tag{13}$$

where

$$T_{i,j}=\begin{cases}I_{n_1+n_2} & \text{for}\quad i=j=0\\ T_{1,0}T_{i-1,j}+T_{0,1}T_{i,j-1} & \text{for } i,j=0,1,...\ \ i+j>0\\ 0 & \text{for}\ \ i<0\ \text{or/and}\ j<0\end{cases} \tag{14}$$

From definition of inverse matrix and (13), we have

$$[I_{n_1+n_2} - T_{1,0}s^{-1} - T_{0,1}z^{-1}]\left(\sum_{i=0}^{\infty}\sum_{j=0}^{\infty} T_{i,j}s^{-i}z^{-j}\right) = I_{n_1+n_2} \quad (15)$$

Comparison of the coefficients at the same powers of s and z of the equality (15) yields (14).

Substituting (13) into (11), we obtain

$$\begin{bmatrix} X_1(s,z) \\ X_2(s,z) \end{bmatrix} = \sum_{i=0}^{\infty}\sum_{j=0}^{\infty} T_{i,j}s^{-i}z^{-j}\left(\begin{bmatrix} s^{-1}B_1 \\ z^{-1}B_2 \end{bmatrix}U(s,z) + \begin{bmatrix} s^{-1}X_1(0,z) \\ X_2(s,0) \end{bmatrix}\right) =$$
$$\sum_{i=0}^{\infty}\sum_{j=0}^{\infty}(T_{i,j}s^{-(i+1)}z^{-j}B_{10} + T_{i,j}s^{-i}z^{-(j+1)}B_{01})U(s,z) +$$
$$\sum_{i=0}^{\infty}\sum_{j=0}^{\infty}(T_{i,j}s^{-(i+1)}z^{-j}\begin{bmatrix} X_1(0,z) \\ 0 \end{bmatrix} + T_{i,j}s^{-i}z^{-j}\begin{bmatrix} 0 \\ X_2(s,0) \end{bmatrix}) \quad (16)$$

where $B_{10} = \begin{bmatrix} B_1 \\ 0 \end{bmatrix}$, $B_{01} = \begin{bmatrix} 0 \\ B_2 \end{bmatrix}$.

Applying the inverse transforms to (16), we obtain

$$\begin{bmatrix} x_1(t,i) \\ x_2(t,i) \end{bmatrix} = \sum_{k=0}^{\infty}\sum_{l=0}^{i} T_{k,i-l}B_{10}\int_0^t \frac{(t-\tau)^k}{k!}u(\tau,l)d\tau +$$
$$\sum_{k=0}^{\infty}\sum_{l=0}^{i} T_{k,i-l-1}B_{01}\int_0^t \frac{(t-\tau)^{k-1}}{(k-1)!}u(\tau,l)d\tau +$$
$$\sum_{k=0}^{\infty}\sum_{l=0}^{i} T_{k,i-l}\frac{t^k}{k!}\begin{bmatrix} x_1(0,l) \\ 0 \end{bmatrix} +$$
$$\sum_{k=0}^{\infty} T_{k,i}\int_0^t \frac{(t-\tau)^{k-1}}{(k-1)!}\begin{bmatrix} 0 \\ x_2(\tau,0) \end{bmatrix}d\tau \quad (17)$$

Method 3.

From definition, solution of the differential equation (1a) has the form

$$x_1(t,i) = e^{A_{11}t}x_1(0,i) + \int_0^t e^{A_{11}(t-\tau)}(A_{12}x_2(\tau,i) + B_1u(\tau,i))d\tau \quad (18)$$

and solution of the difference equation (1b) is given by

$$x_2(t,i) = A_{22}{}^i x_2(t,0) + \sum_{k=0}^{i-1} A_{22}{}^{i-k-1}(A_{21}x_1(t,k) + B_2u(t,k)) \quad (19)$$

Substituting (19) into (18), we obtain

$$x_1(t,i) = e^{A_{11}t}x_1(0,i) + \int_0^t e^{A_{11}(t-\tau)}B_1u(\tau,i)d\tau +$$
$$\int_0^t e^{A_{11}(t-\tau)}A_{12}A_{22}^i x_2(\tau,0)d\tau +$$
$$\sum_{k=0}^{i-1}\int_0^t e^{A_{11}(t-\tau)}A_{12}A_{22}{}^{i-k-1}B_2u(\tau,k)d\tau + \quad (20)$$
$$\sum_{k=0}^{i-1}\int_0^t e^{A_{11}(t-\tau)}A_{12}A_{22}{}^{i-k-1}A_{21}x_1(\tau,k)d\tau =$$
$$\overline{x}_1(t,i) + \sum_{k=0}^{i-1} P_{i-k-1}x_1(t,k)$$

where

$$\overline{x}_1(t,i) = e^{A_{11}t}x_1(0,i) +$$
$$\int_0^t e^{A_{11}(t-\tau)}[A_{12}A_{22}^i x_2(\tau,0) + B_1u(\tau,i)]d\tau +$$
$$\sum_{k=0}^{i-1}\int_0^t e^{A_{11}(t-\tau)}A_{12}A_{22}{}^{i-k-1}B_2u(\tau,k)d\tau \quad (21)$$

$$P_j f(t) = \int_0^t e^{A_{11}(t-\tau)}A_{12}A_{22}{}^j A_{21}f(\tau)d\tau, \quad j \in Z_+$$

Substituting (20) into (19), we obtain

$$x_2(t,i) = A_{22}{}^i x_2(t,0) + \sum_{k=0}^{i-1} A_{22}{}^{i-k-1}B_2u(t,k) +$$
$$\sum_{k=0}^{i-1} A_{22}{}^{i-k-1}A_{21}e^{A_{11}t}x_1(0,k) +$$
$$\sum_{k=0}^{i-1}\int_0^t A_{22}{}^{i-k-1}A_{21}e^{A_{11}(t-\tau)}B_1u(\tau,k)d\tau +$$
$$\sum_{k=0}^{i-1}\int_0^t A_{22}{}^{i-k-1}A_{21}e^{A_{11}(t-\tau)}A_{12}A_{22}^k x_2(\tau,0)d\tau + \quad (22)$$
$$\sum_{k=0}^{i-1}\sum_{l=0}^{k}\int_0^t A_{22}{}^{i-k-1}A_{21}e^{A_{11}(t-\tau)}A_{12}A_{22}{}^{k-l-1}B_2u(\tau,l)d\tau +$$
$$\sum_{k=0}^{i-1}\sum_{l=0}^{k}\int_0^t A_{22}{}^{i-k-1}A_{21}e^{A_{11}(t-\tau)}A_{12}A_{22}{}^{k-l-1}A_{21}x_1(\tau,l)d\tau$$

Solutions of hybrid linear system (1) have the form (20) and (22).

4. NUMERICAL EXAMPLE

Transfer function of the hybrid system is given by

$$T(s,z)=\frac{2sz+s+3z+2}{sz-0.1s+0.9z-0.1} \quad (23)$$

and its realization has the form ($n = 1$, $m = 1$)

$$A_{11}=[-0.9],\ A_{12}=[1\ \ 0],\ A_{21}=\begin{bmatrix}0.01\\1.1\end{bmatrix},\ A_{22}=\begin{bmatrix}0.1 & 0\\1 & 0\end{bmatrix},$$
$$B_1=[1],\ B_2=\begin{bmatrix}0.1\\1\end{bmatrix},\ C_1=[1.2],\ C_2=[2\ \ 1],\ D=[2] \quad (24)$$

Let the initial conditions be given by $x_1(0,0)=0$, $x_2(0,0)=\begin{bmatrix}0\\0\end{bmatrix}$, $x_1(0,i)=1$, $x_2(t,0)=\begin{bmatrix}1\\1\end{bmatrix}$ for $i = 1,2,\ldots,$ $t\in[1,\infty)$ and input $u(t,i)=1$ for $t\geq 0$ and $i\geq 0$.
Find $x_1(1,1), x_2(1,1)$.

Using method 1 we obtain:

$$\begin{aligned}
x_1(1,1)&=\sum_{k=1}^{\infty}\sum_{j=0}^{1}X_{k,j}^{1}\frac{1^k}{k!}u(0,1-j)+\\
&\sum_{k=1}^{\infty}\sum_{j=0}^{1}X_{k,j}^{11}\frac{1^{k-1}}{(k-1)!}x_1(0,1-j)+\\
&\sum_{k=1}^{\infty}X_{k,2}^{12}\frac{1^k}{k!}x_2(0,0)=\\
&\sum_{k=1}^{\infty}\frac{1^k}{k!}(X_{k,0}^{1}u(0,1)+X_{k,1}^{1}u(0,0))+\\
&\sum_{k=1}^{\infty}\frac{1^{k-1}}{(k-1)!}(X_{k,0}^{11}x_1(0,1)+X_{k,1}^{11}x_1(0,0))+\\
&\sum_{k=1}^{\infty}X_{k,2}^{12}\frac{1^k}{k!}x_2(0,0)
\end{aligned} \quad (25a)$$

$$\begin{aligned}
x_2(1,1)&=\sum_{k=1}^{\infty}\sum_{j=1}^{1}X_{k,j}^{2}\frac{1^k}{k!}u(0,1-j)+\\
&\sum_{k=1}^{\infty}\sum_{j=1}^{1}X_{k,j}^{21}\frac{1^{k-1}}{(k-1)!}x_1(0,1-j)+\\
&\sum_{j=1}^{1}X_{0,j}^{2}u(1,1-j)+\sum_{k=1}^{\infty}X_{k,2}^{22}\frac{1^k}{k!}x_2(0,0)+X_{0,2}^{22}x_2(1,0)=\\
&\sum_{k=1}^{\infty}\frac{1^k}{k!}X_{k,1}^{2}u(0,0)+\sum_{k=1}^{\infty}\frac{1^{k-1}}{(k-1)!}X_{k,1}^{21}x_1(0,0)+X_{0,1}^{2}u(1,0)+\\
&\sum_{k=1}^{\infty}X_{k,2}^{22}\frac{1^k}{k!}x_2(0,0)+X_{0,2}^{22}x_2(1,0)
\end{aligned} \quad (25b)$$

Taking into account the initial conditions and the input we obtain

$$\begin{aligned}
x_1(1,1)&=\sum_{k=1}^{\infty}\frac{1}{k!}(X_{k,0}^{1}+X_{k,1}^{1})+\sum_{k=1}^{\infty}\frac{1}{(k-1)!}X_{k,0}^{11}\\
x_2(1,1)&=\sum_{k=1}^{\infty}\frac{1}{k!}X_{k,1}^{2}+X_{0,1}^{2}+X_{0,2}^{22}\begin{bmatrix}1\\1\end{bmatrix}
\end{aligned} \quad (26)$$

If we make three iterations, then the solution takes the form

$$\begin{aligned}
x_1(1,1)&=\sum_{k=1}^{3}\frac{1}{k!}(X_{k,0}^{1}+X_{k,1}^{1})+\sum_{k=1}^{3}\frac{1}{(k-1)!}X_{k,0}^{11}=\\
&(X_{1,0}^{1}+X_{1,1}^{1})+\frac{1}{2}(X_{2,0}^{1}+X_{2,1}^{1})+\frac{1}{6}(X_{3,0}^{1}+X_{3,1}^{1})+\\
&X_{1,0}^{11}+X_{2,0}^{11}+\frac{1}{2}X_{3,0}^{11}=B_1+A_{12}B_2+\\
&\frac{1}{2}(A_{11}B_1+A_{11}A_{12}B_2+A_{12}A_{21}B_1)+\\
&\frac{1}{6}(A_{11}^{\ 2}B_1+A_{11}^{\ 2}A_{12}B_2+A_{11}A_{12}A_{21}B_1+\\
&A_{12}A_{21}A_{11}B_1)+1+A_{11}+\frac{1}{2}A_{11}^{\ 2}\\
x_2(1,1)&=\sum_{k=1}^{3}\frac{1}{k!}X_{k,1}^{2}+X_{0,1}^{2}+X_{0,2}^{22}\begin{bmatrix}1\\1\end{bmatrix}=\\
&X_{1,1}^{2}+\frac{1}{2}X_{2,1}^{2}+\frac{1}{6}X_{3,1}^{2}+X_{0,1}^{2}+X_{0,2}^{22}\begin{bmatrix}1\\1\end{bmatrix}=\\
&A_{21}B_1+\frac{1}{2}A_{21}A_{11}B_1+\frac{1}{6}A_{21}A_{11}^{\ 2}B_1+B_2+A_{22}\begin{bmatrix}1\\1\end{bmatrix}
\end{aligned} \quad (27)$$

Substituting (24) into (27), we obtain final value

$$x_1(1,1)=1{,}261$$
$$x_2(1,1)=\begin{bmatrix}0{,}207\\2.752\end{bmatrix} \quad (28)$$

Using method 2, we obtain:

$$\begin{aligned}
\begin{bmatrix}x_1(1,1)\\x_2(1,1)\end{bmatrix}&=\sum_{k=0}^{\infty}\sum_{l=0}^{1}T_{k,1-l}B_{10}\frac{1^{k+1}}{(k+1)!}u(0,l)+\\
&\sum_{k=0}^{\infty}\sum_{l=0}^{1}T_{k,1-l-1}B_{01}\frac{1^k}{k!}u(0,l)+\\
&\sum_{k=0}^{\infty}\sum_{l=0}^{1}T_{k,1-l}\frac{1^k}{k!}\begin{bmatrix}x_1(0,l)\\0\end{bmatrix}+\sum_{k=0}^{\infty}T_{k,1}\frac{1^k}{k!}\begin{bmatrix}0\\x_2(0,0)\end{bmatrix}
\end{aligned} \quad (29)$$

Taking into account the initial conditions and the input we obtain

$$\begin{aligned}
\begin{bmatrix}x_1(1,1)\\x_2(1,1)\end{bmatrix}&=\sum_{k=0}^{\infty}T_{k,1}B_{10}\frac{1}{(k+1)!}+\\
&\sum_{k=0}^{\infty}T_{k,0}B_{10}\frac{1}{(k+1)!}+\sum_{k=0}^{\infty}T_{k,0}B_{01}\frac{1}{k!}+\sum_{k=0}^{\infty}T_{k,0}\frac{1}{k!}\begin{bmatrix}1\\0\end{bmatrix}
\end{aligned} \quad (30)$$

If we make three iterations then the solution takes the form

$$\begin{bmatrix} x_1(1,1) \\ x_2(1,1) \end{bmatrix} = T_{0,1}B_{10} + B_{10} + B_{01} + \begin{bmatrix} 1 \\ 0 \end{bmatrix} + T_{1,1}B_{10}\frac{1}{2} +$$

$$T_{1,0}B_{10}\frac{1}{2} + T_{1,0}B_{01} + T_{1,0}\begin{bmatrix} 1 \\ 0 \end{bmatrix} + T_{2,1}B_{10}\frac{1}{6} +$$

$$T_{2,0}B_{10}\frac{1}{6} + T_{2,0}B_{01}\frac{1}{2} + T_{2,0}\frac{1}{2}\begin{bmatrix} 1 \\ 0 \end{bmatrix} =$$

$$\begin{bmatrix} 0 \\ A_{21}B_1 \end{bmatrix} + \begin{bmatrix} B_1 \\ 0 \end{bmatrix} + \begin{bmatrix} 0 \\ B_2 \end{bmatrix} + \begin{bmatrix} 1 \\ 0 \end{bmatrix} + \frac{1}{2}\begin{bmatrix} A_{12}A_{21}B_1 \\ A_{21}A_{11}B_1 \end{bmatrix} + \tag{31}$$

$$\frac{1}{2}\begin{bmatrix} A_{11}B_1 \\ 0 \end{bmatrix} + \begin{bmatrix} A_{12}B_2 \\ 0 \end{bmatrix} + \begin{bmatrix} A_{11} \\ 0 \end{bmatrix} +$$

$$\frac{1}{6}\begin{bmatrix} (A_{11}A_{12}A_{21} + A_{12}A_{21}A_{11})B_1 \\ (A_{21}A_{11}A_{11})B_1 \end{bmatrix} +$$

$$\frac{1}{6}\begin{bmatrix} A_{11}A_{11}B_1 \\ 0 \end{bmatrix} + \frac{1}{2}\begin{bmatrix} A_{11}A_{12}B_2 \\ 0 \end{bmatrix} + \frac{1}{2}\begin{bmatrix} A_{11}A_{11} \\ 0 \end{bmatrix}$$

and

$$x_1(1,1) = 1{,}247$$
$$x_2(1,1) = \begin{bmatrix} 0{,}107 \\ 1{,}753 \end{bmatrix} \tag{32}$$

Using method 3, we obtain:

For $i = 0$, we have

$$x_1(1,0) = e^{A_{11}}x_1(0,0) + \int_0^1 e^{A_{11}(1-\tau)}A_{12}x_2(\tau,0)d\tau +$$

$$\int_0^1 e^{A_{11}(1-\tau)}B_1u(\tau,0)d\tau =$$

$$e^{A_{11}}x_1(0,0) + e^{A_{11}}A_{11}^{-1}A_{12}x_2(0,0) - A_{11}^{-1}A_{12}x_2(1,0) + \tag{33}$$

$$e^{A_{11}}A_{11}^{-1}B_1u(0,0) - A_{11}^{-1}B_1u(1,0)$$

$$x_2(1,1) = A_{21}x_1(1,0) + A_{22}x_2(1,0) + B_2u(1,0)$$

Substituting the initial conditions and the input, we have

$$x_1(1,0) = -A_{11}^{-1}A_{12}\begin{bmatrix} 1 \\ 1 \end{bmatrix} + e^{A_{11}}A_{11}^{-1}B_1 - A_{11}^{-1}B_1 = 1{,}1771$$

$$x_2(1,1) = A_{21}(-A_{11}^{-1}A_{12}\begin{bmatrix} 1 \\ 1 \end{bmatrix} + e^{A_{11}}A_{11}^{-1}B_1 - A_{11}^{-1}B_1) + \tag{34}$$

$$A_{22}\begin{bmatrix} 1 \\ 1 \end{bmatrix} + B_2 = \begin{bmatrix} 0{,}218 \\ 3{,}948 \end{bmatrix}$$

and, for $i = 1$

$$\begin{aligned} x_1(1,1) &= e^{A_{11}}x_1(0,1) + e^{A_{11}}A_{11}^{-1}A_{12}x_2(0,1) \\ &- A_{11}^{-1}A_{12}x_2(1,1) + e^{A_{11}}A_{11}^{-1}B_1u(0,1) - A_{11}^{-1}B_1u(1,1) \end{aligned} \tag{35}$$

where

$$x_2(0,1) = A_{21}x_1(0,0) + A_{22}x_2(0,0) + B_2u(0,0) = B_2 \tag{36}$$

Substituting the given data, we obtain

$$\begin{aligned} x_1(1,1) &= e^{A_{11}} + e^{A_{11}}A_{11}^{-1}A_{12}B_2 - A_{11}^{-1}A_{12}\begin{bmatrix} 0.218 \\ 3.948 \end{bmatrix} \\ &+ e^{A_{11}}A_{11}^{-1}B_1 - A_{11}^{-1}B_1 = 1{,}263 \end{aligned} \tag{37}$$

Final value

$$x_1(1,1) = 1{,}263$$
$$x_2(1,1) = \begin{bmatrix} 0{,}218 \\ 3{,}948 \end{bmatrix} \tag{38}$$

Remark 1.

Obtained results for $x_1(1,1)$, $x_2(1,1)$ are different for different method (Tab. 1). To obtain some valid results more computations for i = 2, 3,… need to be performed. The number of iteration k in (27) and (31) need to be also increased.

Tab. 1. Final values for $x_1(1,1)$, $x_2(1,1)$ (for k = 3)

State variable	Method 1	Method 2	Method 3
$x_1(1,1)$	1,261	1,247	1,263
$x_{21}(1,1)$	0,207	0,107	0,218
$x_{22}(1,1)$	2,752	1,753	3,948

5. MATLAB/SIMULINK SIMULATIONS

Using Simulink toolbox we can model given transfer function (25) in the form

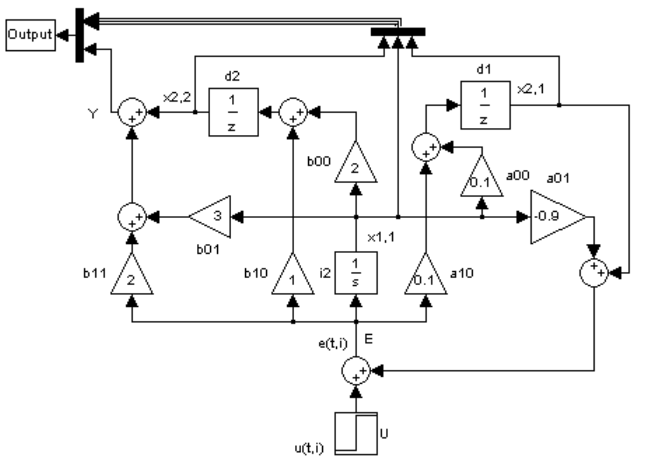

Fig. 1. Matlab/Simulink state variable diagram for transfer function (25)

Simulating i from 0 to 10 with sample time equal one, we obtain ending values of the simulation:

$$x_1 = 1{,}249$$
$$x_2 = \begin{bmatrix} 0{,}125 \\ 2{,}499 \end{bmatrix} \quad (41)$$
$$y = 6{,}249$$

Next step is implementation of considered methods in Matlab.
For simulations we use given initial conditions and input, also the number of iterations is increased (in (29) and (33)).
After performing some simulations, we obtain the following results
Table 2 contains the final values from simulations for three methods. Those results are the state vectors $x_1(t,i)$, $x_2(t,i)$ for $t = 1$ and $i = 6$ with $k = 30$.
Figure 2 shows the diagram generated by Matlab. Diagram shows changes of the values of state vectors with the number i of steps.

Tab. 2. Final values

State variable	Method 1 (dash dot line)	Method 2 (dash dash line)	Method 3 (solid line)	Simulink response
x_1	1,143	1,147	1,148	1,249
x_{21}	0,123	0,124	0,124	0,125
x_{22}	2,376	2,386	2,387	2,499
Execute time [s]	21,744	18,251	0,032	

For $t = 1$, $i = 12$ and $k = 30$ we obtain

Tab. 3. Final values

State variable	Method 1 (dash dot line)	Method 2 (dash dash line)	Method 3 (solid line)
x_1	1,143	1,147	1,148
x_{21}	0,123	0,124	0,124
x_{22}	2,376	2,386	2,387
Execute time [s]	78,266	64,172	0,031

For $t = 10$, $i = 6$ and $k = 30$ we obtain

Tab. 4. Final values

State variable	Method 1 (dash dot line)	Method 2 (dash dash line)	Method 3 (solid line)
x_1	1,250	1,250	1,250
x_{21}	0,125	0,125	0,125
x_{22}	2,500	2,500	2,500
Execute time [s]	21,844	18,251	0,016

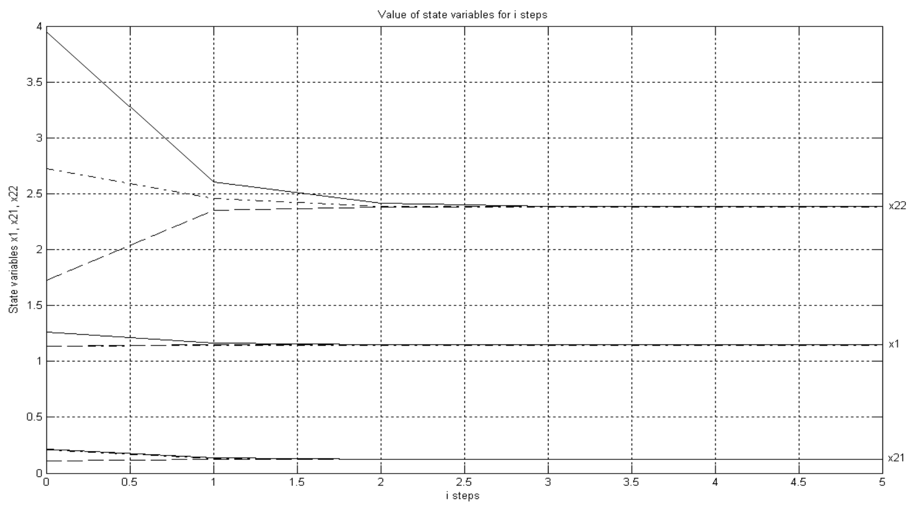

Fig. 2. Computational results for $t = 1$ and $i = 6$ with $k = 30$.

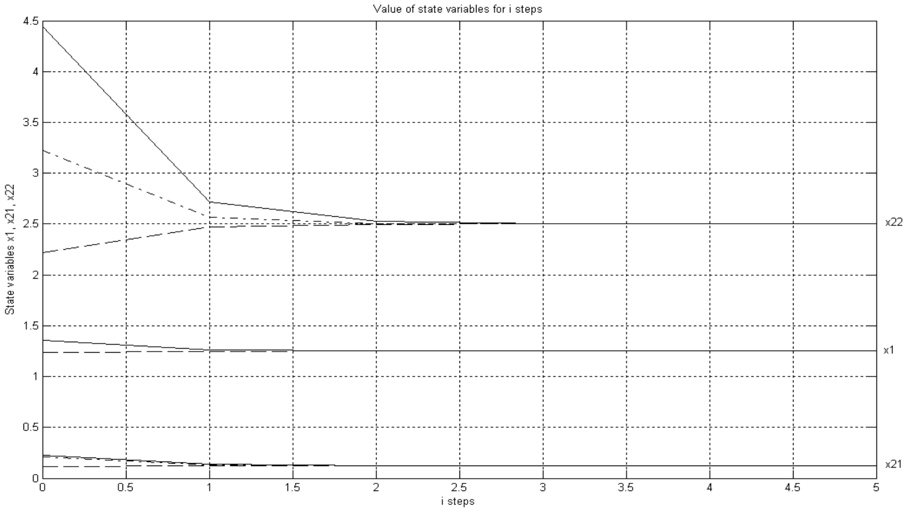

Fig. 3. Computational results for $t = 10$, $i = 6$ and $k = 30$

6. CONCLUDING REMARKS

General conclusion is that all three methods gives the same final results.

The first two methods are similar. To compute the solution $x(t,i)$ using those methods we do not need to know the values of the solution in the previous steps but we have to compute in the first method the matrices $X^1_{k,i}, X^2_{k,i}$ using the determining equations (3) or the matrices $T_{i,j}$ defined by (14) in the second method. In the third method the solution $x(t,i)$ is computed recursively using the initial conditions.

From the simulations it follows that the three methods give similar results after at least three steps.

The calculations have been performed on the Pentium M – 1,7GHz processor with 1GB RAM.

REFERENCES

1. **L. Benvenuti, L. Farina** (2004), *A tutorial on the positive realization problem,* IEEE Trans. Autom. Control, vol. 49, No 5, pp. 651-664.
2. **L. Farina, S. Rinaldi** (2000), *Positive Linear Systems; Theory and Applications*, J. Wiley, New York.
3. **T. Kaczorek** (2003), *Some recent developments in positive systems,* Proc. 7th Conference of Dynamical Systems Thdeory and Applications, pp. 25-35, Łódź.
4. **T. Kaczorek** (2001), *Positive 1D and 2D systems*, Springer Verlag, London.
5. **T. Kaczorek** (2006), *A realization problem for positive continues-time linear systems with reduced numbers of delay*, Int. J. Appl. Math. Comp. Sci., Vol. 16, No. 3, pp. 325-331.
6. **T. Kaczorek** (2006), *Realization problem for positive multivariable discret-time linear systems with delays in the state vector and inputs*, Int. J. Appl. Math. Comp. Sci., ol. 16, No. 2, pp. 101-106.
7. **T. Kaczorek** (2004), *Realization problem for positive discrete-time systems with delay*, System Science, Vol. 30, No. 4, pp. 17-13.
8. **T. Kaczorek** (2005), *Positive minimal realizations for singular discrete-time systems with delays in state and delays in control*, Bull. Pol. Acad. Sci. Techn., Vol 53, No 3.
9. **T. Kaczorek, M. Busłowicz** (2004), *Minimal realization problem for positive multivariable linear systems with delay*, Int. J. Appl. Math. Comput. Sci., Vol. 14, No. 2, pp. 181-187.
10. **T. Kaczorek, Ł. Sajewski** (2008), *Solution of 2D singular hybrid linear system*, 14th International Congress of Cybernetics and Systems of WOSC (submited).
11. **J. Klamka** (1991), *Controllability of dynamical systems*, Kluwer Academic Publ., Dordrecht.
12. **J. Kurek** (1985), The *general state-space model for a two-dimensional linear digital system*, IEEE Trans. Austom. Contr. AC-30 , June, pp. 600-602.
13. **V. M. Marchenko, O. N. Poddubnaya** (2005), *Solution representation and relative controllability of linear differential-algebraic system with several delays*, Doklady Mathematics, Vol. 72, No. 2, pp. 824-828.
14. **V. M. Marchenko, O. N. Poddubnaya, Z. Zaczkiewicz** (2005), *Hybrid control and observation systems in symmetric form*, Proc. Of the IEEE Conf. "RoMoCo", Poznań, Poland.
15. **R. B. Roesser** (1975), *A discrete state-space model for linear image processing*, IEEE Trans. on Automatic Control, AC-20, 1, pp. 1-10.

This work was supported by the State Committee for Scientific Research of Poland under the grant NN 514 1939 33.

RATIONALE FOR MU-SYNTHESIS CONTROL OF FLEXIBLE ROTOR-MAGNETIC BEARING SYSTEMS

Jerzy T. SAWICKI*

*Department of Mechanical Engineering, Cleveland State University,
2121 Euclid Avenue, SH-245, Cleveland, OH 44115, USA

j.sawicki@csuohio.edu

Abstract: The emergence of sophisticated formal control synthesis tools provokes important questions for any prospective user: why learn to use these new tools, what will they offer me? In synthesis of magnetic bearing controllers, it turns out that the range of stabilizing controllers is often quite narrow so that the difference between a poor controller and an "optimal" one may be small. Hence, the product of formal control synthesis tools often looks and performs much like what a reasonably clever control engineer would produce by hand. This paper demonstrates that the real value of these tools lies in a) generation of a performance benchmark which can be used to firmly establish the best performance relative to a specification and b) change of design parameter space to one which is relatively easy to maintain and represents a durable investment from an engineering process view.
Keywords: Robust control, flexible rotor, mu-synthesis, uncertainties.

1. INTRODUCTION

Magnetic bearing systems for rotating machinery represent an archetypal challenge for multi-input, multi-output (MIMO) control: they inherently involve multiple interacting control mechanisms and many conflicting performance objectives. As such, they would appear to be a perfect application of formal MIMO control design techniques such as μ-synthesis. However, the control culture of the magnetic bearings technical community is largely classical and many clever approaches have been developed to enable classical, essentially single-input, single output (SISO) methods to produce reliable and robust solutions to this control problem. A large part of the reason behind this is, quite simply, that classical SISO methods are more widely understood by controls engineers and have a much larger experience base on which to draw. Consequently, most commercial developers view tools like μ-synthesis with considerable trepidation.

Compounding this view is the simple fact that most published examples of μ-synthesis control for AMB systems produce only incremental improvements over hand-synthesized controllers and even this comparison is suspect since optimization of hand-synthesized controllers is largely an art for systems with this level of complexity. We argue here that the primary reason for applying a method like μ-synthesis to AMB control problems is to obtain a better engineering process rather than to obtain substantial performance enhancements. Because μ-synthesis is genuinely an optimization process and because the performance index that it optimizes has a very clear connection to real engineering practice, μ- can at least provide a benchmark against which other controllers may be measured. This alone justifies some level of investment in the method. But more importantly, μ- represents a change in parameter space - the set of knobs that a control designer can turn - and this new parameter space arguably leads to a better engineering process. In particular, investments in this alternate process are easier to translate to different control problems, easier to document, and easier to transfer to new engineers. In order to develop this argument, this paper first outline what is viewed to be the *natural* primary objectives or specifications of AMB controller synthesis. Then the connection between these objectives and the μ-synthesis problem will be developed, highlighting what is retained exactly, what is retained approximately, and what is lost. Then, the actual μ-synthesis problem will be discussed, emphasizing that it is essentially a minor last step once a well structured analysis process for the control objectives has been assembled. That is, most of the engineering effort is applied to developing machinery for assessing the performance of *any* controller relative to these objectives: if this machinery is constructed in a particular way, then μ-synthesis is automatic and requires no significant further effort by the engineer. To illustrate the concepts, an AMB supported machine tool spindle example will be presented. Inevitably, the discussion is heavily invested in the machinery of μ-analysis and synthesis as well as that of H_∞ analysis and synthesis. However, most of the central details can only be provided in sketch because of space limitations: the interested reader is referred to any of numerous authoritative texts on these subjects, for instance (Zhou et al., 1996; Goodwin, 2001; Green and Limebeer, 1995).

2. AMB MACHINING SPINDLE REFERENCE EXAMPLE

To illustrate the concepts presented here, consider the AMB supported machine tool spindle with cross-section shown in Fig. 1. The spindle rotor is supported by two radial bearings and one thrust bearing. The maximum static radial load capacities are approximately 1400 and 600 N for the front and rear bearings, respectively, and the maximum axial capacity for thrust bearing is 500 N. The spindle reaches a rotational speed of 50,000 rpm at 10 kW. The AC motor acts on the rotor between the thrust and rear radial bearing.

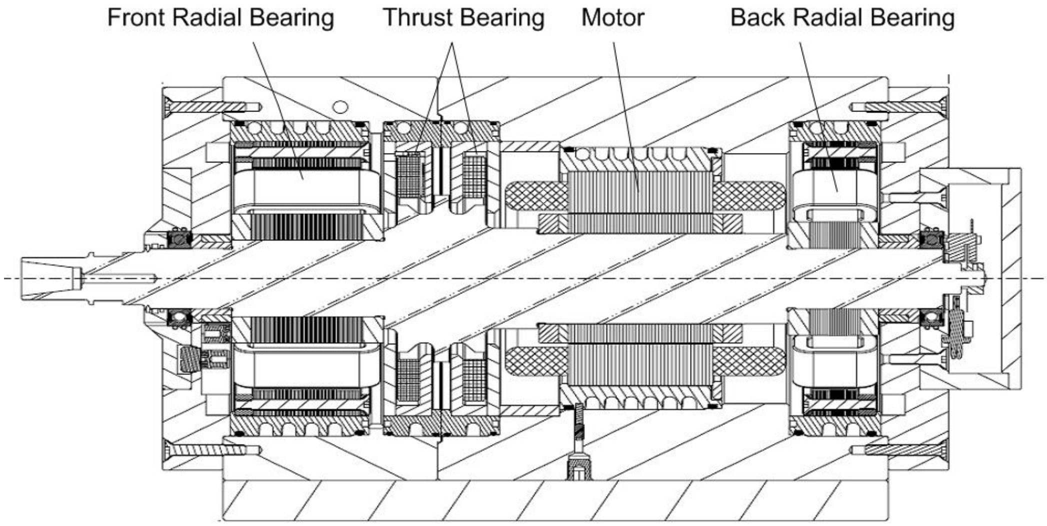

Fig. 1. High-speed machining spindle supported on active magnetic bearings

The total rotor mass is 6.85 kg while the total length is 464 mm. The first two free-free flexible modes are at frequencies 1070 Hz and 1985 Hz. The actuators are driven by transconductance power amplifiers with bandwidth of about 2400 Hz and a gain of 1 volt/amp. Control is implemented digitally with a sampling rate of 10 kSa/sec. The full system model includes rotor (64-element FEM model modally truncated to include two rigid body modes and two flexible modes), actuator properties, amplifier dynamics, computational delay (by Padé approximation), and sensor dynamics.

3. AMB CONTROLLER DESIGN: OBJECTIVES

Most applications of AMB systems for rotating machinery are primarily concerned with steady behavior: analysis focuses on response to steady sinusoidal loads such as mass unbalance, shaft bow, aerodynamic loads, and sensor noise. Such an approach is even commonly adopted when considering transient phenomena such as compressor surge. Notable exceptions to this include applications to systems subject to extreme impact loading such as underwater naval vessels. For systems which are linear (really the dominant behavior of AMB systems), this focus on sinusoidal response has a deeper theoretical justification which dictates that the “worst case”1 bounded signals that can act on linear (time invariant) systems are sinusoidal.

The literature contains many detailed application examples where the performance objectives in AMB controller synthesis are elucidated (Sawicki et al., 2007; Fittro and Knospe, 1999; Sawicki and Maslen, 2006, 2007; Namarikawa and Fujita, 1999). Generally, the obvious objectives include an adequate stability margin and adequate management of external loads. Given the underlying nonlinear character of AMB systems, a common secondary objective is to maintain operation in an essentially linear regime, avoiding numerous sources of nonlinearity including actuator magnetic saturation, amplifier voltage saturation, and actuator nonlinearity due to large journal displacements.

At the most conceptual level, the AMB system may be described by the block diagram indicated in Fig. 2 in which the control inputs u are signals delivered to the power amplifiers, the measurements y are signals received from position sensors, the loads w are forces or electrical noise acting on the system, and performance measures z are those signals that the engineer will monitor in assessing adequate management of the loads w.

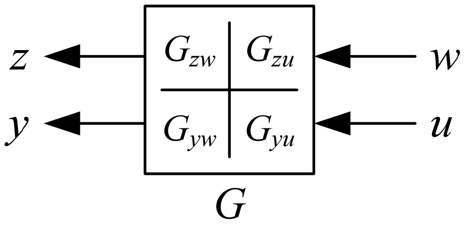

Fig. 2. An AMB system represented as a four block problem

In describing these signals, each will have a natural engineering description and these diverse descriptions will need to be adapted to a uniform and mathematically tractable form for purposes of assessment and design. It is assumed that the signals y and u are self-explanatory and will typically have units of volts. More important is the character of the signals w and z. The exogenous signals w will be a combination of forces (rotor unbalance, gravity load, process loads, impacts) and sources of measurement signal corruption: generally, electrical noise. Some of these have a nice description as a combination of simple basis functions ($\sin\omega t$, $\cos\omega t$, 1.0, e^{at}) with unknown but bounded amplitudes. A simple example is mass unbalance which will typically act at many locations along a rotor and will be described at each location as

$$\begin{Bmatrix} f_x \\ f_y \end{Bmatrix}_i = me_{u.i}\Omega^2 \begin{Bmatrix} \sin\left(\Omega t + \phi_i\right) \\ \cos\left(\Omega t + \phi_i\right) \end{Bmatrix} \tag{1}$$

in which $me_{u.i}$ is a known level of mass unbalance at each location, but with a relatively confident bound: $me_{u.i} < me_{u.i,\,max}$.

Signals such as electrical noise are a bit more difficult to describe but may be represented in terms of spectral bounds. In this case, the spectrum of the signal is expected to lie below a specific bounding curve: assume that there is a stable transfer function $W_w(s)$ whose magnitude exceeds the expected amplitude of the noise signal at every frequency. This means that there is a choice of signal $\hat{w}$ whose RMS amplitude is less than 1.0 for which $w=W_w\hat{w}$ recovers the expected noise signal. Ideally, the amplitude of W_w is as small as possible at every frequency, while still preserving this relationship. Often, when the spectrum of the signal η might be complicated, W_w significantly overbounds the range in the interest of keeping the complexity of W_w low.

The end result is a description of the exogenous signals which takes the form

$$w(s) = W_w \hat{w}(s) \tag{2}$$

in which the elements of $\hat{w}(t)$ are expected to be periodic with amplitude less than or equal to 1.0. The weighting function W_w accounts for spectral bounds which vary with frequency as in the case of mass unbalance (increases with the square of frequency out to some maximum rotation rate).

In the case of the performance signals, the requirement for adequate performance will ideally take the form of

$$z_{i,\min} \le z_i(t) \le z_{i,\max} \;:\; -\infty < t < \infty \tag{3}$$

Examples of such performance specifications include rotor contact clearance, actuator magnetic flux density, and power amplifier output voltage and current. Most commonly, the limits are symmetric so that we may require

$$\frac{z_i(t)}{z_{i,\max}} \le 1 \;:\; -\infty < t < \infty \tag{4}$$

More generally, this nondimensionalization may be written as

$$z = W_z \hat{z} \;:\; \hat{z}_i(t) \le 1.0 \tag{5}$$

in which the scaling of the elements of z is encapsulated by the weighting function W_z. In this manner, W_z is a performance specification in that it stipulates limitations on permissible range of the performance variables z_i.

4. THE SYSTEM MODEL

In its most precise description, the dynamic mapping G indicated in Fig. 2 is nonlinear but it is standard practice to use a linear approximation throughout most of the design process. In the sequel, we will assume specifically that G is linear time invariant (LTI) and may be represented as a matrix of transfer functions. For most AMB systems, such a representation retains sufficient fidelity to permit it to carry the design and analysis nearly to completion. A very thorough design process would conclude by connecting the resulting controller to a fully nonlinear model of the AMB-rotor system and use transient simulations to establish that the linear assumptions have not missed critical performance or stability features. This assumption that G is LTI is central to $\mu-$synthesis and is a first limitation of the design process. Of course, similar assumptions underlie most practical controller synthesis processes: the most notable exceptions would be Lyapunov methods (Tsiotras et al., 2000) or variants such as backstepping (de Queiroz and Dawson, 1996) but these methods have received only very limited attention in the AMB literature and are generally not practical to apply to high ordered models G as arise when rotor flexibility is considered.

In a similar manner, it is common to model the controller as also LTI for the bulk of the design and analysis work. Certainly, commercial AMB controllers often contain nonlinear elements (Lindlau and Knospe, 2002; Cole et al., 2000), but these are assumed either to play a role in extending the linear operating regime (output feedback linearization, for instance) or to operate only when the system is under duress. As such, the controller may be described by a matrix transfer function H and the closed loop system indicated in Fig. 3 maps nondimensional exogenous signals $\hat{w}$ to nondimensional performance measures $\hat{z}$ via

$$\hat{z}(s) = W_z^{-1}\left[G_{zw} + G_{zu}H\left(I - G_{yu}H\right)^{-1}G_{yw}\right]W_w\hat{w} \equiv P\hat{w}(s) \qquad (6)$$

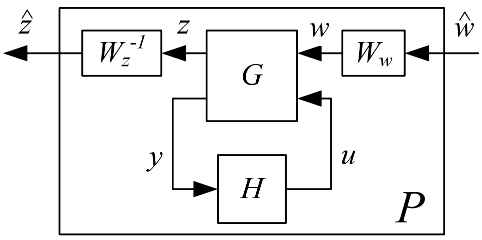

Fig. 3. An AMB system with controller closed loop

Here, the weighted closed loop performance function P can be introduced as a shorthand notation for the more complex expression

$$P = W_z^{-1}\left[G_{zw} + G_{zu}H\left(I - G_{yu}H\right)^{-1}G_{yw}\right]W_w \qquad (7)$$

5. PERIODIC FUNCTIONS

The performance problem, then, is to establish that

$$\hat{z}_i(t) \le 1.0 \;:\quad -\infty < t < \infty$$

when $\hat{z}(s) = P\hat{w}(s)$ and $w_i(t)$ is any periodic signal with amplitude less than or equal to 1.0. First, note that if P is stable, then the homogenous responses $\hat{z}_i$ will also be periodic. If they are periodic, then there is a fundamental connection between the amplitudes of $\hat{z}_i$ and their peak temporal values. Hence, assume that the same normalization holds: that $|\hat{z}_i| \le 1$ is a sufficient condition to meet the temporal requirement. Primarily, this assumption means that we neglect the transient response and assume that the engineering analysis is predominantly concerned with steady state (periodic) response. Obviously, very close satisfaction of periodic response bounds may imply that the transient response violates the temporal bound: one approach to managing this shortcoming is to be a bit conservative in establishing the periodic constraint.

With this, the performance requirement becomes

$$|\hat{z}_i(t)| < 1.0, \quad \hat{z}(s) = P\hat{w}(s), \quad |\hat{w}_i(t)| < 1.0 \qquad (8)$$

in which both $\hat{z}$ and $\hat{w}$ are assumed to be periodic functions whose amplitudes may be represented in RMS terms. Of course, this condition should be met for the *worst case* choice of $\hat{w}$. In particular, the elements of $\hat{w}$ should be worst case periodic functions and the combination of bounded amplitudes should maximize $\hat{z}$. Fortunately, it may be proved that, for an LTI operator P, the worst case periodic function is a sinusoid of single frequency. Thus, a sufficient condition for satisfying (8) is that

$$|\hat{z}_i(t)| < 1.0, \quad \hat{z}(t) = P(j\omega)\hat{w}\sin\omega t, \qquad |\hat{w}_i| < 1.0, \quad \omega \in \Re \qquad (9)$$

Relative phase of the exogenous signals in (9) is managed by assuming that the $\hat{w}_i$ are complex numbers. Under this assumption, the functions $\hat{z}_i$ may also be represented as $\hat{z}_i(t) = \hat{z}_i \sin\omega t$ and (9) becomes

$$|\hat{z}_i(t)| < 1.0, \quad \hat{z} = P(j\omega)\hat{w}, \quad |\hat{w}_i| < 1.0, \quad \omega \in \Re \qquad (10)$$

6. SINGULAR VALUE ANALYSIS

Equation (10) still represents a worst case condition in that we must assure that none of the elements $\hat{z}_i$ has modulus exceeding 1.0 for any frequency or for any possible combination of $\hat{w}_i$ which are only constrained to have modulus less than 1.0. For the moment, neglect the frequency dependence and focus on the possible combinations of $\hat{w}_i$.

The notion that we need $|\hat{z}_i| < 1$ for any combination of $|\hat{w}_i| < 1$ has a nice engineering interpretation but here we introduce another simplification in order to make the problem more mathematically tractable. Rather than requiring that each element of $\hat{w}$ have modulus less than 1, require that the sum of the squares is less than one: $\sum|\hat{w}_i|^2 = |\hat{w}_i|_2^2 < 1$. Certainly, this condition may only be met if | $\hat{w}_i$ |<1 so it is a sufficient but not necessary constraint on w. Further, rather than requiring that $|\hat{z}_i| < 1$, require that $\sum|\hat{z}_i|^2 = |\hat{z}_i|_2^2 < 1$. Again, this is conservative in that it is a sufficient condition for the stipulation on ˆz but not necessary. Thus, if it is true that

$$|\hat{z}|_2 = |P\hat{w}|_2 < 1, \text{ for } \forall|\hat{w}|_2 < 1 \qquad (11)$$

then it is also true that $|\hat{z}_i| < 1$.

The value of the condition indicated by (11) is that it may be tested without performing an exhaustive search on feasible $\hat{w}$. In particular, a necessary and sufficient condition for meeting (11) is that the *maximum singular value* of P is less than 1.0:

$$\bar{\sigma}(P) \le 1 \Leftrightarrow |\hat{z}|_2 = |P\hat{w}|_2 < 1 \;\; \forall|\hat{w}|_2 < 1$$

Of course, as in (10), P is a function of frequency so that a sufficient condition to meet (10) is that

$$\bar{\sigma}(P) \le 1 \;\; \forall\omega \in \Re$$

or, equivalently

$$\sup_{\omega\in\Re}\bar{\sigma}\left(P\left(j\omega\right)\right)\le 1.0 \tag{12}$$

The left side of Eq. (12) defines the H_∞ norm of the transfer function $|P|_\infty$ and indicates the worst case possible gain from the signal $\hat{w}$ to the signal $\hat{z}$. It is assumed implicitly that P represents a stable LTI dynamic system.

6. WEIGHTING FUNCTIONS

The weighted plant model for the reference example is shown in Fig. 4. For the machine tool spindle problem, the loads were assumed to act at the bearing locations while each of the position sensors was assumed afflicted with noise. The bearing loads are summarized in Tab. 1 while the sensor noise was 0.6 micrometers broad-band. The performance measures included amplifier voltage (limited to 300 volts), coil current (limited to 7 amps above a 5 amp bias), and journal displacement at the two bearing locations (limited to 50 micrometers at frequencies above 0.002 Hz, and 0.5 micrometers below this).

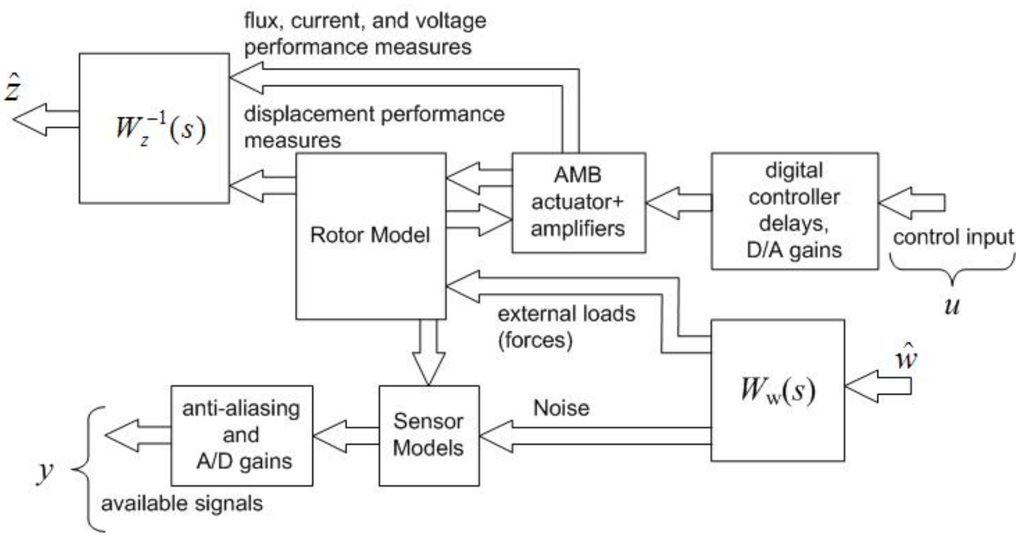

Fig. 4. Weighted model: weighting functions W_w and W_z normalize the load and perfiormance signals

Tab. 1. Bearing load parameters

	tool tip end	drive end
DC load	300 N	130 N
first break	0.0001 Hz	0.001 Hz
midfrequency load	80 N	50 N
second break	40 Hz	40 Hz

7. MODEL UNCERTAINTIES

A significant goal of μ-synthesis is to design controllers which are robust to variations in plant dynamics. A simple example is the effect of gyroscopics: the dynamics of the rotor at standstill are substantially different from those observed when spinning at 16000 RPM. The rotor model contains the rotor spin rate explicitly:

$$M\ddot{x}+\left(D+\Omega G\right)\dot{x}+Kx=f \tag{13}$$

in which the gyroscopic behavior of the rotor mass is represented by the matrix G and Ω is the spin speed of the rotor. If a controller is designed for the rotor with Ω = 0, then there may be no guarantee that the system will be stable for other values of Ω: obviously undesirable.

In the μ-framework, uncertainties are represented as feedback gains connected to the plant where the nominal value of the feedback gain is zero but it is understood that the gain could lie anywhere inside a real range or complex disk. By convention, the size of this range is chosen to be 1.0. As an example, suppose that our rotor had a seal acting at some location along the shaft. The seal might have some nominal cross-coupled stiffness of 1000 N/m but with uncertainty of ± 300 N/m:

$$\begin{Bmatrix} f_{s,x} \\ f_{s,y} \end{Bmatrix} = \begin{bmatrix} 0 & 1000\pm 300 \\ -1000\mp 300 & 0 \end{bmatrix}\begin{Bmatrix} x \\ y \end{Bmatrix} \tag{14}$$

This can be represented by

$$\begin{Bmatrix} f_{s,x} \\ f_{s,y} \end{Bmatrix} = \begin{bmatrix} 0 & 1000 \\ -1000 & 0 \end{bmatrix}\begin{Bmatrix} x \\ y \end{Bmatrix} + 300\begin{bmatrix} 0 & \pm 1 \\ \mp 1 & 0 \end{bmatrix}\begin{Bmatrix} x \\ y \end{Bmatrix} \tag{15}$$

The first part of the relationship defines the *nominal* behavior and would be included in the core model. The second part defines a feedback with nominal value of zero. The scale 300 N/m would be applied to the input or output matrices tying this feedback into the rotor model and the remnant would be the uncertainty matrix, denoted Δ.

The product of adding weighting functions and uncertainty representations to the base model is depicted in Fig. 5.

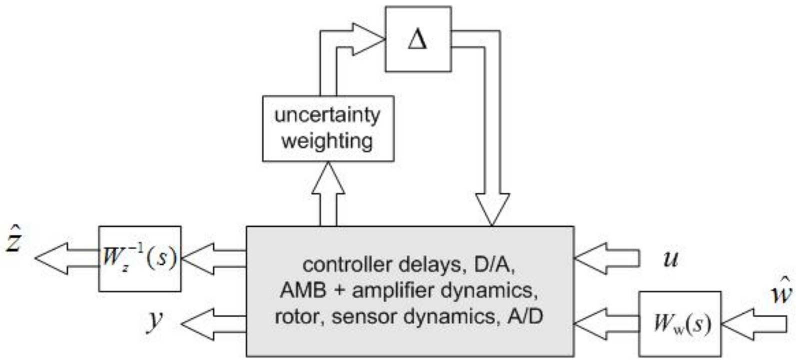

Fig. 5. Model with weighing functions and uncertainty added

For the machine tool spindle, the primary uncertainties were judged to be actuator properties, modal properties for the two bending modes retained, and, of course, rotor speed. The uncertainties in actuator gain and bearing negative stiffness were modeled as 3% and 15% real uncertainties of nominal value, respectively. The modal frequencies of the first and second modes were modeled as 1% complex uncertainty of nominal value for each mode. These latter uncertainties discourage the synthesis machinery from introducing controller dynamics that precisely cancel the dynamics associated with these modes as, for instance, very sharp notch filters. Rotor speed was modeled as 8000 RPM with an uncertainty of 100% in order to obtain a stabilizing controller for the speed range
from 0 to 16000 RPM.

8. THE MU-SYNTHESIS PROBLEM

Having established that assessment of stability robustness and robust performance of an AMB system may be written as a problem in computing the maximum structured singular value, or μ, of the closed loop system, it is natural to consider the possibility that a controller could be automatically synthesized to minimize this μ measure and thereby maximize the robust stability and robust load rejection of the resulting system. This is the objective
of μ-synthesis.

Concisely, μ-synthesis seeks to find that controller H for which the maximum structured singular value of the closed loop system P is minimized. As with H_∞ synthesis, once the specification is established, solving for the controller is a matter of “turning a crank”. That is, reasonably effective computational tools exist to solve this problem. An example is the function “dksyn” provided by the Robust Control Toolbox of MatLab (The MathWorks, 2004).

Unlike the H_∞ synthesis problem, solutions to the μ-synthesis problem cannot be found closed-form and require iteration. The most common iteration scheme is called $D-K$ iteration. While the details of this iterative process are beyond the scope of this paper, it is worth pointing out that $D-K$ iteration adds order to the controller beyond the order of a comparable H_∞ controller so that the order of a μ-controller can be substantially larger than that of the plant plus its weighting functions. This iterative character of the solution can also sometimes lead to failure of the solution which, in this case, does not always imply non-existance of a solution.

Several μ-controllers were designed for the system described by Fig. 1 and just two examples are illustrated in Fig. 6, where one of the controllers was optimized to achieve the best machining performance in terms of high surface finish quality. Both controllers were implemented as discrete time, state-space systems with a sampling rate of 10 kHz. The resulting optimized controller was 88th order and was reduced to 44th order by model order reduction using Hankel singular value based algorithms. Differences between the controllers were generated by changing the performance and load weighting functions.

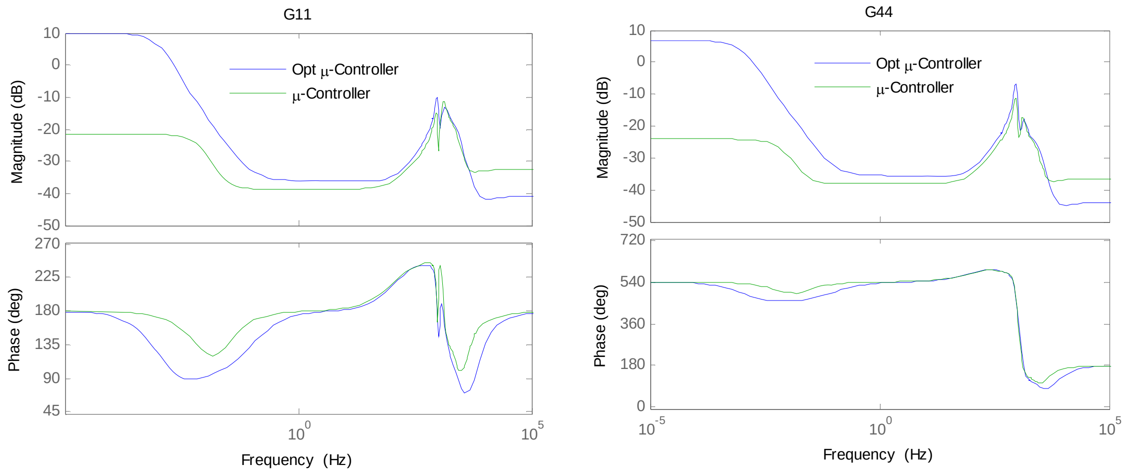

Fig. 6. Comparison of two μ-controllers; one is optimized for machining

To determine the spindle stiffness at the tool tip, with the rotor supported on each the PID, the μ-controller, and the optimized μ-controller, impact testing was carried out with an instrumented hammer. The results presented in the upper plot of Fig. 7 show the advantage of μ-controllers, especially in the vicinity of the first and second modes, where the PID stiffness is significantly lower. Over the wide range of frequencies the PID controller is much less stiff while the optimized μ-controller provides the highest stiffness.

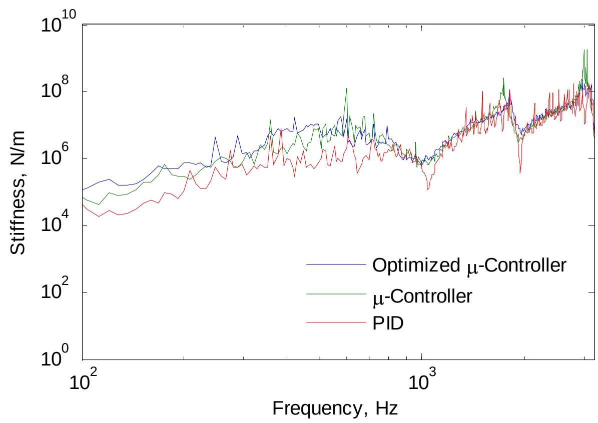

Fig. 7. Stiffness of the spindle at the tool tip extracted from the hammer test for PID and μ-controllers

9. CONCLUSIONS

A well formulated performance assessment tool for evaluating controllers for AMB systems (and practically any other essentially linear system with primarily steady state performance objectives) can be efficiently constructed in the form of a μ-analysis problem. Such a tool is compatible with any linearized AMB/rotor model and any linear controller and, as such, is entirely suitable for assessment of hand-synthesized controllers such as PID with notches and other specialized embellishments. At the same time, having produced such an assessment tool, automated synthesis is just a short step away and involves essentially no investment on the part of the controller design engineer.

The presented simulation and experimental results show the potential of μ-synthesized control of AMB machining spindles for improved cutting performance. In particular, the μ-controllers were able to realize substantially higher broad-band spindle tip stiffness that could be achieved (through manual tuning) by the PID + notch controller. Perhaps a more important advantage is the structure of the synthesis process provided by $\mu-$synthesis. In particular, the synthesis outcome is guided by choice of performance functions and load models and the resulting closed loop performance reflects these functions in a direct manner. Consequently, there is less need for synthesis tricks with the μ- approach. Further, the μ- approach provides

a convenient and rational repository for accumulating system knowledge through model and weighting function refinement. Finally, the μ-approach can provide guarantees of robustness to wide ranges of system parameter such as the operating speed range without requiring gain scheduling or other special techniques: all μ-synthesized controllers developed in the course of this study were stable over the entire operating range while aggressive PID + notch designs did not reliably meet this requirement.

REFERENCES

1. **Zhou, K., Doyle, J. C., and Glover, K.** (1996), *Robust and Optimal Control*. Prentice-Hall, Inc.
2. **Goodwin, G. C.** (2001), *Control System Design*. Prentice-Hall, Inc.
3. **Green, M., and Limebeer, D. J. N.** (1995), *Linear Robust Control*. Prentice-Hall, Inc.
4. **Sawicki, J.T. and Maslen, E.H., Bischof, K.R.** (2007), "Modeling and Performance Evaluation of Machining Spindle with Active Magnetic Bearings," *Journal of Mechanical Science and Technology*, 21(6), pp. 847-850.

5. **Fittro, R., and Knospe, C.** (1999), "μ control of a high speed spindle thrust magnetic bearing", *In Proceedings of the 1999 IEEE International Conference on Control Applications*, Vol. 1, pp. 570–575.
6. **Sawicki, J.T. and Maslen, E.H.** (2007), "Rotordynamic Response and Identification of AMB Machining Spindle," Paper GT2007-28018, *Turbo ASME Turbo Expo Conference*, May 14-17, Montreal, Canada.
7. **Sawicki, J.T. and Maslen, E.H.** (2006), "AMB Controller Design for a Machning Spindle using μ-Synthesis," *The Tenth International Symposium on Magnetic Bearings (ISMB-10*), Martigny, Switzerland, August 21-23.
8. **Namarikawa, T., and Fujita, M.** (1999), "Uncertain model and μ-synthesis of a magnetic bearing", *In Proceedings of the 1999 IEEE International Conference on Control Applications*, Vol. 1, pp. 558–563.
9. **Tsiotras, P., Wilson, B., and Bartlett, R.** (2000), "Control of zero-bias magnetic bearings using control Lyapunov functions", *In Proceedings of the 39th IEEE Conference on Decision and Control 2000*, Vol. 4, pp. 4048–4053.
10. **de Queiroz, M. S., and Dawson, D. M.** (1996), "Nonlinear control of active magnetic bearings: a backstepping approach". *IEEE Transactions on Control Systems Technology,* 4(5), September, pp. 545–552.
11. **Lindlau, J. D., and Knospe, C. R.** (2002), "Feedback linearization of an active magnetic bearing with voltage control" *IEEE Transactions on Control Systems Technology,* 10(1), January, pp. 21–31.
12. **Cole, M. O. T., Keogh, P. S., and Burrows, C. R.** (2000), "Fault-tolerant control of rotor/magnetic bearing systems using reconfigurable control with built-in fault detection". *Proceedings of the Institution of Mechanical Engineers, Part C: Journal of Mechanical Engineering Science,* 214(12), pp. 1445–1465.
13. The MathWorks (2004), *Robust Control Toolbox User's Manual*, 3rd ed. The American Society of Mechanical Engineers, Natick, MA.

MICROELECTROMECHANICAL FLYING ROBOTS - STATE OF THE ART

Krzysztof SIBILSKI[*]

[*]Katedra Robotyki i Automatyki, Wydział Mechaniczny, Politechnika Białostocka, ul. Wiejska 45 C, 15-351 Białystok

sibilski@hot.pl

Abstract: Micro Air Vehicles (MAVs) are miniature airplanes constructed from state-of-the-art materials, designed to be small, light, and highly resilient. Current applications include surveillance, reconnaissance, and munitions. Many of the planes, because of their size, have unconventional designs with respect to the wings and control surfaces. Instability introduced by the small non-traditional aircraft designs must be addressed, to eliminate the need for an expert pilot for aircraft control and navigation. In this paper we present a state-of-the-art technology development focused on the technologies and components required to enable flight at small scales, including flight control, power and propulsion, navigation, multi-purpose structures, advanced communications and information systems, Micro-electro-mechanical Systems (MEMS), advanced sensors, and lightweight, efficient high-density power sources.

1. INTRODUCTION

The term "micro aerial vehicle" (MAV) can be a bit confusing, in the case this name is given a too literal interpretation. Usually it is assumed, that it is a model of an aeroplane treated as miniature, so the "micro" term regards a class of significantly small aircraft [12]. It should be emphasised, though, that microaeroplanes are not small versions of "big" aeroplanes. They should be treated an entirely new cattegory of unmanned aerial vehicles. The definition created for the use of programmes finances by American DARPA agency states, that MAVs are flying vehicles of overall dimensions not greater than 15 cm (6 inches). Overall dimensions are understood here as wing span, height, length or width. From this stems the fact, that the objects belonging to this class are significantly smaller than other unmanned aircraft being developed or used nowadays. In other words "microaeroplane" is a kind of flying robot, characterised by high manoeuvrability, able to carry miniaturised devices and sensors to dangerous locations. This device can perform various missions: scouting, searching, determining contamination or carrying micro explosive charges.

Although limitation of microaeroplane dimensions to 15 cm can seem too arbitrary, it stems from physical and structural solutions and first of all from little Reynolds numbers of flow around wings. The range of small Reynolds numbers in which MAVs operate means a significant difference in physical processes accompanying their flight. Physics of flight of these aircraft is closer to aerodynamics and flight dynamics of birds and large insects than to that of aeroplanes.

Despite the fact that naturalists have been studying problems of insects and birds flight for over fifty years, until now many problems concerning their flight remain unexplained.

Performance, load capacity or manoeuvrability of modern unmanned aeroplanes is far lower than the performance and "load capacity" of bees and wasps or manoeuvrability of dragonflies. Therefore it could be stated, that until the physics of phenomenon accompanying flight in small Reynolds numbers is thoroughly determined, the flight capabilities of miniature aircrafts will be limited. In other words MAVs development apart from "theoretical" problems connected with modelling of their aerodynamics, flight control and dynamics, and generate a lot of serious technical problems. One of those is the integrations of systems mounted inside of the apparatus. Because of small size of the cargo space of a microaeroplane the distribution of the necessary devices, units and on-board sensors becomes an extremely serious problem. The conception used in "large" aeroplanes, consisting in filling the inside of the airframe with necessary instruments and then equipment – programme integration in this case is practically impossible. The scale of complexity of the problem of integration of MAV systems can be better understood while studying figure 1.

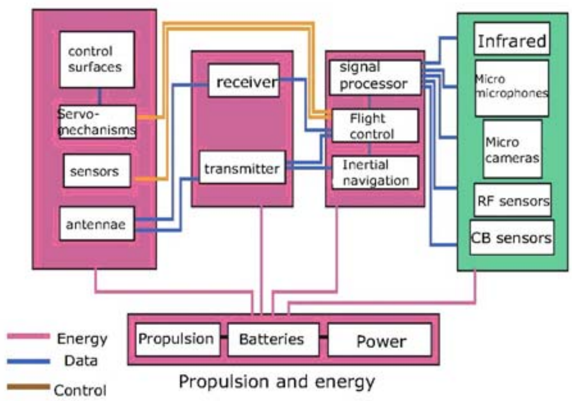

Fig. 1. Integration of MAV systems [22]

Many systems and subsystems presented in fig. 1 belong to the group of microelectronical and microelectromechanical devices. It should be noted, that even individual modules can be of bigger volume than the available one. From the electronic point of view the core of the microaeroplane are: on-board computer and communication modules. These elements are crucial links of a chain connecting the sensors mounted on the microaeroplane and the ground station. They also play the role of controllers of modules of stabilization and control of the flight and of the MAW propulsion system. On the diagram presented in fig. 1 the significant meaning of subsystems of power supply, energy storage and propulsion. Their role is not only providing the power necessary for performing the flight. They are also an energy source for all systems on-board of a microaeroplane. The required functionality of such aircrafts connected with small dimensions and little lift is a serious technological challenge. All systems mounted on them have to be characterised by very large scale of integration. The systems should also be multi-functional. Many of them have to comprise integral elements of airframe structure. And so e.g. the wings of microaeroplane have to be at the same time a system of antennae and be the location of sensors. The power source can be integrated with the fuselage, etc. The degree of “synergism” required when developing a microaeroplane is incomparably higher than the one obtained when designing a “conventional” aeroplane.

Probably the most difficult element of the MAV to design is the system of flight control, which should by highly autonomous and should operate instantaneously. Relatively strong forces and moments caused by laminar flow (in entire flight range) act on the microaeroplane. Moreover it is very difficult to foresee the conditions in which the flight will take place. Because of little mass and dimensions (moments of inertia) the effects of unsteady flow caused by gushes of the air and manoeuvres will significantly influence the aerodynamic loads of the microaeroplane. This is obvious because of extremely low unitary load of lifting surface of this aircraft.

The propulsion system of the microaeroplane has to be characterised by little dimensions and satisfy extremely high demand for power and energy, necessary for correct operation of systems installed on-board. Additional condition posed to the propulsion system is acoustic silencing of its operation. This is a necessary condition to ensure non-detectability of missions performed by the microaeroplane. Decrease of the necessary power can be obtained through decreasing the wing loading. This means increasing the wing surface and decreasing the mass of the microaeroplane. E.g. the famous human-powered aircraft (winner of Kramer award) Gossamer Albatross has gigantic wings (and at the same time little mass), therefore it can be propelled with seemingly insignificant power of human muscles. However, the dimensions of microaeroplanes are limited to 15 cm. Therefore, in this case, constructing “enormous” wings is impossible. The only way of increasing MAVs’ wing surface is by increasing their chord, which in turn causes a decrease of their aspect ratio – and consequently problems with three-dimensional flow. The use of microelectromechanical technologies, little demand for energy of highly integrated microelectronical systems, the use of multifunctional modules – these are the ways to radically decrease the energy demand.

Another problem in need of a solution is the MAV navigation. It seems that an almost perfect solution is the use of GPS. Alternatively, in the case of indoor mission when GPS signal is to small, inertial navigation systems can be used, because of the fact that miniature accelerometer and gyroscope platforms are available nowadays. For a microaeroplane to be a fully operational reconnaissance device it needs to be able to perfectly handle avoiding obstacles and finding path in the area of its flight. Therefore a condition necessary for correct operation of a MAV is equipping it with systems of artificial intelligence. It can be stated, that a reconnaissance MAV should be autonomously acting, flying cybernetic device. It should be remembered, that direct controlling of a microaeroplane by an operator will not always ensure flight stabilization (e.g. after encountering a gush of wind) nor will it cause avoiding of a suddenly appearing obstacle. Therefore MAVs have to operate autonomously in a large portion of their flight.

Another very serious problem is the maintenance of communication between the MAV and the operator. Because of the small dimensions of a MAV the antennae of this device are small, and maintenance of a wide-enough band of data transmission (2-4 Mbit/sec), necessary for transmission of image provided by a video microcamera is an extremely difficult task. Control functions require much narrower band of data transmission (of the order of 10 kbit/sec). Of course compression of images allows decreasing of the wideness of the data transmission band.

MAVs should be equipped with systems of sensors necessary for performing reconnaissance and supervisory missions. The sensors can include microcameras (acting in the visible range and infrared), radio wave receivers of multiple frequencies, biochemical sensors, radiation counters, microphones, etc. These sensors should be integrated with the MAVs systems. Nowadays, miniature video cameras, weighing 1 gram and having the resolution of 1000x1000 pixels and energy consumption of the order of 25 miliwatts are available. Specialists claim, that significant decrease of mass and dimensions of such video cameras is possible, with simultaneous increase of resolution.

2. BIOLOGICAL INSPIRATIONS OF MAV DESIGN

2.1. BIONICS, what it is *

Many MAV developers have opted for fixed wing or rotary wing aircraft designs but most analysts agree that the best solutions to building smaller MAVs closer to the centimeter-scale may be inspired from nature. Through the process of evolution, organisms have experimented with form and function for at least 3 billion

* This paragraph is summary of paper by prof Dickinson: (1999) [7]

years before the first human manipulations of stone, bone, and antler. Although we cannot know for sure the extent to which biological models inspired our early ancestors, more recent examples of biomimetic designs are well documented. For example, birds and bats played a central role in one of the more triumphant feats of human engineering, the construction of an airplane. In the 16th century, Leonardo da Vinci sketched designs for gliding and flapping machines based on his anatomical study of birds. More than 300 years later, Otto Lilienthal built and flew gliding machines that were also patterned after birds. Lilienthal died in one of his own creations, in part because he failed to solve a difficult problem for which animals would eventually provide another critical insight: how to steer and maneuver. The wing warping mechanism that enabled Orville and Wilbur Wright to steer their airplane past the cameras and into the history books is said to have been inspired by watching buzzards soar near their Ohio home. It is perhaps not surprising that early aeronautical engineers were inspired by Nature given that the performance gap was so large and obvious. Because birds can fly and we cannot, only the most foolhardy or arrogant individual would design a flying craft without some reference to natural analogs. Most engineering projects, however, take place successfully without any explicit reference to Nature, in large part because natural analogs do not exist for most mechanical devices. One would need to search far and wide for a natural analog of a toaster. Nevertheless, in recent years there seems to be growing interest on the part of engineers to borrow design concepts from Nature. The discipline has grown to the point that books, articles, conference sessions, and university programs labeled Bionics or Biomimetics are quite common. In the case of aerodynamics, biomimetic approaches appeal to roboticists, because the performance gap between mechanical devices and their natural analogs is so large. One reason for the growing interest in Bionics is that fabrication methods are much more sophisticated than they used to be. Because of innovations in Materials Science, Electrical Engineering, Chemistry, and Molecular Genetics, it is possible to plan and construct complicated structures at the molecular or near molecular level. Examples include buckyballs, nanotubes, and the myriad of microelectromechanical devices (MEMs) constructed with technology derived from the silicon chip industry. Integrated circuits themselves play a role in Bionics projects aimed at constructing smart materials or mimicking the movement, behavior, and cognition of animals. In short, biological structures are complicated, and we are only now beginning to possess a sophisticated enough tool kit to mimic the salient features of that complexity.

Another reason for the increasing popularity of Bionics is simply that we know much more about how plants and animals work than we used to. The overwhelming success of Biology, practiced at the cellular and subcellular levels, has overshadowed many substantial advances in our knowledge of processes that operate at higher levels of biological complexity. Taking examples from studies on animal locomotion, biologists now understand how basilisk lizards walk on water, how penguins minimize drag, and how insects manage to remain airborne, phenomena that, until recently, were poorly understood. The solutions to such puzzles do not impact the world of Science as does, say, sequencing the human genome. They do, however, identify specific structure - function relationships, and, as such, can provide assistance to engineers faced with analogous problems. The fields of Biology that use principles of Structural Engineering and Fluid Mechanics to draw structure - function relationships are Functional Morphology or Biomechanics. These disciplines are of particular use to Bionics engineers, because the behavior and performance of natural structures can be characterized with methods and units that are directly applicable to mechanical analogs. The result of precise spatial and temporal regulation is a complex exoskeleton that is tagmatized into functional zones. Limbs consist of tough, rigid tubes made of molecular plywood, connected by complex joints made of hard junctures separated by rubbery membrane. The most elaborate example of an arthropod joint is the wing hinge, the morphological centerpiece of flight behavior (see fig. 2). Fig. 2 shows hinges system of flying insects. The horizontal hinge ① occurs near the base of the wing next to the first axillary sclerite. This hinge allow the wing to flap up and down. The vertical hinge ② is located at the base of the radial vein near the second axillary sclerite (2AX), and is responsible for the lagging motions of wing. The torsional hinge ③ appear to be more complicated interaction of sclerite and deformable folds.

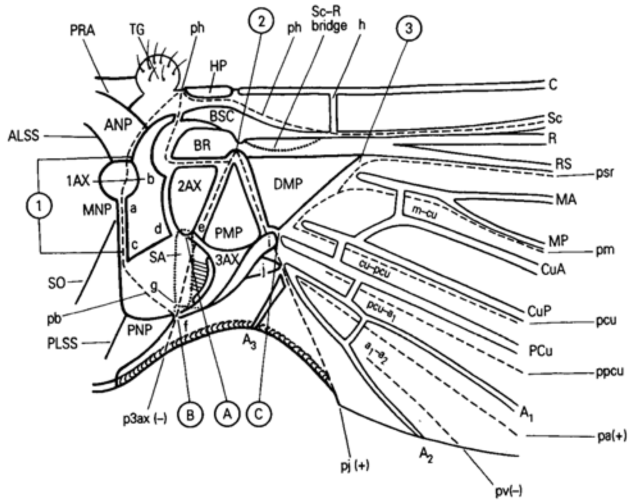

Fig. 2. Insect Axillary Apparatus. Region at the base of the wing containing all the intricate mechanical components. First axillary sclerite (1AX), articulates with the anterior notal process and forms the horizontal hinge. Second axillary sclerite (2AX) articulates with an extension of the thoracic wall. The 2AX is responsible for the pleural wing process (PWP), and support the radial vein, (main mechanical axis for the wing). Third axillary sclerite (3AX) is responsible fopr wing flexing, and play role of the vertical hinge.

The hinge consists of a complex interconnected tangle of five hard scleratized elements, imbedded within thinner, more elastic cuticle, and bordered by the thick side walls of the thorax. In most insects, the muscles that actually power the wings are not attached to the hinge. Instead, flight muscles cause small strains within the walls of the thorax, which the hinge then amplifies into large oscillations of the wing. Small control muscles attached directly to the hinge enable the insect to alter wing motion during steering maneuvers. The indirect muscles do not directly effect wing. They are attach to the tergum, and distort the thoracic box when contracted. This distortion transmits forces to the wing. There are two bundles of indirect muscles: dorsolongitudinal (DLM), and dorsoventral (DVM). The dorsolongitudinal muscles span the length of the tergum, the dorsoventral muscles extend from the tergum to the sternum. The direct muscles connect directly from the pleuron (thoracic wall) to individual sclerites located at the base of the wing. The subalar and basalar muscles have ligament attachments to the subalar and basalar sclerites. Resilin is a highly elastic material and forms the ligaments connecting flight muscles to wing apparatus, and it is 100 times greater energy storage capabilities than muscle. There are other muscles that are directly inserted into the first and third axillary sclerite (see fig. 3)

Although the material properties of the elements within the hinge are indeed remarkable, it is the structural complexity as much as the material properties that endow the wing hinge with its astonishing characteristics. Sometimes it is not the actual morphology that endows a biological structure with its functional properties, but the intelligence with which it is used. Intelligence does not necessarily imply cognition; it may simply reflect the ability to use a structure in an efficient and flexible manner.

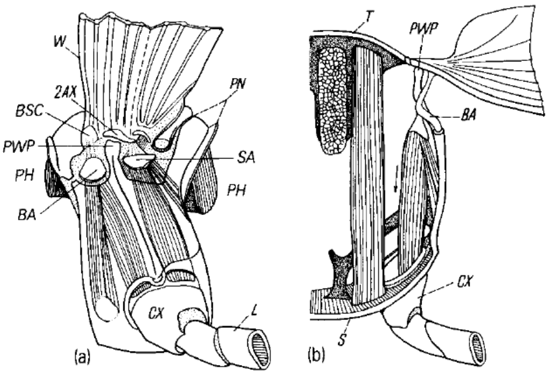

Fig. 3 The direct flight mucles within the wing bearing segment: (a) lateral view; (b) crosssectional view.

Although most biological structures are not intelligent by human standards, they nevertheless outperform most bricks and I - beams. A good example is the insect wing (fig. 4). The wing is the structure with membranous cuticle stretched between veins in the wing. Unlike an aircraft wing, it is neither streamlined nor smooth. Folds facilitate deformation during flight. Veins increase the mechanical rigidity of the wing (alternate in concave and convex patterns). Radial vein is the longitudinal rotational axis of the wing, about which occur pronation and supination.

Engineers and biologists have long struggled to explain how a bumblebee (or any insect) remains in the air by flapping its wings. Conventional steady-state aerodynamic theory is based on rigid wings moving at a uniform speed. Such theory cannot account for the force required to keep an insect in the air. The solution to this paradox resides not in the intrinsic properties of wings, but rather in the way that insects use them. By flapping the wings back and forth, insects take advantage of the unsteady mechanisms that produce forces above and beyond those possible under steady-state conditions. Several research groups are actively attempting to construct miniature flying devices patterned after insects. Their challenge is not simply to replicate an insect wing, but to create a mechanism that flaps it just as effectively. Intelligent structures do not always function the same way; they adapt to local functional requirements. Even the simplest plants and animals sense their world, integrate information, and act accordingly. Feedback-control mechanisms are extremely important features that endow organisms with flexibility and robustness. Even plants, which lack a nervous system, can nevertheless grow leaves and branches toward light, roots toward water, or spatially regulate growth so as to minimize mechanical stress. The functions of biological structures cannot be fully understood or accurately mimicked without taking this complex dynamic feedback into account. Of all the properties of biological entities (with the possible exception of self-replication), it is their intelligence and flexibility that is perhaps the most difficult to duplicate in an artificial device. The next decade should be exciting for the field of Bionics. Just as biologists are discovering the structural and physiological mechanisms that underlie the functional properties of plants and animals, engineers are beginning to develop a fabrication tool kit that is sophisticated enough to capture their salient features. As the performance gap between biological structures and our mechanical analogs shortens, engineers may feel increasingly encouraged to seek and adopt design concepts from Nature. Although the devices they construct may at first appear alien, their origins in the organic world may endow them with an odd familiarity.

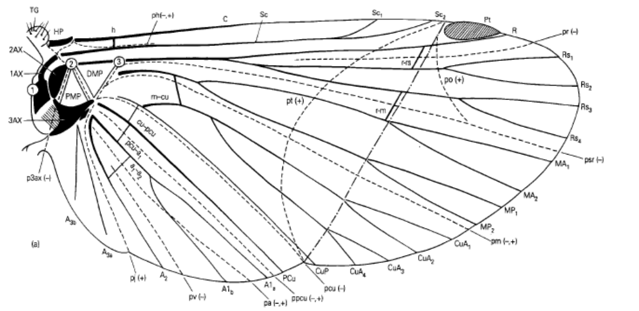

Fig. 4. The insect wing layout

As it was discussed, biological flying insects use flapping wings to attain amazing capabilities for hovering and maneuvering. Most of the recent work on Biological Micro Aerial Vehicles (BMAVs) bas been on the scale of avian flight which is quite different from insect flight. Notable examples in this list include the Caltech RTCLA Omithopter (Pornsin-Sirirak et al [30]), the Delf University of Technology (R. Ruijsink) [www.delffly.nl], the Georgia Tech Entomopter (Michelson) [23, 24], the Arizona University (Shkakaryev) [18], the France ROBUR project [6, 19 . The UC Berkeley developed the Micromechanical Flying Insect (MFI) project. This BMAV distinguishes itself with a wingspan of only 25 mm, almost an order of magnitude smaller than all the others (this translates into roughly three orders of magnitude difference in mass). The work on the MFI has been documented in a number of areas including design and fabrication, actuator development, thorax dynamics, sensing, and aerodynamic simulation [13, 32, 33, 34, 46, 47].

The success of insect-scale BMAVs depends on exploitation of unsteady aerodynamic mechanisms (in particular, delayed stall, rotational lift, and wake capture) which have only recently been elucidated by Dickinson et al [7, 8]. There has been some success with computational methods to estimate forces generated by flapping wings [9, 10, 29, 32, 36] but both the models and algorithms need to be improved in order to get better agreement with experimental values. The only reliable means to determine the forces generated by the flapping wing is to measure them directly.

Current works on MAV with flapping wings required introduction of a new notion, animalopter. Animalopter means a flying object constructed by man, which flies is a way similar to natural animalopters (i.e. like natural creatures: birds, insects and bats), i.e. by moving wings. For this reason we shall avoid the name microaeroplane, which as a rule means a device with immobile wings. Therefore we are dealing with an *entomopter,* if it is an artificial insect, or an *ornitopter,* if we are dealing with an artificial bird.

Wings of an animalopter are a multifunctional device, which create not only the aerodynamic lift, but also thrust, and, last but not least, can control the flight. Because of the complex equipment mounted on the animalopter, it can be stated, that the animalopter is a *flying micro-electro-mechanical robot*.

Animalopter is of dimensions similar to the dimensions of a small bird (or a bat) and a large insect. The thing that distinguishes animalopter from an ordinary radio-controlled small aeroplane are air operations, usually beyond the operator's sight range and on *small* Reynolds numbers (of the order of ten to a hundred thousand). The data of how the motion of wings and the body change during flight is interesting not only *per se,* but also in order to understand the mechanisms, which take place during flight and their mathematical modelling.

If one wanted to search for analogies with artificial objects, then because of the complex motion in relation to the body, animalopter is more similar to a helicopter that to an aeroplane. Therefore many concepts stemming from helicopter flight mechanics found use in flight biomechanics, of course after taking into account animalopters' specificity.

Bird's wing anatomy is quite well known and described. Feathers create a lifting surface with a highly complex structure and shape, which causes the entire wing to become a lifting surface of elastic and permeable profile, with numerous vortex diffusers, such as down and elastic feather radiuses. Moreover appropriate motions of the wings enable a change of their span, lift and sweep during flight, and motions of muscles and tendons inside the wings enable among others a change of camber of a wing profile. Analogously to insects, birds are also able to actively control the flight. Thanks to appropriate wing motions and arrangement of feathers they control the flow around the wings. The aim of this action, as in the case of insects, is minimalising of power needed for flight, reaching maximal velocity or maneouvrability, or fulfilling the requirements of flight in special conditions.

2.2. Flapping wings degrees of freedom

Insect wing motion appear to be not simply up and down. It is much more complex (see fig. 5). Fig. 5 shows insect's wing tip trajectory. Such complex motion can be considered as being composed of three different rotations: flapping, lagging, feathering, and spanning. Flapping is a rotary motion of the wing around the longitudinal axis of the animalopter (this axis overlaps with the direction of flight velocity). Thus "up and down" motion is realised. Lagging is a rotary wing motion around the "vertical" axis, i.e. it describes "forward and backward" motion. Feathering is a rotary motion around longitudinal wing axis. During that motion changes of attack angle of the wing occur.

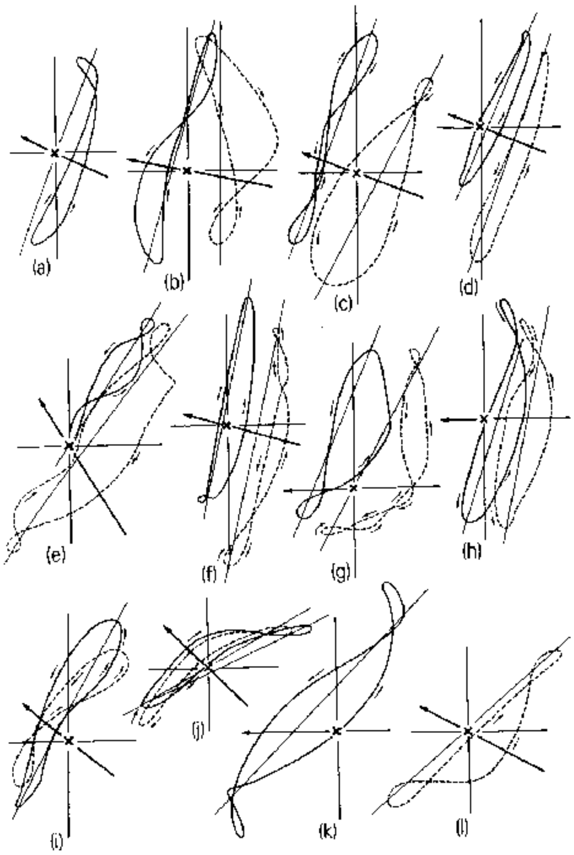

Fig. 5. Wingtip trajectories

Detailed analyses of kinematics are central to an integrated understanding of animal flight [1, 2, 8, 9, 10, 17, 20, 21, 25, 26, 27, 28, 32, 35, 37, 38, 39, 40]. Concluding, four degrees of freedom in each wing are used to achieve flight in the Nature: flapping, lagging, feathering, and spanning. This requires a universal joint similar the shoulder in a human. A good model of such joint is the articulated rotor hub (Fig. 6). *Flapping* is a rotation of a wing about longitudinal axis of the body (this axis lies in the direction of flight velocity), i.e. "up and down" motion. *Lagging* is a rotation about a "vertical" axis, this is the "forward and backward" wing motion. *Feathering* is an angular movement about the wing longitudinal axis (which may pass through the wing center of gravity). During the feathering motion the wing changes its angle of attack.

Similar to insets, the motion of a bird wing may be decomposed into: *flapping*, *lagging*, *feathering* (the rigid body motions) and also into more complex deflections of the surface from the base shape (*vibration modes*).

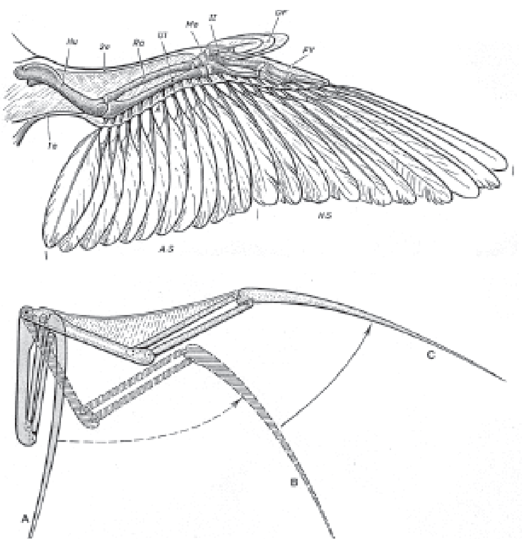

Fig. 6. Bird wing hinges anatomy, and wing folding

Insects with wing beat frequencies about 20 Hz generally have very restricted lagging capabilities. Insects such as alderfly (*Apatele alni*) and mayfly (*Ephemera*) have fixed stroke planes with respect to their bodies. Thus, flapping flight is possible with only two degrees of freedom: flapping and feathering. In the simplest physical models heaving and pitching represent these degrees of freedom. *Spanning* is an expanding and contracting of the wingspan. Not all flying animals implement all of these motions. Unlike birds, most insects do not use the spanning technique.

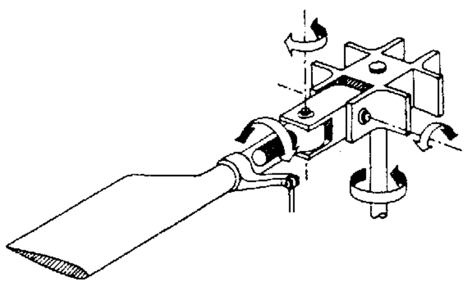

Fig. 7. Articulated joints of a helicopter main rotor

Spanning is a motion, which causes changes of wing aspect ratio. Not all animalopters use these motions. Unlike the birds, most insects do not use this technique. A significant question arises: which of these motions should be taken into account to obtain adequate description?

During level flight a bird has to flap its wings to generate aerodynamic lift and thrust to overcome terrestrial gravity force and drag. Instantaneous forces on the wings change during the cycle because of the changes of wing shape, deformability of joints, attack angle, turning of the wings, rotary velocity of the wings, elastic properties, flight velocity etc. A key issue here is the understanding of how complex motions of so complicated object generate aerodynamic forces. No wonder, that aerodynamics of flapping wings is thought to be the most difficult field of aeroplane and helicopter aerodynamics. The issue is further complicated by the fact, that this is an aerodynamics of small Reynolds numbers. It also needs to be emphasized, that conventional flight mechanics can only be a guide and not an authority while analysing animalopter's flight dynamics. It is enough to realise, that the moments of inertia of movable parts change, and, moreover, the changes are different on each wing. Geometric parameters also undergo changes, e.g. wing aspect ratio. Stabilization of motion is a serious problem. A way to understand animalopters' motion is a thorough kinematic, which is connected with the choice of levels of freedom. An extremely serious problem is controlling such an object. This is caused by the fact, that wings do not have typical control surfaces, like ailerons (not to be confused with a kind of feathers!). Influencing the motion is possible only by changes of amplitudes and frequencies of flapping and turning the wings. It has been observed, though, that anima lots are capable of performing incredible acrobatic manoeuvres, which would not be possible without appropriate "control devices". Knowledge on this topic is in the process of being gathered.

Insects fly by oscillating (plunging) and rotating (pitching) their wings through large angles, while sweeping them forwards and backwards. The wingbeat cycle (typical frequency range: 5–200 Hz) can be divided into two phases: downstroke and upstroke (see Fig. 8*a*).

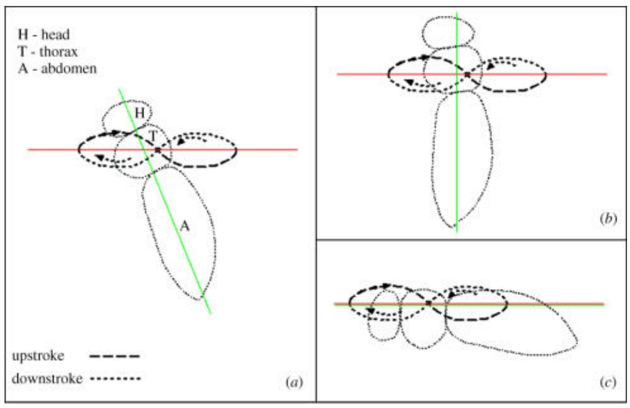

Fig. 8. Generic kinematics of insect in hover: the wing tip traces a 'figure-of eight', when seen from the insect side. The angle between the insect body axis (green) and the stroke plane (red) is constant. Typically, (*a*) the angle is steep; (*b*) one extreme: the angle is $\pi/2$; (*c*) the other extreme: the angle is zero(see Żbikowski and Galiński [48]).

At the beginning of downstroke, the wing (as seen from the front of the insect) is in the uppermost and rearmost position with the leading edge pointing forward. The wing is then pushed downwards (plunged) and forwards (swept) continuously and rotated (pitched) at the end of the downstroke, when the wing is twisted rapidly, so that the leading edge points backwards, and the upstroke begins. During the upstroke, the wing is pushed upwards and backwards and at the highest point the wing is twisted again, so that the leading edge points forward and the next downstroke begins.

Insect wing flapping occurs in a stroke plane that generally remains at the same orientation to the body. The actual angle corresponding to the orientation is an interesting design parameter, (see Fig. 8b, and 8c).

In hover the downstroke and upstroke are equal, resulting in the wing tip approximately tracing a figure-of-eight (as seen from the insect's side). However, the figure-of-eight is not necessarily generic, as other, less regular, closed curves with more than one or no self-intersections are also observed [48]. For two-winged flies (Diptera) a 'banana' shape seems to be common. However, even for Diptera the kinematics in hover can be more complicated, so we settled on the figure-of-eight as 'commonly occurring' for reference purposes.

Since each half-cycle starts from rest and comes to a stop, the velocity distribution of the flapping is non-uniform, making the resulting airflow complex. It is also unsteady, i.e. the aerodynamic force varies in amplitude and direction during each wingbeat cycle. The variability of the force is compounded by the strong influence of the viscosity of air (owing to the small scale) and significant interaction of the wing with its wake (owing to hover). Finally, it is worth mentioning that the thorax–wing system in true flies (Diptera) is resonant, which contributes to the efficiency of propulsion. This feature was not implemented in the presented mechanism, but it is considered for a future design in the form of electro-mechanical resonance [zb].

2.3. Insect wing kinematics and propulsion

Insect wing kinematics are essentially spherical, while the trace of the wing tip is usually photographed from the insect's side. The result is an orthogonal projection of the spherical trace on to the plane of the animal's longitudinal symmetry. The resulting planar figure for a hovering insect's wing is always closed. As far as can be discerned from the available (noisy) data, e.g. for flies, the actual shape may be a figure-of-eight or a banana shape, but can be irregular and sometimes the trace has no self-intersections. Owing to the inherent experimental difficulties, the kinematic and aerodynamic data from free-flying insects are sparse and uncertain, and it is not clear what aerodynamic consequences different wing motions have, despite notable progress (e.g. Dickinson et all. 1998; Lehmann & Dickinson 1998; Lehmann 2004). Since acquiring the necessary kinematic and dynamic data remains a challenge, a synthetic, controlled study of insect-like flapping is not only of engineering value, but also of biological relevance.

There are two phases in each half-cycle of the wing beat: translational (wing moving forwards or backwards) and rotational (at the end of each stroke). In order to clearly investigate the distinct aerodynamic contributions of each phase, the angle of attack should be constant during translation and rotate through at least 90° during the flip-over. Thus, theoretically attractive kinematics should entail an intermittent rotational motion with reversal. A more subtle aspect is the plunging (up–down) component of flapping. Every time a hovering wing starts (or stops) it sheds a starting (stopping) vortex (Wagner 1925; Żbikowski 2002b) which is then convected according to the airflow evolution. Despite the convection, such a vortex may persist in the vicinity of its original shedding point when the wing revisits that point in the next half-cycle. Then the wing and the vortex will collide and the flow structure is impaired. However, if the wing plunges up and down while moving forwards and backwards, it may be able to avoid hitting the vortex when revisiting the shedding point. In other words, figure-of-eight kinematics with the width of the 'eight' corresponding to the extent of plunging can plausibly be advantageous for aerodynamic reasons. Hence the focus of this work has been idealized wing tip kinematics of that type, so that the results are practical to implement, but scientifically relevant both for engineers and biologists.

Zbikowski and Galinski proposed to implement wing tip kinematics as a spherical, symmetric, self-intersecting curve, which would admit a convenient mathematical description and a simple engineering realization. They considers two options: a) Bernoulli's lemniscate and b) spherical Lissajous curves [48] – see fig. 9.

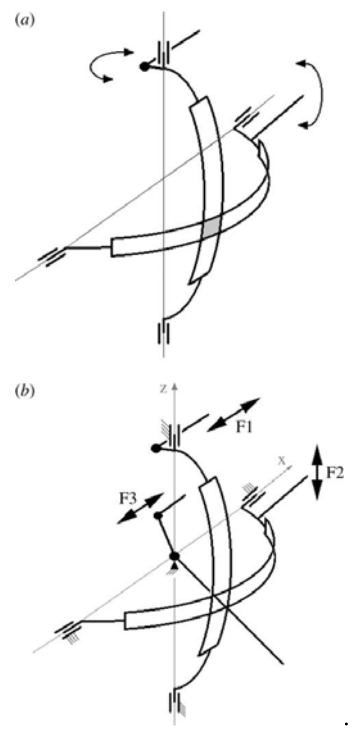

Fig. 9. Spherical double Scotch yoke: (*a*) kinematic diagram; (*b*) concept of the associated flapping mechanism (cf. Zbikowski and Galinski [48])

A spherical figure-of-eight together with decoupled pitching is easily obtainable if each of them have a common apex and if both Scotch yokes are orthogonal.

This combination allows the creation of Lissajous' curves if yokes are driven by sinusoidal inputs, one twice as fast as the other. As a result, a smooth figure-of-eight motion can be obtained, without any excessive accelerations, thus decreasing dynamic loads. The first step was to propose a planar mechanism capable of converting rotary input into reciprocal motion of the figure-of-eight type. This was done by combining orthogonally two Scotch yokes, so that Lissajous curves were generated. The drawbacks of the planar double Scotch yoke, can be avoided if the yokes are made spherical and their translation is exchanged with their rotation. In this configuration, both ends of each yoke are rotated about the same axis, see figure 9*a*. The figure-of-eight generated is then spherical by default, significantly simplifying wing articulation, see figure 9*b* [48].

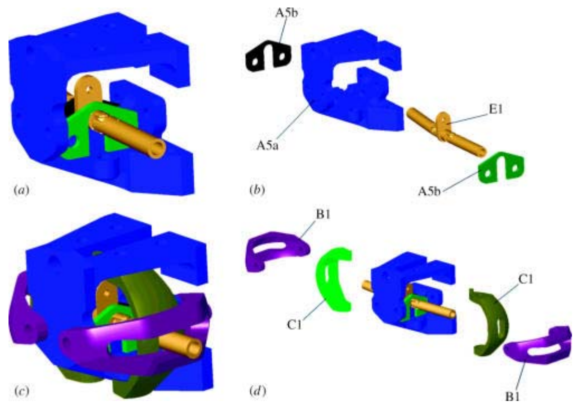

Fig. 10. Practical realization of spherical double Scotch yoke (Zbikowski and Galinski [48])

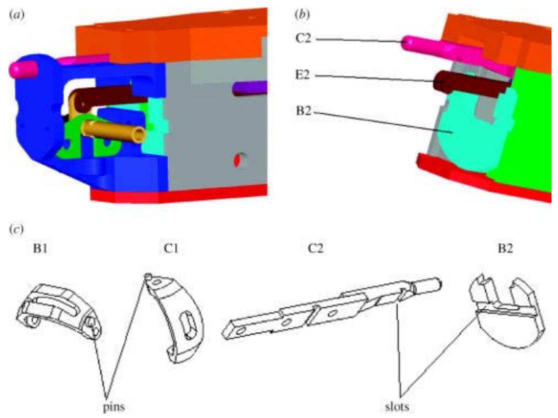

Fig. 11. Details of the driving components [48]

A practical realization of spherical double Scotch yoke realized by Dr Zbikowski and Dr Galinski (Cranfield University asn Warsaw University of Technology) is shown in Fig. 9, and 10. Axle E1 (fig. 9) is attached to frame component A5a by two plates A5b, (fig. 10) so that a mode of slide bearing is created. The axle is equipped with two universal joints for wing articulation and a lever for pitch control. Wings can be attached to the tubes at both axle ends. Yokes C1 and B1 are also attached to frame component A9, so that their axes cross in the centre of the universal joint. The mechanism contains two universal joints and two sets of yokes, to which two wings are to be attached. Universal joints cannot have a common centre, since the lever and attachment bearings have to be located between them.

The kinematics of an insect-like flapping wing for MAVs requires three-dimensional motion which is essentially spherical in character. Spherical double Scotch yoke is a relatively simple mechanism, complying with this requirement and realizing the required figure-of-eight as a spherical Lissajous' curve.

The spherical double Scotch yoke mechanism on the MAV scale was designed, manufactured, assembled and tested. It was found to be quite reliable and met its specifications, performing satisfactorily in tests and generating useful data for further aeromechanical studies. The few problems discovered in the course of the testing are minor and can be resolved by viable modifications.

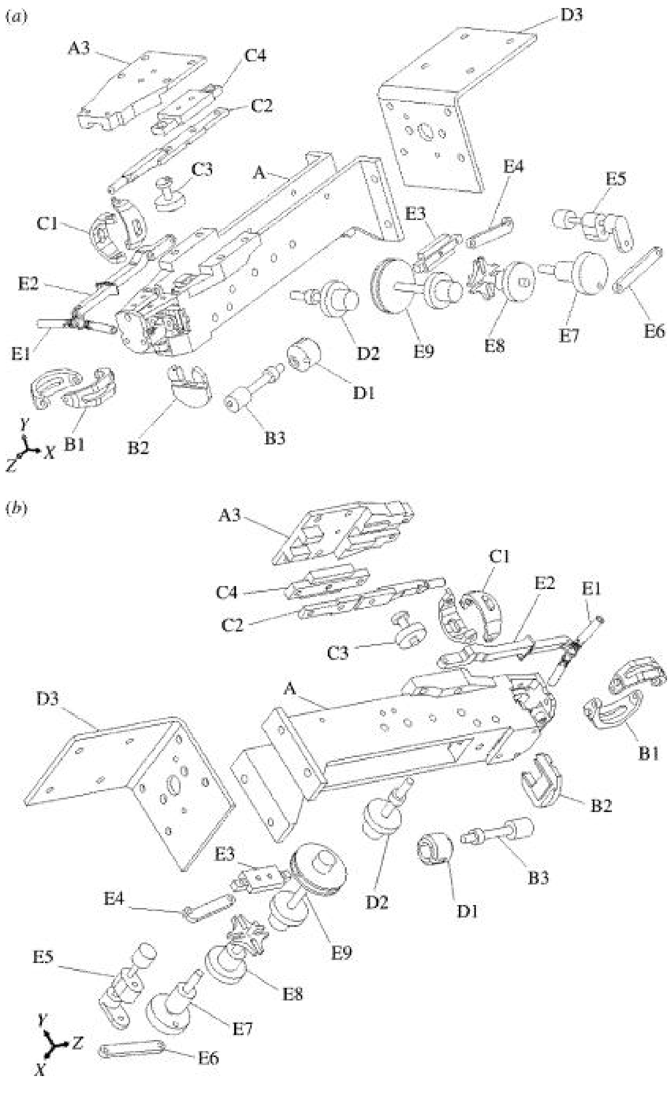

Fig. 12. The exploded view of the complete mechanics

The exploded view of the complete mechanism are presented in figure 12, and a photograph of the assembled mechanism is given in figure 13.

Fig 14 shows another example of mechanical design of flapping wings propulsion. . This mechanism contain two rod-crank parallel mechanisms. It is characterized by minimum energetic consumption for a sinusoidal movement. Other kinematics are possible. Propulsion system 4 brushless motors (30 W, 100g), 0-5 Hz. Symmetrical movements - dihedral ± 50 deg, twist ± 30 deg Dipteran insects drive their wing using indirect flight muscles attached to the exoskeleton dorsally and a deformable section of the exoskeleton call the scutum ventrally. Muscle activation works to depress the scutum while the pleural wing process is attached to the interface of the scutum and exoskeleton. This structure, shown in Fig. 1, is actuated by two sets of muscles: the dorsoventral and dorsolongitudinal muscles. The dorsoventral muscles act to depress the scutum and thus generate the ‘up-stroke’. The dorsolongitudinal muscle acts to shorten the thorax and return the scutum to its relaxed state and thus generates the ‘down-stroke’.

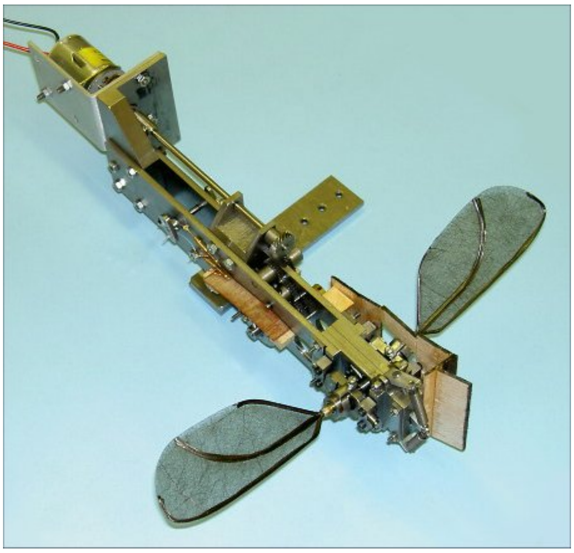

Fig. 13. General view of the Dr. Zbikowski complete mechanism

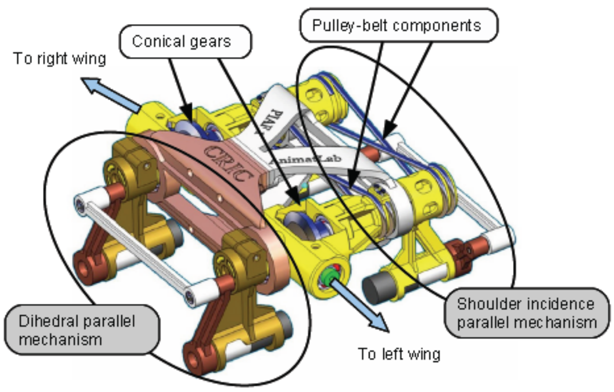

Fig. 14. ROBUR wing propulsion gearbox

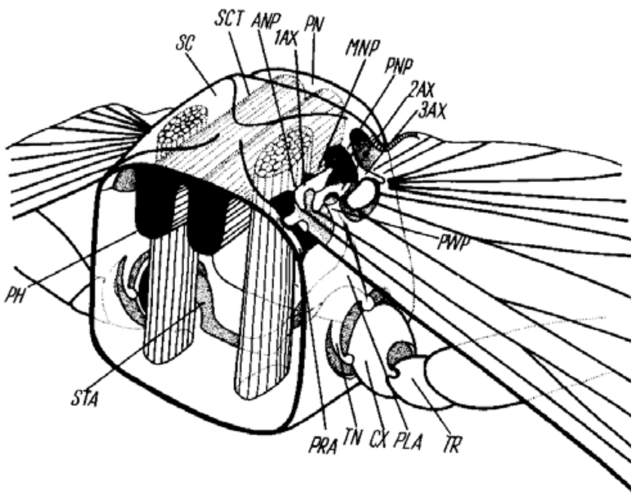

Fig. 15. Simplified diagram of Dipteran wing transmission

Kinematically, the structure in Fig. 15 is essentially a four-bar with a prismatic joint at the input. What is presented here is nearly identical: linear actuator motion is coupled to the wing hinge via a simple transmission which acts to convert this motion to a large flapping rotation at the wing hinge. Thus all the actuator power is used to drive the wings through as large a wing stroke as possible. Additionally, the wings are allowed to rotate along an axis parallel to the span-wise direction. This rotation is passive, but is key to generating lift.

A transmission mechanism is used to transform small actuator motions to large angular wing displacements and to impedance-match the actuator to the load (work done on the surrounding air). There are numerous reasons a large wing stroke is desired: for a given operating frequency a larger stroke amplitude will result in larger instantaneous wing velocities. Also, a larger stroke allows vortices to fully form and stabilize before the stroke reversal. At a ‘macro’ scale, this would be accomplished with a gear system. At the scale of an insect, it is not feasible to produce gears with the necessary efficiency, thus an alternative solution is presented here that is based on low-loss flexure joints.

Significant advances in mesoscale prototyping are enabling rigid, articulated, and actuated microrobotic structures. The robot fly designed by prof. Wood’s team can be a good example of an elegant manufacturing paradigm, employed for the creation of a biologically inspired flapping-wing micro air vehicle with similar dimensions to Dipteran insects. Prof Wood designed a novel wing transmission system which contains one actuated and two passive degrees of freedom. The design and fabrication are detailed and the performance of the resulting structure is elucidated highlighting two key metrics: the wing trajectory and the thrust generated. Construction of the transmission is an exceedingly crucial step. The kinematics and dynamics of the transmission depend strongly upon the concise geometry of each link and flexure. The assumption that it is possible to use a pseudo-rigid-body technique assumes that all joints are properly aligned. To put this in perspective, the smallest link in the transmission system is 300μm in length and the flexure lengths are 80μm. Alignment is controlled by the precision stages of the laser-micromachining system. Fig. 16 shows the resulting transmission system which converts a small linear motion to large angular wing strokes.

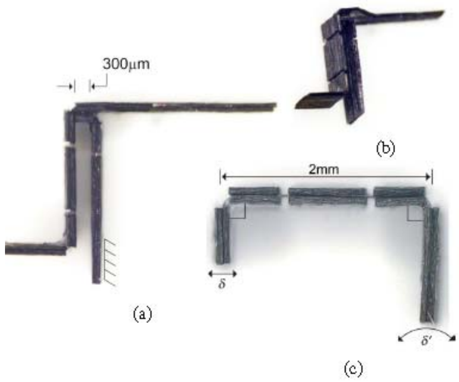

Fig. 16. Designed by prof. Wood MAV transmission system, top view (a) and isometric view (b). The slider-crank for coupling actuator motion to the prismatic input of the transmission is shown in (c) (cf. 44)

The actuators are constructed using the SCM process. In this case, some of the laminae are piezoelectric, thus resulting in bending moments upon the application of an electric field. Fig. 16 shows a completed microactuator.

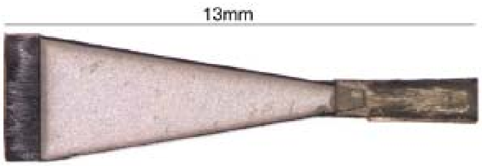

Fig. 17. High energy density piezoelectric bending cantilever [43, 44]

The actuator, wings, and transmission are assembled together onto an acrylic fixture that is created with a three dimensional printer. Care is given to the strength of the mounts so that a solid mechanical ground is established. Detail of the completed structure is shown in Fig. 18.

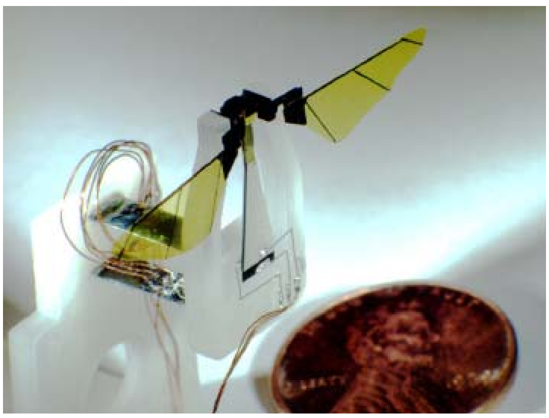

Fig. 18. Completed MAV test fixture mounted to a high sensitivity force transducer (cf. [42 – 44].

2.4. Development of the wing trajectory

The actuated DOF is driven through as large a motion as possible. This is done open-loop with a sinusoidal drive at the resonant frequency. The measured resonant frequency is 110Hz, resulting in an actuator power density of approximately 165W/kg (comparable to good macro-scale DC motors). This is lower than the predicted resonant frequency of 170Hz, most likely due to unmodeled offsets in how the wing is mounted to the transmission. Fig. 18 details the wing motion that this structure can achieve. Note that this motion is qualitatively identical to hovering Dipteran insects. C. Wing force Because of the small force magnitude and high operating frequency, measuring the thrust produced by the wings in real time (with sub-period temporal resolution) is not trivial. A custom sensor was created specifically to measure this force. The design attempts to reconcile two opposing traits: high bandwidth and high sensitivity. To quantify this, the bandwidth of the sensor is desired to be at least 5× the wing drive frequency with a resolution of less than 1% of the weight of the structure. For the details of the design, the reader is directed to [17]. The sensor itself is a parallel cantilever constructed from spring steel with semiconductor strain gages. The completed sensor has a resonant frequency of 400Hz (with the structure attached; slightly lower than desired), and a resolution of approximately 10μN. The structure is fitted to the distal end of the sensor and the device is actuated, starting from rest. The average lift is measured by averaging 50 wing beats after 50 wing beats are elapsed to allow stable periodic vortex formation. The average lift was collected from 10 trials giving an average of 1.14±0.23mN. This would be sufficient to lift a fly weighing over 100mg. A typical time trace of the lift is shown in Fig. 9 for a drive magnitude of 100V peak.

The Harvard Microrobotics lab has recently demonstrated the first step towards recreating these evolutionary wonders with the world's first demonstration of an at-scale robotic insect capable of generating sufficient thrust to takeoff (with external power). The mechanics and aerodynamics of this device are quite similar to Dipteran insects. Biologists have recently quantified the complex nonlinear temporal phenomena that give insects their outstanding capabilities. Periodic wing motions consisting of a large stroke and pronation and supination about an axis parallel to the span-wise direction are characteristic of most hovering Dipteran insects. Previous microrobot designs have attempted to concisely control each wing trajectory in these two dimensions. The robot that is shown here has three degrees-offreedom, only one of which is actuated. Here, a central power actuator drives the wing with as large a stroke as possible and passive dynamics allow the wing to rotate using flexural elements with joint stops to avoid over-rotation. There are four primary components to the mechanical system: the actuator (or 'flight muscle'), transmission (or 'thorax'), airframe (or 'exoskeleton') and the wings. Each is constructed using a mesoscale manufacturing paradigm called Smart Composite Microstructures. This entails the use of laminated lasermicromachined materials stacked to achieve a desired compliance profile. This prototyping method is inexpensive, conceptually simple, and fast: for example, all components of the fly can be created in less than one week. Additionally, the resulting structures perform favorably when compared to alternative devices: flexure joints have almost no loss, ultra-high modulus links have higher stiffness-to-weight than any other material, and the piezoelectric actuators have similar power density to the best DC motors at any scale. After integration, the fly is fixed to guide wires that restrict the motion so that the fly can only move vertically. The wings are then driven open loop to achieve a large angular displacement. This is done at resonance to further amplify the wing motion. The wings exhibit a trajectory nearly identical to biological counterparts. Finally, this 60mg, 3cm wingspan system is allowed to freely move in the vertical direction demonstrating thrust that accelerates the fly upwards. Bench-top thrust measurements show that this robotic fly has a thrust-toweight ratio of approximately two. These results unequivocally confirm the feasibility of insect-sized MAVs. The remaining challenges involve the development of microelectronics appropriate for power conversion, sensing, communication, and control along with the choice of an appropriate power source.

3. STRUCTURAL SYSTEMS OF FLAPPING WINGS MAV

Unlike flying machines, insects can quietly fly in all directions. They show a very useful feature: even if they hit an obstacle (e.g. a wall) they can bounce off it and continue flying and in the worst case to crawl away into safety. Therefore constructors of microaeroplanes watch the structure of insects closely. An authoritative comparative quantity is also the number of kilograms lifted by a unit of engine power. This quantity is called *power load.* For aeroplanes it is 900 W/kg, for birds over 80 W/kg, while for insects maximum 70 W/kg. It can be noted, therefore, that the use of power in Nature is more than 10 times better than in man-made flying machines (compare [4.5, 4.108, 4.110]). Because of small dimensions of MAV cargo space the distribution of necessary devices, units and on-board sensors become a very serious problem. The conception used in “large” unmanned aircrafts consisting in “filling” the inside of the airframe with necessary instruments and next their equipment – programme integration into one system in this case is practically impossible to use.

Initial aerodynamic data have been gathered and more tests, both for force measurement and flow visualization, are planned. The new data will allow a quantifiable study of the aeromechanics of insect-like flapping at the MAV scale. It will also generate information of value for the analysis of insect flight, where similar experiments are difficult to perform. Finally, the progress in understanding of the aeromechanics of insect-like flapping wings will be used to gain additional insights into the flight of real insects. Thus, an engineering study inspired by nature will contribute to a better understanding of nature which, in turn, can be used to further progress the engineering design. This fruitful cycle seems to be a good and practical example of the real value of the interface between engineering and biology.

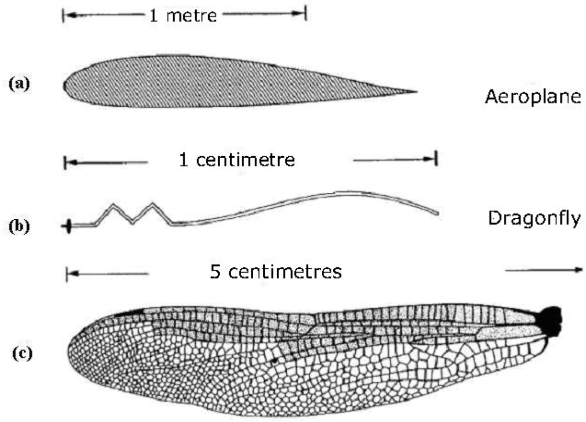

Fig. 19. Comparison of aircraft and dragonfly wing cross-section (airfoil) *a*) aircraft airfoil, *b*) dragonfly wing cross-section, c) dragonfly wing shape

Adult insects consist of three main parts: a head, a thorax, and an abdomen. The propelling system of the insect is the thorax. It consists of three segments connected by flexible joints. Three pairs of legs and one or two pairs of wings are connected to the segments. The abdomen also consists of segments. It contains the following systems: digestive, urinary, circulatory (including the heart), a large part of the respiratory system and the reproductive system. Most of the blood is situated in special chambers, creating a bath for the internal organs, and blood does not dirstibute oxygen, but only purifies the organism and carries fuel, hormones and nutritient media for the tissues. Air gets inside the insect through special openings and is distributed throughout the body by a system of tracheas. The flow of the air is enforced by contracting and expanding special bellows located in the abdomen, and the flow of the air is faster when the insect is flying.

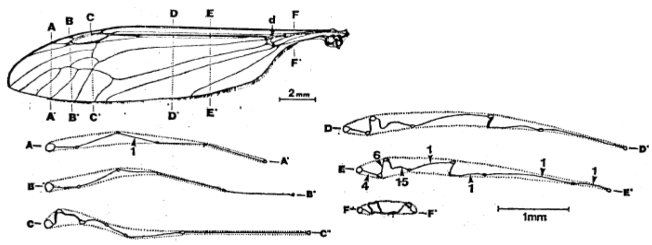

Fig. 20. Folds created on cross-section of a wing generate vortices causing, transformation of wing plate into effective airfoil

The wings of insects are of different shapes, but their structure is similar with all species. It can be stated, that wings of insects have semi-shell structure. The covering are two layers of chitin, thickness of the order of a few micrometers. This covering is enforced by spars (fibres) radiating from the shank in the hole of the body. In the state of rest the wings of an insect are flat. However during a flight they bend one way or the other and deform (fig. 4). Insects can have two pairs of wings or one pair of wings (*diptera*). Some insects equipped with two pairs of wings can set them in motion independently (e.g. dragonflies – *lastes sponsa* – can dislocate pairs of wings during flight by 90^0). However, with most species the pairs of wings work together. With some insects, such as the fly or mosquito, the second pair of wings transformed into little sticks – so called halteres, which act as a balancing system. The wings work in conditions of unsteady of flow (which has a significant influence on their aerodynamic effectiveness).

4. MEMS BASED INSECT CYBORG FLIGHT CONTROL

Insects are characterised by incredible resistance to unfavourable environmental conditions. Probably thanks to that around 750 000 species of insects survived to our times (whereas e.g. the number of species of mammals reaches only around 4 000). Compared with other animals the insects are characterised by a great diversity of shapes and ways of life, however their basic structure is the same. A lifting element of this structure is a hard and at the same time very light external chitin armour (cuticle). It serves not only as an exoskeleton being at the same time attachment place for the muscles, but also as waterproof covering protecting the intestines of the insect from dehydration.

The central computer of insects is their brain, consisting of 400 000 neurons, 98% of which is engaged in transforming information brought by the inset's sensors (e.g. eyes, ocelli, halteres, antennae). The flight control system is governed by less than 3 000 neurons. The motion of the wings is generated by around 20 different muscles. The wings are attached to the fuselage with the use of three joints. This enables performing complicated motions in relation to the fuselage (such mechanism of mounting the wings enables banking in relation to the fuselage of the resultant aerodynamic force and generating controlling forces and moments in a way similar to rotorcrafts – compare [1, 2, 25-30]. Progress ib biology, nad computer sciences allow to find alternative solution of flapping wings MAV design.

The paper [3] reports the first direct control of insect flight by manipulating the wing motion via microprobes and electronics introduced through the Early Metamorphosis Insertion Technology (EMIT). EMIT is a novel hybrid biology pathway for autonomous centimeter-scale robots that forms intimate electronic-tissue interfaces by placing electronics in the pupal stage of insect metamorphosis. This new technology may enable insect cyborgs by realizing a reliable control interface between inserted microsystems and insect physiology. This paper presented design rules on the flexibility of the inserted microsystem and the investigation towards tissuemicroprobe biological and electrical compatibility.

In the case of flight muscle actuation, the main flight powering muscles are located in the dorsal-thorax of the *Manduca sexta* (Figure 21) where electronic implants can be located. The dorsovental and dorsolongitudinal muscle groups move the wings by changing the conformation of the thorax, which supplies the mechanical power for up- and downstrokes. The alternating relaxation and contraction of these muscles create the alternating up- and down-strokes hence the flight. Therefore, the designed probe should target actuating these muscle groups.

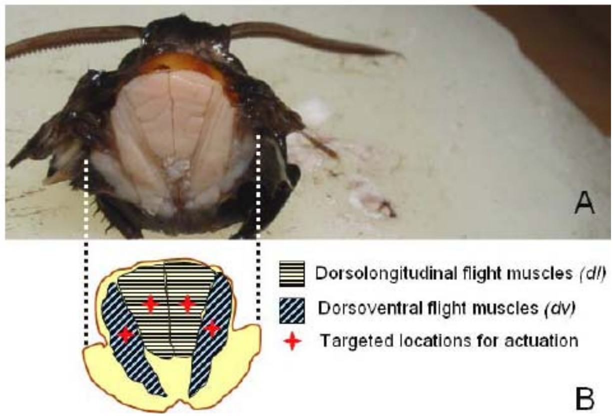

Fig.21. Cross-section (A) and illustrated diagram (B) of the flight muscles powering the up- and down-stroke of Manduca sexta wings (cf. [5])

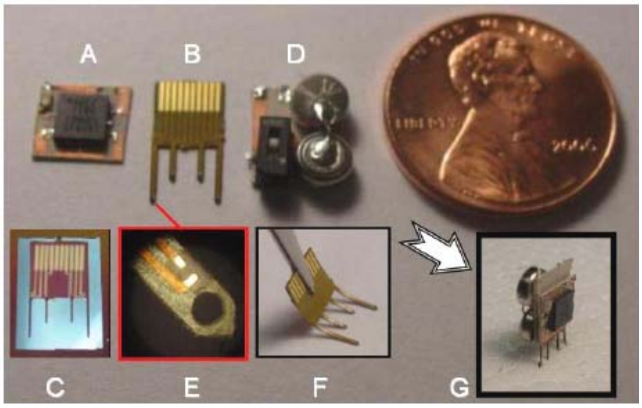

Fig. 22. The microsystem including microprocessor (A), flexible probe (B), silicon probe (C) and battery unit for power (D), the close-up view of the tip in (E) with the hole for muscle growth, the flexibility of the probe (F) and the assembled system (G) (cf. [5]).

The aimed experimental protocols consist of tethered setups where insect flight muscle is actuated through the flexible wires, as well as non-tethered setups where there are no attached wires and free-flight of insect can be realized. We designed and manufactured a flexible probe that can work with both setups (Figure 22B). The microsystem for autonomous control of the probe electronics can be seen in the same figure and consists of three parts: power, probe and control layers. The power layer (Figure 22D) is comprised of two coin batteries and a slide-switch positioned on a printed circuit board (PCB). Each battery has an energy capacity of 8mAh and weighs 120mg. Conductive adhesive was used to attach the batteries to the platform. The control layer (Figure 22A) is- an 8×8mm2 PCB holding the microcontroller (Atmel Tiny13V) and an LED. The microcontroller was electrically connected to the PCB via flip-chip bonding. Wire-bonding was used to connect the PCB to the probe layer. The microfabricated silicon probe is sandwiched between these two layers (Figure 22G). The overall system has dimensions of 8×7mm^2 and total mass of 500 milligrams. The flexible probe can also be used in tethered setups by utilizing a FFC/FPC connector (Figure 23). All-silicon rigid probes, which provide higher stiffness for narrower cross-section enabling higher density probing, were also fabricated and tested (Figure 22C).

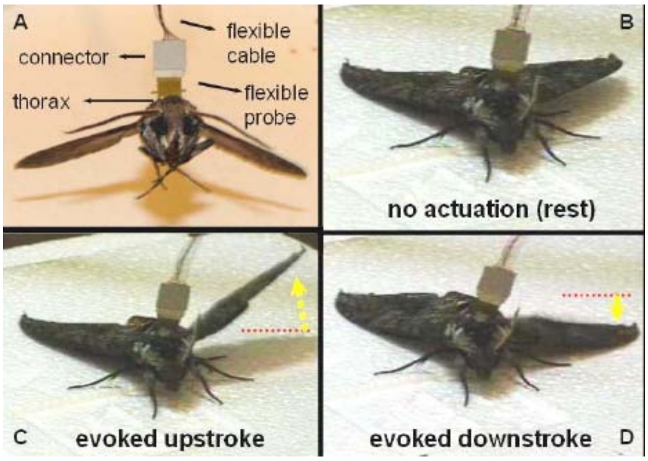

Fig. 23. The evoked up- and downstroke of a "single" wing obtained by applying 5V pulses to the indirect flight muscles (snapshots from the recorded movie). Under natural conditions, moths flap both wings together (cf. [5])

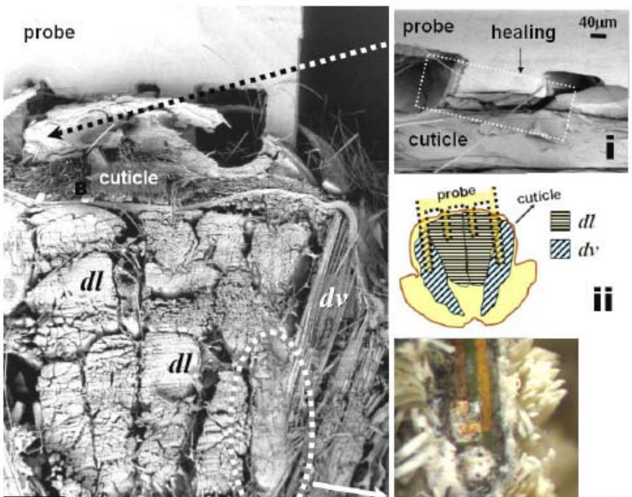

Fig. 24. The crossection of thorax near the probe with explanatory schematic (ii) of thoracic flight muscles. Cuticle sealing (i) and muscle growth (iii) around the probe indicates integration by the body.(dl: dorsolongitudinal flight muscle, dv: dorsoventral flight muscle, see Figure 21) cf [5]

It is possible [5] to demonstrate a reliable hybrid tissue-electronics interface in insects that provides flexibility against tissue movement. Inserting the probes at an early pupal stage ensures that the tissue grows around the probes for a highly natural implant. We also showed down- and up-stroke actuation of each wing separately, through which we were able to affect the flight direction of *Manduca sexta.* The work [5] paves the way for future engineering approaches to utilize the bioelectronic interfaces especially for realizing insect cyborgs.

5. CONCLUSIONS

It should be emphasized, that despite the extraordinary requirements posed for the systems of microaeroplanes, everything points to the fact that modern developments of microelectronics and microelectromechanics already allow constructing a fully-functional miniature aircraft. Also the contemporary knowledge in the field of aerodynamics of little Reynolds numbers (got, among others, thanks to researchers dealing with the problems of flight of birds and insects) allows designing its shape and assessing its dynamic properties. Therefore, it should be expected, that the first generation of microaeroplanes

Therefore, it should be expected, that the first generation of microaeroplanes will be supplied to military units shortly.

REFERENCES

1. **Azuma A, Masato O., Kunio Y.**, (2001), Aerodynamic characteristics of wings at low Reynolds Numbers. *Fixed and flapping wings aerodynamics for micro air vehicle applications*, Ed T, J, Mueller, Progress in Astronautics and Aeoronautics, AIAA, Reston, Va., 341-398
2. **Azuma A.**, (1998), *The biokinetics of flying and swimming*, Springer Verlag, Tokyo
3. **Bolsman C. T., Bjorn P., Goosen H. F. L., Schmidt R. H. M, Keulen F. van,** The Use of Resonant Structures for Miniaturizing FMAVs, *3rd US-European Competition and Workshop on Micro Air Vehicle Systems (MAV07).*
4. **Bergou A., J., Sheng Xu, Wang Z. J.**, (2007), Passive wing pitch reversal in insect flight, *J. Fluid Mech.*, vol. 591, 321–337
5. **Bozkurt A., Gilmour R., Stern D., Lal A**., (2008), MEMS based bioelectronic neuromuscular interfaces for insect cyborg flight control, *MEMS 2008*, Tucson, AZ, USA, January 13-17, 160-163
6. **Doncieux S., Mouret J-B., Muratet L., Meyer J-A.**, (2006), The ROBUR project: towards an autonomous flapping-wing animat, *Proceedings of the 5th European MAV conference and Competition*, Braunschweig, July, 2006
7. **Dickinson M. H.**, (1999), Bionics: Biological insight into mechanical design, *Proceedings of the National Academy of Sciences*, December 7, 1999, vol. 96, no. 25, 14208–14209
8. **Dickinson M, H., Lehmann F. O., Sane S. P.**, Wing rotation and the aerodynamic basis of insect flight, *Science*, Vol. 284, 1954-1960
9. **Ellington C. P.**, (1984) The aerodynamics of hovering insects flight. III Kinematics. *Philosophical Transactions of the Royal Society of London*. Series B. Biological Sciences, 305 (1122), 41-78
10. **Ellington C. P.**, (1999), The novel aerodynamics of insect flight: applications to micro-air-vehicles, *The Journal of Experimental Biology*, 202, 3439–3448
11. **Grasmeyer J. M., Keennon M. T.**, (2001), Development of the Black Widow Micro Air Vehicle, *AIAA-2001-0127 CP*
12. **Hewish M.**, (1999), A bird in the hand, *Janes International Defense Review*, no. 11

13. **Hicks R., Rais-Rohani M**., (1999), Multidisciplinary design and prototype development of a micro air vehicle, *J. of Aircraft*, vol. 36, no. 1, 227-234
14. **Joon-Hyuk Park, Kwang-Joon Yoon, Hoon-Cheol Park**, (2007), Development of bio-mimetic composite wing structures and experimental study on flapping characteristics, *Proceedings of the 2007 IEEE International Conference on Robotics and Biomimetics*, December 15 -18, 2007, Sanya, China, 25-30
15. **Karpelson M., Gu-Yeon Wei, Wood R. J.**, (2008), A review of actuation and power electronics options for flapping-wing robotic insects, *2008 IEEE International Conference on Robotics and Automation*, Pasadena, CA, USA, May 19-23, 2008, 779 - 786
16. **Kroo I., Kunz P.**, (2000), Development of the mesicopter: A Miniature Autonomous Rotorcraft, *Proceedings of the American Helicopter Society Vertical Lift Aircraft Design Conference,* San Francisco, CA
17. **Madejski J.**, (1991), Napędy owadzie i ptasie, Dodatek do książki: *Traktat o śmigłach*, Wyd. PAN, Warszawa
18. **Malladi B., Krashanitsa R., Silin D., Shkarayev S.**, (2007), Dynamic model and system identification procedure for autonomous ornithopter, *Proceedings of the 3rd US-European MAV conference and Competition*, Toulouse, September 2007
19. **Margerie E. de, Mouret J.-B., Doncieux S., Meyer J.-A., Ravasi T., Martinelli P., Grand C.**, (2007), Flapping-wing flight in bird-sized UAVs for the Robur project: from an evolutionary optimization to aeal flapping-wing mechanism, *Proceedings of the 3rd US-European MAV conference and Competition*, Toulouse, September 2007
20. **Marusak A., Pietrucha J., Sibilski K., Złocka M.**, (2001), Mathematical modelling of flying animals as aerial robots, *7th IEEE Inter. Conf. on Methods and Models in Automation and Robotics (MMAR 2001)*, Międzyzdroje, Poland, Aug. 28-31
21. **Maxworthy T.**, (1979), Experiments on the Weis-Fogh mechanism of lift generation by insects in hovering flight. Pat I. Dynamics of the "fling", *J. Fluid Mech.*, Vol. 93, part 1, 47-63
22. **McMichael J. M., Francis M. S.**, (1997), Micro Air Vehicles - Toward a new dimension in flight, *Proceedings of the 23th Annual AUVSI Conference*
23. **Michelson R. C., Helmick D., Reece S., Amarena C.**, A reciprocating chemical muscle (RCM) for Micro Air Vehicle „Entomopter" flight, http://avdil.gtri.gatech.edu/RCM/RCM/Entomopter/AUVSI-7/_EntomopterPaper.htm
24. **Michelson R.C.,** Micro Air Vehicle „Entomopter" Project, http://avdil.grti.gatech.edu/RCM/RCM/Entomopter/EntomopterProject.html
25. **Narkiewicz J., Pietrucha J., Sibilski K**., (2000), Can modern rotorcraft aeromechanics help to design entomopter propulsion ?, *Prace Instytutu Lotnictwa*, no 163
26. **Pietrucha J, Sibilski K.**, (2003), Od stworzeń latających do miniaturowych statków powietrznych, *NIT - Nauka, Innowacje, Technika*, nr 1
27. **Pietrucha J., Poniżnik Z.**, (2004), Kto jest mistrzem latania? Wykorzystanie energii w naturze, *NIT - Nauka, Innowacje, Technika*, nr 3
28. **Pietrucha J., Sibilski K., Zlocka M.**, (2000), Modelling of aerodynamic forces on flapping wings – questions and results, *Proc. of 4th Inter. Seminary on RRDPAE-2000*, Warsaw
29. **Platzer M. F. et al.**, (1993), Aerodynamic analysis of flapping wing propulsion, *AIAA 93-0484CP*
30. **Pornsin-Sisirak T., et. all.**, (2000), MEMS wing technology for a battery-powered ornithopter, *13th IEEE Inter. Conf. On Micro Electro Mechanical Systems (MEMS '00)*, Miyazaki, Japan, Jan. 23-27
31. **Priyadarshi A.K., Gupta S.K., Gouker R., Krebs F., Shroeder M., and Warth S.**, (2007), Manufacturing multi-material articulated plastic products using in-mold assembly. *International Journal of Advanced Manufacturing Technology*, VOL. 32, no 3-4, 250 – 365
32. **Sane S. P.**, (2003), The aerodynamics of insect flight, *The Journal of Experimental Biology* no. 206, 4191-4208
33. **Schenato L., Deng X., Wu W.C., Sastry S.**, (2001), Virtual insect flight simulator (VIFS): A software testbed of insect flight, *IEEE International Conference on Robotics and Automation*
34. **Shyy W, Berg M., Ljungqvist D.**, (1999), Flapping and flexible wings for biological and micro air vehicles, *Progress in Aerospace Sciences*, , Vol. 35, 455-505
35. **Sibilski K**., (2004), Dynamics of flapping wings micro-air-vehicle, *Acta Polytechnica*, vol. 44, no. 2
36. **Singh B., Ramasamy M., Chopra I., Leishman J. G.**, (2004), Insect-based flapping wings for micro hovering air vehicles: experimental investigations, Proceedings of the American Helicopter Society International Specialists Meeting on Unmanned Rotorcraft, Arizona, January, 2004
37. **Smith M. J. C., Wilkin P. J., Williams M. H.**, (1996), The advantages of an unsteady panel method in modelling the aerodynamic forces on rigid flapping wings, *Journal of Experimental Biology*, Vol. 199, 1073-1083
38. **Sunanda S., Kawachi K., Watanabe I., and Azuma A.**, (1993), Performance of a butterfly in take-off flight, *J. of Experimental Biology*, 1993, Vol. 183, 249-277
39. **Tobalske B. W., Dial K. P.**, Flight kinematics of black-billed magpies and pigeons over a wide range of speeds, *Journal of Experimental Biol*ogy, 1996, Vol. 199, 263-280
40. **Weis-Fogh T.**, (1973), Quick estimates of flight fitness in hovering animals including novel mechanism for lift production, *J. of Experimental Biology*, Vol. 59, 169-230
41. **Willmott A. P., Ellington C. P.**, (1997), The mechanics of flight in the hawkmoth *manduca sexta*. Part I. Kinematics of hovering and forward flight; *Journal of Experimental Biology*, 200, 2705–2722
42. **Wood R.**, (2008). Fly, Robot Fly, *IEEE Spectrum*, March 2008, 25 – 29
43. **Wood, R. J.,** (2008), The First takeoff of a biologically inspired at-scale robotic insect, *IEEE Transactions on Robotics*, Vol. 24, No. 2, 341-347
44. **Vörsmann P.**, (2003), MAV State-of-the-Art & Technology Drivers, *Proceedings of the MAV-Workshop*, Elmau, Sept. 22- 24, 2003
45. **Xinyan Deng, Schenato L, S. Shankar Sastry S. S.,** (2006), Flapping flight for biomimetic robotic insects: Part II -flight control design, *IEEE Transactions on Robotics*, Vol.. 22, No. 4, 789-803
46. **Zaeem A. K., Agrawal. S. K.**, (2005), Force and moment characterization of flapping wings for micro air vehicle application, *American Control Conference* , June 8-10, Portland, OR, USA, WeC11.4
47. **Żbikowski R**., (2003), Flapping wing MAVs. *By-invitation-only workshop on Micro Aerial Vehicles - Unmet Technological Requirements*, DLR Institut für Aeroelastik, Göttingen/Germany, Elmau Castle/Germany, September 22 – 24
48. **Żbikowski R., Galiński C.,** (2005), Insect-like flapping wing mechanism based on a double spherical Scotch yoke, *J. Royal Soc Interface*, Vol. 2, no. 3, 223–235